

Geology
GJBX-80-26

GJBX-26 '80

GEOLOGY

National Uranium Resource Evaluation

**GEOMETRIC PATTERN RECOGNITION
TECHNIQUES APPLIED TO LANDSAT
DIGITAL DATA FOR URANIUM EXPLORATION**

EARTH SATELLITE CORPORATION

7222 47th Street (Chevy Chase)
Washington, D.C. 20015

GEOLOGICAL SURVEY OF WYOMING

1979



PREPARED FOR THE U.S. DEPARTMENT OF ENERGY
Assistant Secretary for Resource Applications
Grand Junction Office, Colorado

metadc958472

This report is a result of work performed by Earth Satellite Corporation through a Bendix Field Engineering Corporation Subcontract, as part of the National Uranium Resource Evaluation. NURE is a program of the U.S. Department of Energy's Grand Junction, Colorado, Office to acquire and compile geologic and other information with which to assess the magnitude and distribution of uranium resources and to determine areas favorable for the occurrence of uranium in the United States.

This report was prepared as an account of work sponsored by the United States Government. Neither the United States nor the United States Department of Energy, nor any of their employees, nor any of their contractors, subcontractors, or their employees, makes any warranty, express or implied, or assumes any legal liability or responsibility for the accuracy, completeness, or usefulness of any information, apparatus, product, or process disclosed, or represents that its use would not infringe privately owned rights.

GEOMETRIC PATTERN RECOGNITION TECHNIQUES APPLIED TO
LANDSAT DIGITAL DATA FOR URANIUM EXPLORATION

Earth Satellite Corporation
7222 47th St. (Chevy Chase)
Washington, D.C. 20015

for

BENDIX FIELD ENGINEERING CORPORATION
Grand Junction Operations
Grand Junction, Colorado 81501

October 1979

PREPARED FOR THE U.S. DEPARTMENT OF ENERGY
ASSISTANT SECRETARY FOR RESOURCE APPLICATIONS
GRAND JUNCTION OFFICE, COLORADO
UNDER CONTRACT NO. EY-76-C-13-1664
AND BENDIX SUBCONTRACT NO. 78-187-S

FOREWORD

The work described in this report was performed by a team of Earth Satellite Corporation and Imtech, Inc. personnel. Major contributions were made by Dr. Charles Sheffield, Mr. John Berry, Dr. Jon Dykstra, and Mr. Ira Merin of EarthSat; and by Dr. Azriel Rosenfeld, Dr. David Milgram, and Dr. Sanjy Ranabe of ImTech.

Dr. David Emilia, of Bendix Field Engineering Corporation, and Dr. David Dahlem, of the Department of Energy, provided valuable evaluation, comment and review throughout the course of the project. In addition, Dr. Emilia provided access to invaluable uranium occurrence maps and other relevant materials.

TABLE OF CONTENTS

	<u>Page</u>
ABSTRACT	iii
List of Figures	v
List of Tables	x
List of Plates	xi
1.0 INTRODUCTION	1-1
2.0 OVERALL PROJECT PLAN	2-1
3.0 GEOLOGY	3-1
3.1 Copper Mountain	3-2
3.2 Pumpkin Buttes	3-11
3.3 Gas Hills	3-20
3.4 Grants Mineral Belt	3-23
3.5 San Rafael Swell	3-32
3.6 Marysvale	3-43
3.7 Lake City Caldera	3-54
3.8 Beaverlodge Area, Northern Saskatchewan	3-55
3.9 Northern Michigan	3-66
3.10 Rossing, Southwest Africa	3-69
3.11 South Park, Colorado	3-75
4.0 PROCESSING OF DATA PROCEDURES	4-1
4.1 Texture Measures	4-2
4.2 Display Operators for Texture and Geometric Patterns	4-7
5.0 RESULTS	5-1
5.1 Summary of Texture Measures	5-2
5.1.1 Copper Mountain - Results of Texture Measures	5-14
5.1.2 Pumpkin Buttes - Results of Texture Measures	5-17
5.1.3 Gas Hills Quarter Frame Test Area Texture Measure Results	5-28
5.1.4 Grants - Texture Measure Results	5-35
5.1.5 Namibia - Texture Measure Results	5-44
5.1.6 Marysvale - Texture Measure Results	5-53
5.1.7 San Rafael - Texture Measure Results	5-58
5.2 Display Operators	5-62
5.2.1 Copper Mountain	5-62
5.2.2 Pumpkin Buttes	5-67
5.2.3 Beaverlodge	5-81
5.2.4 Rossing	5-88

	<u>Page</u>
6.0 CONCLUSIONS AND RECOMMENDATIONS	6-1
6.1 Conclusions Regarding the Available Data Base	6-1
6.2 Conclusions Regarding the Completeness of Texture Analysis Tools Used on the Project	6-2
6.3 Conclusions Regarding the Detection of Uranium-Related Textures from Landsat Data	6-3
6.4 Conclusions Regarding the Association of Texture with Uranium Deposits	6-4
6.5 Recommendations	6-5
APPENDICES	
1 - The Use of Texture Measures	A-1.1
2 - The Creation of Eigenpictures	A-2.1
3 - EarthSat Processing of Computer Compatible Tapes and Production of Photo Products	A-3.1
4 - Texture and Lineament Display Operators	A-4.1
5 - Return Beam Vidicon Data from Landsat-3, Thematic Mapper Data from Landsat-D, and Synthetic Aperture Radar Data from SEASAT-1	A-5.1
6 - Computer Output Exhibits, Summary of Runs	A-6.1
7 - Deliverable Image Products	A-7.1
8 - Annotated Geological Bibliography	A-8.1
9 - References on Texture Analysis	A-9.1
10 - Glossary	A-10.1
11 - Use of Landsat X-Directional Derivative Images	A-11.1

ABSTRACT

This report describes the application of texture measures and displays by staff of Earth Satellite Corporation and ImTech to uranium exploration, using data from the Landsat series of spacecraft as the primary information source.

Working together with staff of Bendix Field Engineering Corporation, six training sites were selected, consisting of Copper Mountain (Wyoming), Pumpkin Buttes/Kaycee (Wyoming), Grants (New Mexico), Rossing (Namibia), Marysvale (Utah), and Beaverlodge (Saskatchewan). For each of these sites, displays and/or texture measures were generated, and where possible discrimination functions were developed to separate known uraniumiferous areas from areas of unknown uranium content.

The analysis was applied to the original Landsat spectral bands, to all Eigenbands (linear combinations of the original bands) and to band ratios (visual inspection only). The basic data source for all our analyses was Landsat Computer Compatible Tapes.

Of all data sources and all texture measures, the most successful was the measure pair, Inverse Difference Moment (IDM) plotted against Angular Second Moment (ASM), applied to the third Eigenband of the Landsat data. This measure pair permitted separation of uranium from non-uranium in certain geologies (particularly Pumpkin Buttes/Kaycee) but was unsuccessful in others. Our attempts to develop general discriminants by extending calculated discrimination curves across Landsat frame boundaries, were unsuccessful. We attribute this lack of success in jumping boundaries to variations in Landsat images caused by changes in sun angle, atmosphere and season from one frame to another.

The use of enhanced displays as a tool for analysis showed hints of correlation with uranium occurrences, but the resolution of available data limited the strength of this inference. Broadly speaking, texture and enhanced geometric pattern displays are still too crude to enable any real correlation with uranium to be demonstrated or denied.

Although the results we obtained cannot be described as providing a new tool for uranium exploration, we saw clear evidence that computed texture measures are describing some element of the Landsat data source that cannot be readily observed or analyzed by human interpreters. The success of Eigenband 3 is less surprising, since we had other evidence suggesting that such a band ought to be relevant to image textures.

We conclude that the experiments would be worth pursuing further only in areas with selected geologies, such as that of Pumpkin Buttes. In addition, portions of this work should definitely be repeated as soon as the higher resolution data of Landsat-D becomes available. There were enough hints of success that texture cannot be discounted as a basis for classifying terrain in terms of uranium-bearing potential.

Keywords: Landsat
Uranium
Texture
Image processing
Computer compatible tapes
Exploration
Copper Mountain, Wyoming
Pumpkin Buttes, Wyoming
Grants, New Mexico
Rossing, Namibia
Marysvale, Utah
Beaverlodge, Saskatchewan

LIST OF FIGURES

		<u>Page</u>
Figure 2.1	Processing stages.	2-4
Figure 3.1.1	Index map of Wyoming and northern Colorado showing uranium occurrences, basins, and Precambrian exposures.	3-3
Figure 3.1.2	A generalized stratigraphic column of Wyoming.	3-5
Figure 3.1.3	A generalized geologic map of East Owl Creek Mountains.	3-7
Figure 3.1.4	Diagrammatic cross-section showing Eocene facies across Wyoming. Location of line of cross-section on Figure 3.1.1.	3-9
Figure 3.1.5	Genetic model for uranium deposition at Owl Creek Mountains.	3-10
Figure 3.1.6	Geology of central northern Wyoming.	3-16
Figure 3.2.1	Idealized vertical section across a solution front, showing several superimposed roll front ore deposits.	3-18
Figure 3.4.1	Index map illustrating the Grants Region in relation to major tectonic elements of the San Juan Basin, New Mexico.	3-24
Figure 3.4.2	Geologic map of the southern part of the San Juan Basin and vicinity, showing the uranium deposits.	3-27
Figure 3.4.3	Stratigraphic column for the southern part of the San Juan Basin.	3-28
Figure 3.4.4	Generalized geologic sections showing the stratigraphic relations of the Morrison uranium deposits near Grants and near Laguana, New Mexico.	3-30
Figure 3.5.1	Stratigraphic column, San Rafael Swell area.	3-34
Figure 3.5.2	Map of areas favorable for uranium deposits in the San Rafael Swell area.	3-39
Figure 3.5.3	Map of uranium deposits and mines, San Rafael Swell area.	3-40
Figure 3.6.1	Index map of geographical features in the Marysvale area, west-central Utah.	3-42

		<u>Page</u>
Figure 3.6.2	Stratigraphic column for Marysvale, Utah.	3-46
Figure 3.6.3	Diagrammatic cross-section showing stratigraphic relations of the Mount Belknap Volcanics.	3-47
Figure 3.6.4	Typical pitchblende vein at Marysvale.	3-50
Figure 3.7.1	Generalized geologic map of the Silverton-Lake City area.	3-56
Figure 3.8.1	Index map and geology of the Beaverlodge District.	3-58
Figure 3.8.2	Geology of the Beaverlodge area, northwest Saskatchewan.	3-59
Figure 3.8.3	Stratigraphic column for northwest Saskatchewan.	3-61
Figure 3.10.1	Geologic map of the Rossing area, Southwest Africa.	3-70
Figure 3.10.2	Stratigraphic column for the Rossing area.	3-72
Figure 3.10.3	Cross-section through the Rossing deposit.	3-74
Figure 3.11.1	Geologic map of the South Park area.	3-76
Figure 4.1.1	Pumpkin Buttes, IDM/ASM plot.	4-4
Figure 4.1.2	Pumpkin Buttes, IDM/ASM plot with complex discrimination curve.	4-4
Figure 4.1.3	Marysvale, IDM/ASM plot with vertical discrimination boundary.	4-5
Figure 4.1.4	Pumpkin Buttes, IDM/ASM plot with two discrimination lines.	4-5
Figure 5.1.1	6 x 10 matrix of data combinations.	5-5
Figure 5.1.2	Pumpkin Buttes, IDM/ASM plot for B5	5-6
Figure 5.1.3	Pumpkin Buttes, IDM/ASM plot for B7	5-6
Figure 5.1.4	Pumpkin Buttes, IDM/ASM plot for E1	5-7
Figure 5.1.5	Pumpkin Buttes, IDM/ASM plot for E2	5-7
Figure 5.1.6	Pumpkin Buttes, IDM/ASM plot for E3	5-8
Figure 5.1.7	Pumpkin Buttes, IDM/ASM plot for E4	5-8
Figure 5.1.8	Pumpkin Buttes, ENT/ASM plot for E3	5-9
Figure 5.1.9	Pumpkin Buttes, CON/ASM plot for E3	5-9

	<u>Page</u>	
Figure 5.1.10	Pumpkin Buttes, COR/ASM plot for E3	5-10
Figure 5.1.11	Pumpkin Buttes, IDM/ASM plot for E3	5-10
Figure 5.1.12	Pumpkin Buttes, ENT/IDM plot for E3	5-11
Figure 5.1.13	Pumpkin Buttes, COR/IDM plot for E3	5-11
Figure 5.1.14	Pumpkin Buttes, CON/ENT plot for E3	5-12
Figure 5.1.15	Pumpkin Buttes, COR/ENT plot for E3	5-12
Figure 5.1.16	Pumpkin Buttes, CON/IDM plot for E3	5-13
Figure 5.1.17	Pumpkin Buttes, CON/COR plot for E3	5-13
Figure 5.1.1.1	Uranium Occurrence Map for a Portion of Wyoming	5-15
Figure 5.1.1.2	Copper Mountain, IDM/ASM plot for E3	5-18
Figure 5.1.2.1	Uranium Occurrence Map for a Portion of Wyoming	5-20
Figure 5.1.2.2	Classification Map for a Portion of Wyoming	5-21
Figure 5.1.2.3	Pumpkin Buttes, IDM/ASM plot for E3	5-22
Figure 5.1.4.1	Uranium Occurrence Map for a Portion of New Mexico	5-38
Figure 5.1.4.2	Classification Map for a Portion of New Mexico (Line #1)	5-39
Figure 5.1.4.3	Classification Map for a Portion of New Mexico (Line #2)	5-40
Figure 5.1.4.4	Grants, IDM/ASM plot for E3, Line #1	5-41
Figure 5.1.4.5	Grants, IDM/ASM plot for E3, Line #2	5-41
Figure 5.1.5.1	Uranium Occurrence Map for a Portion of Namibia	5-47
Figure 5.1.5.2	Classification Map for a Portion of Namibia	5-49
Figure 5.1.5.3	Namibia, IDM/ASM plot for E3	5-50
Figure 5.1.6.1	Uranium Occurrence Map for a portion of Utah	5-54
Figure 5.1.6.2	Classification Map for a portion of Utah	5-55
Figure 5.1.6.3	Marysvale, IDM/ASM plot for E3	5-56
Figure 5.1.7.1	San Rafael, IDM/ASM plot for E3	5-61

	<u>Page</u>
Figure 5.2.1.1	Lineaments drawn on local histogram stretch (band 5) compared with those on texture transform (band 5). 5-65
Figure 5.2.1.2	Lineaments drawn on edge detector (band 5) at threshold = 1. 5-65
Figure 5.2.1.3	Lineaments drawn on edge detector (band 5) at threshold = 2. 5-66
Figure 5.2.1.4	Lineaments drawn on edge detector (band 5) at threshold = 3. 5-66
Figure 5.2.1.5	Comparison between lineaments on band 5 line detector at threshold = 3 versus threshold = 2. 5-68
Figure 5.2.2.1	All lineaments drawn on band 5 line detector (Z). 5-72
Figure 5.2.2.2	All lineaments trending at 045° or 135° drawn on band 5 thinned line detector (ZZ). 5-73
Figure 5.2.2.3	Major lineaments trending at 045° or 135° drawn on band 5 line detector (Z). 5-74
Figure 5.2.2.4	Lineament intersections and long lineaments (excluding those trending 045° and 135°) on band 5 thinned line detector (ZZ). 5-75
Figure 5.2.2.5	Lineaments and circulars on Eigenband 1, global histogram stretch (H). 5-76
Figure 5.2.2.6	Lineaments, and extreme dark and light toned areas on Eigenband 1, texture transform (N). 5-77
Figure 5.2.2.7	Dark and light toned areas on Eigenband 3, texture transform (N). 5-78
Figure 5.2.2.8	Circulars and low contrast features on Eigenband 3, local histogram stretch (S). 5-79
Figure 5.2.3.1	Uranium Occurrence Map for the Beaverlodge Area of Saskatchewan. 5-82
Figure 5.2.3.2	All lineaments drawn on band 7 with edge detector at threshold = 1. 5-83
Figure 5.2.3.3	Lineaments trending 045° and 135° drawn on Eigenband 1 with edge detector at threshold = 2. 5-84
Figure 5.2.3.4	Lineaments trending 135° drawn on band 7 with edge detector at threshold = 2. 5-85
Figure 5.2.4.1	Polaroid of edges on band 7 at threshold = 2 for the Rossing area of Namibia. 5-87

		<u>Page</u>
Figure A.1.1	Picture element array and notation.	A-1.2
Figure A.1.2	Examples, coarse texture and array and fine texture array.	A-1.9
Figure A.2.1	Pixels as points in N-space.	A-2.3
Figure A.2.2	Pixel clusters in N-space.	A-2.3
Figure A.2.3	Pixel clusters fitted to an ellipsoid.	A-2.5
Figure A.3.1	Result of additive mixing of colors (three spotlights)	A-3.3
Figure A.3.2	Diagram of the subtractive combinations of colors (such as printing and painting)	A-3.3
Figure A.3.3	Formation of negative images.	A-3.4
Figure A.3.4	Formation of positive images.	A-3.4
Figure A.11.1	Partial interpretation of the Unsmoothed X-Directional Derivative of the Poison Spider Frame, a portion of Wyoming.	A-11.3
Figure A.11.2	Partial interpretation of the Smoothed X-Directional Derivative of the Poison Spider Frame, a portion of Wyoming.	A-11.4

LIST OF TABLES

		<u>Page</u>
Table 5.1.1	Pumpkin Buttes Training Area: Degree of Correct Classification of Known Uranium Occurrences	5-23
Table 5.1.2	Correlation of Texture Measure Output with Known Uranium Distribution for the Pumpkin Buttes Training Area	5-24
Table 5.1.3	Gas Hills Test Area: Degree of Correct Classification of Known Uranium Occurrences	5-30
Table 5.1.4	Correlation of Texture Measure Output with Known Uranium Distribution of the Gas Hills Test Area	5-31
Table 5.1.5	Grants Training Area Line 1: Degree of Correct Classification of Known Uranium Occurrences	5-43
Table 5.1.6	Grants Training Area Line 2: Degree of Correct Classification of Known Uranium Occurrences	5-44
Table 5.1.7	Correlation of Texture Measure Output with Known Uranium Distribution for the Grants Training Area Line 1	5-45
Table 5.1.8	Correlation of Texture Measure Output with Known Uranium Distribution for the Grants Training Area Line 2	5-46
Table 5.1.9	Marysvale Area: Degree of Correct Classification of Known Uranium Occurrences	5-58
Table 5.1.10	Correlation of Texture Measure Output with Known Uranium Distribution for the Marysvale Area	5-59
Table 5.2.1.1	Display Operators Carried Out on Copper Mountain Area	5-64
Table 5.2.2.1	Display Operator Processes Carried-Out on Pumpkin Buttes Area	5-69
Table A.3.1	Results of Various Dye Combinations in a Color Negative	A-3.6

LIST OF PLATES

Plate 1	-	Standard false color composite of Landsat image #1786-17135 (Poison Spider) at a scale of 1:250,000	-	Unbound
Plate 2	-	Standard false color composite of Landsat image #1515-17180 (Grants) at a scale of 1:250,000	-	Unbound
Plate 3	-	Standard false color composite of Landsat image #1383-08264 (Namibia) at a scale of 1:250,000	-	Unbound
Plate 4	-	Standard false color composite of Landsat image #1068-17364 (Overthrust) at a scale of 1:250,000	-	Unbound
Plate 5	-	Standard false color composite of Landsat image #1396-17531 (Uranium City) at a scale of 1:250,000	-	Unbound
Plate 6	-	Standard false color composite of Landsat image #1802-17030 (South Park) at a scale of 1:250,000	-	Unbound
Plate 7	-	Standard false color composite of Landsat image #5433-16342 (Durango) at a scale of 1:250,000	-	Unbound
Plate 8	-	Standard false color composite of Landsat image #1774-16044 (Iron Mountain) at a scale of 1:250,000	-	Unbound
Plate 9	-	Color composite of Eigenbands 1, 2, and 3 of Landsat image #1786-17135 (Poison Spider) at a scale of 1:250,000	-	Unbound
Plate 10	-	Color composite of ratioed Landsat bands (4/5, 5/6, 6/7) for Landsat image #1786-17135 (Poison Spider) at a scale of 1:250,000	-	Unbound
Plate 11	-	Uranium Occurrence Map overlay to plate 1 (Poison Spider)	-	Unbound
Plate 12	-	Classification Map overlay to plate 2 (Poison Spider)	-	Unbound
Plate 13	-	Uranium Occurrence Map overlay to plate 2 (Grants)	-	Unbound
Plate 14	-	Classification Map overlay (using line #1) to plate 2 (Grants)	-	Unbound
Plate 15	-	Classification Map overlay (using line #2) to plate 2 (Grants)	-	Unbound
Plate 16	-	Uranium Occurrence Map overlay to plate 3 (Namibia)	-	Unbound
Plate 17	-	Classification Map overlay to plate 3 (Namibia)	-	Unbound

Plate 18	- Uranium Occurrence Map overlay to plate 4 (Overthrust)	- Unbound
Plate 19	- Classification Map overlay to plate 4 (Overthrust)	- Unbound
Plate 20	- Uranium Occurrence Map to plate 5 (Uranium City)	- Unbound
Plate 21	- Unsmoothed X-Directional Derivative of Eigenband-1 #1786-17135 (Poison Spider) at a scale of 1:250,000	- Unbound
Plate 22	- Smoothed X-Directional Derivative of Eigenband-1 #1786-17135 (Poison Spider) at a scale of 1:250,000	- Unbound

NOTE: These plates are presented in reduced microfilm form in the bound packet at the back of this report. The reproducible master copies from which the microfilm sets were made are on open file at Bendix Field Engineering Corporation, Grand Junction, Colorado.

1.0 INTRODUCTION

Since the launch of the first Landsat satellite in 1972, this series of spacecraft has found use in a wide variety of natural resource applications. One of the more surprising results of using the data has been the discovery that Landsat Computer Compatible Tapes contain much more information than can be presented in any single photograph. As a result, a number of methods have been developed to maximize the use of multispectral data from the four MSS channels. These methods include image ratioing, linear (digital) combinations of images, and spectral clustering. Each of these techniques is concerned with manipulation of spectral properties of the data.

In this project, the question of the enhancement of spatial properties of the data is addressed. Spatial properties reveal themselves through a number of different image features: scene texture, preferred directions, linear patterns, preferred spatial frequencies, and preferred shape of ground features. This study has concentrated on two of these: image texture, and image geometric patterns. It has sought to correlate these image properties with the presence of uranium deposits in selected areas of the United States, Canada, and South Africa. Both computer-generated measures and human analysis of enhanced images have been employed.

Just as the use of Landsat for spectral analysis is limited by virtue of the narrow spectral window observed by the spacecraft (four bands in the range 0.5 to 1.1 micrometers, with no data in the geologically important 1.5 to 1.7 or 2.1 to 2.6 micrometer regions), so also is the use of texture and spatial information limited by the spatial resolution of the observing instruments. The basic picture element (pixel) size for Landsat-1 and -2 is 79 meters by 57 meters. Landsat-3 has the same

resolution for the MSS, but also has a Return Beam Vidicon (RBV) with spectral window 0.5 to 0.75 micrometers, and resolution of about 35 meters. However, data from the RBV is not yet available except in small quantities and for limited areas, and it was not possible to use it on this project.

By the use of digital enhancement methods, the effective resolution of the Landsat MSS data can be somewhat improved, perhaps to 50 meters. This is especially true when we are interested in looking at linear features, where high-contrast linears as narrow as 20 to 25 meters can often be seen (such as bridges over water, roads through vegetated areas, etc.). Even with enhancement, however, it is certain that texture finer than about 20 meters will not be seen on Landsat data, regardless of the degree of computer processing, contrast adjustment, or output scale. Since many natural textures of geological interest are much finer than 20 meters, it was recognized at the outset that the task of correlating texture and uranium would not be an easy one. The correlation would have to be with some more extensive texture feature of the surface, which would then itself have to be correlated with mineralization.

Since it was anticipated that such a more extensive class of texture feature would, if present, be new and perhaps unpredictable on the basis of geological fore-knowledge, it was decided at the outset that a wide class of texture measures, texture displays, and geometric pattern enhancers ought to be tried on the project. Previous experience in the use of texture indicators (Reference 1) has shown that texture is a subtle and complex entity.*

The human eye sees "texture" readily in an image, and can quickly classify it as coarse or fine. In objective terms, however, numerical

* Texture References are given in Appendix 9.

measures of texture as estimated by humans are affected by a number of other variables. Overall brightness, contrast, image polarity (positive or negative), and color all influence the evaluation of texture. In a computerized approach, the first requirement is to define numerical measures of texture that stand independent of such variables as brightness and contrast. This has been done by a number of research workers, and the basis for the texture measure adopted in this project is described in Reference 2. A summary of the meaning and computation methods for the measures used is given in Appendix 1 and in the Glossary of Appendix 10.

Recent work in the evaluation of multispectral image data has also suggested that linear combinations of individual bands may prove more useful for texture analysis than any single spectral band (Reference 3). Thus, although the emphasis of the work on this project was spatial rather than spectral analysis, some preliminary spectral processing was performed in order to obtain a variety of band combinations on which texture operations could be performed. As will be seen later when we describe the results of the study, this pre-processing proved to be very valuable, since the best texture discrimination was obtained using a band combination.

Previous attempts to make inferences based solely on computerized measures of texture from Landsat imagery had not been very successful (Reference 4). It was therefore decided that, in parallel with computer analyses, the active involvement of geologists was essential. The geological staff were used in three separate roles: as independent evaluators of enhanced image products, as selectors of suitable image areas for the training of computer algorithms, and as evaluators of the effectiveness of computer measures and displays of image texture.

2.0 OVERALL PROJECT PLAN

The performance of the project was divided into 14 distinct but interdependent activities. In this Section these activities are described in summary, without presenting any of the results. Those follow in later sections.

2.1 Activity 1 - Selection of Training and Test Areas

Based upon an analysis of available geological information and available Landsat imagery, five areas were selected for training of computer algorithms. Five areas were also selected for testing of the methods suggested as a result of training area analysis. In the course of the project, a sixth training and a sixth test area were added (see Section 5), with the recognition that the processing of test areas would be meaningless unless some satisfactory discrimination could be proposed from analysis of the corresponding training area. In general, each training area was chosen to reflect some different type of uraniferous structure, with some appropriate non-uraniferous but otherwise similar area nearby. Test areas, where possible, were of similar geological type to the corresponding training area. Selection of test and training areas was done by the project Technical Monitor and EarthSat geological staff, working together.

2.2 Activity 2 - Collection and Evaluation of Information on Training and Test Sites

When the training and test sites had been identified, all available information (maps, reports, and Landsat coverage) was collected and reviewed by EarthSat staff. It also proved possible in the course of the project to visit several of the training and

test site on field trips; however, those field trips were not part of the original information available on the sites.

2.3 Activity 3 - Acquisition of Landsat Computer Compatible Tapes

Following the review of dates, season, cloud cover, and image quality of the available Landsat coverage of the training and test areas, CCT's (one of each area) were ordered from the EROS Data Center.

2.4 Activity 4 - Pre-Processing of Landsat Scenes

The pre-processing of the CCT's called for the generation of two different types of tapes:

- a. Tapes for use in generating image products.
- b. Tapes for use with computer texture algorithms.

Both sets of tapes were radiometrically corrected using EarthSat software to reduce the "striping" of the image caused by variable sensitivity of the six sets of detectors used in each spectral band of the Landsat spacecraft. In addition, both sets of tapes were geometrically corrected for the effects of earth rotation, earth curvature, variations in scan mirror speed and sweep angle, and effects of changes in satellite altitude and attitude. However, the tapes for use with the texture analysis were not "squared", which adds sets of scan lines to an image to produce a correct ratio of horizontal to vertical scale. It was felt that squaring of this type would add a spurious texture and reduce the utility of the texture measures.

In addition to the spectral bands recorded by Landsat, band combinations (Eigenbands) were also generated, for use in both the

image products and the computerized texture analyses. A full discussion of the logic for the use of Eigenbands, and of the mathematical operations used to generate them, is given in Appendix 2.

In order to distinguish the tapes for computer processing of texture from those used in generation of image products, the prefix R- will be added in describing the former set of tapes. As will be seen from the processing flow chart of Figure 2.1, subsequent processing history of image product tapes and R-tapes is completely different.

2.5 Activity 5 - Contrast Adjustment and Edge Enhancement of Product Tapes

(Note: Activities 5 through 7 proceeded substantially in parallel with Activities 8 through 12.)

Image product tapes were edge-enhanced for geological interpretation, and a computer adjustment of contrast was performed to create output images with the best possible degree of detail and interpretability. (These are standard operations used in all EarthSat's GEOPIC line of image products.)

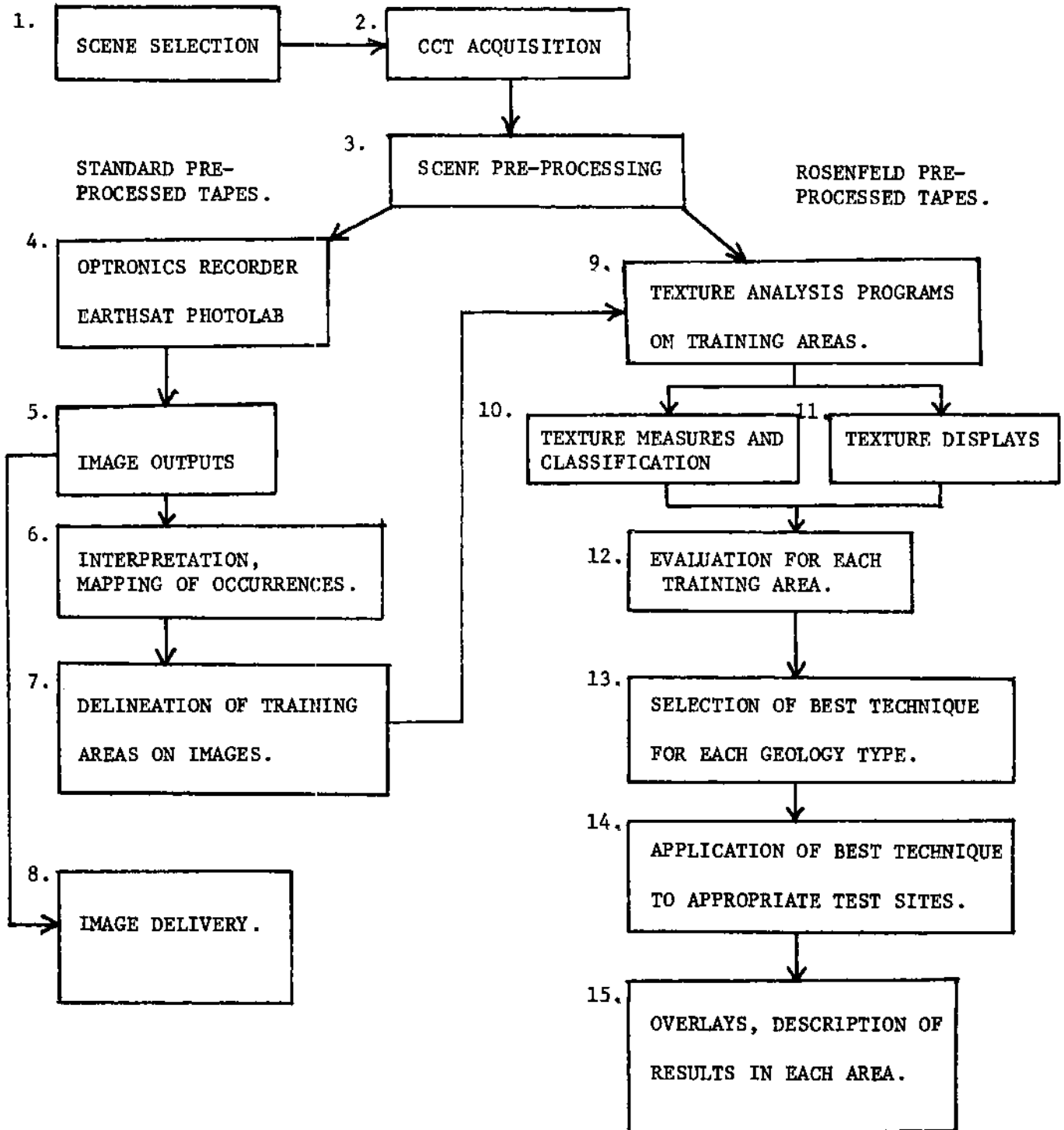
2.6 Activity 6 - Generation of Color Composite Image Products

The processed tapes were written to film using an Optronics P-1500 film recorder.** This was done for both the Landsat original spectral bands and for the Eigenbands.

** The recorder equipment was changed during the project. This caused both delay and a need for re-calibration of some of the imagery.

FIGURE 2.1

PROCESSING STAGES.



In EarthSat's photolab, each spectral band is used to create a single black-and-white film positive. Color prints are produced by pin registration of three black-and-white positives to produce a color negative, and finally a color print. The procedure is described in full in Appendix 3. Here, it is appropriate to note that the green, red, and infrared of the original Landsat image are represented by blue, green, and red on the standard EarthSat GEOPIC product, and other colors on the print are generated by the standard rules for additive color (green + red = yellow, etc.).

2.7 Activity 7 - Mapping for Uranium Occurrences

Using 1:250,000 scale prints of the image products, and the collateral information collected from maps and reports, known uranium occurrences were delineated for each training area. Sub-areas were drawn on image overlays, for use in computer analysis of texture and lineaments.

2.8 Activity 8 - Window of R-Tapes

Using the delineated sub-areas on the Landsat images, particular row and column numbers were identified on the R-tapes, and windows selected corresponding to these sub-areas. These were then extracted and stored in separate computer storage, for subsequent processing with texture and lineament analysis programs.

2.9 Activity 9 - Image Texture Measures

Texture measures were computed for the windowed training areas. A total of ten different measures were computed, and the results displayed as two-dimensional plots, with one value shown

for each 64 x 64 pixel sub-area. The computations performed, and the meaning of each of the computed texture measures, are described in Appendix 1. The output of this activity was a series of data plots for manual interpretation.

2.10 Activity 10 - Image Texture and Lineament Displays

In parallel with Activity 9, a series of image texture displays and lineament enhancements were computed and produced as CRT screen outputs for evaluation. This set of operators is described in Appendix 4. The output of this activity was a set of texture images and lineament images for manual interpretation.

2.11 Activity 11 - Evaluation of Texture Measures, Texture Displays, and Lineament Displays for Each Training Area

EarthSat geologists reviewed the results of the texture and lineament enhancement operators, in terms of the known occurrences of uraniferous and non-uraniferous regions within the training areas. Based on this analysis, correlations were made of the apparent success of each type of operator for each corresponding type of geology. In practice, since it was not feasible to try all measures for all areas, the process proceeded by a narrowing of the options explored from one training area to the next, so that the first training areas inevitably were subjected to more detailed analysis than those studied later. The possible effects of such an approach are discussed later in this report. Clearly, the ideal approach would be to try every measure for every area, but time and cost limits prohibited this.

2.12 Activity 12 - Selection of the Preferred Techniques for Particular Geologies

The best procedure (evaluated subjectively by EarthSat staff) for separating uraniferous and non-uraniferous areas was chosen for each training area. At this stage, some techniques were eliminated completely from further consideration. As a consequence, some associated test areas were also eliminated from further consideration, since without a promising tool of correlation of scene with uranium deposits, there was no measure against which areas of test areas could be evaluated. All the techniques, and their relative success and failure, are described later in this report.

2.13 Activity 13 - Application to Test Areas

The promising techniques were applied to the appropriate test areas, and overlays generated that separated uraniferous from non-uraniferous areas, on the basis of the statistics developed from the training area analysis. These overlays were in turn analyzed by geological staff to see how well the computer overlays seem to correspond to probable uranium deposits.

2.14 Activity 14 - Results

The final task on the project was the overall evaluation of the results. Each geology was discussed in terms of the discrimination functions developed from the training areas, and where relevant, the success of the discrimination function on the corresponding test area. Overall conclusions were also drawn as to the probable general utility of texture as an additional data source

in the uranium exploration process, including the extrapolation to Landsat-D and the use of the Landsat-3 RBV data (see also Appendix 5 for a discussion of the characteristics of these instruments).

3.0 GEOLOGY

The general geology and the uranium geology of the training and test areas chosen was studied from published sources, and is described in this section. References quoted are to be found, with comments upon their content and degree of usefulness, in the Annotated Bibliography, Appendix 8.

Three of the areas were visited in the field: Copper Mountain (Wyoming), South West Africa (Namibia), and the Lake City Caldera (Colorado), area. In addition, the Gas Hills area was a principal topic of discussion at the 1978 Wyoming Geological Association meeting, which was attended by EarthSat staff. These visits were extremely useful in acquainting us with the complexities of each area, and in helping us to direct our efforts toward the techniques most likely to be successful. They also re-emphasized that each mining district is unique geologically, so that a grouping into Training/Test pairs is inevitably somewhat arbitrary. Therefore, techniques that appear to work in a training area may not work, or may need extensive "tuning" to work, in the corresponding test area.

Personnel of the Grand Junction field office of Bendix Field Engineering Corporation gave great assistance with data and in discussions of the uranium geology of the Marysvale, Lake City Caldera, and San Rafael Swell areas, and we would like to record our thanks to them.

As a result of knowledge gained from the field visits and discussions with field geologists, several changes were made in the training and test areas chosen. In the case of the Lake City Caldera area, it became apparent that knowledge of the uranium geology of the area was inadequate for it to serve as a training area, and in the case of Gas Hills it was realized that ground disturbance due to mining and related

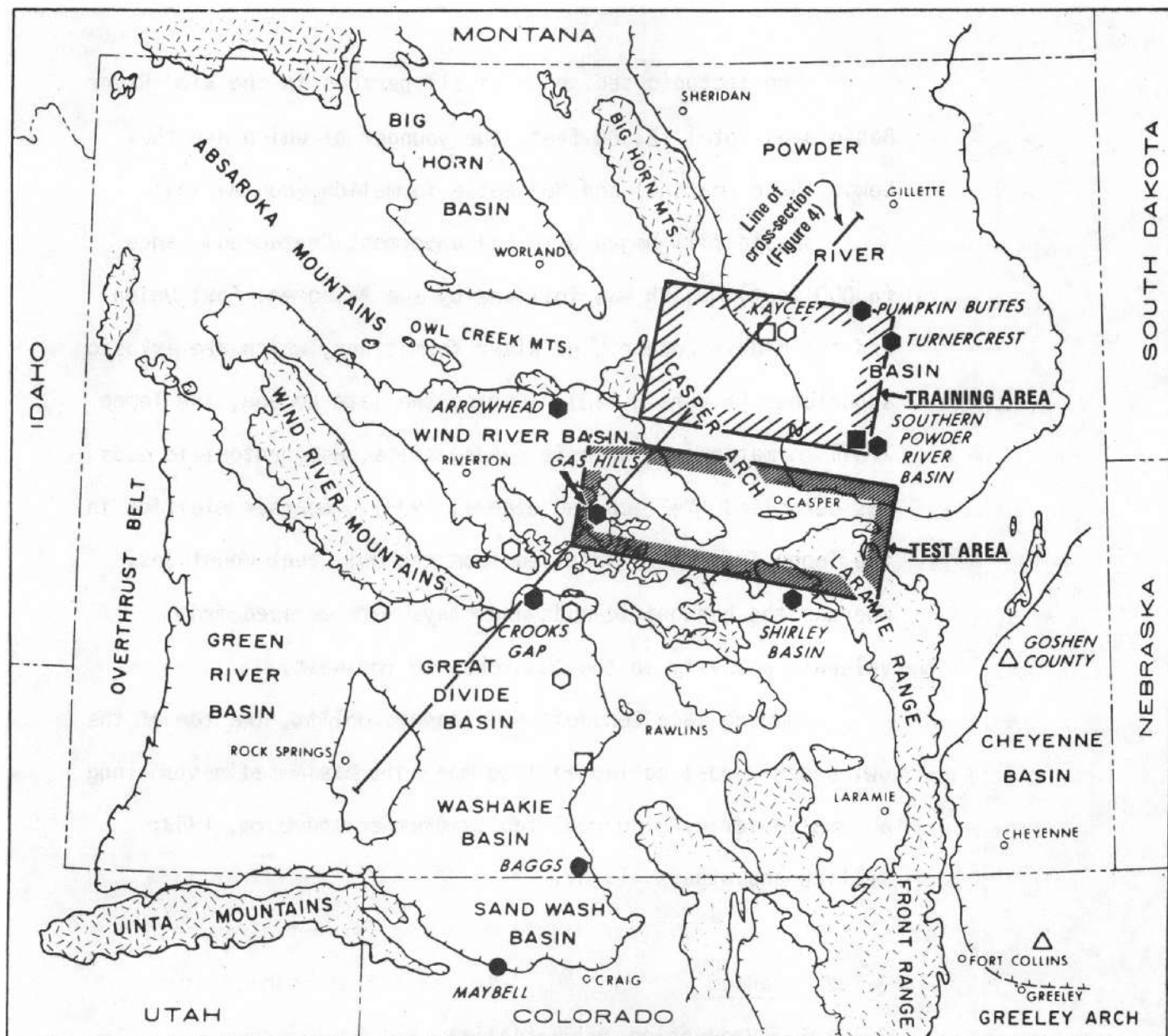
activities had affected almost all the potentially uranium-bearing ground. The Marysvale area therefore replaced Lake City as the training area for this kind of deposit, and Pumpkin Buttes replaced Gas Hills for the roll-front type. It was also apparent that the Rossing area was in the very early stages of exploration, and that a statistically significant number of pegmatite deposits was not yet known in the area.

3.1 Copper Mountain



3.1.1 Geology

The Copper Mountain area lies on the north flank of the Wind River Basin, along the toe of the Owl Creek thrust (Figure 3.1.1 and Figure 3.1.3). North of this major thrust, which has approximately 36,000 feet of throw (Keefer and Love, 1963), granitic and metamorphic rocks crop out topographically higher in the Owl Creek Mountains than in the Wind River Basin (Figure 3.1.4). These granites are 2.65 b.y. old (Nkomo and others, 1978), and were intruded at a relatively low temperature into older metasediments. They carry slightly anomalous uranium values of about 15 ppm.

Development of the Wind River Basin began in latest Cretaceous time (Laramide orogeny), and reached a climax in early Eocene time with initiation of the Owl Creek thrust. Epeirogenic uplift in late Cenozoic times (Keefer and Love, 1963) lifted the basin floor to its present elevation. The basin is asymmetric, with its deepest part close to the Owl Creek thrust (Keefer and Love, 1963).



— LEGEND —

-  BASIN OUTLINE
-  PRECAMBRIAN ROCKS EXPOSED

SIGNIFICANT URANIUM OCCURRENCES





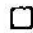

-  MIOCENE HOST
-  EOCENE HOST
-  EOCENE HOST (NO DEVELOPMENT)
-  PALEOCENE HOST
-  PALEOCENE HOST (NO DEVELOPMENT)
-  UPPER CRETACEOUS HOST (NO DEVELOPMENT)

Fig. 3.1.1 Index map of Wyoming and northern Colorado showing uranium occurrences, basins, and Precambrian exposures, with training and test areas for this project indicated also.

(After M.O. Childers, 1974)

Pre-tectonic sediments of all periods in the Wind River Basin area total 12,500 feet, the younger of which are the Lewis shale (marine) and Meeteetse formation (non-marine).

Basin fill began with the uppermost Cretaceous Lance (6,000 feet), which was followed by the Paleocene Fort Union and the middle Eocene Wind River formations, which are arkosic sandstones (Figure 3.1.2). During the late Eocene, the Tepee Trail formation, of arkosic sands, silts, and bentonitic muds was deposited (Yellich and others, 1978). Coarser clastics in the Tepee Trail were supplied from the Owl Creek Mountains, whereas the bentonitic muds and clays were derived from volcanic activity in the Absarokas to the west.

During late Cenozoic epeirogenic uplift, the toe of the Owl Creek thrust collapsed into the soft basin sediments along a complex series of normal faults (Keefer and Love, 1963; Yellich and others, 1978).

3.1.2 Uranium

3.1.2.1 Production and Potential

Shallow uranium occurrences, in both the Tepee Trail formation and Precambrian rocks, have been known along the collapsed toe of the Owl Creek thrust since the early 1950's. Production began in 1955, at the Little Mo-Arrowhead Mine, and totals about 500,000 lbs. of U_3O_8 . Other mines and prospects in the area are the Bonanza, Day Berger, De Pass, and Last Hope. The North Canning deposit is at present being evaluated.

	SYSTEM	FORMATION	CHARACTER
TERTIARY	PLIOCENE	North Park Formation	Tuff, Sandstone, Bentonitic claystone
	MIOCENE	Browns Park Formation	Tuffaceous sandstone, Conglomerate, Marl
	OLIGOCENE	White River Formation	Tuffaceous claystone, Arkosic conglomerate
	EOCENE	Green River Formation	Shale, Marlstone, Sandstone
		Wasatch Formation	Sandstone, Shale, Claystone
		Wind River Formation	Sandstone, Shale, Conglomerate
PALEOCENE	Fort Union Formation	Sandstone, Shale, Coals	
CRETACEOUS	UPPER	Lance Formation	Sandstone, Shale, Coals,
		Lewis Formation	Gray shale, Lenticular sandstone beds
		Mesaverde Formation	Sandstone, Shale, Coals
		Cody Shale	Gray shale, Lenticular sandstone
		Frontier Formation	Shale, Sandstone
		Mowry Shale	Shale, Some bentonite beds
	LOWER	Thermopolis Shale	Black shale, Some sandstone
		Cloverly Formation	Sandstone, Conglomerate, Bentonitic claystone
JURASSIC	UPPER	Morrison Formation	Siliceous claystone, Silty sandstone
		Sundance Formation	Glauconitic sandstone, Shale
	MIDDLE	Gypsum Springs Formation	Siltstone, Gypsum, Anhydrite
	LOWER	Nugget Sandstone	Massive bedded sandstone
TRIASSIC	Chugwater Formation	Red shale, Siltstone, Gypsum beds	
	Dinwoody Formation	Dolomitic siltstone, Shale, Sandstone	
PERMIAN	Phosphoria Formation	Phosphatic dolomite, Mudstones	
PENNSYLVANIAN	Tensleep Formation	Sandstone, Limestone, Chert	
	Amsden Formation	Shale, Limestone, Some Sandstone	
MISSISSIPPIAN	Madison Limestone	Massive bedded limestone	
DEVONIAN	Darby Formation	Dolomite, Shales	
SILURIAN	(Missing)		
ORDOVICIAN	Bighorn Dolomite	Massive dolomite	
CAMBRIAN	Gallatin Limestone	Shaley limestone, Limestone	
	Gros Ventre Formation	Fissile shale, Some limestone	
	Flathead Quartzite	Conglomeratic sandstone	
PRE-CAMBRIAN		Granite - Shist	

Fig. 3.1.2. A generalized stratigraphic chart of Wyoming.

Interest in, and exploration activity at, the Copper Mountain area remains high, and it appears that there may be other regions along the toes of Wyoming thrust faults favorable for this type of deposit.

3.1.2.2 Ore Genesis

Ore is found in the Tepee Trail formation associated with hematitic alteration "halos," abundant carbon trash and, in the Little Mo area, with asphaltic material.

Ore is also found at Copper Mountain in conglomerates and coarse-grained arkoses immediately overlying the granite surface and, at Day Berger, within bentonitic claystones and freshwater limestone.

At the Last Hope prospect, detailed underground mapping indicated association of uranium with fractures in the Precambrian mafic rocks and with asphalt (Yellich and others, 1978).

The North Canning deposit also lies within the upper thrust plate, in fractured and altered granite and metamorphic rocks along the high-angle normal North Canning fault, which was formed by collapse of the toe of the Owl Creek thrust. Uranium is not confined to the Precambrian rocks, but also occurs in overlying conglomerates, sandstones, and siltstones of the Tepee Trail formation, as sooty pitchblende, uraninite, and coffinite. Uranium appears to occur at permeability changes (Yellich and others, 1978), and particularly along the crush zone of the North Canning fault. It also appears to

EAST OWL CREEK MOUNTAINS GEOLOGIC MAP

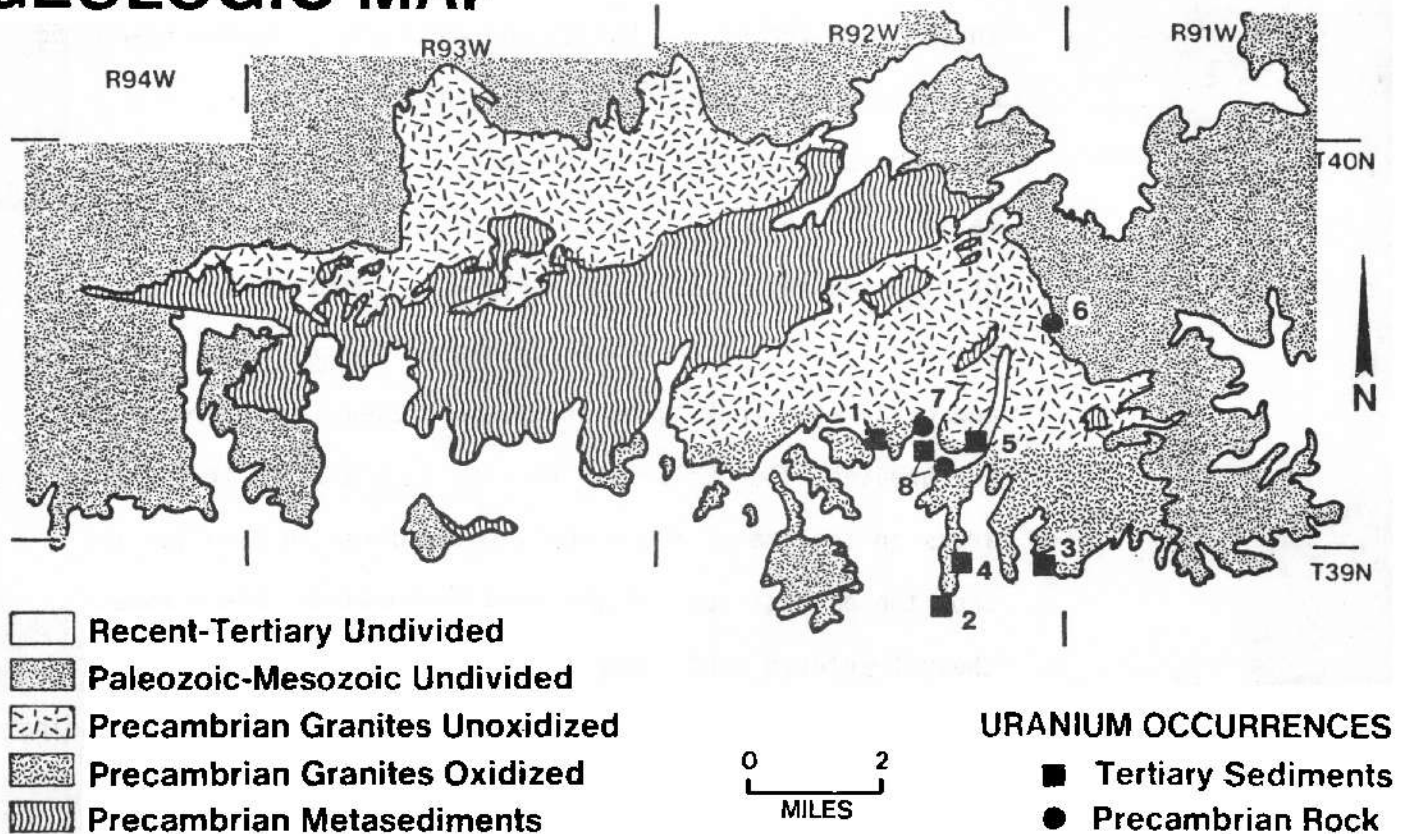


Figure 3.1.3 East Owl Creek Mountains geologic map with index of uranium occurrences. 1) Arrowhead Mine, 2) Bonanza Mine, 3) Schroeckingerite, 4) Day-Berger Prospect, 5) Hesitation Prospect, 6) De Pass Mine, 7) Last Hope Project Drift, 8) North Canning Deposit. (After Yellich, Cramer, and Kendall, 1978)

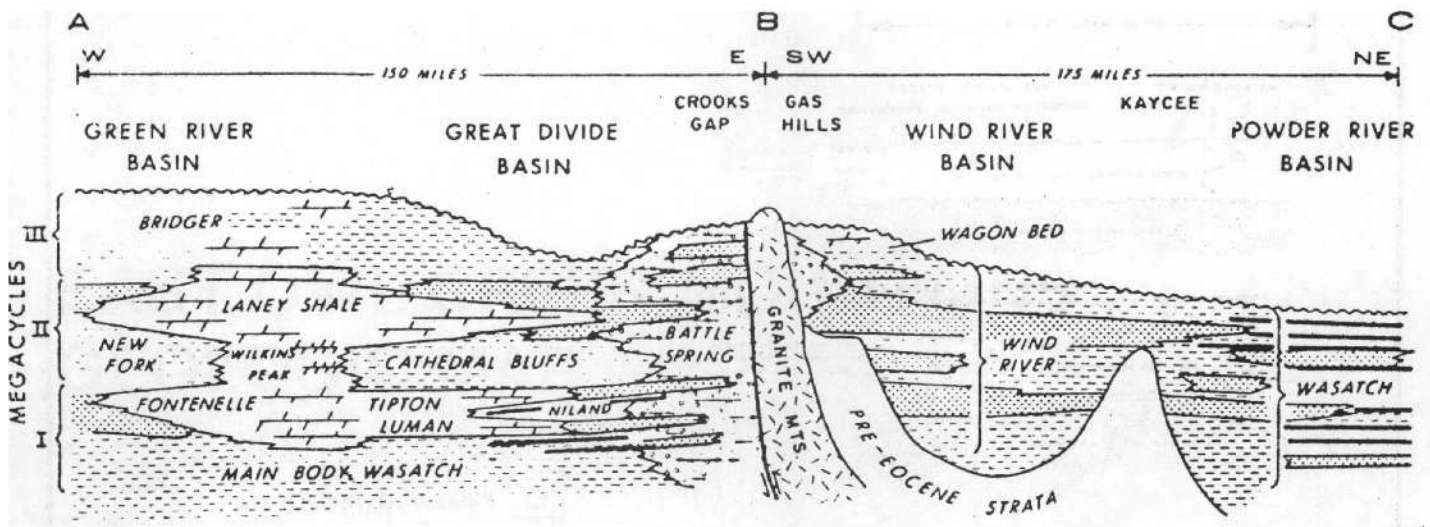
have been precipitated in contact with mafic metamorphic rocks, particularly chloritized rock, containing calcium carbonate and pyrite.

Geologists working in the area (Yellich and others, 1978) propose a genetic model in which warm, highly corrosive basinal brines containing hydrocarbons traveled upwards through the toe of the thrust and encountered downwards-moving meteoric waters which contained uranium leached from the Precambrian rocks and from the bentonitic Tepee Trail formation (Figure 3.1.5). Uranium was precipitated where the uranium-bearing oxidized meteoric waters met reducing environments which were caused either by the presence of pyritic and calcareous rock types or by the presence of hydrocarbons. The greatest fluid flow was through tectonically fractured areas in the toe of the thrust, which directly overlies and caps the deepest part of the Wind River Basin. Therefore, these fractured rocks were most altered by the ascending solutions and uranium was deposited in them from the descending solutions in economic quantities.

There is disagreement with this hypothesis, but it is the only one well worked out. Inferences for Landsat exploration must therefore be based upon it.

3.1.3 Ore Guides Which May Be Detectable By Geometric Pattern Recognition Techniques Applied to Landsat

At Copper Mountain, ore is associated with intense fracturing along secondary faults at the toe of the thrust.



—LEGEND—



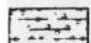
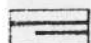
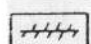
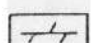
-  Large stream facies (carbonaceous sandstones, shales, siltstones: reducing)
-  Small stream and mudflat facies (Mainly banded mudstones: oxidizing in part)
-  Piedmont facies (unsorted conglomerates sandstones, mudstones)
-  Swamp facies (coals, carbonaceous shales)
-  Locustrine evaporite facies (includes trona)
-  Locustrine facies (carbonate rocks and shale)

Fig. 3.1.4 Restored diagrammatic cross-section showing Eocene facies across Wyoming. Location shown on Figure 1. (After M.O.Childers, 1974)

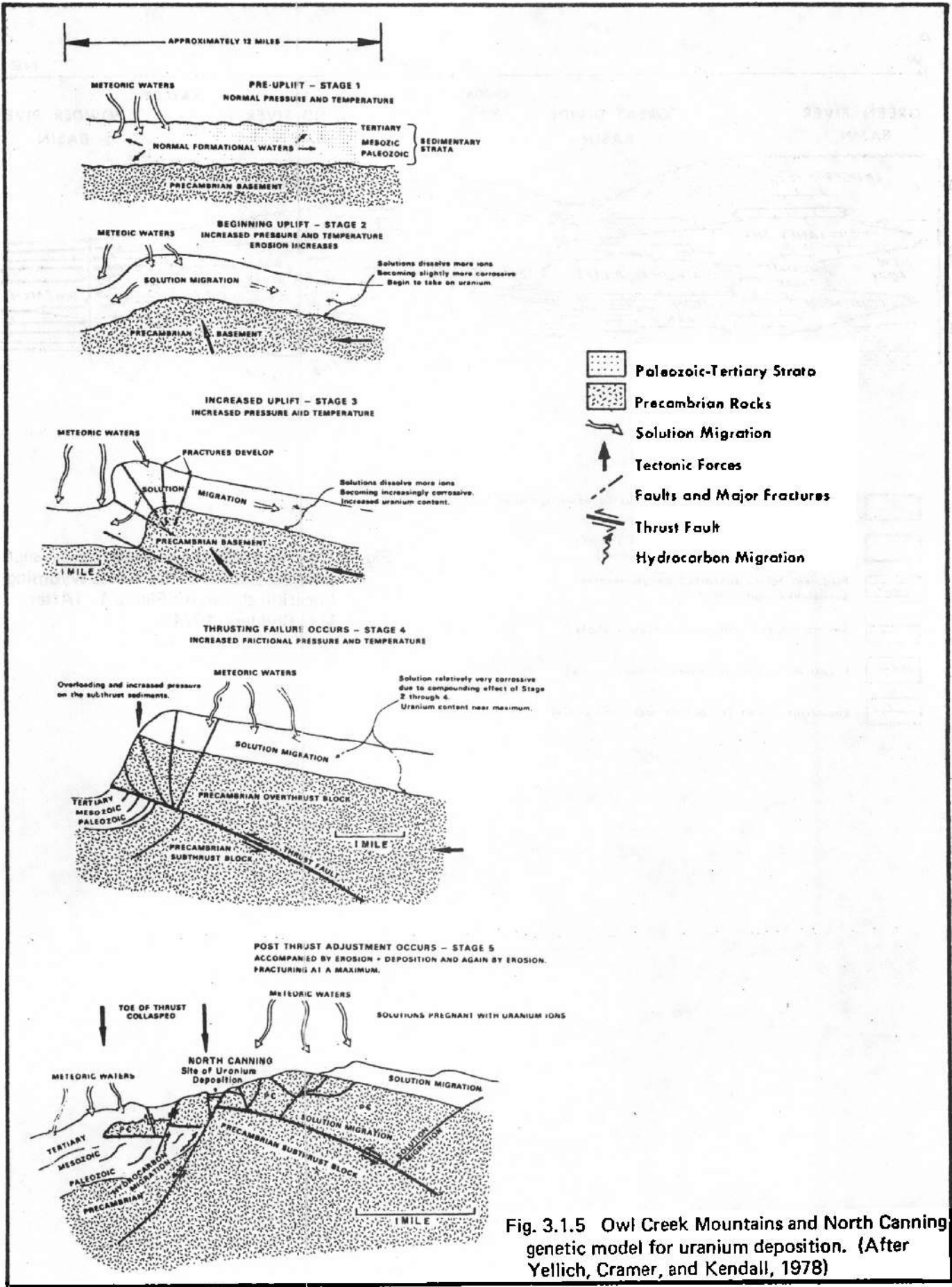


Fig. 3.1.5 Owl Creek Mountains and North Canning genetic model for uranium deposition. (After Yellich, Cramer, and Kendall, 1978)

This should be detectable as very fine texture with the texture measures, and as an area generally lacking in strong lineaments (because of the relatively coarse resolution of Landsat) by the lineament mapping technique.

The toe of the thrust itself should be recognizable as both a lineament (or set of lineaments) and as a major textural change between igneous and metamorphic rocks to the north and sediments to the south.

Known uranium occurrences at Copper Mountain are also associated with granite of hypidiomorphic-granular texture which occurs along the southern and southeastern margins of the Owl Creek Mountains (Nkomo and others, 1978) as opposed to xenomorphic-granular to cataclastic textures which occur elsewhere in the range. The former granite weathers to rounded iron-stained surfaces, whereas the latter type weathers to more angular, less iron-stained surfaces. It might be expected that the interplay of a different surface texture and spectral reflectances values would give rise to distinctive values of the Landsat texture measures, and thus lead to identification of areas of "favorable" granite.

3.2 Pumpkin Buttes

3.2.1 Geology

The Pumpkin Buttes uranium area is on the west flank of the Powder River Basin, a topographic and structural basin in northeastern Wyoming (see Figure 3.1.1).

The Basin is flanked on the west by the Bighorn Mountains, on the south by the Laramie Range, and on the northeast by the Black Hills. Structural relief between the Basin and its flanks is 24,165 feet, as measured on the top of the Precambrian over 115 miles on a northwest-southeast line through Pumpkin Buttes. The Powder River Basin is a Laramide structure, and near Pumpkin Buttes is filled with approximately 6,000 feet of Oligocene, Eocene, and Paleocene rocks and 7,000 feet of Cretaceous rocks, overlying 3,100 feet of older Mesozoic and Paleozoic sediments (Figure 3.1.6).

The Eocene sediments were principally derived from a source to the southeast, perhaps the paleo-Wind River. Cretaceous rocks in the Powder River Basin are marine, whereas the Paleocene (Fort Union formation) and Eocene (Wasatch formation) are fluvial floodplain and channel deposits (see stratigraphic column, Figure 3.1.2), which include coal beds and are generally reduced.

During Oligocene time, uplift terminated the influence of the major northward-flowing stream and the basin was buried beneath sediments (White River formation) derived from the Bighorn Mountains and from volcanic centers to the west.

The uranium at Pumpkin Buttes is contained in lenticular sandstone units, scattered through the otherwise fine-grained Wasatch formation (Sharp and others, 1964). The sands range from a few feet to 100 feet thick, and on an average are from 20-30 feet thick. They are elongated shoestrings filling channels cut in claystone and siltstone, and range from 100

feet wide to, most often, 4-5 miles wide and 6-8 miles long. Channels often bottom on carbonaceous or coaly beds and their central parts have the greatest porosity. The sandstones are cross-bedded, with sets 1-2 feet thick, and contorted bedding occurs locally in association with "trash piles" - pockets of sand, mudstone fragments, and carbonaceous debris. A few mudstone lenses, and mud-flake conglomerates, occur in basal pockets of the sandstones, which are generally clean.

Calcareous concretions of various shapes and sizes occur in the sandstone. Pyrite occurs in association with wood fragments in drab unweathered sandstone, and patches of silicification are known.

In the Pumpkin Buttes area, a lense-shaped region of these drab Wasatch sandstones has been oxidized or hydrated (Sharp and others, 1964) to red, to a depth below land level of at least 500 feet. This zone occurs over the intersection of two folds (Sharp and others, 1964) that were active in the Tertiary and may have influenced groundwater regimes. The oxidation-reduction front is very sharp, but in some areas thin lenses of reduced sandstone have been left behind by it.

3.2.2 Uranium Deposits

3.2.2.1 Production and Potential

About 250 uranium occurrences, containing up to 5,000 tons of ore at 0.3% U_3O_8 are known within an area of 350 square miles centered on Pumpkin Buttes. This area has not

been extensively mined, hence ground surface disturbance is minimal, which is the reason this area was chosen for training rather than Gas Hills or Shirley Basin. At Gas Hills and Shirley Basin, open pits and spoil heaps cover a large portion of the area of interest, precluding the use of the technique. At the currently high price of uranium, the potential of the Pumpkin Buttes area might be quite great, especially where the uranium lies at shallow depths (Sharp and others, 1964) around the fringes of the down-dip extension of the oxidized zone.

3.2.2.2 Ore Genesis

The deposits are associated with irregularly distributed calcite, manganese oxide, or hematitic zones in the sandstones, and are thus themselves irregular in shape and distribution.

All deposits occur within a stratigraphic interval of 500-1,000 feet below the top of the Wasatch formation.

Three modes of occurrence are present; and may be combined in an individual deposit:

- a) Oxidized uranium minerals disseminated in sandstone and distributed around calcite enriched sandstone, and along redox fronts in the sandstones.
- b) Oxidized uranium in or around manganese oxide nodular concretions.
- c) Nodular concretions of uraninite with pyrite.

3.2.2.2.1 Disseminated Oxidized Uranium Minerals

Yellow to greenish-yellow uranium minerals occur in drab sandstones along color contacts with red sandstones, and around calcite concretions which themselves preferentially occur on the redox interface (Figure 3.2.3). Thin tongues of drab sandstones surrounded by red sandstone, or along the basal contact with shale, are especially favorable places. The best deposits of this type occur around the periphery of the major tongue of red sandstone noted above.

3.2.2.2.2 Uranium With Manganese Oxides

These concretions are zoned, with the uranium enclosed in an outer shell of barren manganese oxide. Many manganese oxide nodules appear to be localized by patches of woody or coaly material. Although these concretionary areas may be 10-20 feet across, they are of little economic importance since they are found within the red, barren sandstones.

3.2.2.2.3 Uraninite Concretions

These appear much like the manganese oxide concretions in habit. They have a core of pyrite or, occasionally, woody material. Most of these concretions have been found relatively near the ground surface and thus have rich weathering halos of oxidized uranium minerals around them. They are small (up to one foot long) and, therefore are economically unimportant except where found in association with roll-front (Type (a) of 3.2.2.2) deposits.

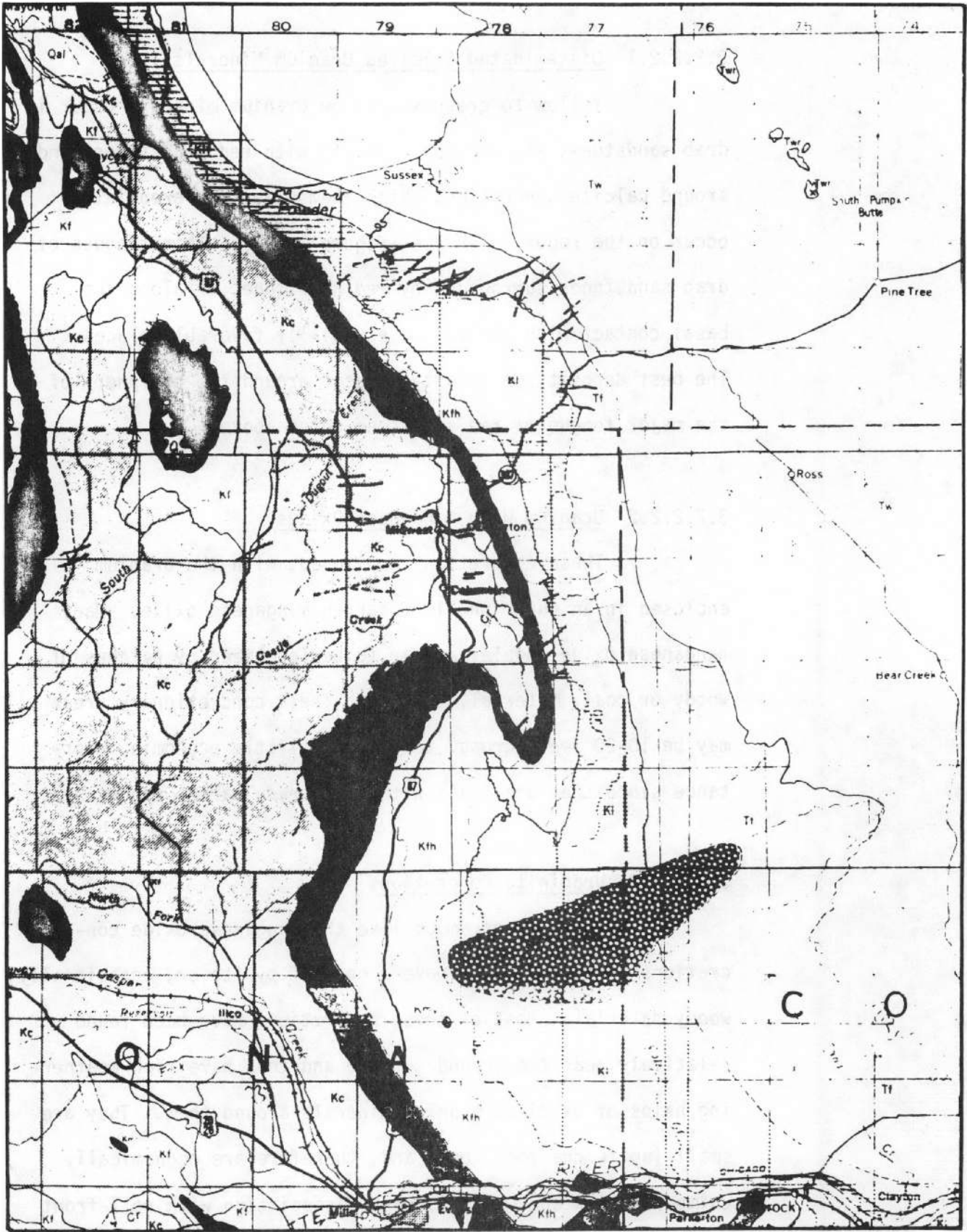


Figure 3.1.6.a. A portion of the geological map, Wyoming. Scale is approximately 1:250,000.

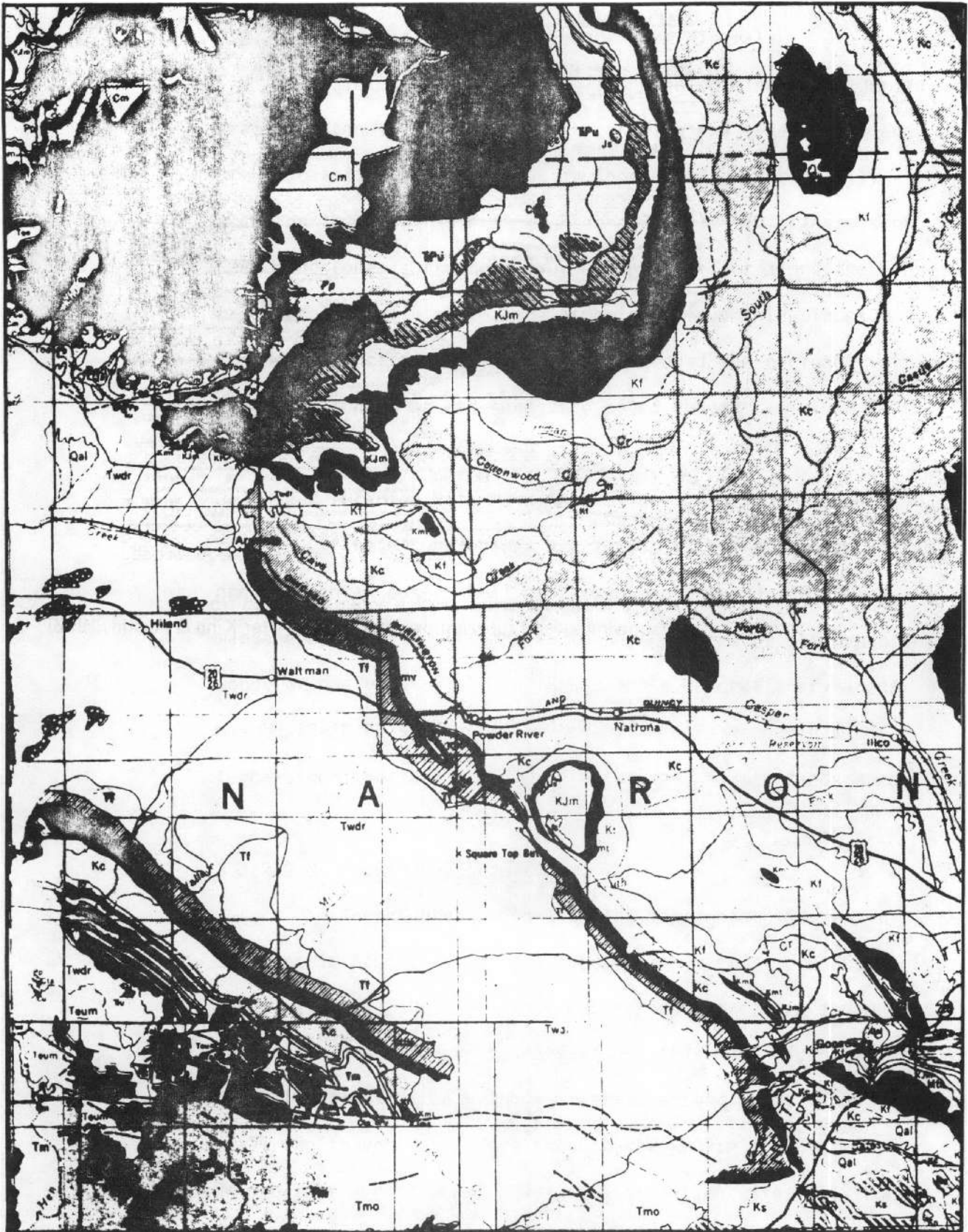


Figure 3.1.6.b. portion of the geological map, Wyoming.
Scale is approximately 1:250,000.

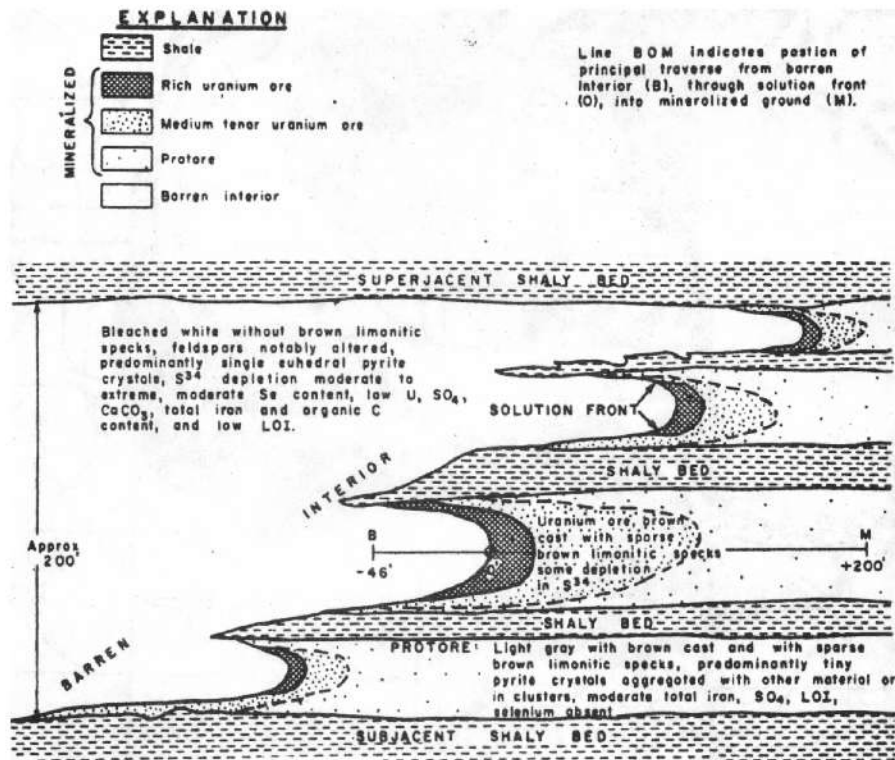


Fig. 3.2.1 Idealized vertical section across a solution front, showing several superimposed ore veins. (After King & Austin, 1966)

3.2.3 Ore Guides Which May Be Detectable by Geometric Pattern Recognition Techniques Applied to Landsat

Since no faults or fractures are known to be genetically associated with uranium ore at Pumpkin Buttes, or with Wyoming uranium ore rolls, generally exploration for uranium using this technique must be indirect.

The following features hold promise:

- a) Detection of channel sandstones. The outlines of channel sandstones have been shown to be reflected through several hundred feet of overlying sediment, due to differential compaction of the shales surrounding them. Such differential compaction may show up as double lineaments on the enhanced display operator outputs.
- b) Detection of oxidized/altered ground. Uranium in the Pumpkin Buttes area is associated with a tongue of red oxidized sandstone, which is in turn associated with sporadic calcareous cement. If this sporadic cementation is reflected in a distinctive erosional texture of any kind, it should be shown by the texture output.
- c) Detection of folds controlling location of oxidized tongues. The location of the oxidized tongue at Pumpkin Buttes appears to be controlled by the intersection of north and east trending anticlines (Sharp and others, 1964). Folds in sedimentary rocks should be detected as curving sets of parallel lineaments in the enhanced display operator outputs.

3.3 Gas Hills

3.3.1 Geology

The general stratigraphic section at Gas Hills is very similar to that of the Pumpkin Buttes and Copper Mountain areas (Sections 3.1 and 3.2). However, Gas Hills lies on the south side of the Wind River Basin (Figure 3.1.1), and the ore-bearing arkosic sandstones of the Wind River (Eocene) formation were here laid down by northward-flowing braided tributaries of the paleo-Wind River. The sediments were derived from the Granite Mountains (Zeller, 1957), then an imposing range, but now merely remnants isolated from each other by erosion and Tertiary tectonic movements.

The ore-bearing sandstones are overlain by tuffaceous sandstones of the Eocene Wagon Bed and Oligocene White River formation (Armstrong, 1970). The uranium is thought to have been derived from the tuffaceous component of these strata. East-trending normal faults are common in the area, and large ones along the Beaver Rim show movement down to the south (Zeller, 1957).

3.3.2 Uranium

3.3.2.1 Production and Potential

Mining began in the district in 1954; and by the end of 1976 72.5 million pounds of U_3O_8 had been produced. The area is still a major producer and was perhaps the area where the "roll-front" concept was first developed (Riddell, 1958; quoted by Snow, 1978, p. 332).

3.3.2.2 Ore Genesis

The Gas Hills deposits are the classical "roll-front" uranium deposits. They form where oxidized groundwater carrying dissolved uranium (probably in the range 20-100 ppb) (Granger and Warren, 1978) encounters reduced rock, and precipitates some of its uranium along a narrow front by means of a complex series of oxidation-reduction reactions. Since a critical ingredient in the formation of an ore-roll is an ample supply of groundwater, they are usually found in the more permeable rock-types present, often medium- to coarse-grain channel sandstones which are confined between shales and siltstones. Since groundwater flows more rapidly in the center of the aquifer, the ore-rolls are U-shaped, convex down the direction of groundwater flow (Figure 3.2.1), and towards the sides of the channel.

In the United States, the source of the uranium in the rolls is usually an overlying Tertiary tuff or tuffaceous rock units: acid tuffs are enriched in uranium relative to most other rocks, and release it rapidly upon weathering. Ore rolls are usually found in semi-arid climates where surface streams tend to lose water to the ground, thus providing a ready supply of leach water and a groundwater table at sufficient depths to preserve the ore bodies from weathering.

The Gas Hills satisfy all of these criteria: surface and subsurface drainage is to the north, and the deposits are convex to the north and towards the edges of each

of three large north-trending channel systems. Ample supply of groundwater is provided by headwaters of the White River system which traverses the area.

3.3.3 Ore Guides Which May Be Detectable by Geometric Pattern Recognition Applied to Landsat Imagery

Many faults are present in the area, and those with as little as 10 ft. of throw can often be recognized as lineaments up to a mile long on aerial photographs (Zeller, 1957); however, surface resistivity measurements are even more useful where faults are concealed beneath alluvium (Stahl, 1974). Faults such as those described by Zeller (1957) should be visible on the display operators as linear features. Since the resistivity method depends on varying groundwater chemistry, which is often reflected by subtle differences in surface vegetation, those faults outlined by Stahl (1974) may also be visible on the Landsat display operators. We have found in practice that Eigenband and ratio images are better for displaying groundwater-related phenomena than are any of the standard Landsat imagery.

Some of these faults may have acted as barriers (Zeller, 1957) controlling groundwater movement, and thus have influenced ore deposition, but the vast majority are of little significance to ore-genesis.

It was hoped that differential compaction over the margins of major channel systems would cause fracturing and

jointing sufficient to be detected by the display operators as lineaments and by the texture measures as areas of distinct textures. We have been able to observe such differential compaction features on Landsat, using a conventional photointerpretative approach, in areas of stacked barrier beach deposits of the Powder River Basin of Wyoming.

It was also thought possible that areas of altered (oxidized ground) would show different erosional textures which might be detectable by the techniques employed. However, it seems that these techniques are of too coarse a resolution and are not able to detect such subtle and localized features (see Section 5).

3.4 Grants Mineral Belt

3.4.1 Geology

The Grants Mineral Belt (Figures 3.4.1 and 3.4.2) stretches 95 miles from southeast of Laguna to Gallup, New Mexico, and has been mined and explored intensively since 1951. The mineral belt comprises four districts (from east to west), Laguna, Ambrosia Lake, Smith Lake, and Church Rock (Fitch, 1971), and has produced ore from the Todilto limestone (Jurassic), and the Westwater Canyon and Brushy Basin members of the Morrison formation (see stratigraphic column, Figure 3.4.3), in the upper Jurassic San Rafael group.

The mineral belt lies on the north flank of the Zuni uplift, with regional dip into the San Juan Basin to the

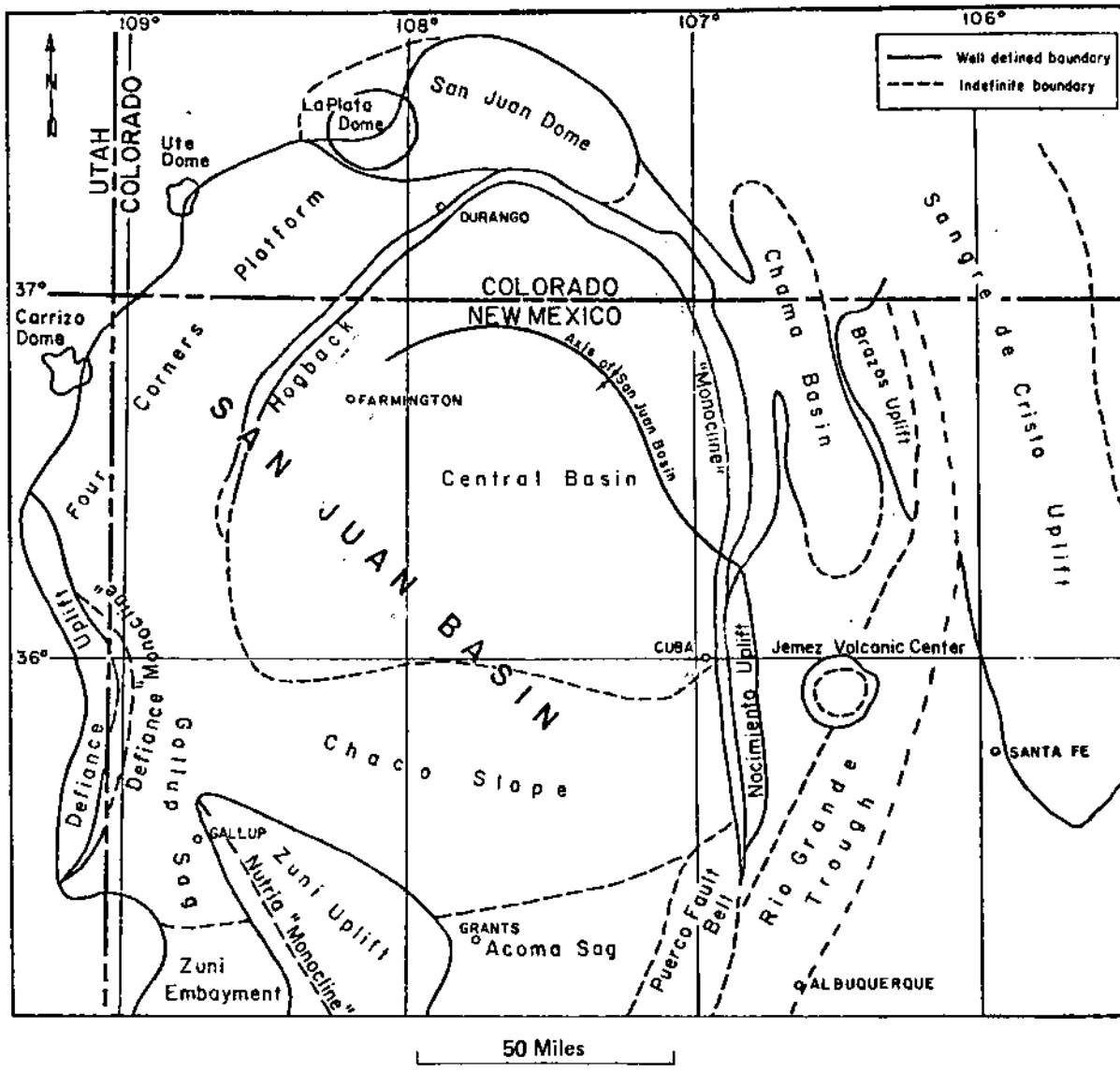


Fig. 3.4.1 Grants Region in relation to major tectonic elements of the San Juan Basin.

(Modified from Vizcaino and O'Neill, 1977)

northeast. It is bounded by the Rio Grande trough or rift on the east, and the Gallup sag on the west (Kelley, 1963). Intrusive and extrusive rocks of the Mt. Taylor and Zuni volcanic fields intrude and overlie parts of the eastern end of the belt. The core of the Zuni uplift, south of the mineralized belt, is composed of metamorphosed Precambrian rock; whereas the mineral belt itself is underlain by sedimentary rocks of Permian to Cretaceous age (Hilpert and Moench, 1960).

The uranium-bearing rocks were deposited by braided streams flowing to the northwest and the northeast (Westwater Canyon member and "Jackpile sandstone"). Gentle tectonic movements took place in the late Jurassic-Cretaceous interval, resulting in pre-Dakota erosional pinch-out of the Morrison formation along a line 15-20 miles south of, and parallel to, the Grants Mineral Belt. Gentle warps with north-south axes formed during this episode, as well as prominent sandstone breccia pipes, which cut the Westwater Canyon and Brushy Basin members (Hilpert and Moench, 1960). The breccia pipes are occasionally mineralized, and may have been formed by dewatering of shales within the Morrison formation (Recapture member).

Subsequent tectonic activity included: pronounced Laramide (Cretaceous-Eocene) movements resulted in the formation of the Zuni uplift, the San Juan Basin, and much faulting. The formation of a regional arch, followed by development of a low-relief surface, took place in mid-Tertiary

times (Kelley, 1963). During Pliocene uplift, the Rio Grande Rift was formed and Mt. Taylor igneous activity was initiated (Kelley, 1963).

3.4.2 Uranium Deposits

3.4.2.1 Production and Potential

The Grants Mineral Belt has been, and continues to be, the most productive uranium district in the U.S. From 1951-1970, the Belt has produced 158 million lbs. of U_3O_8 . Early production was from the Todilto limestone, in the Ambrosia Lake district. This was quickly over-shadowed by Westwater Canyon member production from the Poison Canyon and Ambrosia Lake trends. Later, the Jackpile area in the Laguna district became dominant.

Exploration continues to be intense and new ore bodies are being discovered. The interest appears to be moving north, into the San Juan Basin. Many companies are using Landsat image interpretation to guide this exploration.

3.4.2.2 Ore Genesis

The deposits in the Grants Mineral Belt fall into two groups: those associated with the Todilto limestone and those in Morrison formation sandstones. The sandstone deposits are the more important of the two groups, having produced over 90% of the uranium ore from this region.

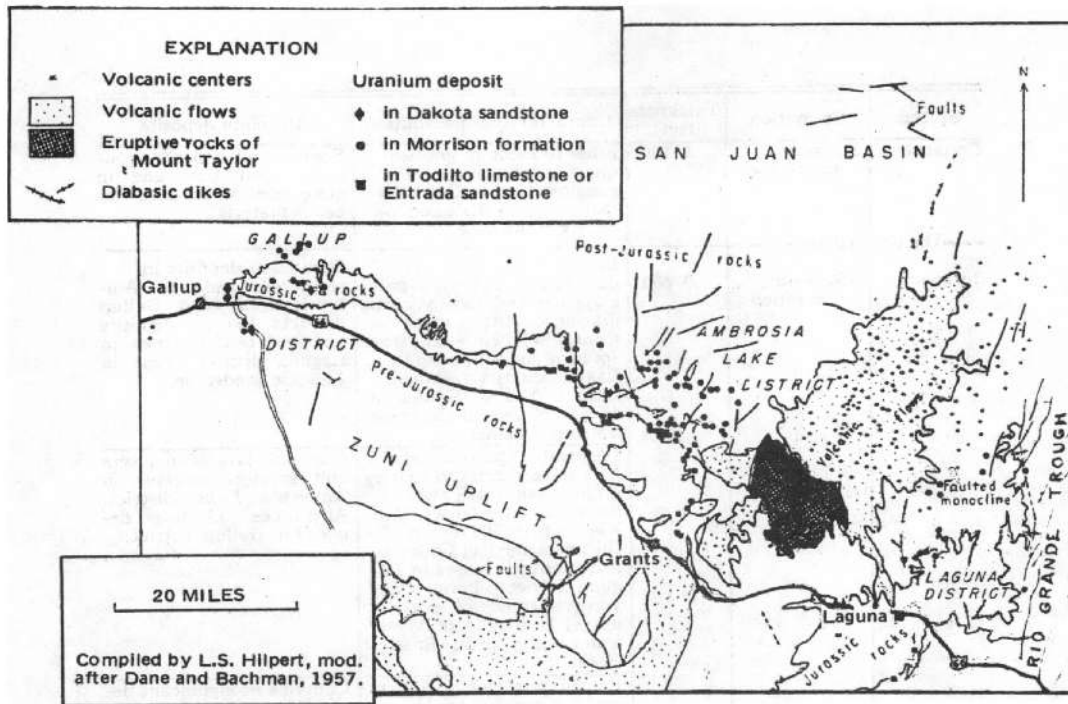


Fig. 3.4.2 Geologic map of the southern part of the San Juan Basin and vicinity, showing the uranium deposits.
(Modified from Hilpert and Moench, 1960)

System	Formation	Thickness (feet)	Character and distribution	Uranium deposits
Cretaceous	Dakota sandstone	5-100	Fine- to medium-grained quartz sandstone, locally conglomeratic. Generally carbonaceous shale and locally coal at base.	Some small deposits, generally near base and in close relation to carbonaceous material.
—Unconformity—				
Jurassic	Morrison formation	0-600	Brushy Basin member; dominantly a greenish-gray claystone and, locally, thick arkosic sandstone units. Contains Jackpile sandstone (of local usage) at top in Laguna district. Ranges from 0 feet at Gallup to about 500 feet in thickness north of Laguna.	Significant deposits in sandstone beds in Ambrosia Lake and Gallup districts. Largest deposits and greatest reserves in Laguna district occur in Jackpile sandstone.
			Westwater Canyon member; arkosic, fine- to coarse-grained sandstone and some claystone lenses. Ranges from 300 feet in thickness north of Gallup to discontinuous lenses in Laguna district. Poison Canyon sandstone (of local usage) is tongue of Westwater Canyon in Brushy Basin.	Contains largest deposits and greatest reserves in Ambrosia Lake district. Also moderately large deposits in Gallup district.
			Recapture member; fine- to medium-grained, friable sandstone and some silty claystone beds. Occurs in distinctive alternating light-gray and reddish-brown units 5-10 feet thick. From 20-170 feet thick; absent at least locally in Laguna district.	Contains no significant deposits.
	Bluff sandstone	175-330	Fine- to medium-grained quartz sandstone. Dominantly a thick-bedded unit with some relatively thin interbedded siltstone units near the base.	Contains no deposits.
	Summerville formation	100-220	Fine-grained sandstone beds, generally 1 to several feet thick, alternating with thinner beds of siltstone.	Contains a few small deposits, only where underlying Todilto limestone is mineralized.
Todilto limestone	0-85	Fetid dense gray laminated limestone; massive in upper part. Ranges from pinch-out near Gallup to maximum thickness in Laguna district. Includes an upper unit of anhydrite and gypsum in Laguna district that ranges from discontinuous masses at south to continuous unit to the north.	Contains small to fairly large deposits. Most are in Ambrosia Lake district. The anhydrite-gypsum member is barren.	
Entrada sandstone	150-250	Reddish-orange fine-grained quartz sandstone; lighter colored at top. Generally thins eastward. In Laguna district two distinct units—a lower reddish-orange unit and an upper white unit.	Contains a few small deposits in Laguna and Ambrosia Lake districts—all at top of formation.	

Fig. 3.4.3 Sequence of formational units containing uranium deposits along the southern part of the San Juan Basin, New Mexico. (Modified from Hilpert and Moench, 1960)

3.4.2.2.1 Limestone Deposits

The Todilto limestone is thin (0-160 feet), of wide areal extent, and is divided into a lower limestone and an upper gypsum member of more restricted areal extent (Hilpert and Moench, 1960). Uranium occurs in the lowermost 40 feet of the limestone. This interval is fetid, fine-grained, gray and thin-bedded and is subdivided into three units (from the base): platy, crinkly, and thick-bedded limestone. Uranium is usually associated with the platy limestone in which the fine bedding is undisturbed. The crinkly limestone appears to have enterolithic folds, perhaps after gypsum. The thick-bedded limestone is recrystallized and brecciated (Hilpert and Moench, 1960).

All uranium deposits in the Todilto are associated with intraformational folds (re-interpreted by Perry, 1963 (in Kelley, 1963) as reefs). Uranium mineralization occasionally extends down into the Entrada formation and up into the Summerville formation, both of which are conformable with the Todilto formation. In both these cases, such mineralization is thought to be secondary and remobilized.

Uranium in the Todilto is associated with fluorite, galena, and barite (Granger, 1968). This fact, combined with the occurrence of fluorite veins in the Zuni uplift to the south, has caused many to suggest hydrothermal activity.

3.4.2.2.2 Sandstone Deposits

Sandstone ore bodies occur in the Westwater Canyon and Brushy Basin members of the Morrison formation (Figure 4).

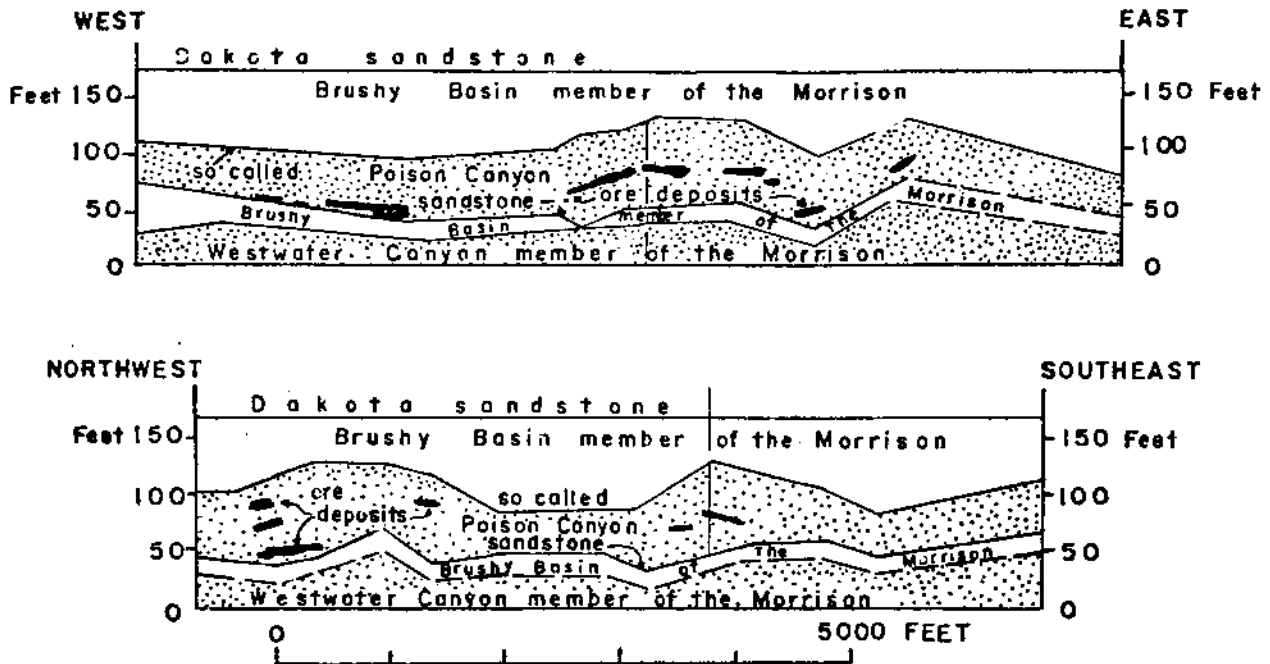


Fig. 3.4.4a Generalized geologic sections showing the stratigraphic relations of the Morrison uranium deposits northwest of Grants, New Mexico.

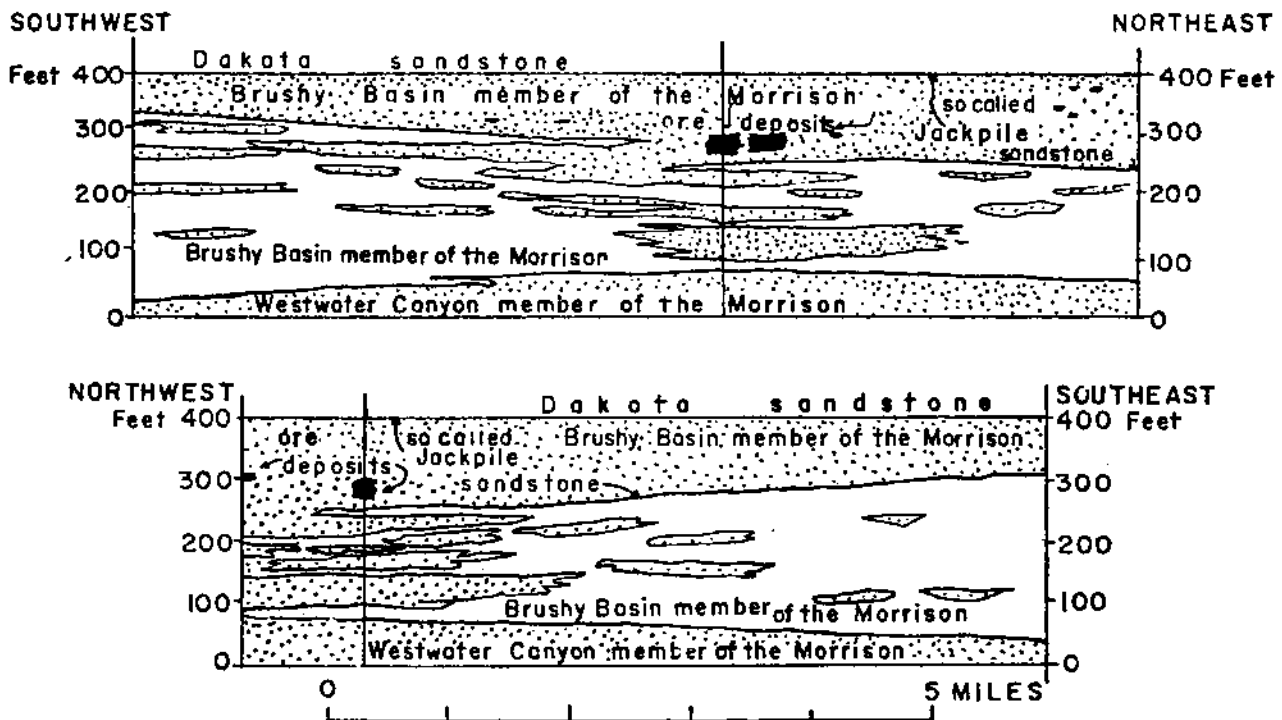


Fig. 3.4.4.b Generalized geologic sections showing the stratigraphic relations of the Morrison uranium deposits north of Laguna, New Mexico.

Some authors, however, place all upper Morrison sandstones in the Westwater Canyon, and all shales and siltstones in the Brushy Basin (e.g. Santos, 1963) since the two members inter-finger extensively. In the Laguna district, the Jackpile sandstone, a 15 mile wide, 35 mile long channel sand at the very top of the Morrison, carries rich ore bodies.

The primary, or "trend" ore, is intimately associated with a black organic residue which impregnates the sandstones, and has been determined as a humic acid derivative. Carbonized logs and other plant remains are also occasionally mineralized. The ore also tends to be concentrated around clay galls and in thin lenses or fingers of sandstone which are surrounded by mudstone. However, ore is also reported (e.g. Hilpert and Moench, 1960, and Reinhardt, 1952) to be associated with thickening of sandstone lenses.

In the Ambrosia Lake district the ore steps up through the Westwater Canyon to the north. Since the Westwater Canyon dips north, this suggests an association with an old water table. The primary ore occurs in thin, irregular lenses of fairly wide areal extent. It is elongated and aligned parallel to the outcrop, and generally concordant, but cross-cuts the bedding in detail.

Secondary or "stack" ore occurs as irregular and superimposed lenses which are related to subsidiary faults or fractures but not related to the major faults of the area.

3.4.3 Ore Guides Which May Be Detectable by Geometric Pattern Recognition Techniques Applied to Landsat

The main ore trends of the Grants Mineral Belt are associated with channel sandstones such as the "Jackpile" and those of the Poison Canyon and Ambrosia Lake trends. Thus, as at Pumpkin Buttes, textures or lineament sets due to differential compaction fracturing over the fringes of the sand bodies are of interest. Isolated areas of texture that is elsewhere associated with sandstone may be of assistance in locating isolated sandstone tongues included in predominantly shale sections. This may be useful in that uranium orebodies tend to be concentrated near the margins of sandstone bodies.

"Stack" ore bodies are associated with subsidiary faults and fault intersections. Thus, it may be expected that the edge or lineament displays may pinpoint favorable places for "stack" ore.

Alteration is present in the Grants Belt, but is pervasive and subtle; its detection is therefore not likely to aid greatly in prospecting for ore.

3.5 San Rafael Swell Area

3.5.1 Geology

The San Rafael Swell is a large, broad anticlinal structure, very well shown on Landsat imagery, in eastern Utah. The stratigraphy of the area is shown on Figure 3.5.1: the outer rim of the structure is composed of resistant

aeolian and fluvial sandstone of the Glen Canyon Group (Triassic). The interior of the Swell is underlain by Permian and lower Triassic rocks. Outside the topographic rim, the Swell is flanked by Jurassic rocks, including the uranium-bearing Morrison formation.

Of the units shown on Figure 3.5.1, only the Moenkopi, Chinle, Kayenta, Curtis, and Morrison formations contain lithologies commonly considered favorable for Colorado Plateau-type uranium deposits. However, the Permian White Rim sandstone contains asphalt in one area, which may be favorable, whereas the Moenkopi, Kayenta (upper Triassic), and Curtis (Jurassic) formations are not known to contain any significant amounts of uranium. Discussion will therefore be confined to the Chinle and Morrison formations.

3.5.1.1 Chinle Formation

The lower part of Chinle formation contains bentonite, a possible primary source of uranium and hosts most of the known uranium occurrences in the San Rafael Swell area. The Shinarump member (Figure 3.5.1) is absent in the San Rafael Swell area. The Temple Mountain and Monitor Butte members are difficult to distinguish and the Petrified Forest member is absent. Therefore, the only members of the Chinle which are of interest for uranium in the Swell area are the sub-Moss Back (Mickle and others, 1977: combined Temple Mountain and Monitor Butte) and the Moss Back members.

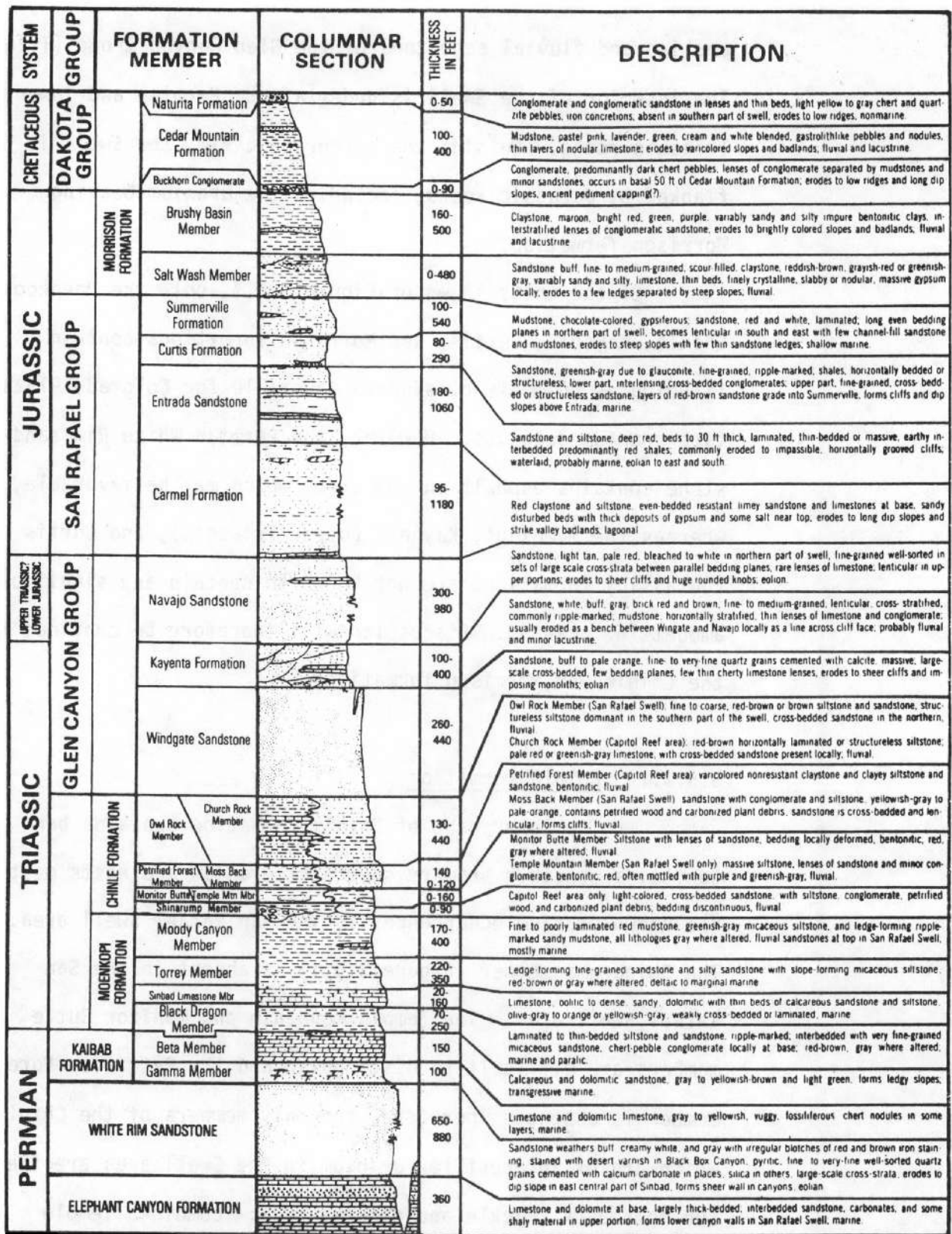


Figure 3.5.1. Generalized stratigraphic column, San Rafael Swell and Capitol Reef, Utah. (after Mickle, et al, 1977)

Sub-Moss Back Member

This unit ranges from 0-160 feet in thickness, but is usually less than 30 feet. It consists of thick-bedded mottled siltstone with sandstone to conglomeratic lenses (Temple Mountain lithology), interbedded with well sorted fine-grained feldspathic sandstone, rippled sandstone, and bedded siltstone (Monitor Butte lithology). The siltstones are varicolored but dominantly red, and some of the mottling appears to be due to highly weathered carbonaceous material. Siltstones of this unit are locally altered to purplish and greenish gray colors. Syn-depositional slumping within them may indicate proximity to paleochannels.

Paleochannels are marked by lenticular sandstones filling intraformational scours or scours eroded into the Moenkopi. Most of the uranium is contained in these sandstones (e.g. at the Delta Mine, Lucky 7 Prospect, Green Vein Mesa, etc.), which are up to 30 feet thick.

Moss Back Member

The Moss Back is composed of sandstone, subordinate conglomerate, and thin laterally discontinuous beds of claystone and siltstone, and ranges from 0-120 feet in thickness. Rapid variations in thickness exist within the Moss Back, which are due to extensive development of channel scours at the base. The center of the Moss Back channel system seems to have crossed approximately the center of the Swell, where the

member is thick-bedded and thicker than it is to the southwest or northeast. In the southern and central parts of the Swell, the Moss Back fines upwards from quartz-pebble conglomerate through medium-grained sandstone and limestone pebble conglomerate to fine-grained cross-bedded sandstone. The conglomerates contain coalified and silicified logs, with finer plant debris along bedding planes. The thick-bedded sandstone is petroliferous.

3.5.1.2 Morrison Formation

The Morrison formation surrounds the San Rafael Swell except on the southeast side of the Swell, where it was removed by erosion. It ranges from 290-780 feet in thickness and consists of a lower Salt Wash member and an upper Brushy Basin member. The Salt Wash unconformably overlies the Summerville formation.

Salt Wash Member

The Salt Wash is a light-colored fluvial sandstone with interbeds of red and green mudstone. Its thickness ranges from 0-480 feet and it pinches out in the southwestern part of the Swell. It appears to represent a large alluvial fan deposited by aggrading braided streams diverging from a common source in south-central Utah.

Brushy Basin Member

The Brushy Basin conformably overlies the Salt Wash, and is composed of variegated mudstone from 160-500 feet thick,

with subordinate siltstone, sandstone, and freshwater limestone. Color banding is not always parallel to bedding. A yellowish-tan ("buckskin") color is regarded locally as a guide to favorable ground and may originate in weathering of organic material in carbonaceous mudstones.

Whereas the Salt Wash represents mainly channel-fill sandstone, the Brushy Basin represents mainly overbank silts and muds, and the contact between them probably represents a change in energy regime. Whereas clay in the Salt Wash are predominately illite, clay in the Brushy Basin is mainly montmorillonite, probably after volcanic ash (Mickle and others, 1977).

3.5.1.3 Structure

The present northeast trending Swell is superimposed on a Permo-Triassic northwest trending fold whose activity is reflected in the thickness of facies of the Moenkopi and Chinle formations.

Both bedding-plane and high angle faults are present. Bedding-plane and related faults near the Moenkopi-Chinle contact strike about N25E and although there is probably little movement on them, they may have induced a secondary permeability in relatively tight, fine-grained sediments, which allowed uranium bearing groundwaters to circulate through them.

Various sets of high-angle faults are apparent, most with throws of less than 200 feet. Lineaments, of which there

are many, interpreted from Landsat imagery, are parallel to and extend the important north-northeast trending set of faults. Although the faults and the uranium mineralization are of apparently the same age (Laramide), there appears to be no correlation between the two.

Fourteen (14) collapse structures are known in the Swell: six (6) have some uranium but only one (1) has been of sufficient grade to produce commercially.

3.5.2 Uranium Occurrences and Favorability

3.5.2.1 Chinle Formation

Outside the Green River District, which is in Morrison rocks, all important San Rafael uranium deposits are at the base of the Chinle with the exception of that at the Temple Mountain collapse feature and the Dexter 7 mine, which is located on a fault. Producing areas (Figure 3.5.2 and Figure 3.5.3) fall into a north and south belt, of which the south belt is by far the most important. Both belts coincide with areas of thick sub-Moss Back development, and thin Moss Back member: they are thought to represent main distributary channel areas.

3.5.2.2 Morrison Formation

The Green River District on the east side of the Swell, has, as of July 1977, produced 2.4 million pounds of U_3O_8 from the Salt Wash member. Production is primarily from

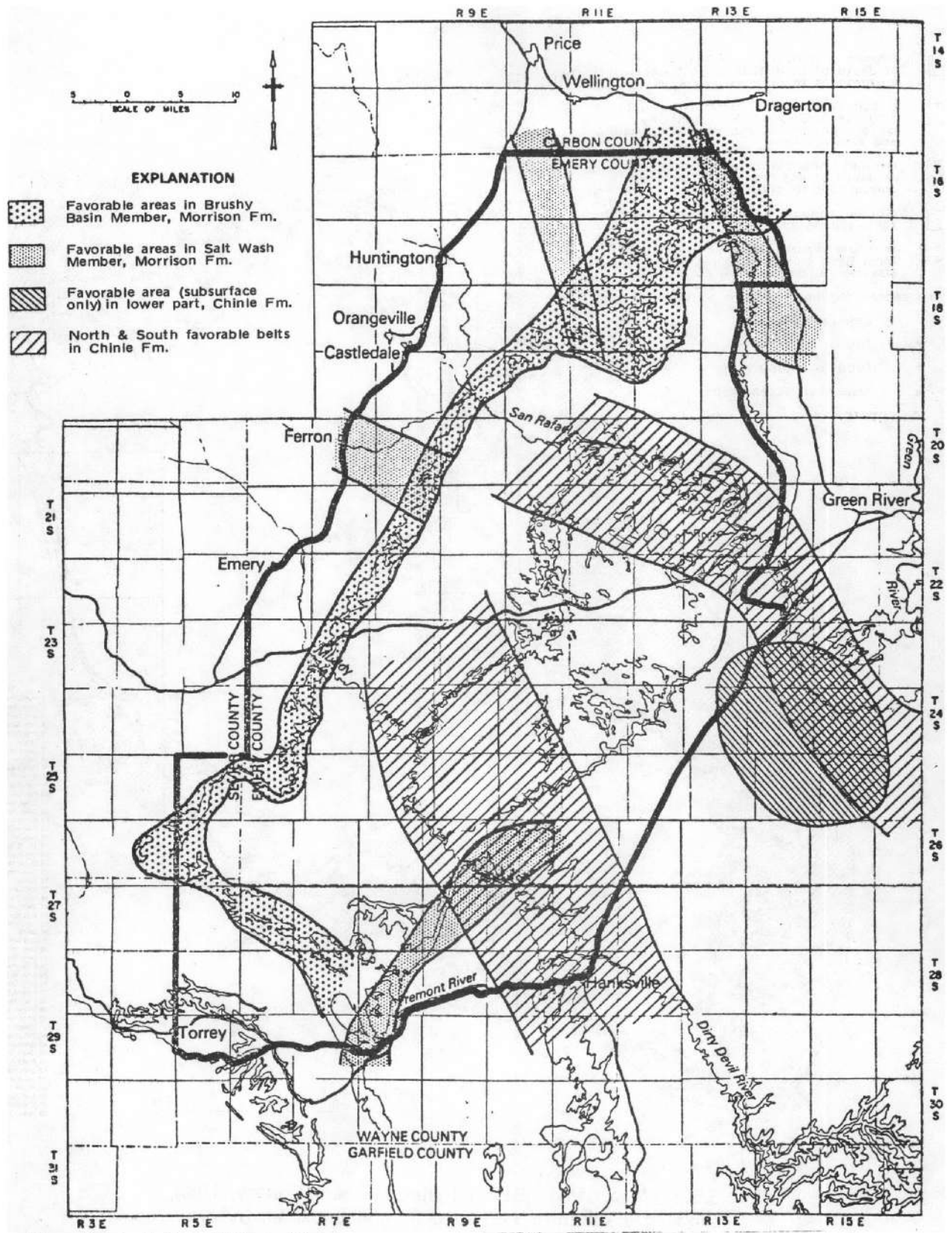


Fig. 3.5.2 Areas favorable for uranium deposits, San Rafael Swell, Utah. (After Mickle and others, 1977)

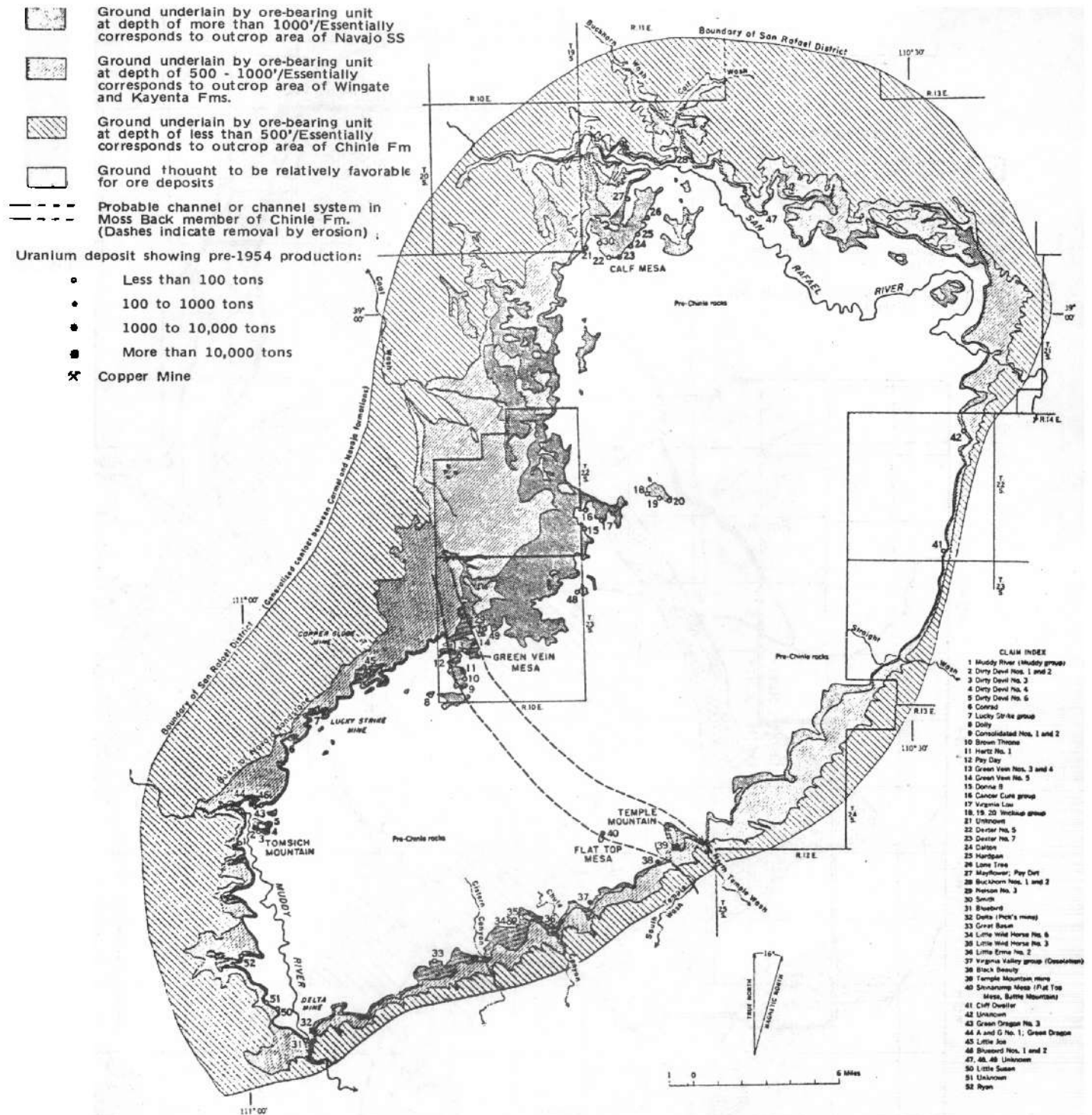


Fig. 3.5.3 Map of San Rafael District, Emery County, Utah, showing uranium deposits and ground underlain by ore-bearing unit (Johnson, 1957)

the uppermost continuous sandstone of the Salt Wash. Favorability of the Salt Wash, according to Mickle and others (1977), is shown on Figure 3.5.2, and is based on occurrence of known deposits and of thick potentially ore-bearing sandstones in the unit.

The Brushy Basin member on the west side of the Swell (Figure 3.5.2) it is altered to "buckskin" color. Here it is considered a potential large volume, low grade resource by Mickle and others (1977).

3.5.3 Ore Guides Which May Be Detectable by Geometric Pattern Recognition Applied to Landsat

In this area, textures due to thick sandstones in the Chinle formation and Salt Wash member of the Morrison formation should be associated with areas favorable for uranium production. Compaction fractures over channel flanks may be particularly good guides.

Since high angle faults are not correlated with uranium occurrences (Mickle and others, 1977), and the obvious Landsat lineaments are definitely correlatable with fault sets, automatic lineament mapping would not be expected to be of assistance.

Unfortunately, along the east side of the Swell, the rocks dip steeply, and everywhere there are many sandstones in the section which will give rise to textures similar to the target sandstones. Therefore it is likely that, due to inherent limitations of Landsat resolution, and to the size of

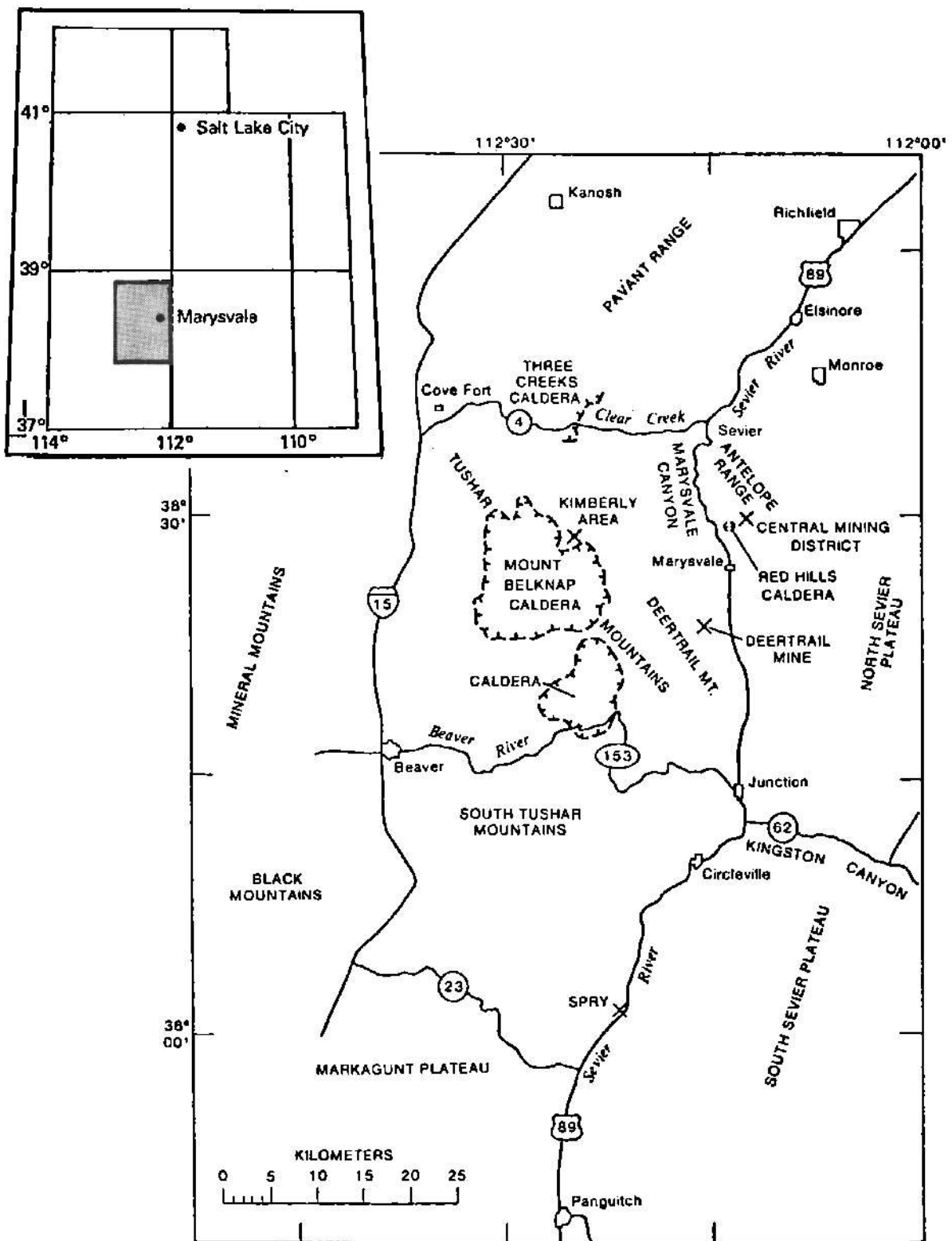


Fig. 3.6.1 . . . Index map of geographical features in the Marysvale area, West-central Utah.

of the windows required for statistical validity of the texture measures, the resolution of the texture measure will be far too coarse to distinguish potentially uraniferous from non-uraniferous ground.

3.6 Marysvale

3.6.1 Geology

Approximately 6,000 feet of Paleozoic and Mesozoic sedimentary rocks similar to the strata of the Colorado Plateau underlie the volcanic rocks of the Marysvale uranium area. These rocks are exposed in the Tushar Mountain Range (at the Deer Trail Mine) just west of Marysvale (Figure 3.6.1) and are only sparsely exposed within the Marysvale uranium area itself. Although the Shinarump and Chinle formations (Stratigraphic Column, Figure 3.6.2) yield numerous uranium-bearing deposits on the Colorado Plateau, they have not been found to be uraniferous in the Deer Trail mine area. The sedimentary rocks near the Marysvale uranium area are deeply buried beneath volcanic rocks.

The Bullion Canyon Volcanic series is a complex Oligocene (28-31 m.y.) assemblage of rocks ranging from coarse latite agglomerate to fine tuff, interspersed with latite or andesite flows. These rocks accumulated around a cluster of generally intermediate composition volcanos located in the Tushar Mountains, the Antelope Range and the Northern Sevier Plateau. Alunite alteration is associated with this volcanic activity. The alunite occurs as masses and veins principally in the tuff.

During the late Oligocene (23-26 m.y.), quartz monzonite and associated masses intruded through the sedimentary rocks to the Bullion Canyon Volcanics. These intrusive masses form part of an east-west trend extending from the San Francisco Mountains to the Sevier Plateau. The intrusives are scattered, frequently separated by several miles and range in size from about an acre to several miles across. In the central mining area of Marysvale (located just north of the town of Marysvale), is a quartz monzonite intrusive which penetrates the Bullion Canyon Volcanics and is roughly two miles in diameter. The quartz monzonite intrusive is the principal host rock for uranium-bearing veins (Kerr, 1968; Steven and others, 1977).

The Mount Belknap Volcanic series is a late Miocene (17-21 m.y.) heterogenous assemblage of ash-flow tuffs, lava flows, associated pyroclastic breccia, and intrusive rhyolite (Figure 3.6.3). A 20 million year old fine-grained granite which cuts the Marysvale quartz monzonite was apparently emplaced during the early period of Mount Belknap activity (Steven and others, 1977). The Mount Belknap assemblage is a result of repeated rhyolite eruptions from the Mount Belknap and Red Hills calderas which formed 18-19 million years ago in response to eruptions of gas-rich rhyolite as flow tuffs (Steven and others, 1977). Uranium-bearing rhyolite dikes cutting the quartz monzonite and granite are believed to be feeders to these calderas. After the accumulation of the volcanic rocks, there was a period of argillic alteration.

This alteration is associated with the uranium-molybdenum-fluorine alteration in the central uranium mining area at Marysvale (Kerr, 1968; Steven and others, 1977).

Basin-range faulting began after eruption of the Mount Belknap Volcanics and continued through much of the remainder of Cenozoic time. The Sevier River formation consists of fluvial and minor lacustrine sediments that were deposited in basins that developed concurrently with faulting. Basalt flows were erupted widely but in low volumes during the period of Sevier River sedimentation (Kerr, 1968).

3.6.2 Uranium Deposits

3.6.2.1 Production and Potential

Gold and silver have been mined in the Marysvale area since the 1860's, with the peak of activity at the turn of the 20th Century (Callaghan, 1973), and only sporadic activity in the past 50 years. Alunite was discovered in the Tushar Mountains in 1910, exploited for potash during World War I and investigated for aluminum potential during World War II.

Uranium was discovered in 1949 in the Antelope Range, 6 kilometers north of Marysvale. These deposits had produced over 1,000,000 pounds of U_3O_8 by 1960, after which they became no longer economic. The recent increases in the price of uranium have sparked new exploration in the Marysvale area.

SERIES	ISOTOPIC AGE (million years)	STRATIGRAPHIC UNIT
Holocene Pleistocene Pliocene		Alluvium Basalt flows Sediments Sevier River Formation and included basalt flows
Miocene	13.7 - 20.0	Mount Belknap Volcanic Series
Oligocene	26.0	Quartz monzonite and related intrusives.
	29.5 - 31.5	Bullion Canyon Volcanics
Paleocene and Eocene		Flagstaff Formation and Tertiary conglomerate.
Cretaceous		Price River Formation
Jurassic		Arapien Formation Navajo Sandstone (quartzite)
Triassic		Chinle Formation Shinarump Formation Moenkopi Formation
Permian		Kaibab Formation Toroweap Formation Queantoweap (Talisman) Formation Pakoon Formation
Pennsylvanian		Callville Limestone

Fig. 3.6.2 Stratigraphic column, Marysvale, Utah, area. (Simplified from Callaghan, 1973)

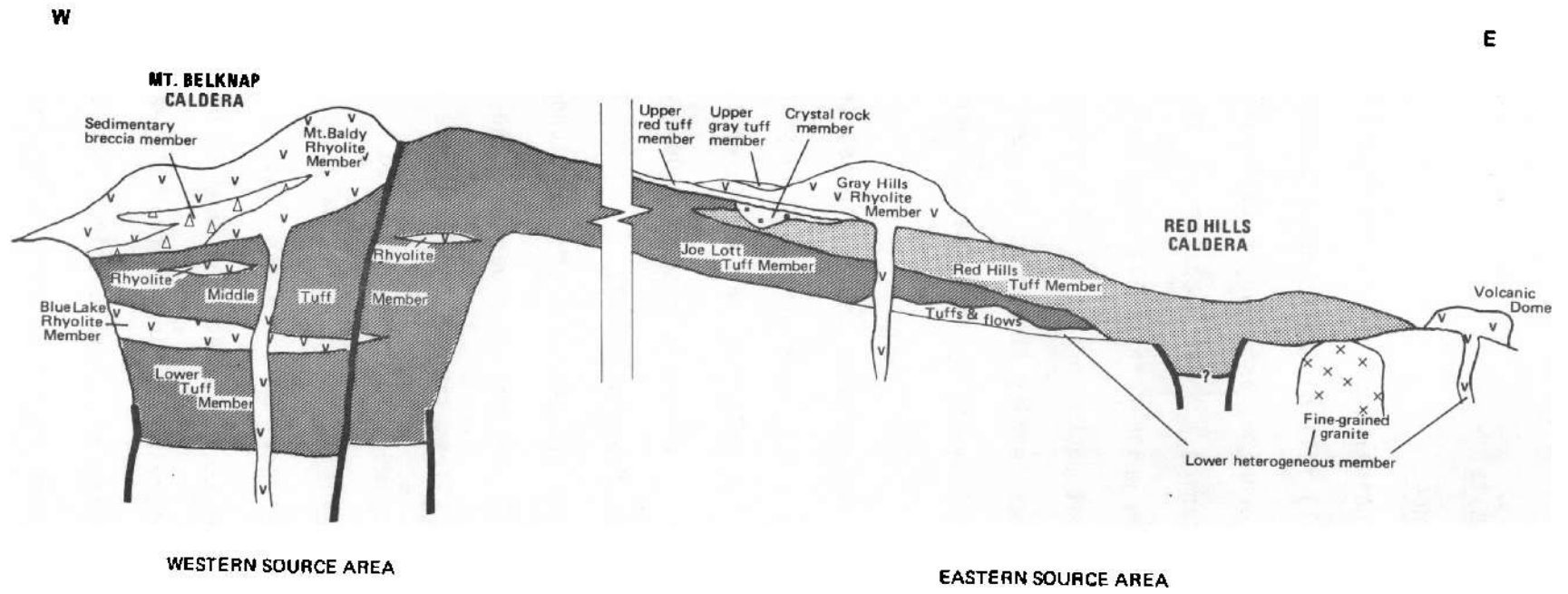


Fig. 3.6.3 Diagrammatic cross-section showing stratigraphic relations of the Mount Belknop Volcanics. Vertical scale exaggerated.
Modified from Steven, et al, 1977.

3.6.2.2 Ore Deposits

3.6.2.2.1 Occurrence

The principal type of uranium deposit occurs as veins (Figure 3.6.1) filling faults and fractures in the quartz monzonite, granite, and younger tuff members of the Mount Belknap Volcanics. These deposits are associated with argillic alteration which Kerr (1957) described as a change of feldspar in the host rocks to various clay minerals. The faults and fractures bearing the veins are vertical and in the main mining district typically trend between N55E-N65E (Kerr, 1968).

Within these faults and fractures, the veins commonly pinch and swell, some ore being in pronounced shoots. Mineralization in faults occurs in hydrothermally altered rock as narrow, locally quartz-rich, discontinuous veins separated by clay gouge or as breccia cement.

The veins are composed of pitchblende, fluorite, pyrite, and locally, molybdenum minerals. The pitchblende may occur as veinlets alternating with thin layers of the other minerals, disseminated in a matrix composed of these minerals, or as breccia cement (Walker and Osterwald, 1956; Kerr, 1957). The ore-bearing portions of the veins range in length from less than 100 feet to 1,500 feet and tend to be vertical. The width of the ore-bearing portion is typically about 4 to 5 feet, at vein intersections or junctions as much as 20 feet. In general, the grade of ore in veins is higher where the wall rock is quartz monzonite rather than it is where the wall rock is fine-grained granite (Kerr, 1968).

Within two to ten feet on either side of ore-bearing veins, a complete change may be observed from unaltered wall rock to the most advanced alteration of the core (Figure 3.6.4). In quartz monzonite, chlorite replaces augite and andesine is replaced by montmorillonite and kaolinite in the early stages of alteration. In later stages, illite and sericite replace orthoclase and kaolinite replaces chlorite, augite, andesine, and biotite. Early stages of granite alteration are represented by sericitization of feldspars plus chlorite replacement of biotite. In later stages kaolinite and montmorillonite replace sericite. The core of the veins in the quartz monzonite and granite consists of pitchblende, fluorite, pyrite, and molybdenum-bearing minerals.

Pitchblende also occurs disseminated in rhyolitic vitrophyre dykes, which cut both quartz monzonite and granite. These dykes are believed to be part of a feeder system which contributed to the overlying Mount Belknap Volcanic Series (Kerr, 1968, 1957).

Numerous supergene uranium minerals occur in the area and with few exceptions are localized in or within several feet of primary uranium-bearing veins. The most common minerals are uranophane, uranotil, and autunite. Numerous other minerals can be found; torbernite, phosphuranylite, schroëckingerite, zippetite, tyuyamunite, and umohoite (Walker and Osterwald, 1956). Ore grade concentrations commonly represent the near surface altered extensions of the primary veins, as the oxidation of the primary uranium minerals occurred essentially in place. No supergene enrichment occurred and the uranium content of

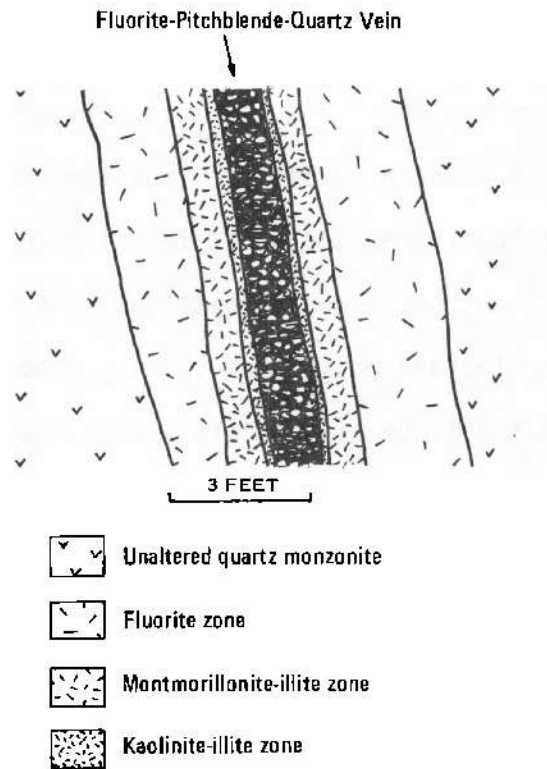


Figure 3.6.4. Typical pitchblende vein, Marysvale, Utah. (After Kerr, 1968)

the weathered zone remains the same as in the primary ore. The secondary minerals most commonly fill fractures or coat fracture surfaces while lesser amounts are disseminated in the veins and wall rock (Walker and Osterwald, 1956).

The assemblage of secondary uranium minerals depends on the type and degree of wall rock alteration, the primary uranium minerals of the veins and the depth beneath the ground surface. Autunite, torbernite, and metatorbernite are rare or lacking in surface outcrops and are found principally as disseminations and fracture coatings in argillized quartz monzonite ten feet or more beneath the ground surface. Autunite was found in partly oxidized veins at depths of 400 feet, hence, it has a relatively large vertical range. Torbernite and metatorbernite typically do not have as great a vertical range (Walker and Osterwald, 1956). Uranophane and uranotil occur only as fracture coatings and veinlets in quartz monzonite, granite, and rhyolite. Concentration of these minerals occur from the surface to depths of 200 feet and are most commonly within ten feet from the primary uranium-bearing veins. They are most abundant in surface or near-surface exposures, indicating that they are the most stable of the secondary uranium minerals at near-surface weathering conditions (Walker and Osterwald, 1956).

3.6.2.2.2 Ore Genesis

The Mount Belknap volcanic activity was ultimately derived from a single magma source, which fed two calderas (the Mount Belknap and Red Hills calderas). The fine grained

granite which cuts the quartz monzonite in the main mining district is a coarse grained representative of the Mount Belknap magma source (Steven and others, 1977). According to Files (1978), the hydrothermal fluids accomplishing the uranium mineralization at Marysvale and within the Mount Belknap caldera were also derived from the same magma source as the Mount Belknap volcanics.

Files (1978) cited Marysvale as an example of a generalized model for uranium mineralization during the caldera cycle. Magmatic differentiation, concentrating uranium in late stage magmatic fluids provides the source for subsequent mineralization. The collapse of the Red Hills and Mount Belknap calderas created numerous fractures and channelways through which mineralizing solutions traveled (Steven and others, 1977). Files suggests that extensive hydrothermal mineralization has occurred along these volcano-tectonic fractures. Pitchblende and secondary minerals are most common in the NE trending faults, less common in the NW trending faults and rare or absent in the N trending faults (Walker and Osterwald, 1956). In the main mining district, most uranium-bearing veins occur in vertical, N55-65E faults (Kerr, 1968).

Frequently the intersections of uranium-bearing veins and the quartz monzonite-rhyolite contact are loci for ore concentration. Apparently the mineralizing solutions traveled through the fractured quartz monzonite to the overlying rhyolite, which was more susceptible to reaction and thus underwent extensive mineralization.

Major uranium mineralization appears to have taken place several million years after the Mount Belknap Volcanic activity, late in the caldera cycle. The major deposits occur mainly as veins in faults and fractures, cutting the quartz monzonite, granite and rhyolite tuff of the Mount Belknap Series. These deposits are believed to be of hydrothermal origin and are usually associated with an argillic wall rock alteration (Steven and others, 1977; Kerr, 1968, 1957).

This argillic wall rock alteration affects various lithologies to a different extent. Quartz monzonite and granite show several stages of alteration in terms of progressive mineral changes (see Section 2.2.1 above), while the tuff is so susceptible to alteration that these stages are not distinguishable. Alteration halos along a vein in the granite are not as wide as the corresponding halo in the quartz monzonite, thus the granite appears less susceptible to the alteration than the quartz monzonite (Kerr, 1968, 1957).

3.6.3 Ore Guides Which May Be Detectable by Geometric Pattern Recognition Techniques Applied to Landsat

Several such guides to uranium ore in this district are worth mentioning:

1. Uranium in veins is nearly always associated with argillic alteration. These argillic areas are bleached white or yellow clay-like soft masses (Kerr, 1968). This phenomenon may give rise to distinctive erosional or weathering textures which may be recognizable in the texture output.

2. Uranium is associated with vertical fractures trending NE and occasionally NW. These fractures should be detectable as lineaments by the automatic lineament mapping algorithm. North-south faults are not of exploration interest.

Other guides which are not expected to be detectable by geometric pattern recognition techniques applied to Landsat are:

3. Most of the vein quartz in the main mining area is clear to milky white, but near concentrations of pitchblende it is smoky to almost black in color (Walker and Osterwald, 1956).
4. Purple to almost black fluorite, either in coarse crystals or in fine grained powdery masses is present in virtually all pitchblende-bearing veins (Walker and Osterwald, 1956).
5. Colorless or pale green fluorite is present in alteration halos around uranium-bearing veins (Walker and Osterwald, 1956).

3.7 Lake City Caldera Area

The Lake City caldera lies within the larger and slightly older Uncompahgre caldera, and formed 22.5 m.y. ago. Similarly the Silverton caldera, to the southwest, lies within the San Juan caldera, which, together with the adjoining Uncompahgre caldera forms the San Juan Volcanic Depression (Lipman and others, 1973). All metal production (\$500 million) of the several districts associated

with these two pairs of calderas (e.g. Red Mountain, Lake City, Telluride) is related to the Lake City/Silverton caldera cycle, although hydrothermal activity and alteration were both prominent during the Umcompahgre caldera cycle (28 m.y.) and preceding andesitic stratovolcanic phase (35-30 m.y.). The northern part of the volcanic pile lies on Cretaceous rocks and the southern part on Precambrian rocks (Lipman and others, 1973).

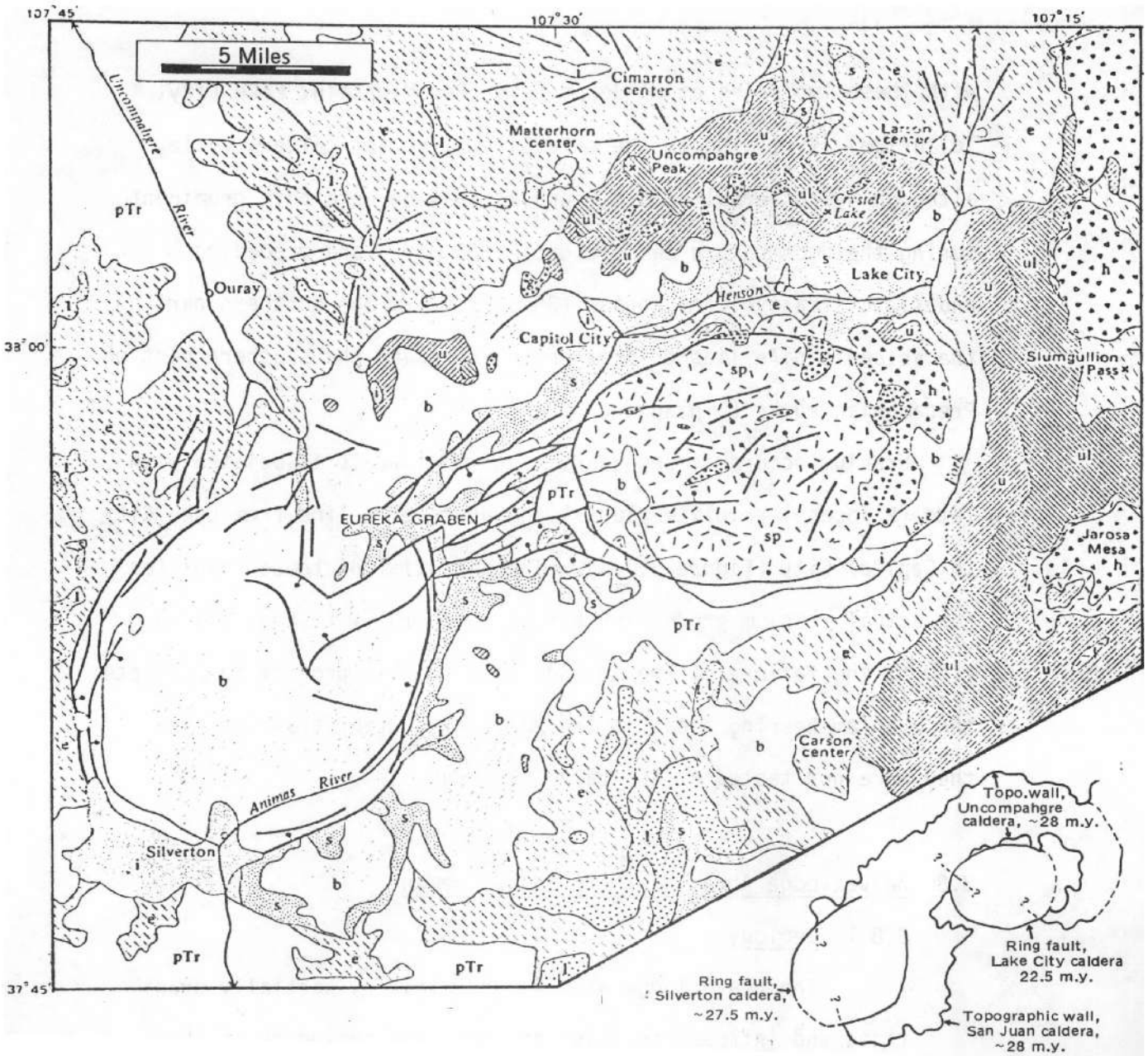
Uranium occurs as secondary uranium minerals associated with late (Pliocene) rhyolite plugs lying north of a line from Lake City to Capitol City (Figure 3.7.1). The potential of these rhyolites for actual uranium production has not been fully tested, and in view of the failure of the methods used in this project to indicate the uranium-bearing areas in the Marysvale, Utah, training area, they were not tested at the Lake City area.

3.8 Beaverlodge Area, Northern Saskatchewan

3.8.1 Geology

The Beaverlodge area is underlain by partially granitized and intruded pelitic and psammitic sediments of the Tazin Group, of Alpebian (2,300 m.y.) age (Figures 3.8.1, 3.8.2, and 3.8.3). Folding, on three superimposed sets of axes, and metamorphism, which ranges from upper greenschist facies to lower granulite facies, occurred during the Hudsonian Orogeny (1,700-1,900 m.y. B.P.).

The Martin formation was deposited, apparently as graben fill (Olsson, 1974) on the planed and subsequently faulted basement surface at about 1,650 m.y. B.P. (Figure 3.8.3). Its base is a coarse sedimentary breccia, passing



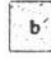
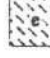



ASH-FLOW SHEETS



LAVAS

INTRUSIVES

-  Sunshine Peak Tuff (Miocene)
-  Upper ash-flow sheets (Oligocene) - Fish Canyon, Crystal Lake, Carpenter Ridge, Wason Park, and Rat Creek Tuffs
-  Sapinero Mesa (and Eureka Member) Tuff (Oligocene)
-  Lower ash-flow sheets (Oligocene) - Dillon Mesa, Blue Mesa, and Ute Ridge Tuffs

-  Quartz latitic lavas of Lake City caldera and basaltic lavas of the Hinsdale Formation (Miocene)
-  Upper lavas around margins of Uncompahgre caldera (Oligocene)
-  Lower caldera lavas and volcanoclastic rocks (Oligocene) - Henson and Burns Formation
-  Early intermediate-composition lavas and breccias (Oligocene)

-  Rhyolite and granite intrusives of Lake City caldera (Miocene)

-  Intermediate-composition intrusives (Oligocene) - mainly monzonite
-  Dikes

 Pre-Tertiary rocks

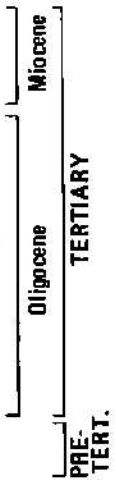
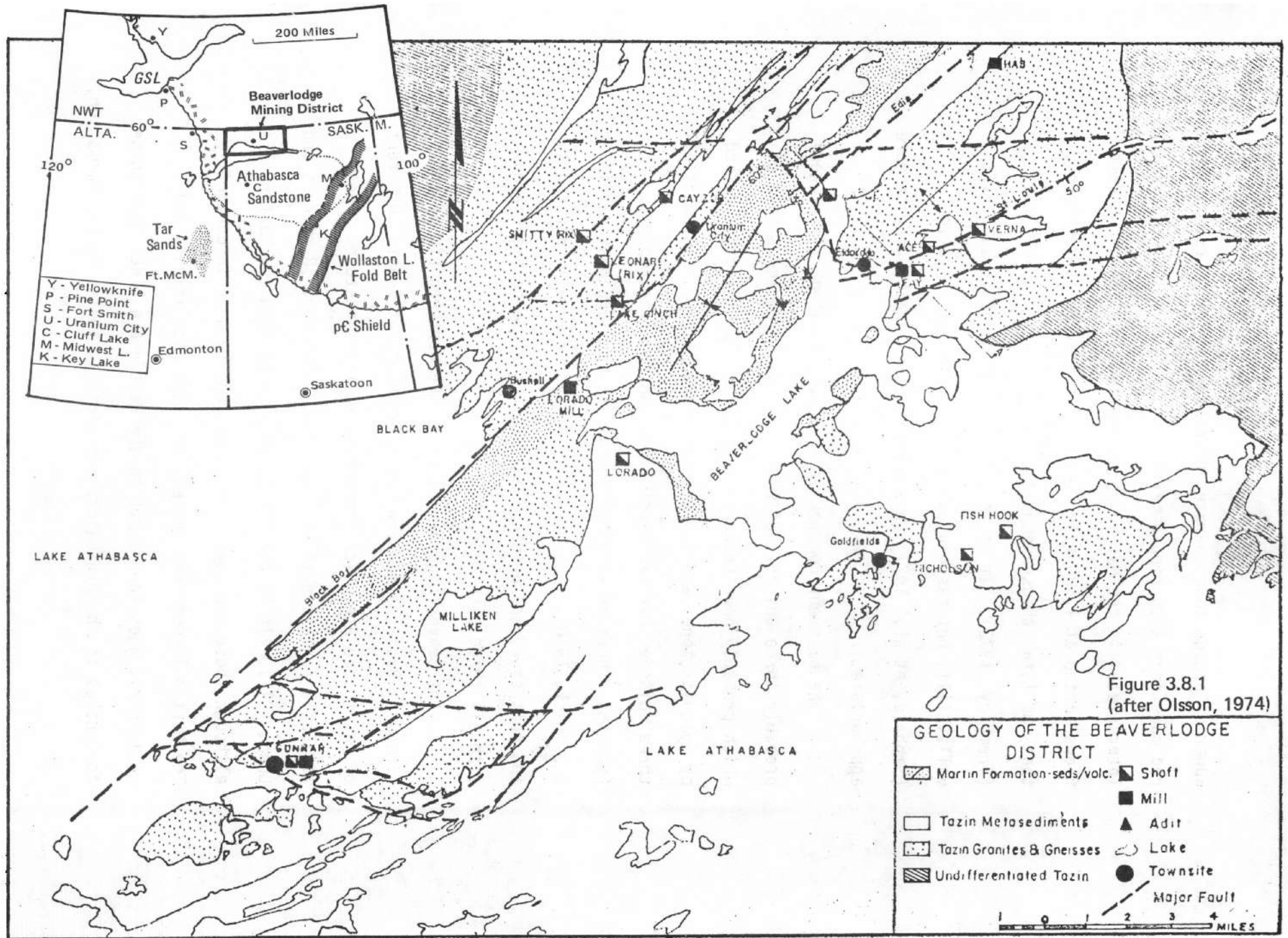


Fig. 3.7.1 Generalized geologic map of the Silverton-Lake City area. (Lipman, et al, 1973)

upwards through conglomerate and arkose to red siltstones and red mudstones with ripple-marks and mud-cracks (Olsson, 1974). Intercalated in the Martin formation are andesite and basalt flows (dated at 1,630 m.y. B.P.) and sills; it is possible that the total thickness of this formation is 19,500 feet (Tremblay, 1972). It is tempting to interpret it as a rift valley fill, but associated volcanics are calc-alkaline (Sibbald, et al., 1977), and a Great Basin analogy may be more appropriate.

The basement complex is intensely faulted. There were probably three episodes of faulting, the first and second of which probably have reverse throw (Beck, 1970) and are marked by mylonite zones and heavy gouge respectively. Faults of all three episodes partially coincide, and the final episode (perhaps others as well) is normal in sense and post-Martin in age (Beck, 1970). The main fault trends are east, northwest, and northeast, and uranium deposits appear to be associated with all three directions.

The Beaverlodge area lies on the northern rim of the Athabasca Basin, a shallow basin filled by at least 5,000 feet of undeformed Athabasca formation, mostly sandstone. The Athabasca formation is well-dated at 1,350 m.y. (Ramackers and Dunn, 1977). It is thought to be younger than the Martin, although these two cover formations are nowhere in contact. The Martin is deformed whereas the Athabasca is not, and radiometric ages for basalt in the Martin are older than those for shales in the Athabasca. In contrast to the Martin formation,



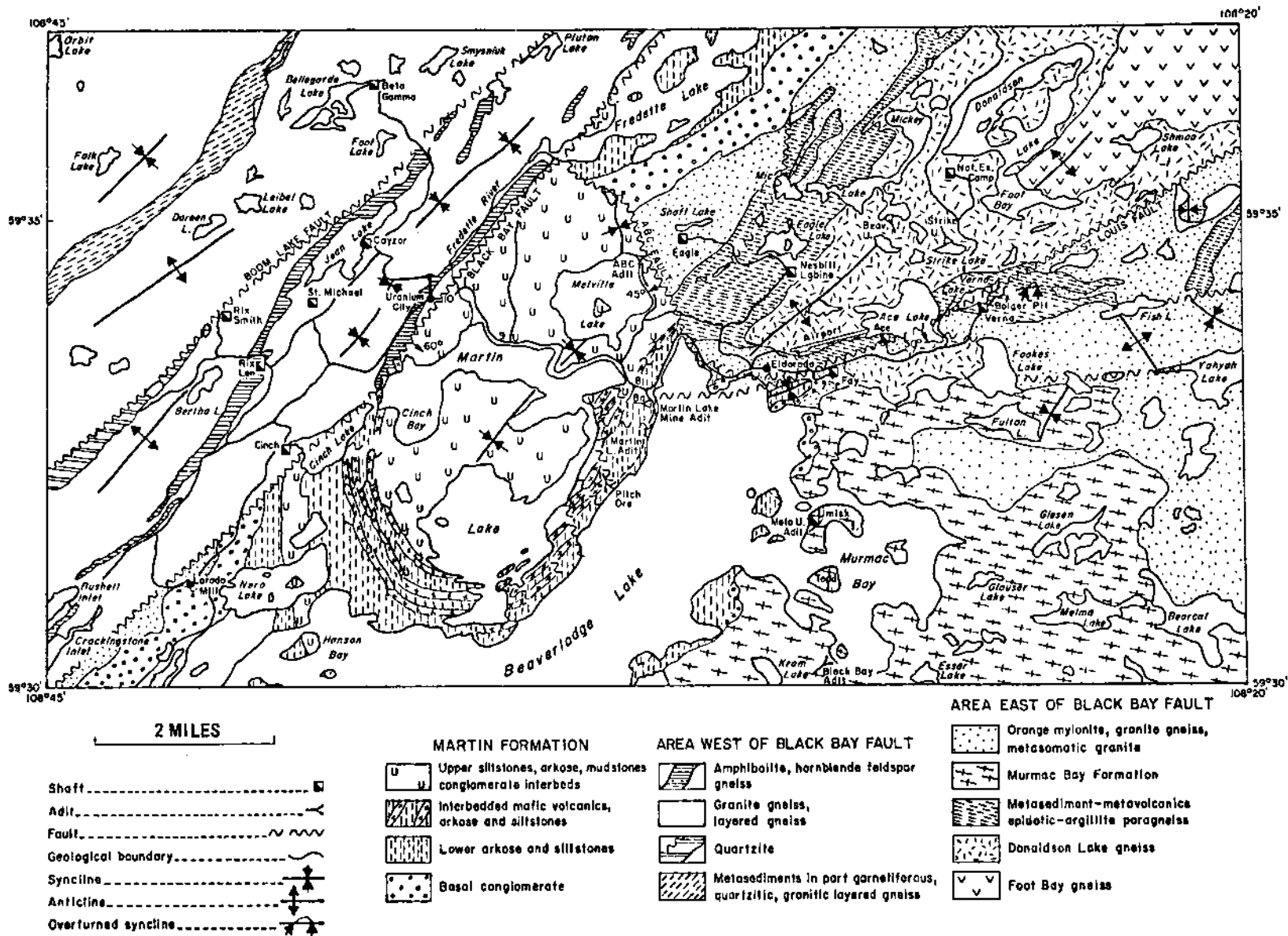


Figure 3.8.2. Geology of the Beaverlodge area, northwest Saskatchewan (after Simpson, 1973).

the Athabasca formation is a thin and very extensive stable platform deposit composed of mature fluvial sediments. It is underlain by a thick regolith, with which most of the uranium at Key Lake, Rabbit Lake, and elsewhere is associated.

Post-Athabaskan events include intrusion of late Precambrian diabase dikes, formation of the Paleozoic Carswell impact structure and deposition of Cretaceous sediments. However, these are not thought to have any significance in localizing uranium deposits, though changes in groundwater regime at several epochs may have led to local mobilization of uranium and enrichment or impoverishment of pre-existing deposits.

3.8.2 Uranium Deposits

3.8.2.1 Production and Potential

Several hundred showings of uranium occur in an area of about 500 sq. mi., centered on Uranium City (Beck, 1970). Nineteen mines were brought into production in the 1950's, with a total daily production in that period of 4,500 tons of ore grading 0.2% U_3O_8 . Two of these were major deposits: the Gunnar, depleted in 1963, and the Eldorado Nuclear group of ore bodies, which are still in production.

Areas of similar geology around the rim of the Athabasca Basin to the southwest, southeast and south, are now the scene of a very large uranium "play". These areas probably have a potential one or two orders of magnitude greater than that of the Beaverlodge area alone, making the Athabasca Basin one of the world's greatest uranium provinces. The literature on new discoveries in this vast area is very sparse. The area involved is so large that no more than one or two deposits are

PLEISTOCENE	
CRETACEOUS	Grand Rapids Formation Clearwater Formation McMurray Formation
DEVONIAN	Methy (Winnipegosis) Formation McLean River Formation La Loche Formation
HELIKIAN	Carswell Formation Athabasca Formation (1350 ± 50 m.y.) Martin Formation (1630 ± 180 m.y.)
--HUDSONIAN OROGENY-- (1735 m.y.)--	
APHEBIAN	Many Islands Group Thluicho Lake Group Tazin Group (in part?) Wollaston Group Wollaston, Mudjatik, and Virgin River domain granitoid gneisses (in part?)
--KENORAN OROGENY-- (2480 m.y.)--	
ARCHEAN	Tazin Group Western granulites Wollaston, Mudjatik, and Virgin River domain granitoid gneisses (in part?)

Fig. 3.8.3 Stratigraphic column for northwest Saskatchewan.

located within a single Landsat frame, making statistical evaluation of Landsat techniques difficult. Since the ore controls at Beaverlodge and the newer deposits are thought to be almost identical, the Beaverlodge area may be used as a model for the development of methods applicable to the Athabasca Basin as a whole, and to similar areas in the United States.

3.8.2.2 Ore Genesis

Beaverlodge uranium showings fall into two groups: syngenetic and epigenetic. Only the epigenetic deposits have proved commercially viable to date. The syngenetic bodies are of interest because they are similar in many ways to the Rossing deposit in Southwest Africa, and also because several large low-grade deposits are known in the Charlebois Lake area of Saskatchewan.

3.8.2.2.1 Syngenetic Deposits

The 50 known deposits of this type occur as disseminations of grains of uraninite associated with biotite in pegmatites, and occur as three types (Beck, 1970):

1. Lit-par-lit zones of pegmatite in alaskitic gneiss.
2. Irregular bodies of pegmatite in migmatite zones.
3. Isolated dike-like pegmatites.

Tremblay (1970) showed by geochemical means that the source of the pegmatite uranium was the quartzites and to some extent the argillites of the Tazin Group; he assumed that

the uranium was originally contained in these rocks in detrital form. He demonstrated that uranium was progressively mobilized during granitization from the quartzites to be reconcentrated in the pegmatites. Final remobilization and reconcentration to form vein deposits was by fluids issuing from the pegmatites.

In the following respects: 1) presence of metamorphic quartzites partially granitized to alaskitic rocks, and 2) mobilization of the above to form alaskite pegmatities with U_3O_8 , the syngenetic deposits of Beaverlodge are similar to those of the Rossing area of South West Africa (Section 3.10). At Rossing, however, field evidence suggests derivation of uranium from an argillaceous rock, now a biotite gneiss.

3.8.2.2.2 Epigenetic Deposits

These are stated (Dahlkamp, 1977) to occur in structures subsidiary to major faults, and to range in type from massive veins and stockworks (Robertson, 1974) to disseminations in the Tazin Group and, rarely, Martin formation. Whereas Robertson (1974) emphasizes structural control by zones of mylonitization and brecciation, Dahlkamp points out that individual ore lenses are parallel to bedding, and that certain very competent or very incompetent lithologies may cap the ore. The primary uranium minerals are deposited by open-space filling in thousands of small fractures, and are economic where fracture density is high. Tremblay (1970) shows that these high fracture density areas occur in dilatational zones at F_2/F_3 fold intersections.

The ore deposits are also spatially related to the pre-Martin (or perhaps Athabasca) unconformity, as are all commercial deposits in the Athabasca Basin. In the Beaverlodge district, however, the ores are not quite as closely related to the unconformity as elsewhere, occurring from 0-2,000 feet below it.

The ore bodies are also associated with intense red hematitic alteration, this is, however, not an infallible guide to ore. Chloritization, epidotization, silicification, albitization and the introduction of calcite are also associated with the ore (Dahlkamp, 1977).

Radiometric ages for the syngenetic deposits cluster at 2,200 m.y. (perhaps the date of original sedimentary deposition), and at 1,930 m.y. (Dahlkamp, 1977), marking the remobilization into pegmatitic rocks early in the Hudsonian Orogeny (Dahlkamp, 1977). Concordia plots of U/Pb ages from the epigenetic deposits suggest initial deposition at about 1,780 m.y. (Koeppel, 1968), predating of the Martin formation, with episodic lead loss occurring at 1,110 m.y., 270 m.y., and within the last 100 m.y. This complex history of mineralization corresponds to an equally complex paragenetic sequence in the veins, beginning with open-space-filling colloform pitchblende, and ending with sooty pitchblende, as described by Tremblay (1972). The existence of deposits intermediate in type between epigenetic and syngenetic, and of a pegmatite (1,815 m.y.) cutting pitchblende ore-zones at the Gunnar mine,

suggests a long and episodic history of uranium mineralization. This includes concentration, partial dispersion and re-concentration of uranium, from initial sedimentary protore to uraniferous pegmatites to veins and supergene enrichment.

3.8.3 Geometric Patterns and Textures Associated with Ore Deposits

At Beaverlodge the following ore-controls fall under this heading:

1. Faulting - Major faults, and the subsidiary structures issuing from them, appear to be a major control. These should be recognized by the automatic lineament mapping program.
2. Unconformity - Most of the major deposits lie within a few hundred feet stratigraphically of the pre-Martin unconformity. The differences in texture between the greenschist facies, tightly folded, refolded and intruded Tazin Group rocks and the slightly folded sediments of the Martin should be amenable to mapping by the texture measure techniques.
3. Brecciation and mylonitization - Most ores are associated with fine brecciation or with mylonite zones. These should have a much finer surface texture than the less broken rocks, and should therefore be distinguished by texture measure techniques.

4. Alteration - The bright red hematitic, chloritized and silicified alteration zones should have topographic and spectral textures or patterns which differ from those of the unaltered country rock.
5. Fold intersections - Fold intersections should be recognizable as zones of rapid change in orientation of automatically-mapped linear features.

3.9 Northern Michigan

3.9.1 Geology

The oldest rocks present in the area are gneisses of the "Southern Complex" near Watersmeet and Marenisco, Michigan. These extend southeast into Wisconsin and are probably (Kalliokoski, 1976) correlative with the 3.8 b.y. old Minnesota Valley complex. Greenstones and granites of the Michigan "Northern Complex" are of Superior (2.70-2.75 b.y.) age.

The Northern and Southern Complexes are overlain by rocks of the Penokean cycle (1850-1950 m.y.). Penokean rocks of the Marquette trough area along the eastern edge of the Landsat image, are predominantly sediments in the north, volcanics in the south. Granitic to dioritic plutons of this age are common in northeastern Wisconsin. Major faulting, up to the south, of Penokean age is present along the eastern part of the Michigan-Wisconsin border. The Penokean rocks are interpreted (Kalliokoski, 1976) as a continental margin to the north, with a volcanic/plutonic belt to the south.

The Baraboo quartzites and quartz-pebble conglomerates, representing shallow shelf conditions, were deposited during

the interval 1500-1800 m.y., and were intruded by the Wausau (syenite) and Wolf River batholiths. The Red River quartz-monzonite phase of the latter has some uranium associated with it.

The upper Precambrian is represented by the copper-bearing Keweenaw lavas and overlying sediments (including the Copper Harbor conglomerate), which trend northeast across the northwest part of the Landsat image.

In the north-central part of the Landsat image are discontinuous outcrops of the Jacobsville fluviatile sandstone, which Kalliokoski (1976) thinks are also of Upper Precambrian age. These sandstones lie on an old unconformity representing a surface of long and deep weathering, reminiscent of that beneath the Athabasca sandstone in the Beaverlodge uranium area.

3.9.2 Uranium Deposits

Three general types of radioactive mineral occurrence are known in the area:

1. Primary uranium in igneous rocks - e.g., in syenites, Green's Creek pegmatite, Republic migmatite.
2. Syngenetic monazite in the Goodrich quartzite.
3. Supergene uranium in mid-Precambrian metasediments, granitic rocks, and metadiabase and in Keweenaw felsites.

Kalliokoski (1976) proposes for this latter type, which has the greatest potential for production, a "Lake Superior" type uranium model:

1. Leeching of uranium from carbonaceous shale of Upper Marquette Range supergroup.
2. Re-deposition of the uranium, in various rocks, associated with deep weathering of the "soft iron ores" and with deposition of the Jacobsville sandstone.

These processes may give rise to a number of different occurrence types, all of them variations on a theme:

1. Veins, possibly supergene, in gneiss - e.g., Big Eric's crossing, Wiggins Prospect, and so on. These occurrences are similar to those of Rabbit Lake and of the Beaverlodge area in Canada.
2. Veins, possibly supergene, in metasediments and volcanic rocks - e.g., fractures and breccia zones in black slates of the Michigamme formation, and fractures in oxidized iron-ores and in felsite. These occurrences resemble those of Beaverlodge as well as those of the Alligator River/Rum Jungle area in Australia.
3. In fractures in diabase dykes - e.g., the Haggett Dyke, Taylor Mine, Graphite Quarry, the M&G Mine.

3.9.3 Exploration Using Geometric Pattern Recognition and Texture Measures Applied to Landsat

Kalliokoski's model predicts an association of uranium with the Jacobsville sandstone, which should be recognizable on Landsat. Most of the uranium seems to have been re-deposited

in fractures or breccia zones, which should give rise to recognizable lineaments (in the display outputs) and textures (on the texture measures), respectively.

However, the Michigan area is not only heavily vegetated and modified by human activity, but has also been extensively glaciated, which resulted in development of numerous lakes and peat bogs, similar to those of the Beaverlodge area. Therefore, in view of the lack of positive results in Beaverlodge, and the similar but more severe problems to be expected in applications of the technique in Upper Michigan, it did not seem logical to proceed with this test area.

3.10 Rossing, Southwest Africa

3.10.1 Geology

The Rossing and related deposits occur in the central part of the late Precambrian Damara orogenic belt of Southwest Africa (Figure 3.10.1). Sediments of the Damara group were deposited about 1.0 b.y. BP, and consist in the Rossing mine area of Khan formation sandstones, siltstones, and marls across which prograde Rossing formation shales and limestones (see Stratigraphic Section, Figure 3.10.2).

At about 500 m.y. BP, the sediments were folded and metamorphosed to amphibolite grade, and basement granites were remobilized and rose palingenetically to form mantled gneiss domes such as the Rossing Dome (Figure 3.10.1 and Figure 3.10.3). The sediments, especially the Khan formation, were migmatized and passively intruded by large alaskitic pegmatite bodies. Xenoliths of country rock within the pegmatite are

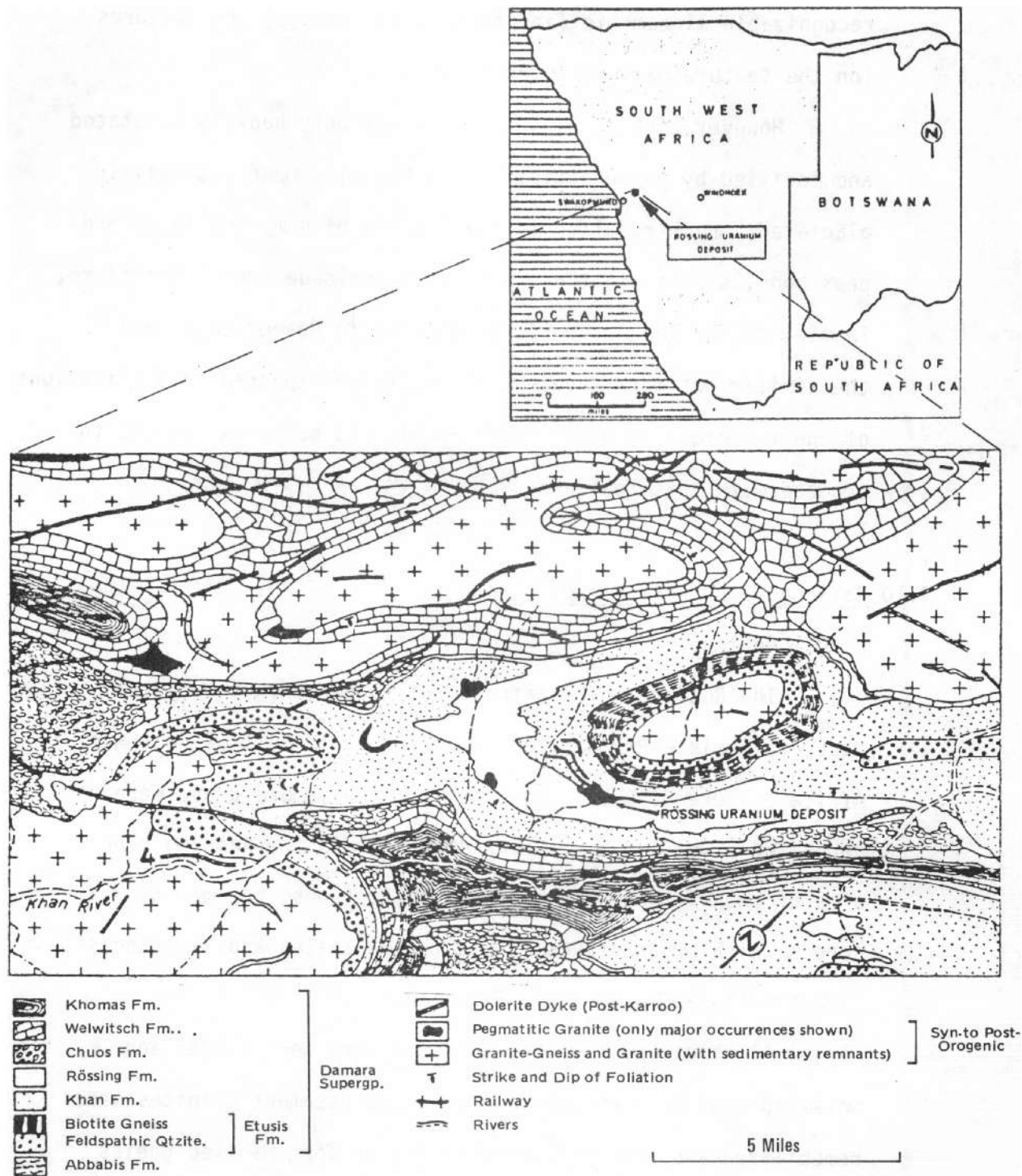


Fig. 3.10.1 Setting of the Rössing uranium deposit in the central portion of the Damaran orogenic belt (after Berning, et al, 1976).

concordant with the surrounding country rocks. From evidence seen in the field south of the Swakop River near Rossing, the uranium minerals seem to have been introduced into the alaskitic pegmatite bodies by leaching of biotite from the Khan formation. As the pegmatite contacts were approached, very dark brown biotite of the Khan formation became progressively paler and less brown, until it was hard to distinguish from muscovite. The same mica occurred in the first few feet of pegmatite, but became clear muscovite within a few feet. Associated with the dark mica in the outer edges of the pegmatite were large (up to one inch) irregular blebs of ilmenite, prominent secondary uranium minerals, and smoky quartz.

Evidence exists suggesting that uranium ore occurs only in association with a particular, very aluminous member of the Khan formation in which the Khan Copper deposit also occurs.

3.10.2 Uranium Ore Bodies

3.10.2.1 Production and Potential

The Rossing is the largest known hard-rock uranium ore body in the world, but it is of relatively low (0.035% U_3O_8) and variable grade. Full production rates of 5,000 s.t. of U_3O_8 per year were achieved in January 1979.

The potential of the area is quite high: at Trekkopje, west of Rossing, is a similar body which is being seriously investigated for mining, and there are other occurrences of similar nature along the Swakop River gorge. In addition, the geologic similarities between the Rossing deposit and large

GROUP	SUBGROUP	FORMATION	LOCAL LITHOSTRATIGRAPHIC UNITS	THICKNESS	REMARKS	
DAMARA (Late pC)	Swakop	Komas		10,000	Biotite - Cordierite - Garnet & Quartz - Biotite Schist	
		Welwitsch		300' - 2000'	Blue Marble, White Marble & Quartz - Biotite Schist	
		Chuos		300' - 1600'	Tillite	
	Hakos	Rössing	Feldspathic Quartzite		160'	
			Upper Biotite - Cordierite Gneiss		130' - 160'	
			Upper Marble		160' - 230'	Includes Granofels & Schist
			Conglomerate		6' - 30'	
			Lower Biotite - Cordierite Gneiss		100' - 130'	Migmatized, incl. Biotite - Hornblende Schist
			Lower Marble		70' - 160'	
NOSIB	Khan	Biotite - Amphibole Schist		30' - 70'		
		Upper Pyroxene - Hornblende Gneiss		230' - 330'	Migmatized	
		Pyroxene - Garnet Gneiss/Amphibolite		100' - 400'	Amphibolite in discontinuous bodies	
	Etusis	Lower Pyroxene - Hornblende Gneiss		230' - 500'	Migmatized	
		Upper Biotite Gneiss		650' - 1000'	Migmatized	
		Marker Quartzite		6' - 25'		
		Lower Biotite Gneiss		500' - 650'	Migmatized	
		Feldspathic Quartzite		650'	Cross-bedding typical	
	Abbabis (pC)		— UNCONFORMITY —		Sillimanite and Quartzo-Feldspathic Augen-Gneiss	

Stratigraphic position of Rössing uraniferous pegmatitic granite (late to post-Damaran tectogenesis).

Fig. 3.10.2 Lithostratigraphy of metasediments in the vicinity of the Rössing Uranium Deposit. (after Berning, 1976)

"protore" deposits in alaskitic pegmatite in the Beaverlodge area (Section 3.8) imply that this general type of uranium occurrence is widespread. However, the low grade typical of these deposits may imply that such deposits will only be economic when extremely accessible.

3.10.2.2 Ore Genesis

Geologists in the field feel that the original uranium concentration is in a particular bed in the Khan formation, since pegmatites are mineralized only where they cut this stratigraphic unit.

From the observations made in the field, uranium and iron were mobilized from the sediment and redeposited in the fringes of the pegmatites. In later stages of pegmatite emplacement, the uranium was probably remobilized and reconcentrated to form ore bodies.

3.10.3 Ore Guides Recognizable by Geometric Pattern

Recognition Techniques Applied to Landsat

The ore at Trekkopje and Rossing occurs in dilatational pressure shadow areas on the noses of large mantled gneiss domes. Although the Rossing dome is well exposed, others in the area do not outcrop and are covered by a thin veneer of desert lag. Therefore, it is of value to establish methods to identify these areas, and this can perhaps be done by:

1. Automatic lineament mapping - These areas should stand out as areas of short random lineaments. They should occur where strong lineaments corresponding to the bedding are strongly inflected.

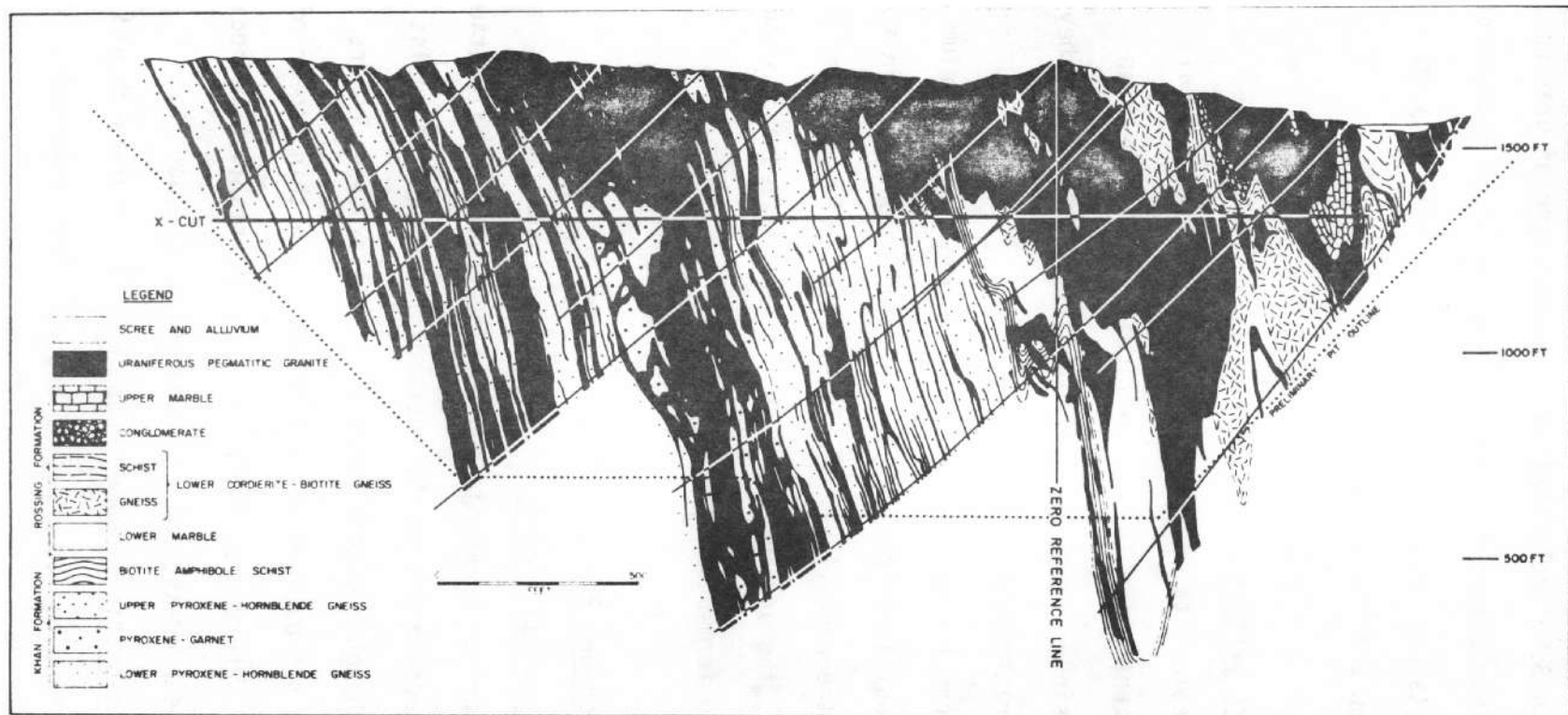


Fig. 3.10.3 Drill section zero showing geology, boreholes, and bulk sampling crosscut.
(after Berning, et al, 1977)

2. Texture Measures - There should be differences in texture between these "pressure shadow" areas of random stresses and the remainder of the area which has strong, oriented stress patterns. These texture differences should arise from different joint and fracture systems imposed by the two different stress regimes.
3. Texture Measures - Since the ore is associated with large pegmatites which, due to their lithology and to their intricate pattern, should have a distinctive texture, it may be possible to further outline favorable areas by using the texture measures to identify intensely pegmatized areas. This texture should be composed of a topographic component coarser than surrounding areas due to the massive nature of the pegmatite, and a tonal component due to the unusually high contrast between pegmatite and host rocks.

3.11 Geology of the South Park Area, Colorado

3.11.1 Geology

This area was chosen as a possible U.S. analog for the Rossing area in South West Africa/Namibia. The Idaho Springs formation of the Colorado Front Range is older than the 1600-1730 m.y. old Boulder Creek granodiorite, which intrudes it (Figure 3.11.1). The Idaho Springs formation is intensely metamorphosed and folded about NNE axes and is lithologically similar to the Damaran sediments of the Rossing area. It

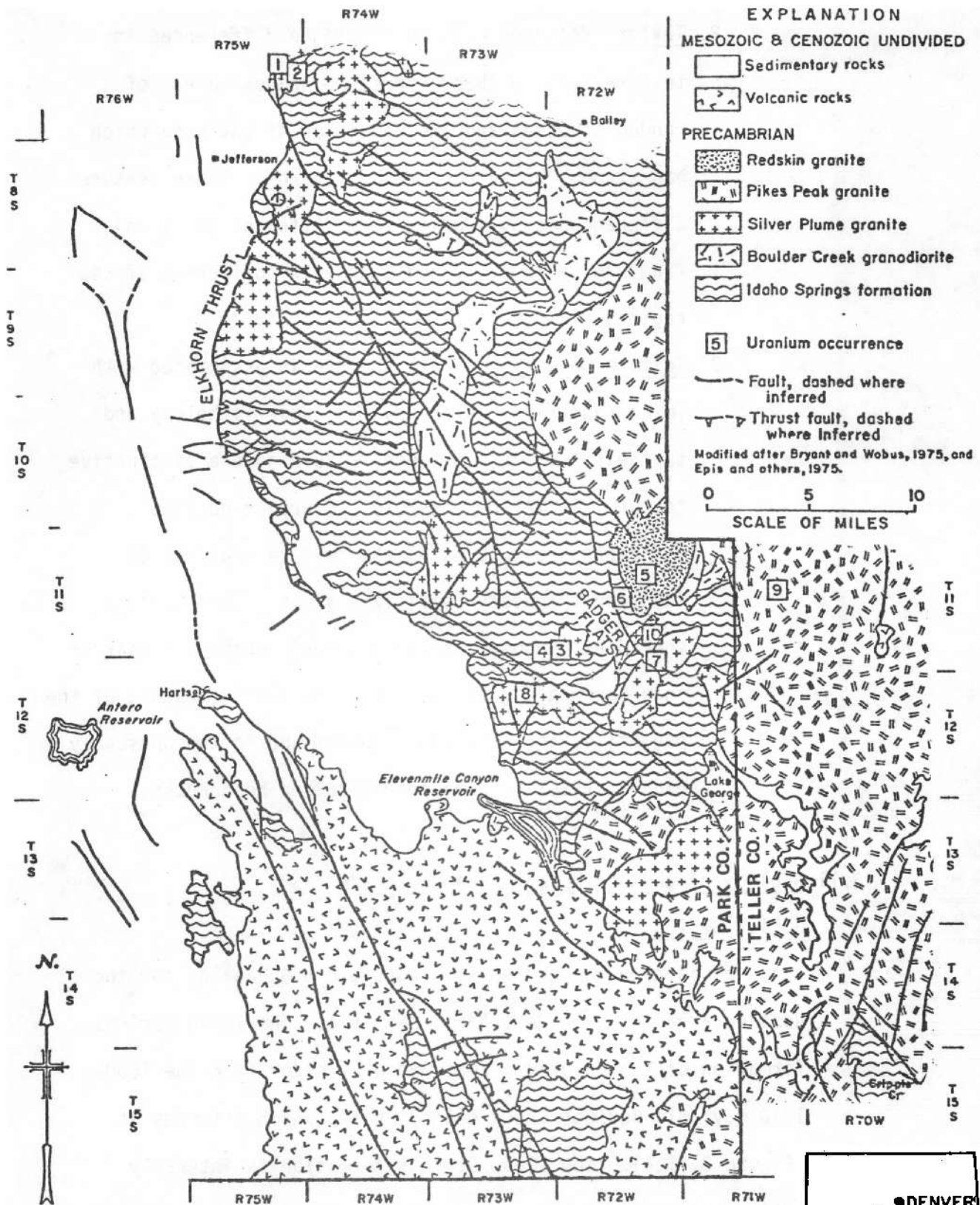


Fig. 3.11.1 Geologic map of South Park Area, Park and Teller Counties, Colorado. (after Gallagher, 1976)



includes calc-silicate gneiss, quartzite and amphibolite, and is dominantly a fine-grained biotite gneiss. In addition, it is extensively migmatized and even granitized in places, as are the Damaran rocks of Rossing. The Idaho Springs formation is considerably (1000 m.y. BP) older than the Rossing rocks, and there are apparently no mantled gneiss domes in the South Park area. Gallagher (1976), however, has described a variant of Idaho Springs formation rocks, which he states has often been mapped as Pike's Peak granite, that consists of metasomatic alaskite rich in small xenoliths of biotite gneiss. A sample of this rock carried 40 ppm eU in the xenoliths and 16 ppm eU in the alaskite.

Most known uranium occurrences in the area are, however, related to northwest fracturing attendant on intrusion of the very much younger Redskin Granite.

In the interval between intrusion of the Boulder Creek granodiorite and the Pike's Peak Batholith, the Silver Plume granite, consisting of numerous small irregular igneous bodies, was intruded into the Idaho Springs formation at 1350 m.y. BP, and gave rise to some retrograde metamorphism. The Redskin Granite is a late phase of the 980-1060 m.y. BP Pike's Peak batholith composite pluton. It is enriched relative to the dominant pink granite of the Pike's Peak batholith in tin, lithium, rubidium, beryllium and fluorine, and contains topaz and fluorite as accessory minerals. Greisen pipes and northwest-trending fractures in the country rock associated with it contain fluorine and beryllium mineralization.

After intrusion of the Redskin Granite, the area was pediplained and then covered by Paleozoic and Mesozoic sediments. Major thrusting to the east along the shallow eastward-dipping Elkhorn Thrust brought Precambrian rocks over Mesozoic and Paleozoic rock. The area was then blanketed by Tertiary andesites, small patches of which remain on topographic highs.

Later Tertiary block faulting gave rise to the South Park Basin, the Tertiary fill of which has some potential for uranium deposits of the Wyoming roll-front type.

3.11.2 Uranium Deposits

3.11.2.1 In Precambrian Rocks

Ten known uranium occurrences exist in the Badger Flats area (Gallagher, 1976) one of which has produced uranium.

Six of these are veins in N30°W trending shears in Redskin, Pike's Peak, Silver Plume and Idaho Springs rocks. Mineralization is autunite, pitchblende, and torbernite and is less than 0.33% U_3O_8 .

A seventh deposit, the Gold Star, is apparently a strongly-altered breccia pipe of volcanic origin (Gallagher, 1976). It is visible on aerial photographs as a circular feature 400 ft. in diameter (i.e., covering about four Landsat pixels). The upper part of the deposit carries sporadic values with a maximum of 3.21% U_3O_8 , and is strongly enriched in lead and zinc.

The remaining three occurrences are in pegmatites, and all have grades less than 0.01% U_3O_8 . Gallagher (1976) indicates that pegmatites probably do not have significant potential for uranium production in this area.

Just northwest of the South Park area, the old Alma Mining District contains 24 uranium occurrences (Pierson and Singewald, 1953), all of them in Tertiary veins, mostly cutting Precambrian rock. This area drains into Tertiary rocks of South Park.

3.11.2.2 In Tertiary Rocks

The Eocene Echo Park alluvium and Oligocene Tallahassee Creek conglomerate were deposited in the paleochannels on an extensive Eocene erosion surface. They contain most of the known Tertiary uranium in the area in association with carbonaceous "trash pockets" (Young and Mickle, 1976). Abundant source rocks are present within the Tertiary section, in the form of Oligocene tuffs (Antero formation) and tuffaceous sediments. This type of deposit was not of prime interest in this project, but its presence on the same Landsat frame was an additional attraction of the area as a test area for the Rossing type of deposit.

3.11.3 Geometric Patterns and Textures Associated with Ore Deposits

Rossing-type deposits might have been detectable here by the same features that, it was hoped, would lead to their recognition in the Rossing area itself: areas of randomly oriented linear features associated with alaskite, and a coarser texture over massive acidic rocks. However, the task was expected to be much more difficult in this area due to:
1) very poor knowledge of the actual occurrence of alaskitic

rocks, and 2) presence of two younger granites whose textural characteristics might be expected to be much the same as those of the alaskites.

This area also has potential for vein-type deposits. If any technique had worked at Beaverlodge, the same technique may have been useful here. The same applies to exploration for Tertiary roll-fronts, to which any measures successful in the Pumpkin Buttes area could have been applied. However, since the techniques used were a total failure at Rossing and almost a total failure at Beaverlodge and Pumpkin Buttes, hence the South Park Area was not run.

4.0 PROCESSING OF DATA: PROCEDURES

At the beginning of the project, we had available a large number of choices of operators for texture processing and geometric pattern displays. We also had six separate training areas and six possible test areas to be considered. One of the first priorities in the project was to decide on appropriate subsets of texture measures (Appendix 1) and geometric pattern displays (Appendix 4) to apply to particular areas, since it was clear that the total possible number of combinations of all measures and displays, for all areas, would imply a prohibitively large number of computer runs.

The principal choices to be made on the selection of texture measures and geometric pattern displays were:

1. The use of difference histogram statistics versus the use of co-occurrence matrices in the calculations.
2. The use of distance-1 or distance-2 sampling for the evaluation of pixel properties.
3. The choice of the single measures (ENT, IDM, etc.--see Glossary of Appendix 10) or measure pairs (ENT/IDM, ENT/ASM, etc.) for discrimination between uraniumiferous and non-uraniferous windows.
4. The choice of display operator (texture transform, local stretch, etc.) for best presentation of enhanced texture information.

Broadly speaking, we tried to tackle the selection problem by proceeding sequentially. Thus, for texture measures we first examined whether difference histogram statistics or co-occurrence matrices (see Appendix 1) seemed statistically stronger for particular training areas. Based on this, we decided which of these two methods should be used

thereafter. We next considered the choice of distance-1 versus distance-2 or some higher distance function. Following that choice, we addressed the question of the best measure, or set of measures, to use for uranium/non-uranium area discrimination. Use of this sequential logic reduced the number of cases to be considered to a level that could be accomplished in the time and scope of the project.

In the case of the display operators, the set of logical decisions was more straightforward. The decisions were limited to the selection of those operators which showed promise in being able to discriminate uraniferous from non-uraniferous ground. We used two training areas (Copper Mountain and Pumpkin Buttes) to evaluate the texture display operators and applied that experience to decide how to proceed thereafter.

4.1 Texture Measures

All these experiments, and their results, are described in Section 5. The practical procedure for calculating texture measures is as follows. Before beginning the texture calculations, the satellite data base is divided into 64 x 64 pixel "windows." This window size was selected based on texture processing experience at the University of Maryland. The choice of window size represents a trade-off between spatial resolution of the window and statistical validity of the window's co-occurrence matrix. A 64 x 64 pixel window provides the best spatial resolution that maintains a statistically valid co-occurrence matrix. The co-occurrence matrix of the 4096 pixel values is generated for each window. From this matrix, the five texture measures are calculated.

The quarter frame "training areas" and "test areas" overlie regions of known and prospective uranium occurrence, respectively. Each quarter frame area consists of over 400 windows. In order to facilitate analysis and maintain reasonable computer costs, smaller "control areas" were selected within each training area. These control areas contain approximately 35 windows over known uraniferous ground and 40 windows over (presumed) non-uraniferous ground. The results of the texture measures calculated for each window are plotted as two dimensional plots, one measure versus another. These plots provide the basis for developing a bounding curve, or a "classification discriminant," for a given control area.

Each window, with its set of measures, can be regarded as a point in two-dimensional space (Figure 4.1.1). Discrimination between uraniferous and non-uraniferous windows is easy if all points from one set are clearly separated from all points of the other, i.e., if a bounding curve can be placed that separates the two sets. In practice, such a bounding curve is not useful unless it also has a simple form (by drawing a sufficiently complex curve, any two sets can be separated (Figure 4.1.2)). For this project we used a linear function as the bounding curve (Figure 4.1.3). Thus, only straight lines would be considered as suitable classification discriminants.

By reference to the IDM/ASM plots, such as the one for the Marysvale control area (Figure 4.1.3), a "best" line can be chosen as a classification discriminant, thus dividing the plot into two fields. Those windows which fall into the uranium field are assigned a uranium classification, and those which fall in the non-uranium

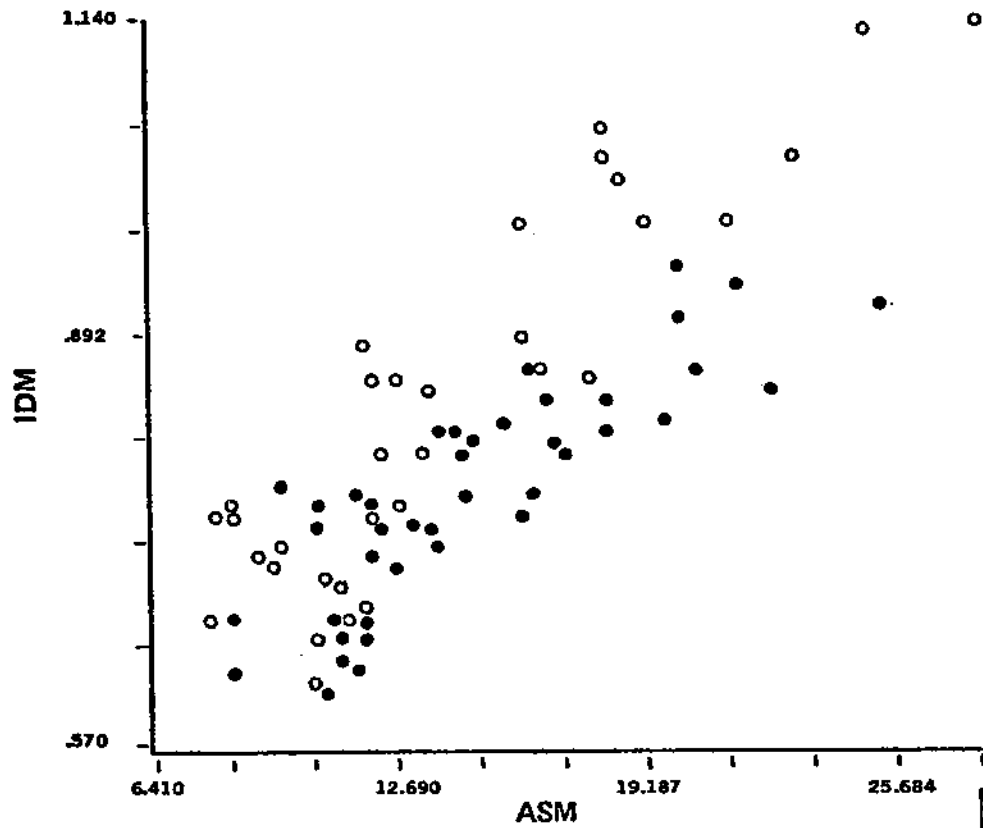


Fig. 4.1.1 Pumpkin Buttes, IDM/ASM plot for E1

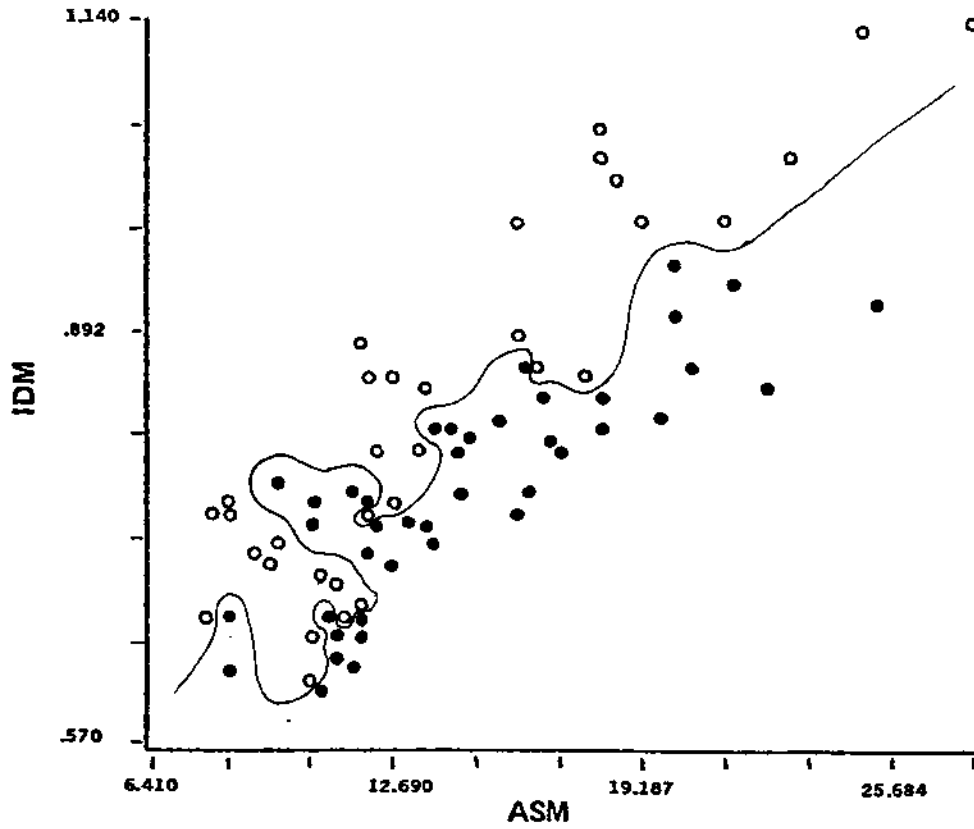
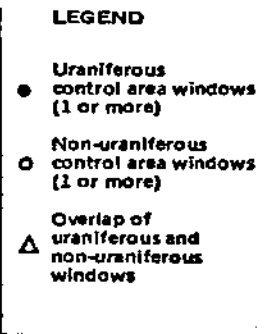


Fig. 4.1.2 Pumpkin Buttes, IDM/ASM plot with complex discrimination curve for E1

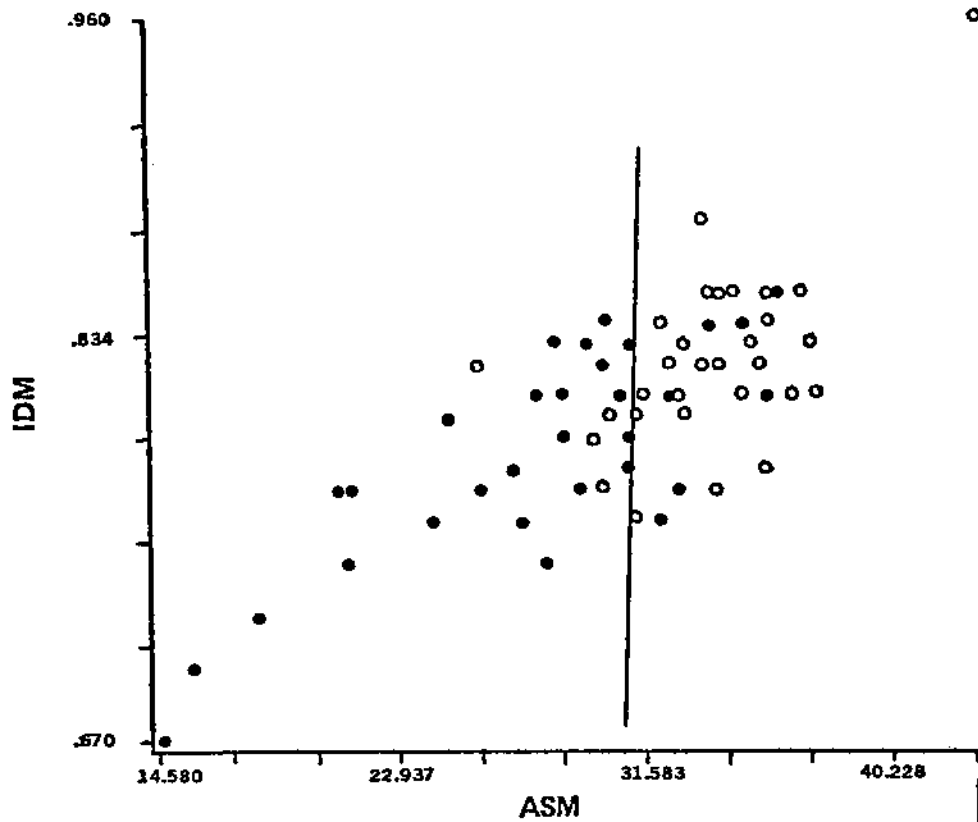
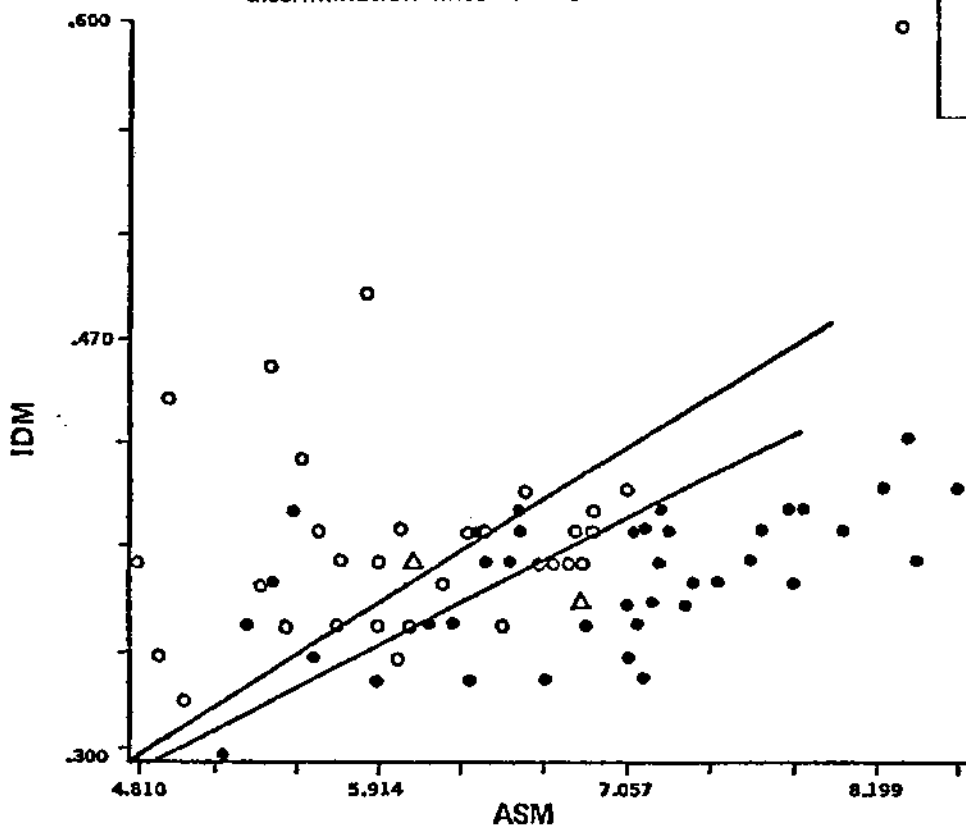


Fig. 4.1.3 Marysvale, IDM/ASM plot with vertical discrimination boundary for E3.

Fig. 4.1.4 Pumpkin Buttes, IDM/ASM plot with two discrimination lines for E3.



LEGEND

- Uraniferous control area windows (1 or more)
- Non-uraniferous control area windows (1 or more)
- △ Overlap of uraniferous and non-uraniferous windows

field are classified as non-uranium. It was necessary at Pumpkin Buttes to draw two lines (Figure 4.1.4) defining a "zone of overlap" in addition to the uranium and non-uranium fields. Those windows which fall within the overlap zone were assigned to a separate category in the final classification.

The sequential logic used in classifying a quarter frame training area is as follows:

1. Select control areas of known uraniferous and presumed non-uraniferous ground.
2. Calculate texture measures for the windows of the control area using the third eigen projection as the satellite data base.
3. Based on the IDM/ASM texture plot, choose a line, or lines, as the classification discriminant(s) dividing the plot into uranium and non-uranium fields.
4. Calculate texture measures for the windows of the quarter frame training area.
5. Test the IDM/ASM values of each window against the line chosen in Step 3, thus classifying the uranium potential of each window.

In classifying a quarter frame test area the line(s) chosen as the classification discriminant(s) at the control areas are applied to the test area. The sequential logic used is as follows:

1. Calculate texture measures for the windows of the quarter frame test area.

2. Test the IDM/ASM values of each window against the chosen line(s) thus classifying the uranium potential of each window.

Quarter frame areas were run for the Pumpkin Buttes and Grants training areas and the Poison Spider test area. The results of these runs are discussed in Section 5.0.

4.2 Display Operators

It was first necessary to decide which image product was the best on which to use the display operators. After trials on the original Landsat bands and on the Eigenbands, it was quickly apparent that Eigenband 1 provides the best data base for lineament interpretation.

The display operators available fell into two groups:

1. "Generalized" operators such as the texture transform and histogram stretches,
2. More specialized operators such as the line and edge detectors.

All of the display operators were tested on two areas. These were the same "control areas" used to establish the texture measure procedure.

As a result of this testing, which included comparison of the displays with the uranium distribution and the geology and topography of the areas, as well as total interpretation of the displays followed by comparison, a decision was made to concentrate on the second group of display operators, since the generalized operator either did not add much to the interpretability of the original image, or gave results that were uninterpretable in geologic terms. After testing in one

additional area, work was further restricted to the edge detector operator rather than the line operator. The line operators appeared insensitive to many of the features, essentially edges or boundaries, which make up "lineaments" on Landsat images, and thus much information was lost. However, the edge operator gave double lines where there really were lines on the ground, and were noisy. Therefore, the choice of operators to be used was limited again, by thresholding the outputs to reduce "noise," and by limiting the number of threshold levels that were examined to those that gave interpretable and, as far as possible, geologically meaningful, results.

5.0 RESULTS

Three different data sources, all obtained from the original Landsat Computer Compatible Tapes, were available for the application of texture measure and texture display operators. These sources consist of computer enhanced color combinations of the original bands of Landsat data (usually chosen as bands 4, 5, and 7); linear combinations of these original bands, consisting of Eigenbands 1, 2, 3, and 4; and band ratios, usually taken to be digital ratios of band 4/band 5, band 5/ band 6, and band 6/band 7. On the figures that follow, bands 4, 5, and 7 are denoted as B4, B5, and B7, and Eigenbands as E1, E2, E3, and E4.

For the Poison Spider frame, containing two training areas (Copper Mountain and Pumpkin Buttes), each of these image products was generated for analysis (Plates 1, 9, and 10). From an inspection of these, it is clear that the ratio products are badly contaminated by striping, which could not be removed by the EarthSat destriping algorithm. This is a property of all ratio products, reflecting the sensitivity of the ratios to detector quantizing effects. The overall effect of this striping on texture measures is considerable.

Although the human eye can compensate for and to some extent ignore the striping, computer measures of texture will be dominated, not by the true texture of the scene, but by the anomalies introduced by different detector sensitivities. Thus, the bulk of the texture in the ratio images is contributed by striping alone. For this reason, the idea of using the ratio products as the data source for computer analysis was abandoned early in the study, leaving the original four bands and the four Eigenbands as candidates for data sources.

The original bands of Landsat data are highly correlated, thus there was little point in working with all four. Bands 5 and 7 were

chosen for analysis, and texture measures and texture displays were developed for training areas using both of them. The four Eigenbands, on the other hand, are uncorrelated with each other, thus it seemed desirable to apply texture analyses to all four. There was an additional logic for working not only with the high-contrast Eigenband 1 and band 2, but also with the low contrast Eigenbands 3 and band 4; namely, earlier work by Lowitz (Reference 4) had suggested that texture information was specifically contained in the higher order Eigenbands.

The remainder of this section will discuss the results obtained from the application of the texture measure and geometric pattern operators to the various training and test areas. The results of the texture analysis at the various study areas are presented in generally the same order as they were processed. The discussion will first present the texture measure results, followed by a discussion of the texture display results.

5.1 Summary of Texture Measures

The first objectives of the texture measure study was to decide on the most favorable method of:

1. Sampling the satellite data, and
2. Calculating the individual texture measures.

Both of these objectives were achieved through an exhaustive study of the Copper Mountain test area. Texture measures were calculated for both the MSS 5 and MSS 7 data bases of the Copper Mountain training area in order to compare the merits of using the co-occurrence matrices vs. difference histograms and sampling at single pixel distances vs. sampling at a distance of two pixels.

As will be discussed later in this section, the texture measures were unsuccessful in being able to separate adequately the uraniferous and non-uraniferous control areas at Copper Mountain. There were, however, three conclusions to be drawn as to the best way to proceed in calculating and analyzing the texture measures:

1. Any advantage of using the co-occurrence matrix over the difference histogram was not apparent from the texture measure results at Copper Mountain; however, previous experience suggested that the co-occurrence matrix would be less sensitive to any overall brightness changes across an individual image, or when moving from one image to another. Previous experience with texture measures also indicates that there is no significant difference between the histogram difference and the co-occurrence matrix methods in terms of their sensitivity to window sample size.
2. Sampling at one pixel distance did appear to have a slight advantage over sampling at two pixel distances. This supported the a priori assumption that textures associated with uranium mineralization would be fine grained and therefore more apparent at close pixel spacings.
3. In presenting the results of the texture measures for analysis, it was found that two dimensional plots (plotting one texture measure against another) provide the best separation of the uraniferous and non-uraniferous control area windows. In all subsequent runs, texture measures were plotted as the ten unique paired combinations of the five measures.

Having decided the best approach for calculating the texture measures, the next objective was to decide which texture measure combination, applied to which satellite data base, best discriminates between the windows of the uraniferous and non-uraniferous control areas. This objective was achieved through the extensive texture study (see Section 4.1) of the Pumpkin Buttes training area. At Pumpkin Buttes, the plots of all ten texture measure combinations were analyzed for a total of six different data bases. The six data bases consisted of band 5, band 7, and the four eigen projections (E1, E2, E3, and E4 -see Appendix 2). The various combinations of the six data bases and ten texture measure pairs can be expressed as a 6 x 10 matrix. From a study of the resulting 60 plots, we selected the IDM/ASM measures calculated from the third Eigenband (E3) as displaying the best discrimination between the windows of the uraniferous and non-uraniferous control areas at Pumpkin Buttes.

The following two collections of texture plots present two transects across the 6 x 10 matrix (see Figure 5.1.1). The first collection of plots (Figures 5.1.2-5.1.7) are the IDM/ASM texture measures for the Pumpkin Buttes control areas applied to the six different data bases (B5, B7, E1, etc.). The second collection, consisting of ten plots (Figures 5.1.8-5.1.17) are the results at the Pumpkin Buttes control areas for the ten texture measure pairs (ENT/ASM, COR/ASM, etc.) applied to the E3 data base.

We should note that the performance of E3 as the best band for the discrimination of texture information is not too surprising. It was already noted by Lowitz (1976) in experiments analyzing data from a seven-channel scanner, that the higher order Eigenbands seem

6 x 10 Matrix

		SATELLITE DATA BASE					
		<i>B5</i>	<i>B7</i>	<i>E1</i>	<i>E2</i>	<i>E3</i>	<i>E4</i>
TEXTURE MEASURE PAIR	<i>ENT/ASM</i>	x	x	x	x	(x)	x
	<i>CON/ASM</i>	x	x	x	x	(x)	x
	<i>IDM/ASM</i>	(x)	(x)	(x)	(x)	(x)	(x)
	<i>COR/ASM</i>	x	x	x	x	(x)	x
	<i>ENT/IDM</i>	x	x	x	x	(x)	x
	<i>COR/IDM</i>	x	x	x	x	(x)	x
	<i>CON/ENT</i>	x	x	x	x	(x)	x
	<i>COR/ENT</i>	x	x	x	x	(x)	x
	<i>CON/IDM</i>	x	x	x	x	(x)	x
	<i>CON/COR</i>	x	x	x	x	(x)	x

Figure 5.1.1 This 6 x 10 matrix is a graphic representation of the various possible combinations of data bases and texture measure pairs. An 'x' is used to designate those combinations processed for the Pumpkin Buttes control areas. An '(x)' is used to designate those combinations presented in this report.

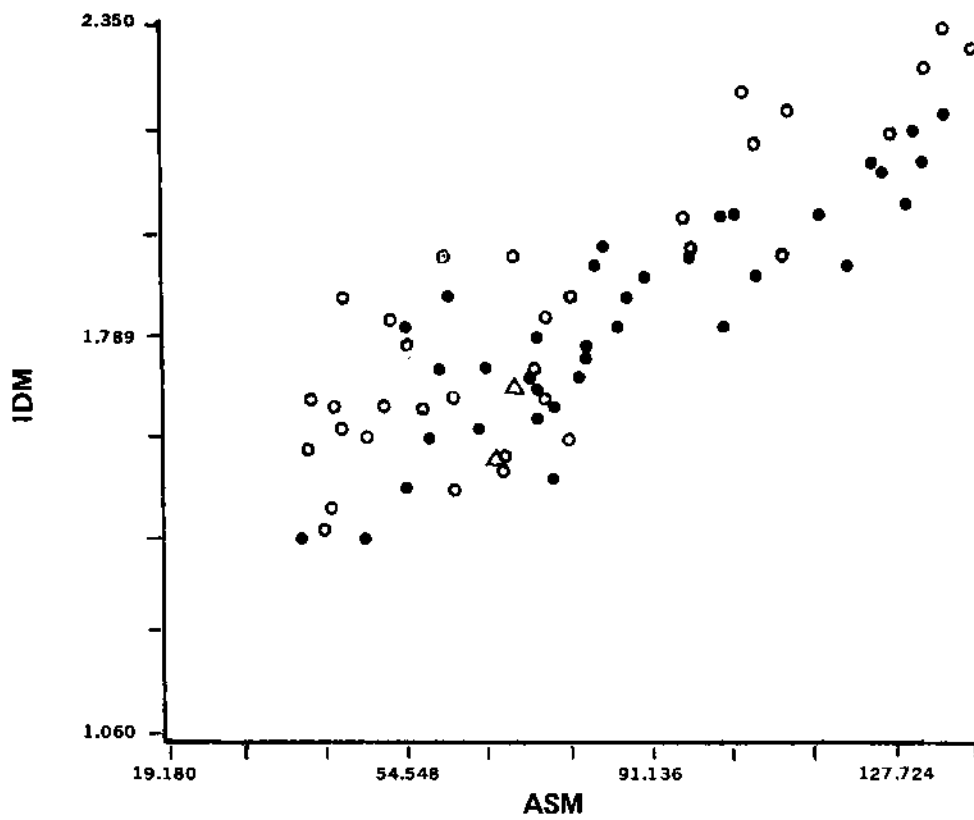


Fig. 5.1.2 Pumpkin Buttes, IDM/ASM plot for B5

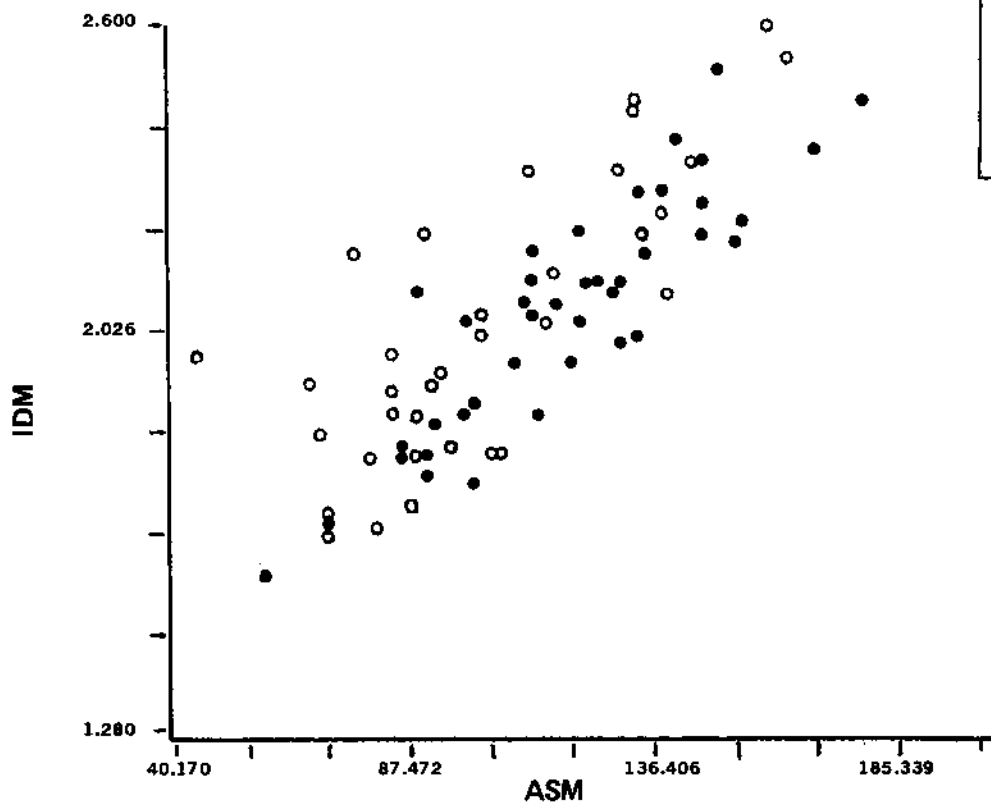


Fig. 5.1.3 Pumpkin Buttes, IDM/ASM plot for B7

LEGEND

- Uraniferous control area windows (1 or more)
- Non-uraniferous control area windows (1 or more)
- △ Overlap of uraniferous and non-uraniferous windows

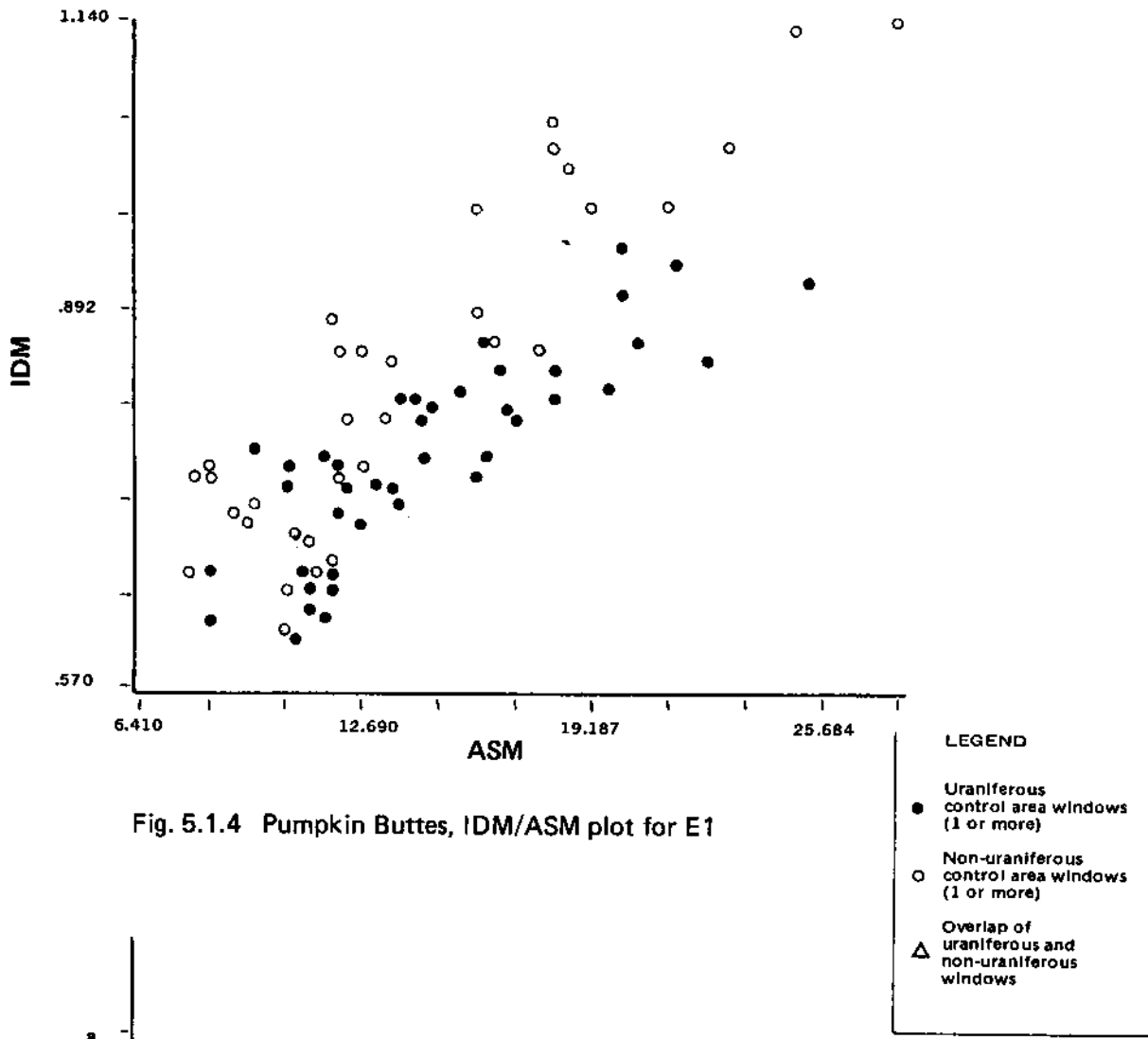


Fig. 5.1.4 Pumpkin Buttes, IDM/ASM plot for E1

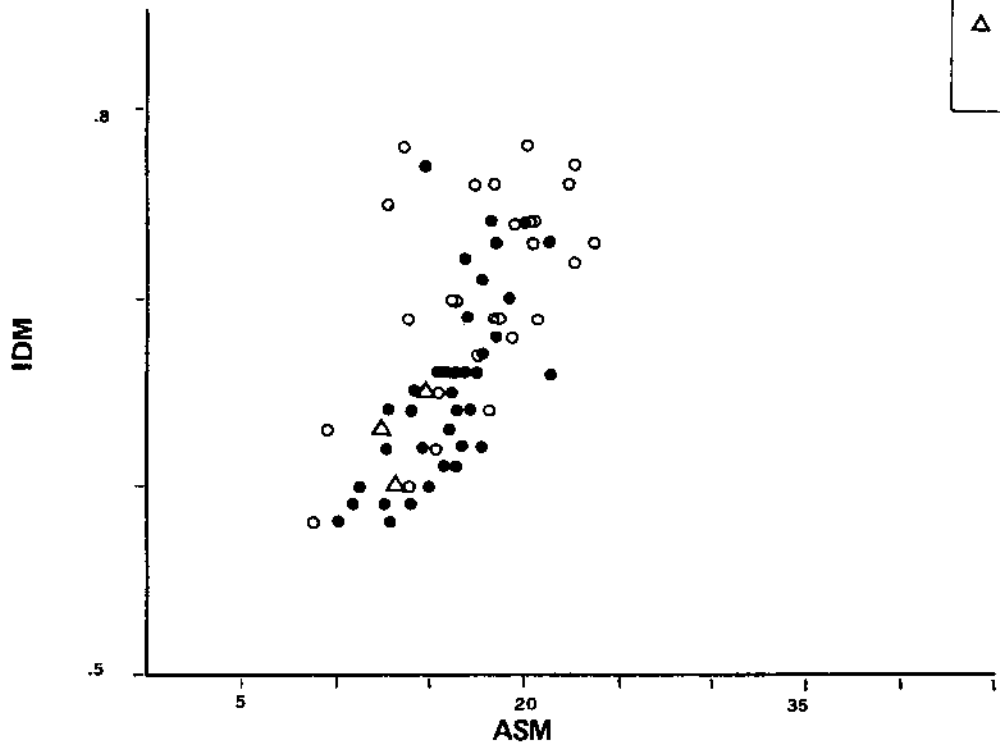


Fig. 5.1.5 Pumpkin Buttes, IDM/ASM plot for E2

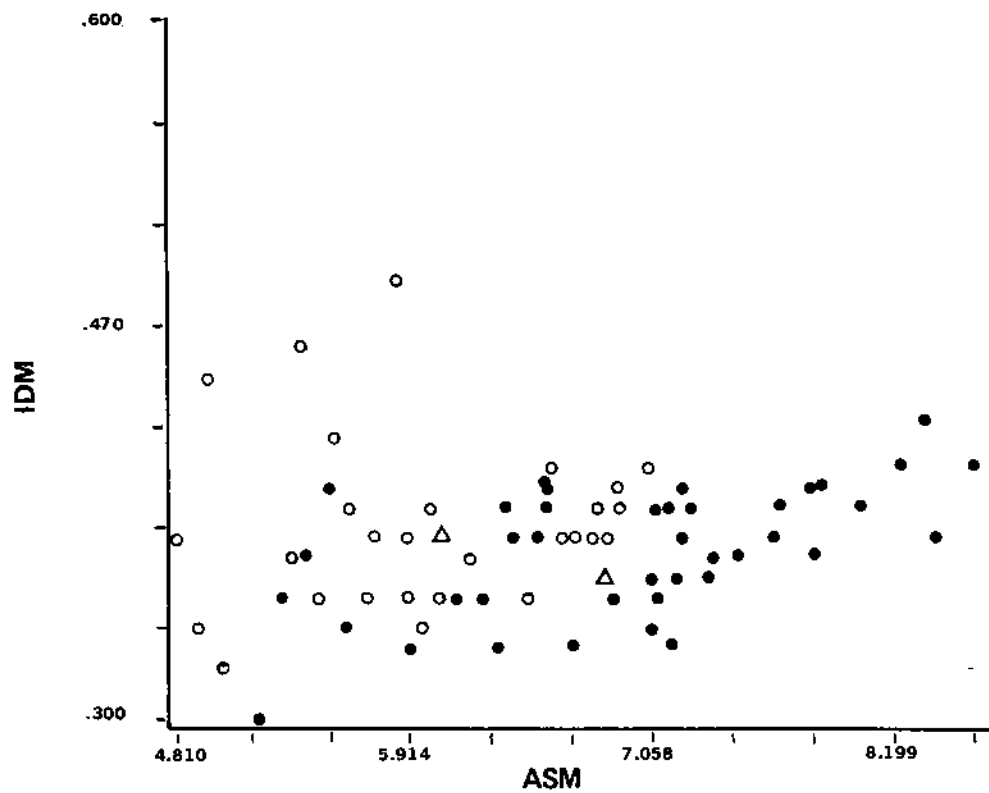


Fig. 5.1.6 Pumpkin Buttes, IDM/ASM plot for E3

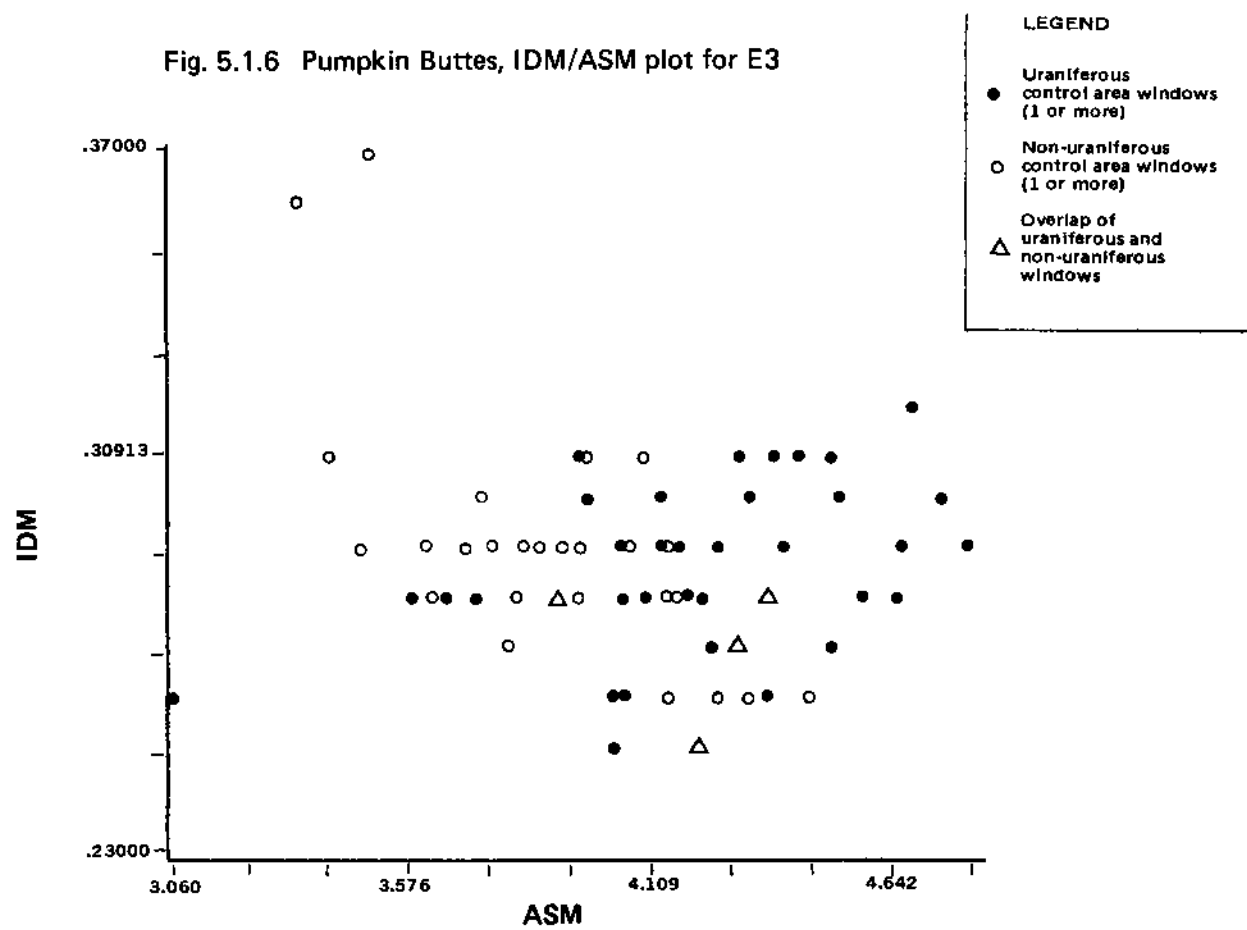


Fig. 5.1.7 Pumpkin Buttes, IDM/ASM plot for E4

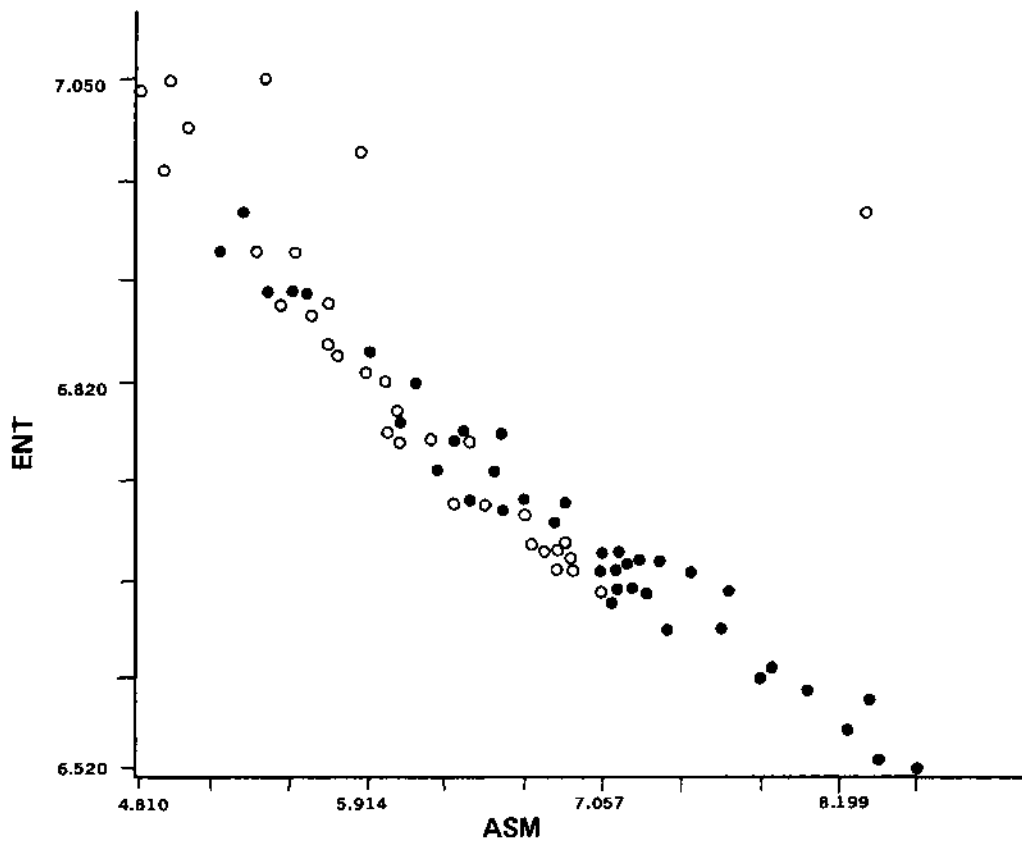


Fig. 5.1.8 Pumpkin Buttes, ENT/ASM plot for E3

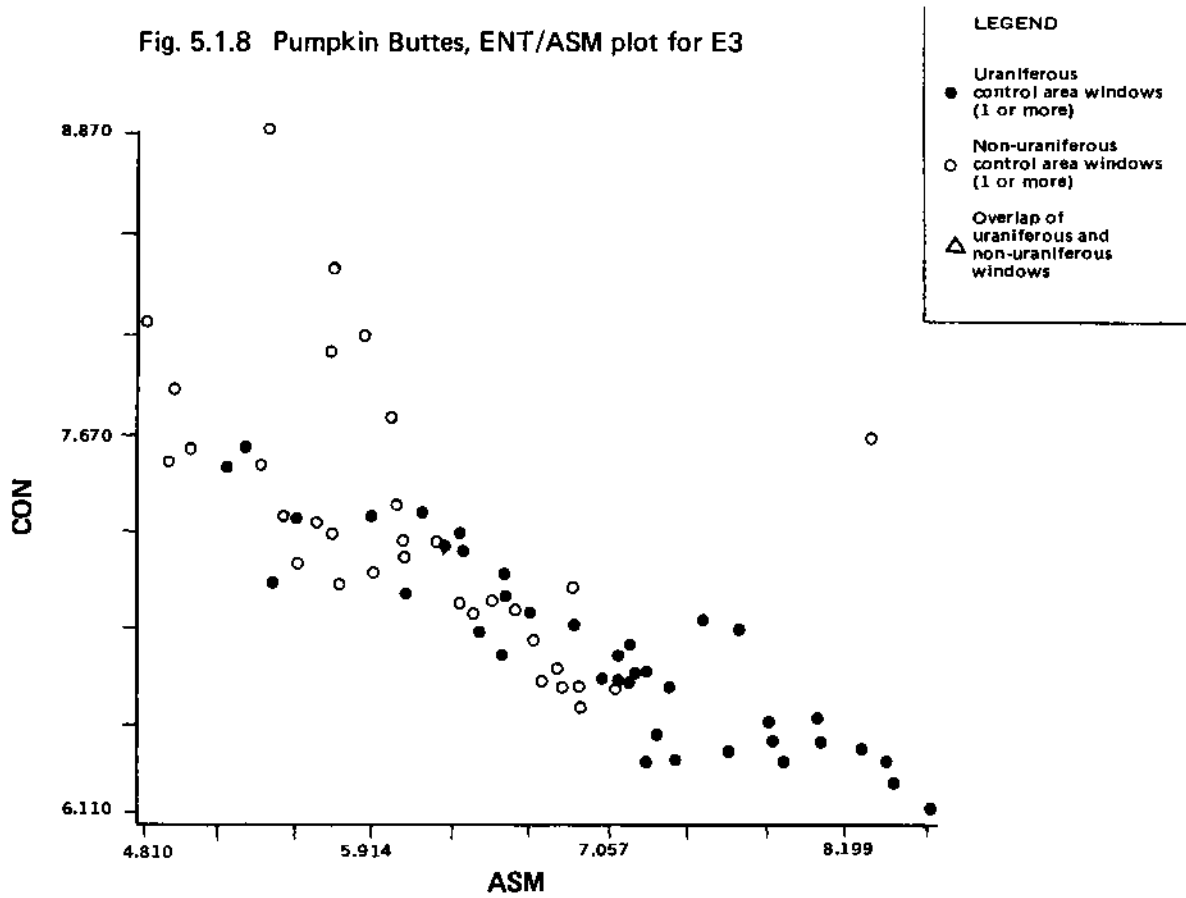


Fig. 5.1.9 Pumpkin Buttes, CON/ASM plot for E3

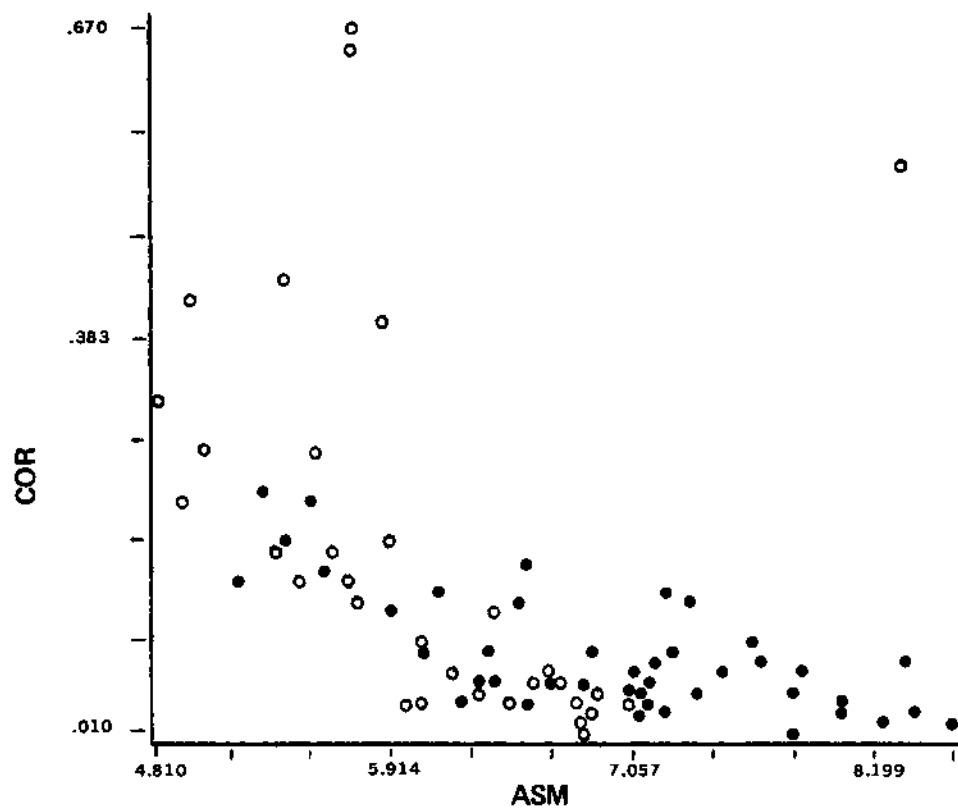


Fig. 5.1.10 Pumpkin Buttes, COR/ASM plot for E3

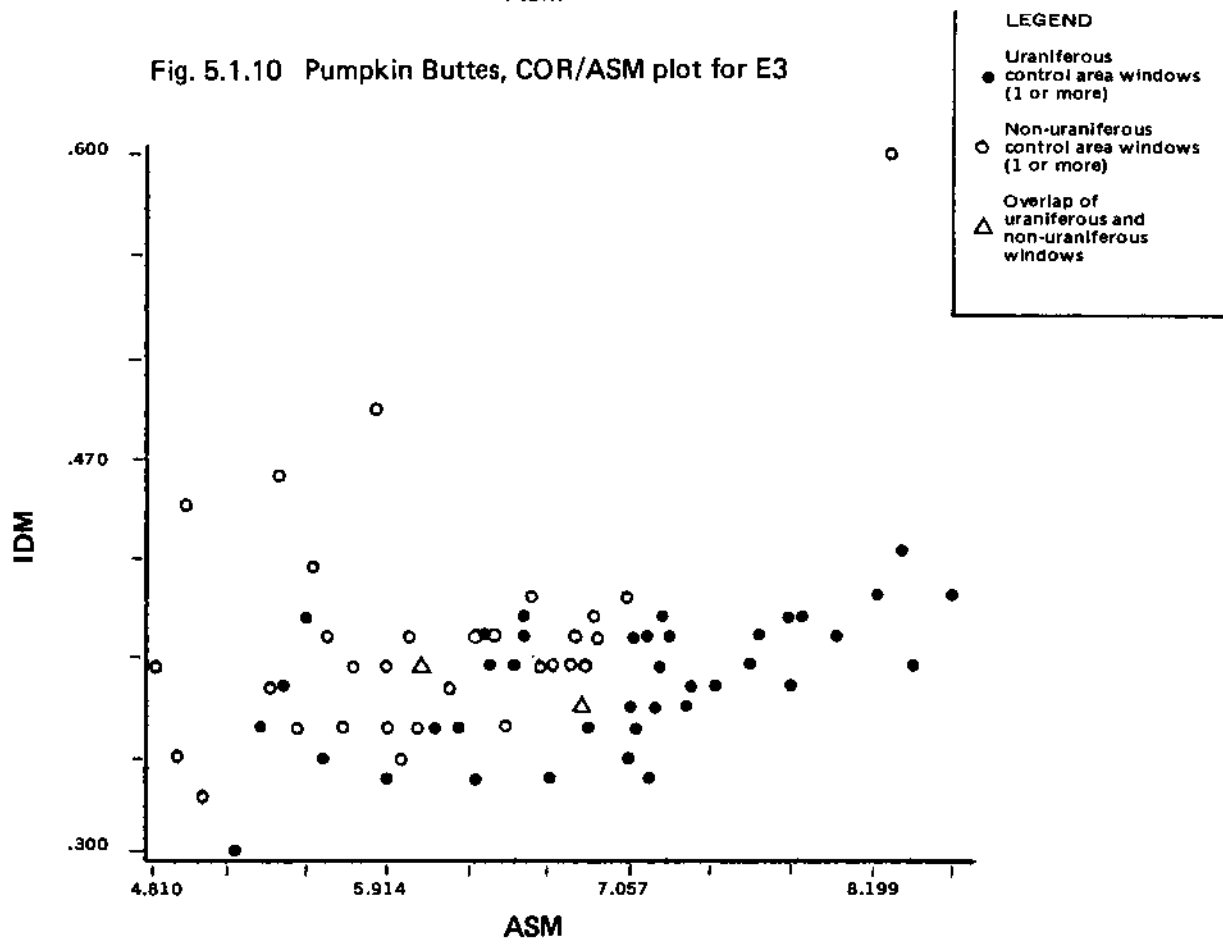


Fig. 5.1.11 Pumpkin Buttes, IDM/ASM plot for E3

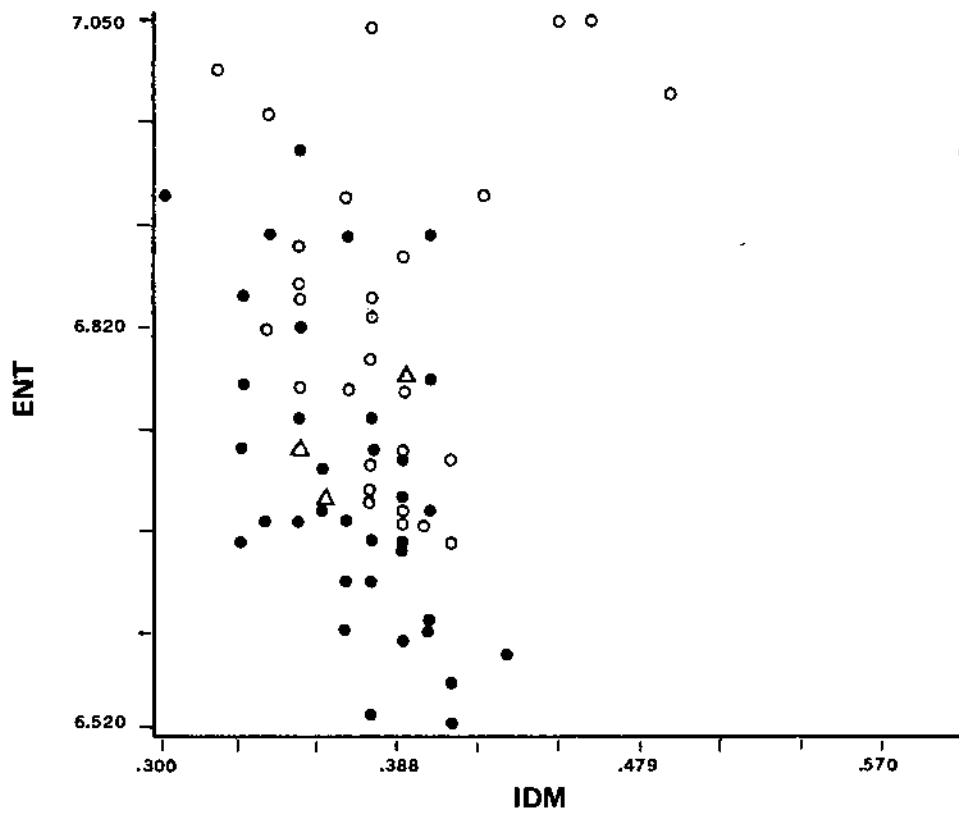


Fig. 5.1.12 Pumpkin Buttes, ENT/IDM plot for E3

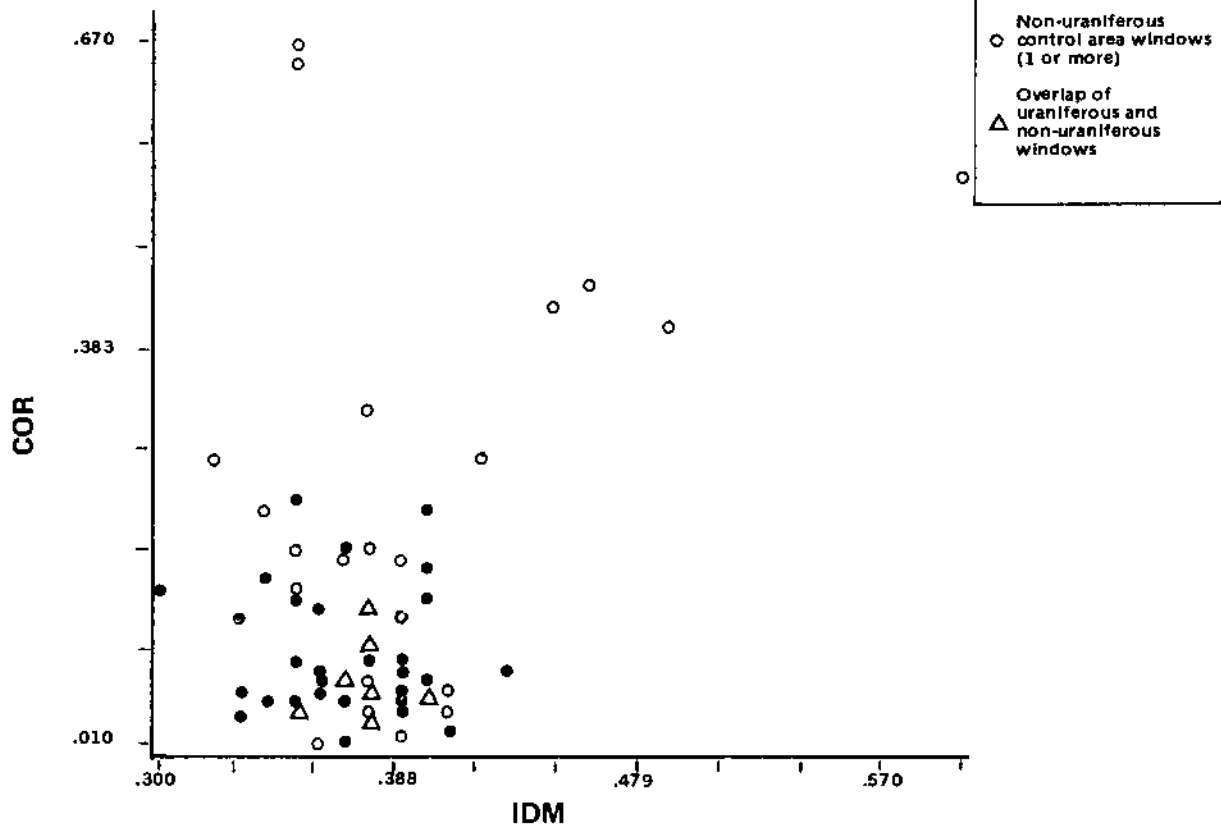
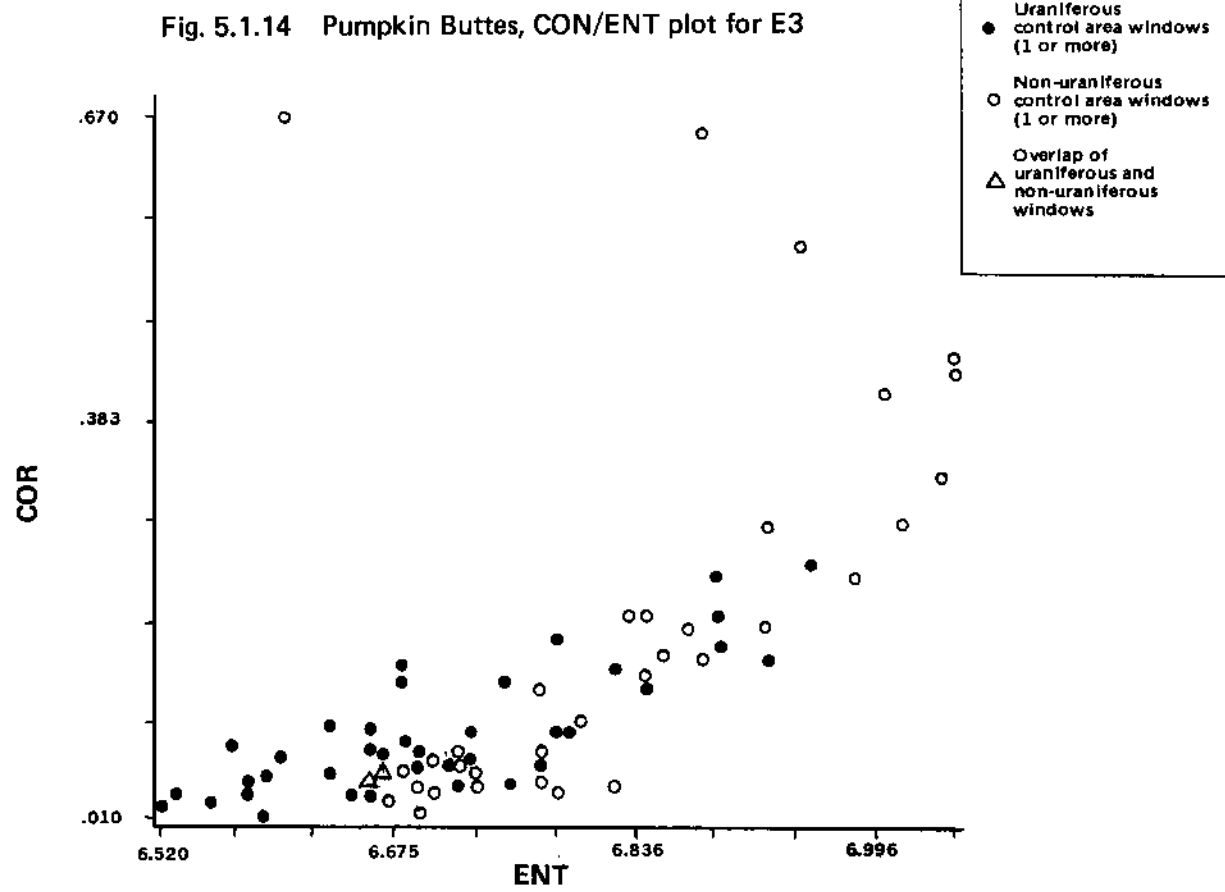
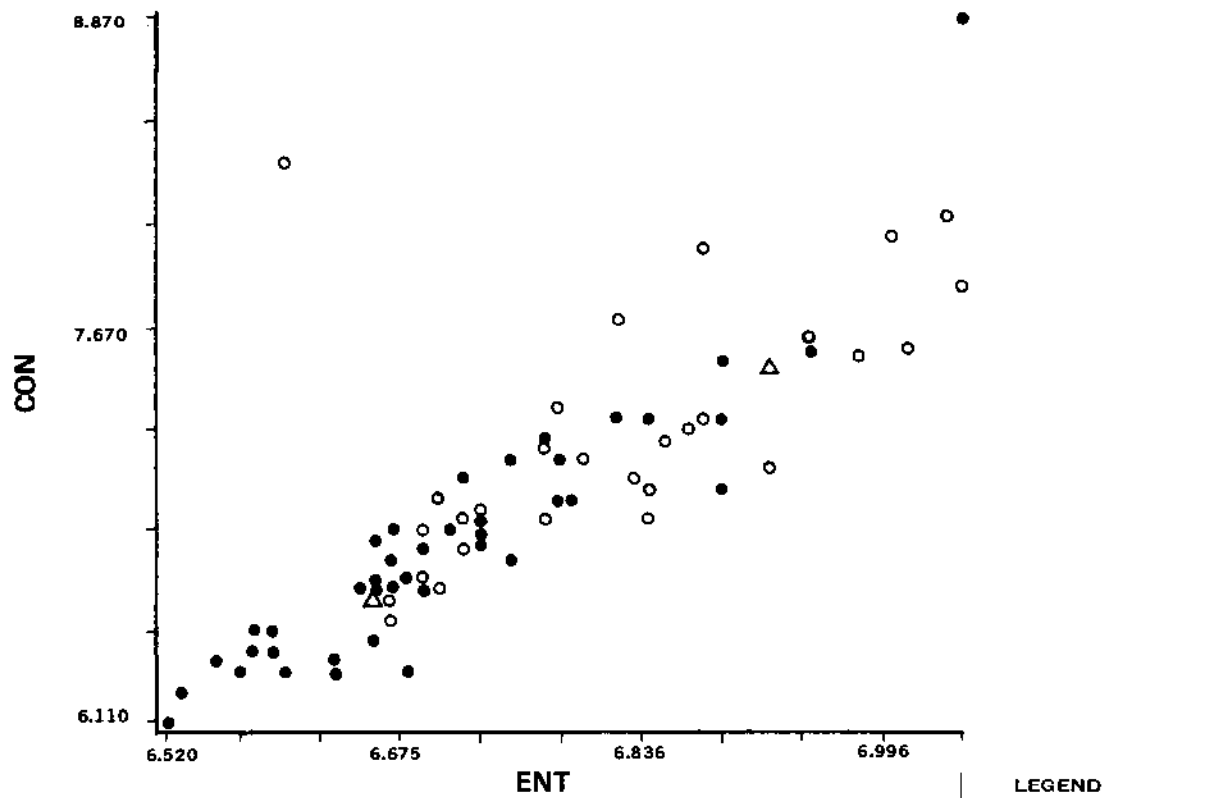
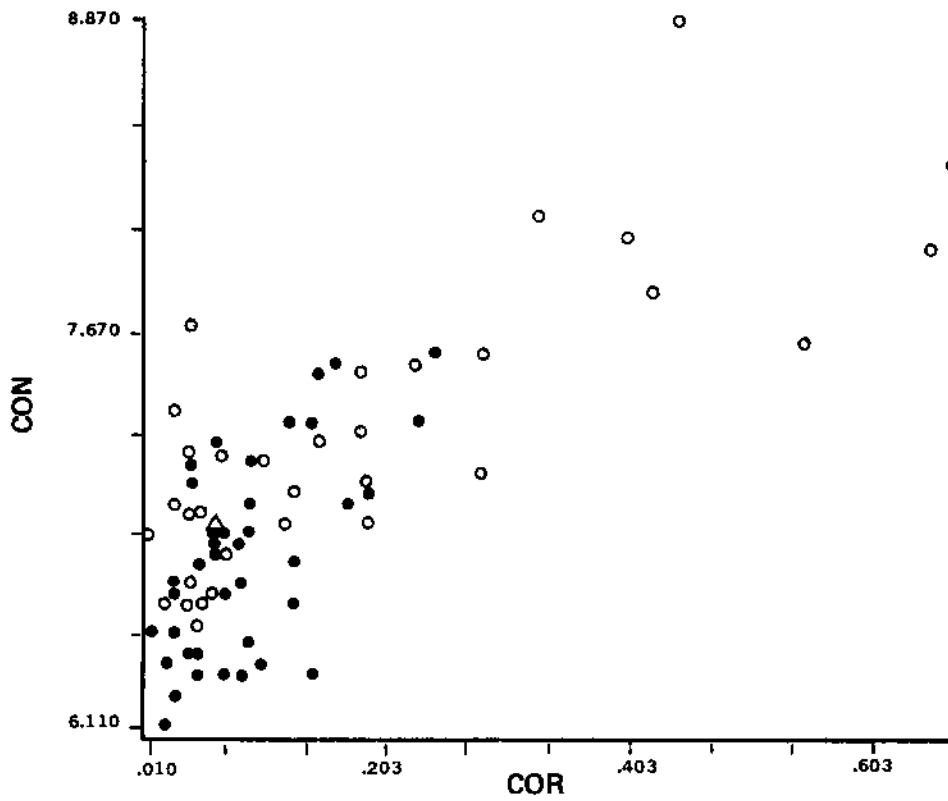
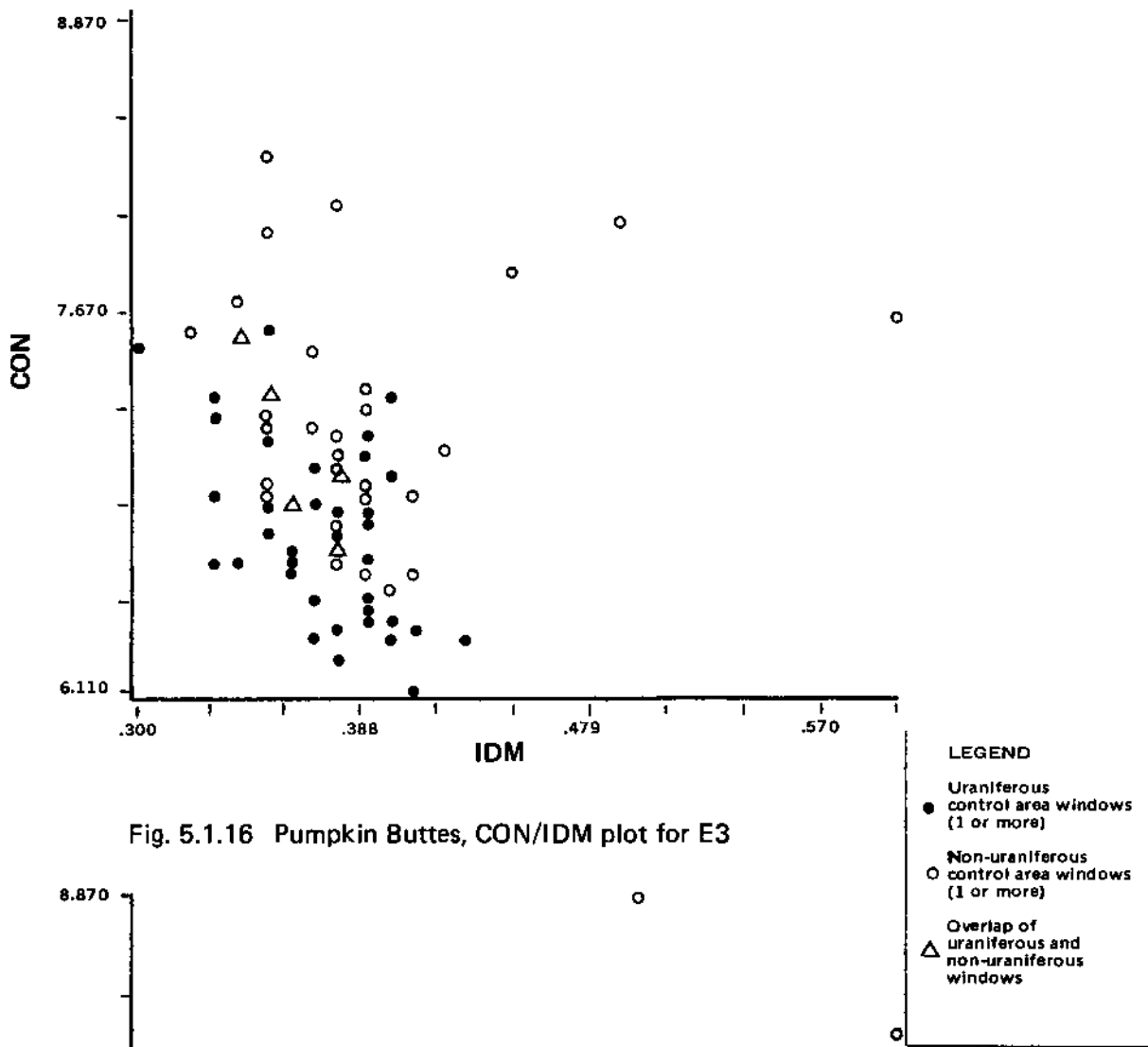


Fig. 5.1.13 Pumpkin Buttes, COR/IDM plot for E3



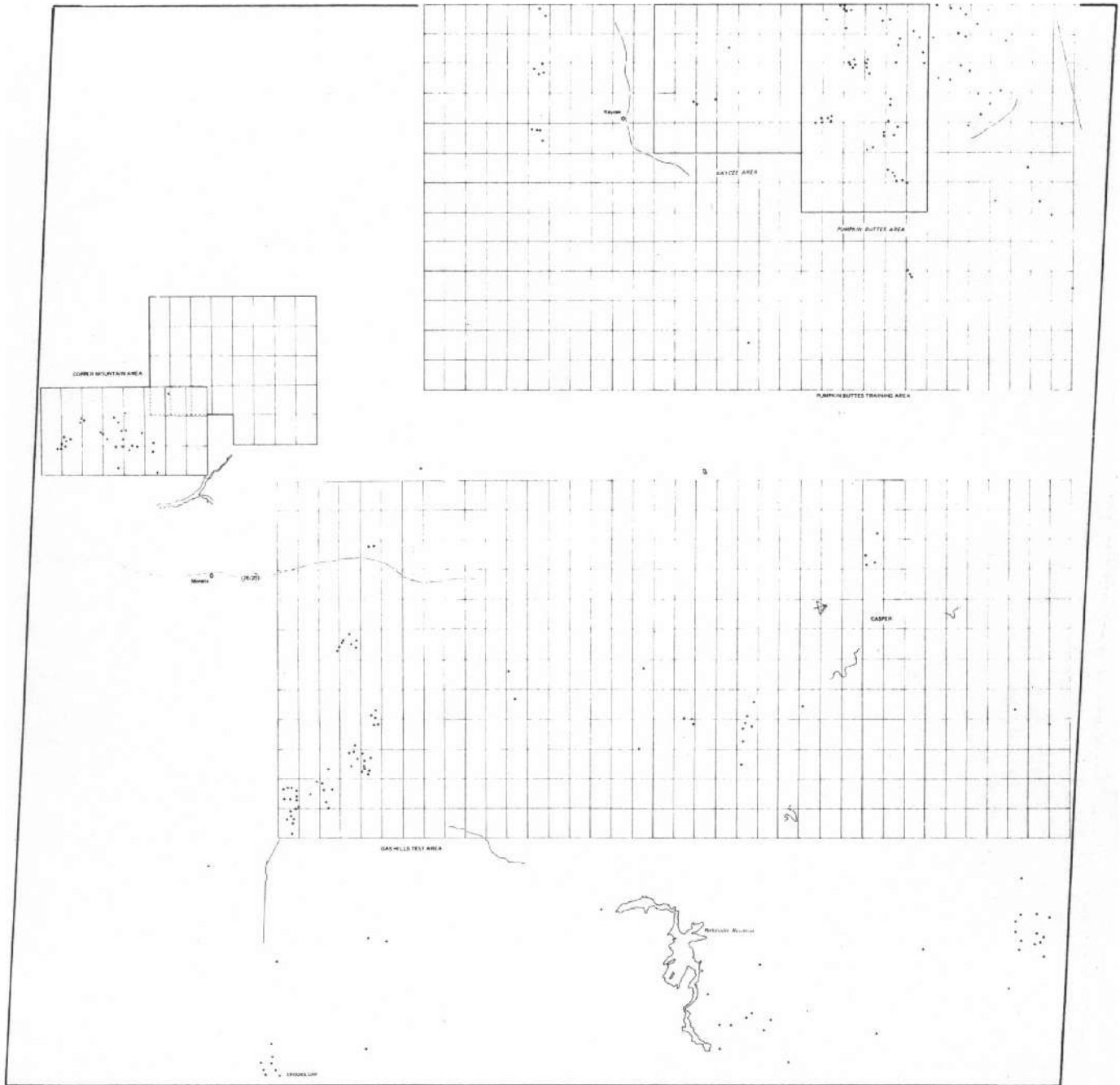


to carry most of the textural information. The logic presented for this fact is that the principal Eigenbands account for most of the large variations in overall scene contrast, leaving the higher order Eigenbands available to pick up the fine changes in grey level that characterize the texture of a scene. Lowitz found that the main texture seemed to be in Eigenbands 3 and 6, with Eigenbands 1 and 2 accounting for most of the scene tonal variance, and Eigenband 7 being largely noise (Reference 4). In our case, Eigenbands 1 and 2 account for most of the variance, and Eigenband 4 is mainly noise.

5.1.1 Copper Mountain - Results of Texture Measures

Two sets of control area windows were selected in the Copper Mountain study area (Plate 11, Figure 5.1.1.1). These were the first sets of windows to be processed, and as such, inexperience led to a slight mistake in registration and resulted in a small overlap of the uraniferous and non-uraniferous areas.

The texture measures for the control area windows were by using the band 5 and band 7 satellite data bases. For both satellite bands, five texture measures were calculated using both the co-occurrences matrices and distance histograms (see Appendix 1). The satellite data used in these calculations were separately sampled at one and two pixel spacings (see Appendix 1). Based on this exhaustive processing, the technique of using the co-occurrence matrix sampled at one pixel spacing was calculated to be the most sensitive to textural information in the satellite data. An additional decision



PREPARED BY
EARTH SATELLITE CORPORATION
WASHINGTON, D. C.

**URANIUM OCCURRENCE MAP
FOR A PORTION OF
WYOMING**

JUNE 1979
C-1152



Figure 5.1.1.1. 4X-reduction of image overlay. See original for details.

drawn from the Copper Mountain work was the choice of displaying the texture measure results as two dimensional plots, rather than one dimensional bar graphs. The two dimensional approach produces ten unique paired combinations of the five texture measures. This decision was based on the observation that the uraniferous and non-uraniferous windows were often able to be differentiated on a two dimensional plot, whereas, they were not able to be clearly differentiated on a bar graph of a single texture measure. Projection of the data points of the two dimensional plots onto one axis will, in effect, produce a one dimensional bar graph. If uraniferous and non-uraniferous windows can be differentiated by a single texture measure in the two-dimensional plot, then the discriminant used will be parallel to one axis (see Figure 4.1.3.). In such a case, a bar graph of the appropriate measure will also discriminate uraniferous from non-uraniferous windows.

The results of the band 5 and band 7 studies at Copper Mountain, although sufficient to determine the best technique for calculating the texture measures, did not adequately separate the uraniferous and non-uraniferous control area windows.

The technique developed at Copper Mountain was next applied to band 5, band 7, and the four Eigenbands for the Pumpkin Buttes control areas (see Section 5.1). From the Pumpkin Buttes control areas (see Section 5.1). From the Pumpkin Buttes study it was concluded that the IDM/ASM plot of the texture measures calculated from the third Eigenband was

the most promising for detecting subtle textures associated with uranium mineralization.

For completeness, the Copper Mountain control area windows were then also processed using the third Eigenband data for the Wyoming scene. The ten texture pair plots were generated and analyzed for the possibility of separating the uraniferous and non-uraniferous windows. As predicted by the Pumpkin Buttes study, the IDM/ASM plot (Figure 5.1.1.2) was indeed the most promising. However, the large degree of overlap in all plots, including IDM/ASM, rendered them useless as a discriminating tool between uraniferous and non-uraniferous windows. The overlap observed on the texture measure plots was far greater than could be explained by the accidental overlap of control area windows.

We conclude from the poor performance of the IDM/ASM and all other texture measure operator pairs that any texture associated with uranium mineralization at Copper Mountain is not detectable by this approach of texture analysis.

5.1.2 Pumpkin Buttes - Results of Texture Measures

Location of uranium occurrences and classification of selected windows for the Wyoming study areas are given as two overlays (Plates 11 and 12, and Figures 5.1.2.1 and 5.1.2.2, respectively) to the GEOPIC false color composite (Plate 1) of Landsat frame #1786-17135.

Two control areas, outlined with bold lines on the overlays (Figure 5.1.2.1), were selected within the Pumpkin

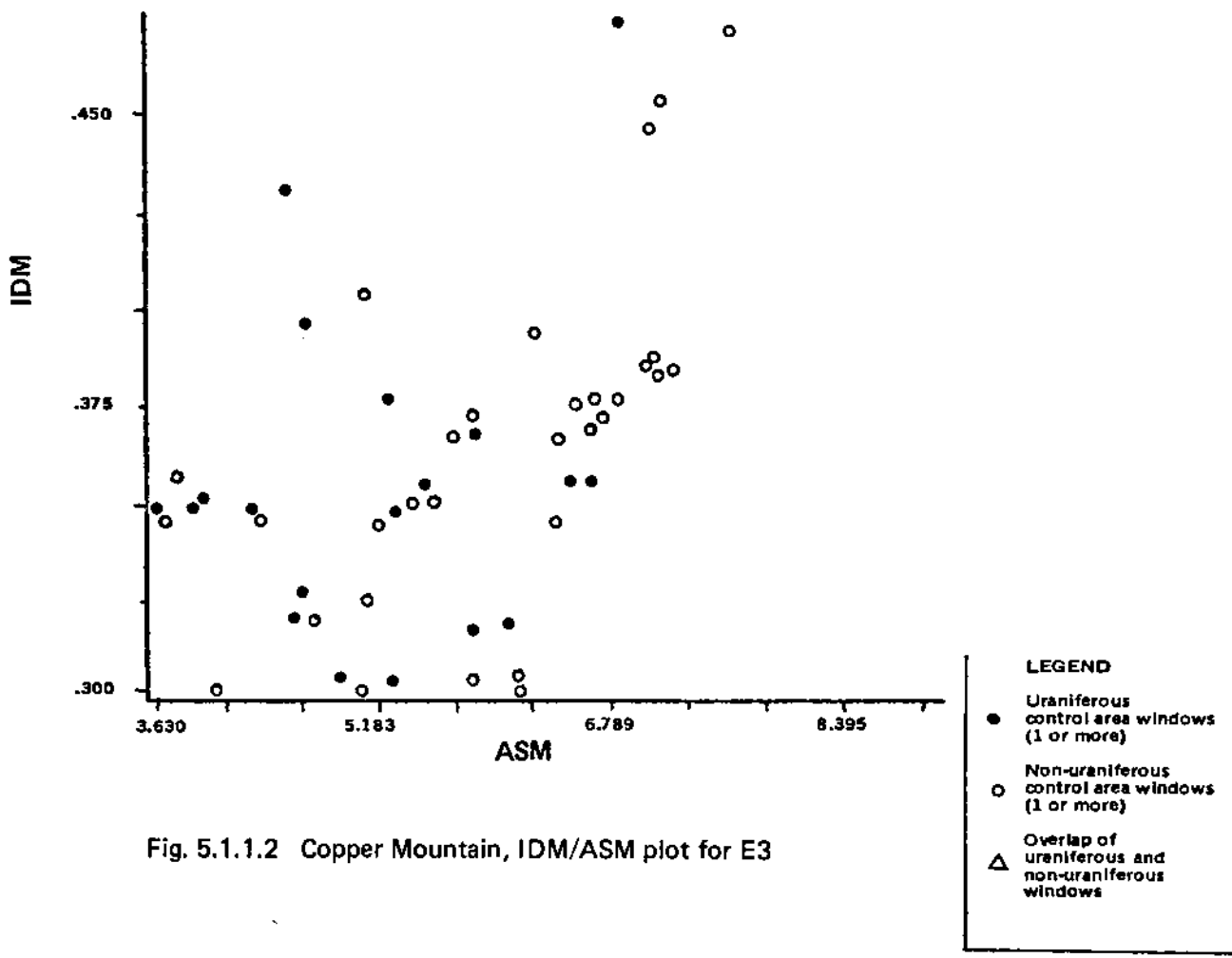
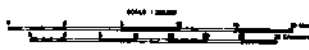
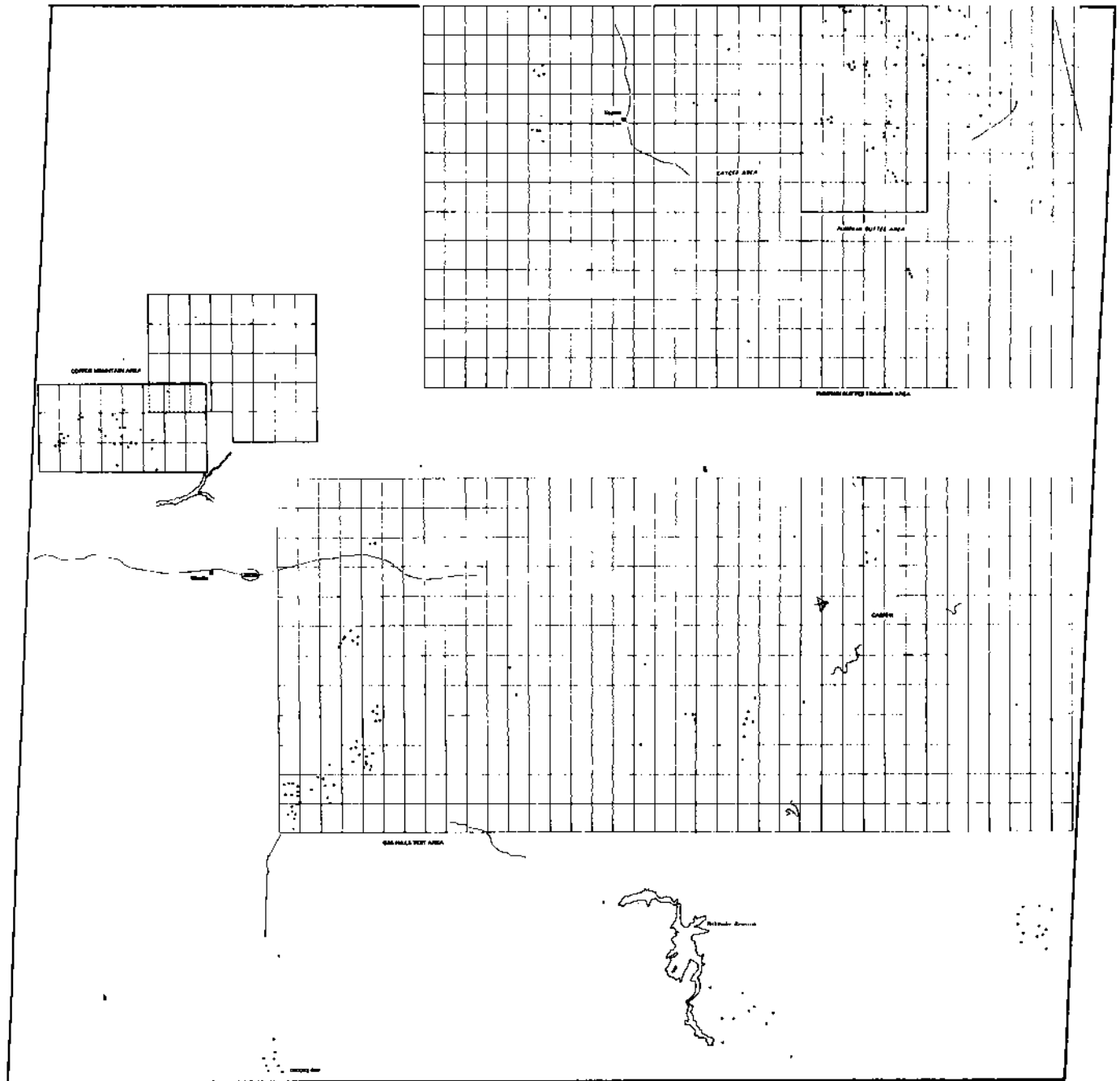


Fig. 5.1.1.2 Copper Mountain, IDM/ASM plot for E3

Buttes training area. The eastern block of windows lies over Pumpkin Buttes proper, comprising the uraniferous control area. Those windows in the western control area overlies the Kaycee area (Figure 5.1.2.1) which is largely non-uraniferous terrain.

The texture measure operators were applied to the third Eigenband (E3) data and the results of the IDM and ASM operators were displayed as a two dimensional plot (Figure 5.1.2.3). Two lines were selected which divided the plot into three fields: an upper field of mostly non-uraniferous control area windows, a lower field of mostly uraniferous control area windows, and a narrow zone of overlap between the two. Following the procedure described in Section 4.1, the quarter frame training and test areas of the Pumpkin Buttes and Gas Hills regions respectively were then processed.

The IDM/ASM measures correctly classified 74% of the known uranium occurrences (Table 5.1.1). However, as seen in Table 5.1.2, this was at the cost of classifying a very large proportion (50%) of the ground involved as being of "high uranium potential." Table 5.1.2 also shows that, in the Pumpkin Buttes area, the method was statistically good at rejecting land with no known uranium deposits: only 2% of the windows classified "non-uraniferous" have a known uranium occurrence, thus 32% of the total area could be eliminated from further consideration on this basis. However, 12% of the windows classified "medium potential" had known uranium occurrences. These two classes account for 68%, or over 2/3 of the ground windowed. From this it follows that approximately 50% of the total area is shown as having high uranium



PREPARED BY
EARTH SATELLITE CORPORATION
 WASHINGTON, D. C.

**URANIUM OCCURRENCE MAP
 FOR A PORTION OF
 WYOMING**

JUNE 1973
 C-253

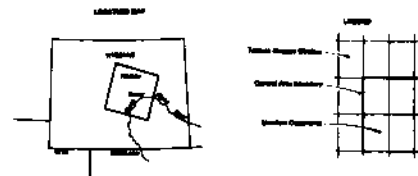
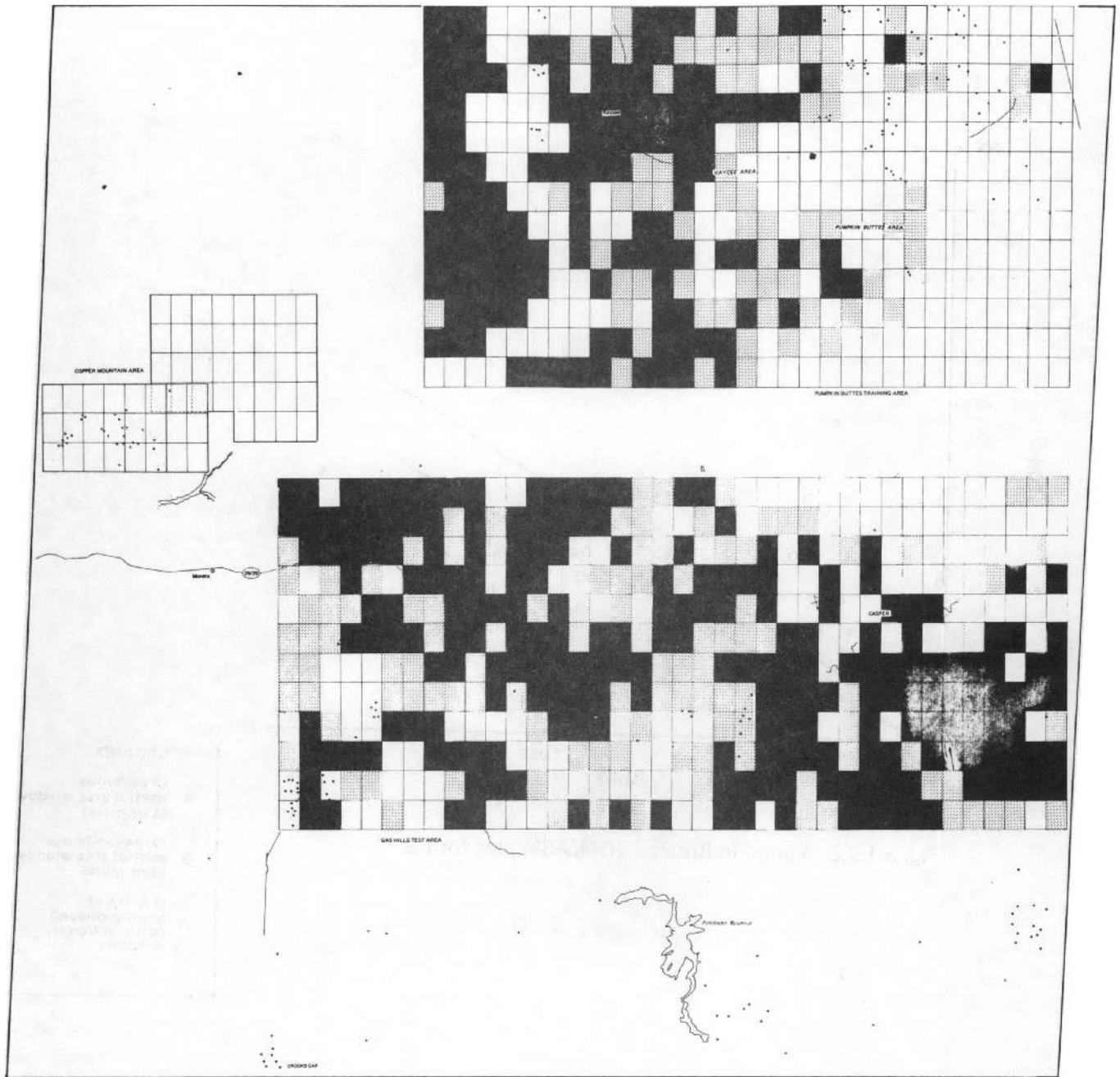


Figure 5.1.2.1. 4X-reduction of image overlay. See original for details.



PREPARED BY
EARTH SATELLITE CORPORATION
 WASHINGTON, D. C.

**CLASSIFICATION MAP
 FOR A PORTION OF
 WYOMING**

JUNE 1969
 C-1193

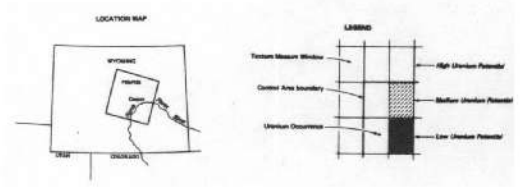


Figure 5.1.2.2. 4X-reduction of image overlay. See original for details.

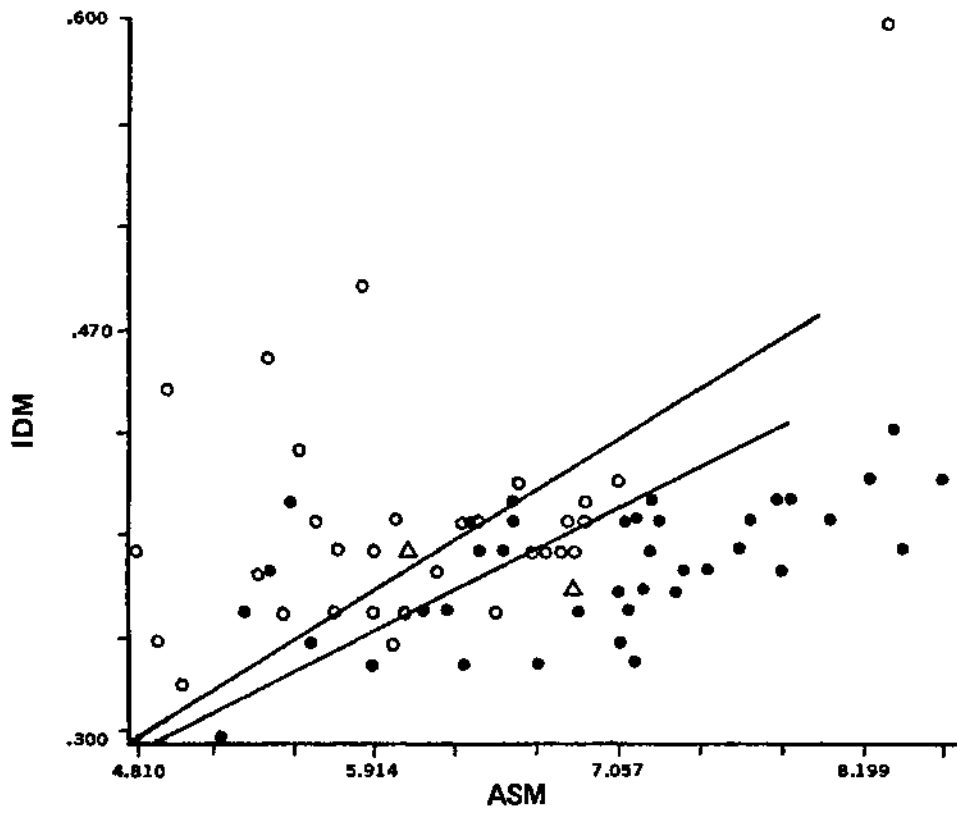


Fig. 5.1.2.3 Pumpkin Buttes, IDM/ASM plot for E3

- LEGEND**
- Uraniferous control area windows (1 or more)
 - Non-uraniferous control area windows (1 or more)
 - △ Overlap of uraniferous and non-uraniferous windows

potential but no known occurrences. The method would appear, therefore, to be very inefficient in the explorationists' sense of drastic restriction of surface area to be surveyed in detail.

Table 5.1.1 Pumpkin Buttes Area: Degree of Correct
Classification of Known Uranium Occurrences

	<u>Number</u>	<u>% of Total</u>
Uranium occurrences falling with windows classified as having high potential for uranium mineralization.	43	74
Uranium occurrences falling within windows classified as having medium potential for uranium mineralization.	10	17
Uranium occurrences falling within windows classified as having low potential for uranium mineralization.	5	9
Totals	58	

Since such a large proportion of the total area was classified as being of "high" or "medium" uranium potential, it is believed that the texture measure was probably identifying some gross textural feature, or set of features, that is related to topography, underlying geology, etc. An attempt

Table 5.1.2 Correlation of Texture Measure Output with Known Uranium Distribution for the Pumpkin Buttes Training Area

(A) Raw Data Values

Classification by Texture Measure Method	Number of Windows with Uranium Deposits	Number of Windows with no Uranium Deposits	Number of Windows in Each Uranium Potential Category
High uranium potential	30	173	203
Medium uranium potential	9	64	73
Low uranium potential	3	127	130
Total number of windows that have or lack uranium deposits	42	364	406

(B) Percentage Values

Classification by Texture Measure Method	Percent of Windows with Uranium Deposits	Percent of Windows with no Uranium Deposits	Percent of Windows in each Uranium Potential Category
High uranium potential	15%	85%	50%
Medium uranium potential	12%	88%	18%
Low uranium potential	2%	98%	32%
Total percent of windows that have or lack uranium deposits	10%	90%	

was made to identify these features, or their signature on data sets such as the band 7 image, in order to help in areas where the classification was of much more obscure meaning (e.g., Gas Hills test area, on the same Landsat frame. These features include ground features such as relief, slope orientation, surface roughness as depicted by contour maps, the drainage network, topographic directionality, geologic structure and stratigraphy, and the apparent texture of the band 7 and Eigenband 3 images.

We also compared the features shown by the various display operators with the IDM/ASM results for parts of the training area. No consistent correlations of IDM/ASM output were found with any obvious features of the various data sets utilized in these comparisons; we can only conclude that the texture operators are influenced by a number of factors related to the spectral responses of different terrains, and that a simple line separation such as we have performed aggregates these in ways that are not obvious to the human eye. If it were practical (with higher resolution data) to run a sufficiently large number of windows, a two-dimensional clustering technique applied to the IDM/ASM output might provide results both more interpretable in general and more useful for uranium exploration.

In general, the IDM/ASM plots appeared to correlate better with a different set of features in the hilly western part of the windowed area than those with which they correlated in the flatter eastern part of the area.

5.1.2.1 Geological Map

A large portion of the Mesozoic sedimentary rocks which underlie low relief areas are classified as uraniferous (Figure 5.1.2.2), while most of the rugged terrain underlain by Mesozoic sedimentary rocks and Precambrian igneous rocks is classified as nonuraniferous. Notable exceptions are the Chugwater and Sundance formations (Figure 3.1.6) which crop out along east-facing slopes and are classified as uraniferous. These are respectively red gypsiferous and greenish-glaucconitic fine-grained sandstones and siltstones. They form prominent, smooth, generally east-facing slopes. There is also some correlation of uraniferous windows with smooth east-facing slopes developed on Frontier formation.

In the eastern part of the training area, the Mesa Verde, Fox Hills, Lance, Wind River, Fort Union, and Wasatch formations (Figure 3.1.6) are generally denoted as uraniferous, except in the Kaycee area where they are classified as non-uraniferous. There are no obvious geological reasons why the latter should be so, or for the few isolated windows also classified as non-uraniferous. It is interesting that the Kaycee area, although well-known as an area of uranium shows, has apparently never produced any uranium commercially.

5.1.2.2 Topographic Map

In the western part of the training area, the "uraniferous" windows correspond to areas of smooth east,

southeast, and northeast facing slopes underlain by the Sundance and Chugwater formations. Areally more limited smooth eastward facing slopes are developed in the Frontier formation: these also are classified uraniferous.

In the eastern part of the training area, there is apparently no topographic difference between non-uraniferous and uraniferous windows, except towards the north (near the town of Kaycee) where there appears to be some tendency for the flatter areas to classify as non-uraniferous.

5.1.2.3 Eigenband 3 (E3)

In the eastern two thirds of the training area (see Figure 5.1.2.2), which has predominantly a very fine (pepper and salt) texture on E3, and is labeled uraniferous by IDM/ASM, coarse textured areas (i.e., ones with large patches darker or lighter than average) are picked out as non-uraniferous. In the western area, the Chugwater formation, which is very dark on E3, is picked out as uraniferous (see Figure 5.1.2.2). Uranium prospects are in fact known in the Chugwater in this vicinity. There is no correlation with coarseness, directionality, tone, or contrast that is consistent throughout the training area.

5.1.2.4 Band 7 (B7)

As expected, band 7 shows less correlation with the IDM/ASM output than does E3. There is no correlation at all with coarseness, directionality, contrast, or drainage features; the only correlation with tone is with the light-toned Chugwater in the western part of the area.

5.1.2.5 Other Features

In the west, gypsiferous beds tend to classify as uraniferous, and limestone beds, as non-uraniferous. There is no correlation between the classification and ground disturbance due to oil production (two oil fields classified "U", ten as "non-U"). There appears to be no correlation with vegetation. The Teapot Dome is classified non-uraniferous and surrounded by uraniferous windows.

5.1.3 Gas Hills Quarter Frame Test Area Texture

Measure Results

An overlay showing the distribution of windows classified "highly favorable," "favorable," and "unfavorable" for uranium is given (Figure 5.1.2.2). Tables 5.1.3 and 5.1.4 summarize how known uranium deposits were classified and how well the window classification agrees with the distribution of known uranium occurrences (Table 5.1.2).

Although the likelihood of a window containing uranium declined slightly from those classified "highly favorable" through those classified unfavorable, the difference is not great; and not significantly different from the 6% of all windows that include uranium occurrences. This area is on the same frame (actually adjacent to), and has very similar geology, as the Pumpkin Buttes training area. Therefore, in this area, the method does not appear to work in the most basic terms of distinguishing uraniferous ground from non-uraniferous ground.

However, examination of band 7 shows that over 50% (6 of 11) of the windows misclassified as "non-uraniferous" lie in two areas of badly disturbed ground: the Gas Hills mining district proper, and along the main highway north from Casper (Figure 5.1.2.1 or 5.1.2.2). These six windows contain 22 of 29 or 76% of the misclassified deposits. The remaining misclassified windows contain one or two scattered occurrences only. Thus, the classification is seen to be rather successful if the presence of disturbed ground in mining areas is allowed for.

However, 27% of the total area was classified as being high potential, and 26% as of medium potential, so the lack of selectivity of the approach is still a problem. In an effort to understand this lack of selectivity, the output of the texture measure classification was compared with other data sets, as was done for Pumpkin Buttes.

In general, low relief areas underlain by Tertiary rocks were classified as uraniferous, while more rugged areas underlain by Mesozoic sedimentary rocks and Precambrian igneous rocks were classified as non-uraniferous. In particular, at most localities within the quarter frame, bentonite-bearing strata were classified as uraniferous, and gypsiferous strata as non-uraniferous. More detailed comparisons between the texture measure window output and individual data sets are described below.

Table 5.1.3 Gas Hills Test Area: Degree of Correct
Classification of Known Uranium Occurrences

	<u>Number</u>	<u>% of Total</u>
Uranium occurrences falling within windows classified as having high potential for uranium mineralization.	31	43
Uranium occurrences falling within windows classified as having medium potential for uranium mineralization.	12	17
Uranium occurrences falling within windows classified as having low potential for uranium mineralization.	29	40
Totals	72	

5.1.3.1 Geological Map

In the western portion of the test area, the Madison and the Chugwater/Dinwoody formations as well as most of the Wind River formation, the Fort Union formation and the Precambrian granite have been classified as non-uraniferous. The Wind River and Fort Union formations consist of shales, sandstones and conglomerates (with coal in the Fort Union formation) and form flatlying areas with gently rolling hills. The Chugwater/Dinwoody and Madison formations respectively

Table 5.1.4 Correlation of Texture Measure Output with Known Uranium Distribution for the Gas Hills Test Area

(A) Raw Data Values

Classification by Texture Measure Method	Number of Windows with Uranium Deposits	Number of Windows with no Uranium Deposits	Number of Windows in Each Uranium Potential Category
High uranium potential	8	114	122
Medium uranium potential	7	110	117
Low uranium potential	11	205	216
Total number of windows that have or lack uranium deposits	26	429	455

(B) Percentage values

Classification by Texture Measure Method	Percent of Windows with Uranium Deposits	Percent of Windows with no uranium Deposits	Percent of Windows in each Uranium Potential Category
High uranium potential	6.5%	93%	27%
Medium uranium potential	6%	94%	26%
Low uranium potential	5%	95%	47%
Total percent of windows that have or lack uranium deposits	6%	94%	

consist of red, gypsiferous shales and sandstones which form steep east-facing slopes that are capped by Precambrian granite. It is interesting to note that no uranium occurrences have been reported from the Chugwater at this locality.

The southeastern portion of the test area is classified as almost entirely non-uraniferous and consists of the Casper, the Chugwater, the Cloverly/Morrison the Mowry and Thermopolis formations which form steep slopes that are capped by Precambrian granite. The Cloverly/Morrison, Mowry, and Thermopolis formations are bentonitic grey shales and sands, while the Casper formation is a grey to tan sandstone and limestone. No uranium occurrences have been reported in this area, which is classified as non-uraniferous.

At most localities throughout the test area, the Lewis/Lance formation and the Mesa Verde formation are classified as either uraniferous or indeterminate. The Mesa Verde contains uranium occurrences along highway 87 north of Casper and at Poison Spring Creek southwest of Casper. These formations consist of grey or grey to tan sandstones and shales with some coal beds, and form flatlying areas or gently rolling hills.

In the northeastern portion of the test area, the Fort Union, the Lance, the Frontier, and Hillard formations are classified as uraniferous. These formations consists of brown-to-grey or grey-to-black sandstones and shales (with coal in the Fort Union) which form flatlying areas with rolling hills.

5.1.3.2 Topographic Map

In the eastern portion of the test area, low-lying flat areas were classified as uraniferous while the steep slopes and uplands were classified as non-uraniferous. In the western portion, no correlation with topography is apparent.

5.1.3.3 Eigenband 3

In general, areas of fine (salt and pepper) texture were classified as uraniferous by IDM/ASM, and coarse texture areas (i.e., ones with darker or lighter than average patches) were classified as non-uraniferous. Located in the north-eastern part of the test area is a large patch of salt and pepper texture, which appears continuous with a similar area in the eastern portion of the quarter frame training area to the north, and represents the Tertiary fill of the southern Powder River Basin.

The Chugwater formation is very dark on Eigenband 3 and is picked out as non-uraniferous. No uranium occurrences are present in the Chugwater in this vicinity; however, in the training area this formation was classified as uraniferous and this contains known uranium occurrences.

No correlation with coarseness, directionality, tone, or contrast can be consistently established throughout this quarter frame test area.

5.1.3.4 Band 7

It is apparent from band 7 that badly disturbed areas of ground are classified non-uraniferous, and that these

areas include the pits and dumps of the Gas Hills mining district. Otherwise, band 7 shows less correlation with the IDM/ASM output than does Eigenband 3. No correlation is apparent with coarseness, directionality, contrast, drainage, or tone.

5.1.3.5 Summary of Texture Measure Results for Pumpkin

Buttes and Gas Hills

When the two quarter frame areas run on the Poison Spider frame are considered together, uraniferous and non-uraniferous windows form a broad pattern. The Powder River Basin is classified as uraniferous, as are areas in the Wind River Basin north of the Gas Hills mining district and areas of Tertiary cover in the Granite Mountains. Heavily disturbed ground in part of the Gas Hills mining area is classified non-uraniferous. Areas of igneous outcrop are classified non-uraniferous and so are central and northern parts of the Wind River Basin.

"Indeterminate" uranium potential areas include much of the Mesozoic of the Powder and Wind River Basin in the Sweetwater Arch. A band of "indeterminate" to "uraniferous" windows cross the Sweetwater Arch approximately along the line of Poison Spider Creek, roughly paralleling the inferred course of the paleo-Wind River. The reason for this is unknown.

Although these are very broad and generalized conclusions, they do indicate that there may be promise in the approach in the sense that the technique can recognize certain

broad textural types of the kind associated with uranium-bearing sediments. However, since approximately half the area is classified as uraniferous, and the area of each window is so large, this may not be of much value in exploration. This latter factor tells us more about the resolution of Landsat imagery than it does about the potential value of the techniques itself. The method did not prove sensitive enough to recognize areas of local uranium enrichment within generally favorable terrain, but that could change with the significantly higher resolution imagery of Landsat-D. With the MSS data of Landsat-1 and -2, however, the method must be regarded as only partially successful.

5.1.4 Grants - Texture Measure Results

Three overlays have been produced for the GEOPIC false color composite (Plate 2) of Landsat bands 4, 5, and 7 for the Grants, New Mexico study area. Figures 5.1.4.1, 5.1.4.2, and 5.1.4.3 are reduced copies of Plates 13, 14, and 15 comprising the "Uranium Occurrence Map" and the two "Classification Maps" (one classification map for each of the two classification discriminants described below) respectively.

Following the procedure described in Section 4.0, control areas were chosen within the Grants training area. The locations of the control areas are shown on the Uranium Occurrence Map. The eastern block of windows overlies uraniferous terrain; the western block characterizes non-uraniferous

terrain. The third Eigenband data for the windows of the two control areas were processed using the five texture measure operators. The results were plotted as a series of two dimensional plots.

Figures 5.1.4.4 and 5.1.4.5 present the IDM/ASM plot with two different linear classification discriminants. The first (line #1, Figure 5.1.4.4) was chosen as the best discriminant between windows of the uraniferous and non-uraniferous control areas. An assessment of the results based on this line is discussed below. In an effort to increase the selectivity and confidence of those windows classified as having a high uranium potential, windows within the uraniferous control area which contained the greatest concentration of mapped occurrences were flagged on the plot (Figure 5.1.4.5). With special attention to these windows, a new line was selected (line #2) which classified as uraniferous only those windows which fell in the field to the right of the line, i.e., in the field with the greatest concentration of flagged windows.

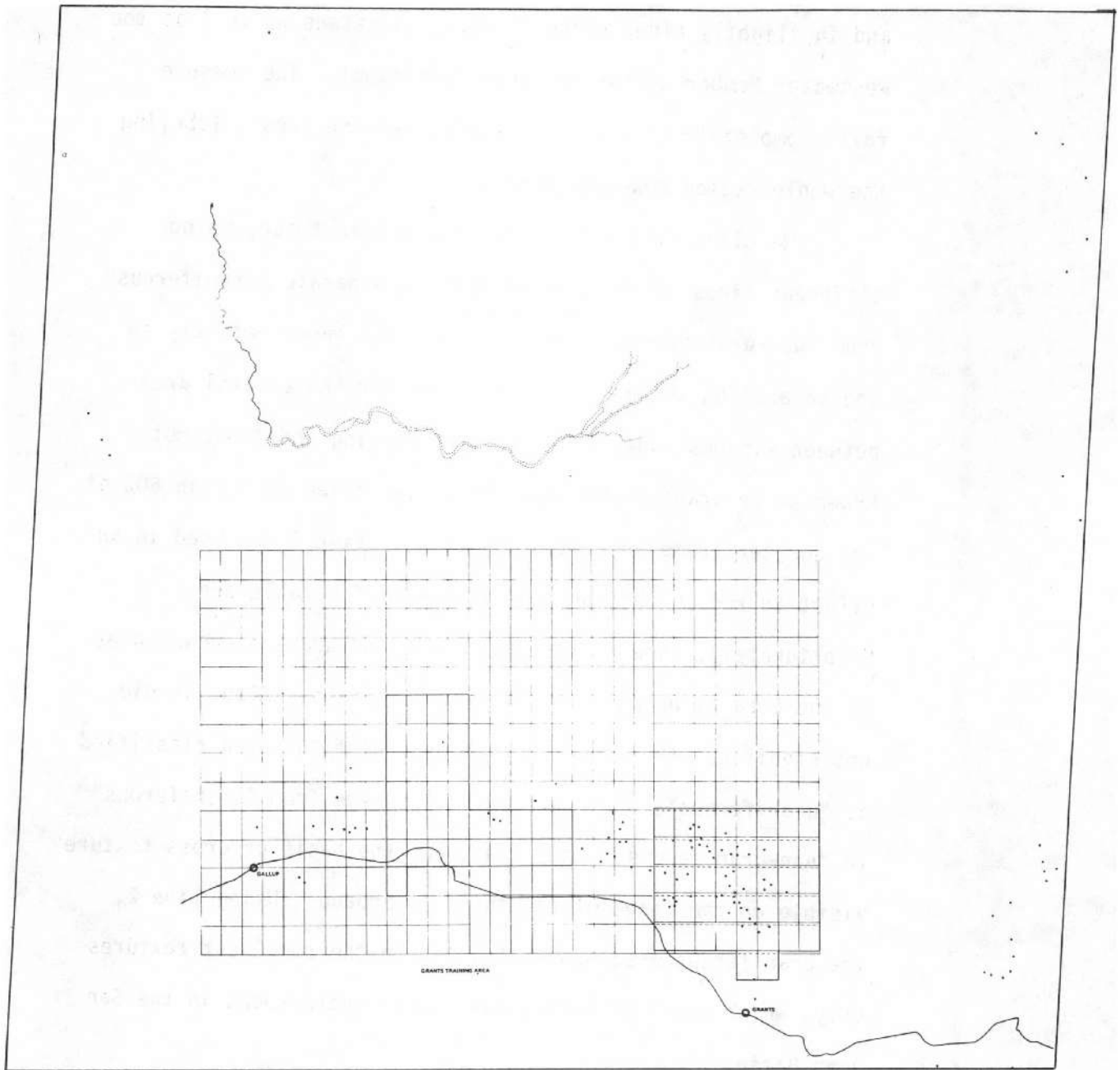
In general, areas labeled as "uraniferous" by the texture measure IDM/ASM correlate with low contrast, medium gray, "salt and pepper" textured areas on the Eigenband 3 image. These same areas are light-toned on the MSS color composite, and generally correspond to low-lying areas of low, gentle relief underlain by Cretaceous and Tertiary rocks.

The eastern part of the area, where the measure was trained, is characteristic of the terrain in which uranium occur; the correspondence with uranium occurrence here is

rather good (see classification map). In the western part of the area, uranium occurs in the somewhat more rugged terrain and in slightly older rocks (Todilto limestone as well as the Westwater Member of the Morrison formation). The measure fails completely to pick out uranium-bearing areas, labeling the whole region non-uraniferous.

We classified the quarter frame area twice, using different lines on the IDM/ASM plot to separate "uraniferous" from "non-uraniferous" areas. Line 1 was based entirely on the separation shown in the print-out for the control area between windows known to be uranium-bearing and those not known to be uranium-bearing. This classified more than 50% of the quarter frame area as uranium-bearing. Line 2 was used in an effort to reduce the apparent amount of favorable area. Unfortunately, line 2 classified half the uranium occurrences in the area as being "non-uraniferous" areas. Also, it did not significantly reduce the proportion of the area classified as "uraniferous"; where windows did change from "uraniferous" to "non-uraniferous," they did so on the basis of gross texture visible on the image of the third Eigenband. Using line 2, the uranium-bearing area was restricted to the smoothest textures only, which occur primarily over unfavorable rocks in the San Juan Basin.

Tables 5.1.5, 5.1.6, 5.1.7, and 5.1.8 summarize the correlation, or lack of it, between the classification and known uranium areas. It is apparent that the degree of misclassification is very high, especially for line 2.



SCALE 1:250,000
 0 1 2 3 4 5 6 7 8 9 10 11 12 13 14 15 16 17 18 19 20 Miles
 0 1 2 3 4 5 6 7 8 9 10 11 12 13 14 15 16 17 18 19 20 Kilometers

PREPARED BY
EARTH SATELLITE CORPORATION
 WASHINGTON, D. C.

**URANIUM OCCURRENCE MAP
 FOR A PORTION OF
 NEW MEXICO**

JUNE 1979
 C-1153

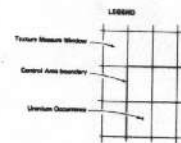
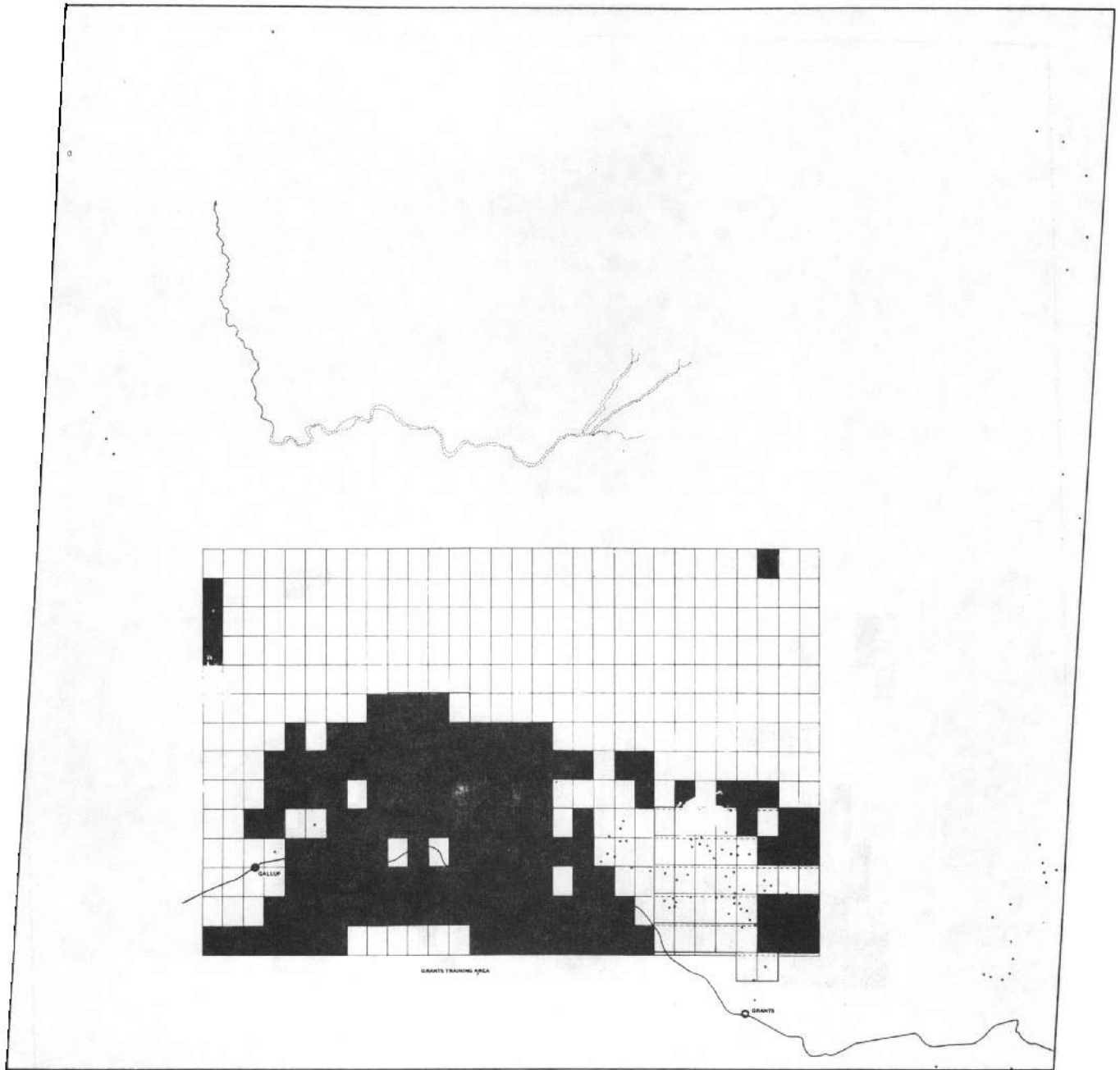


Figure 5.1.4.1. 4X-reduction of image overlay. See original for details



SCALE 1:62,500

PREPARED BY
EARTH SATELLITE CORPORATION
WASHINGTON, D. C.

Line 1
CLASSIFICATION MAP
FOR A PORTION OF
NEW MEXICO

JUNE 1974
E-1152

LOCATION MAP

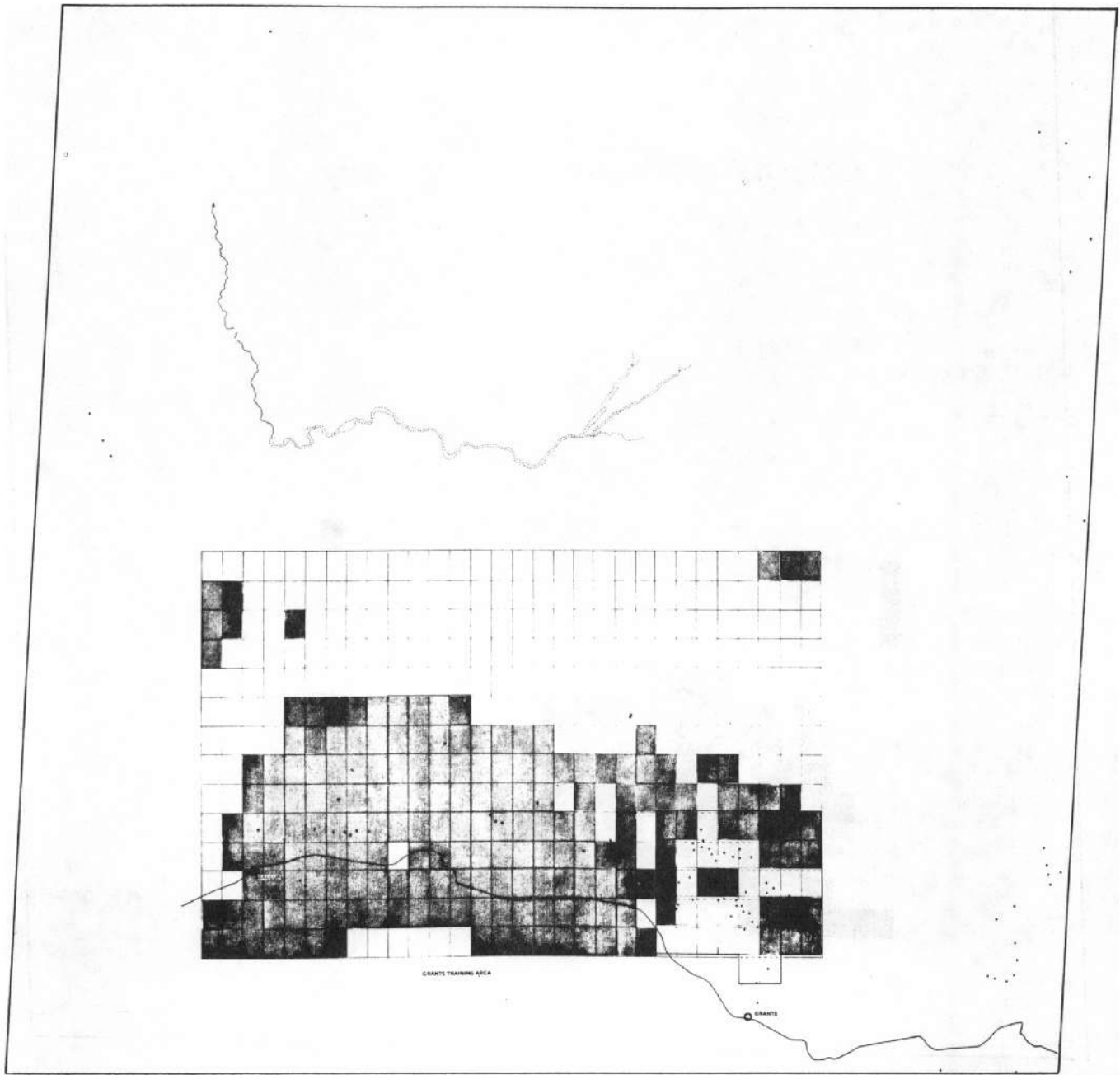
NEW MEXICO

LEGEND

Urban Potential
Urban Circumference
Control Area Boundary

High Urban Potential
Low Urban Potential

Figure 5.1.4.2 4X-reduction of image overlay. See original for details.



PREPARED BY
EARTH SATELLITE CORPORATION
WASHINGTON, D. C.

Line 2
CLASSIFICATION MAP
FOR A PORTION OF
NEW MEXICO

JUNE 1979
C-1162

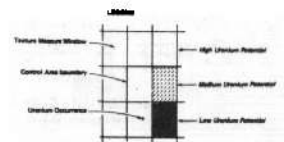


Figure 5.1.4.3 4X-reduction of image overlay. See original for details.

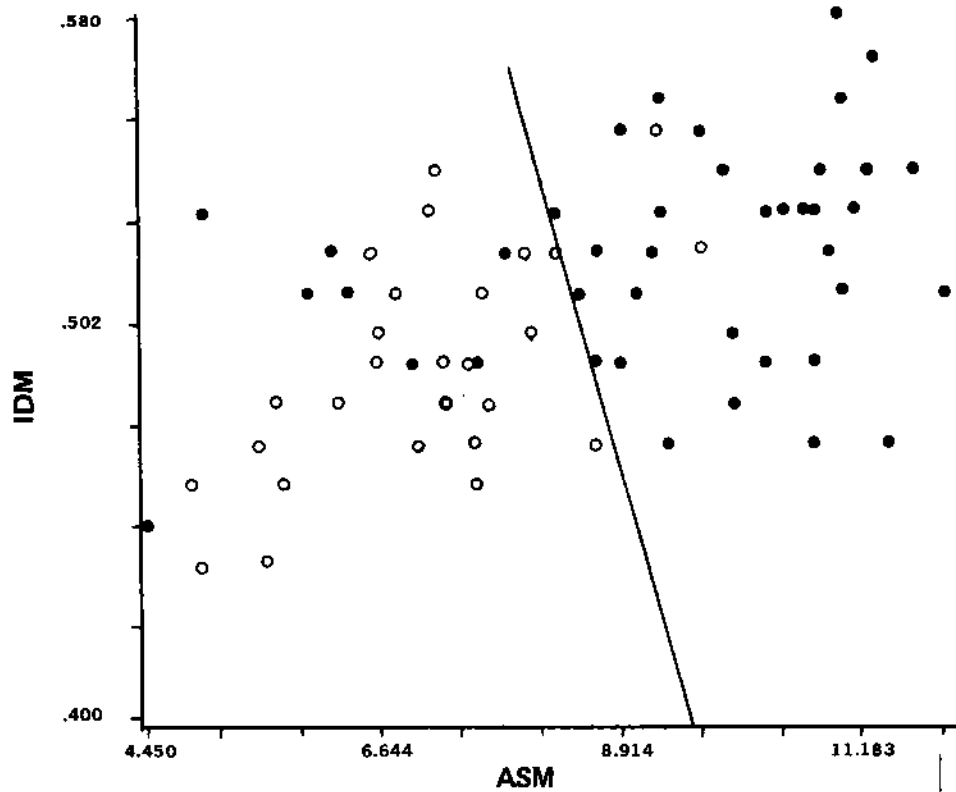


Fig. 5.1.4.4 Grants, IDM/ASM plot for E3, Line 1

- LEGEND**
- Uraniferous control area windows (1 or more)
 - Non-uraniferous control area windows (1 or more)
 - △ Overlap of uraniferous and non-uraniferous windows
 - Many known occurrences

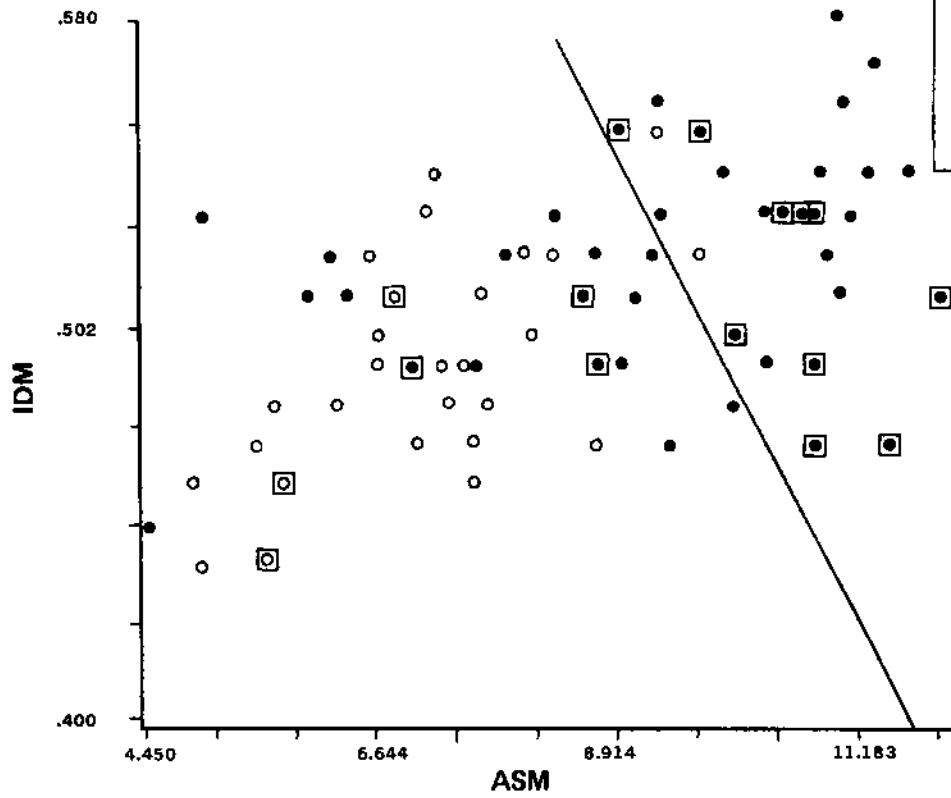


Fig. 5.1.4.5 Grants, IDM/ASM plot for E3, Line 2

Thus, IDM/ASM cannot be considered a valid tool for uranium prospecting in the Grants area. More detailed comments on its relationship to various data sets appear below:

5.1.4.1 Geology

The uppermost unit of the Mesa Verde (the Menefee formation), a grey-orange, non-uraniferous sandstone with interbedded coals, and areas of Quaternary alluvium, are classified uraniumiferous in the western part of the quarter frame; and all older rocks are classified non-uraniferous.

In the eastern part of the quarter frame, where relief is less rugged, the Mancos shale, parts of the Dakota, the Morrison, the Summerville, and the Todilto formations, and even the Triassic rocks are classified as uraniumiferous. These rocks are of highly varied lithology and topographic expression.

The classification of Morrison and Summerville formations as uraniumiferous in this area explains the good correlation with uranium deposits found in the small training area used. The fact that the texture measure is so indiscriminate here, and so restricted to young rocks further west, suggests that it is mainly detecting coarse topographic variations, and has no correlation with geology or the occurrence of uranium.

5.1.4.2 Topographic Map

Steep slopes and upland surfaces, which appear on the Landsat color composite, are classified non-uraniferous. Flat to rolling areas in the San Juan Basin and major valleys

tend to be classified uraniferous. Line 2 eliminates most of the valley areas classified as uraniferous, and restricts this classification to the San Juan Basin and eastern end of the mining region (Grants District).

5.1.4.3 Eigenband 3

Non-uniform, contrasting areas are labeled non-uraniferous by line 1, especially when they are brighter than average. Line 2 restricts the "uraniferous" classification to the most uniform areas of the quarter frame.

Table 5.1.5 Grants Training Area line 1: Degree of Correct Classification of Known Uranium Occurrences

	<u>Number</u>	<u>% of Total</u>
Uranium occurrences falling within windows classified as having high potential for uranium mineralization	59	76
Uranium occurrences falling within windows classified as having low potential for uranium mineralization	19	24
Totals	78	

Table 5.1.6 Grants Training Area Line 2: Degree of Correct
Classification of Known Uranium Occurrences

	<u>Number</u>	<u>% of Total</u>
Uranium occurrences falling within windows classified as having high potential for uranium mineralization	36	46
Uranium occurrences falling within windows classified as having low potential for uranium mineralization	42	54
Total	78	

5.1.4.4 Band 7

No correlations between IDM/ASM output and coarseness, directionality, or contrast of texture on band 7 were noted.

5.1.4.5 Color Composite

Non-uraniferous windows correlate quite well with dark-toned areas on the color composite. This implies that the correlation is with areas that have low reflectivity.

5.1.5 Namibia - Texture Measure Results

In selecting uranium control areas within a training area, we required for this project that at least 70% of the windows contain known uranium occurrences. This maintains a level of confidence that the texture within the windows are characteristic of mineralized ground. Only eight occurrences were found in

Table 5.1.7 Correlation of Texture Measure Output with Known Uranium Distribution for the Grants Training Area
Line 1

(A) Raw Data Values

Classification by Texture Measure Method	Number of Windows with Uranium Deposits	Number of Windows with no Uranium Deposits	Number of Windows in Each Uranium Potential Category
High uranium potential	27	230	257
Medium uranium potential	0	0	0
Low uranium potential	15	180	195
Total number of windows that have or lack uranium deposits	42	401	452

(B) Percentage values

Classification by Texture Measure Method	Percent of Windows with Uranium Deposits	Percent of Windows with no Uranium Deposits	Percent of Windows in each Uranium Potential Category
High uranium potential	11%	89%	57%
Medium uranium potential	0	0	0
Low uranium	8%	92%	43%
Total percent of windows that have or lack uranium deposits	9%	90%	

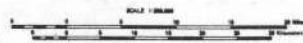
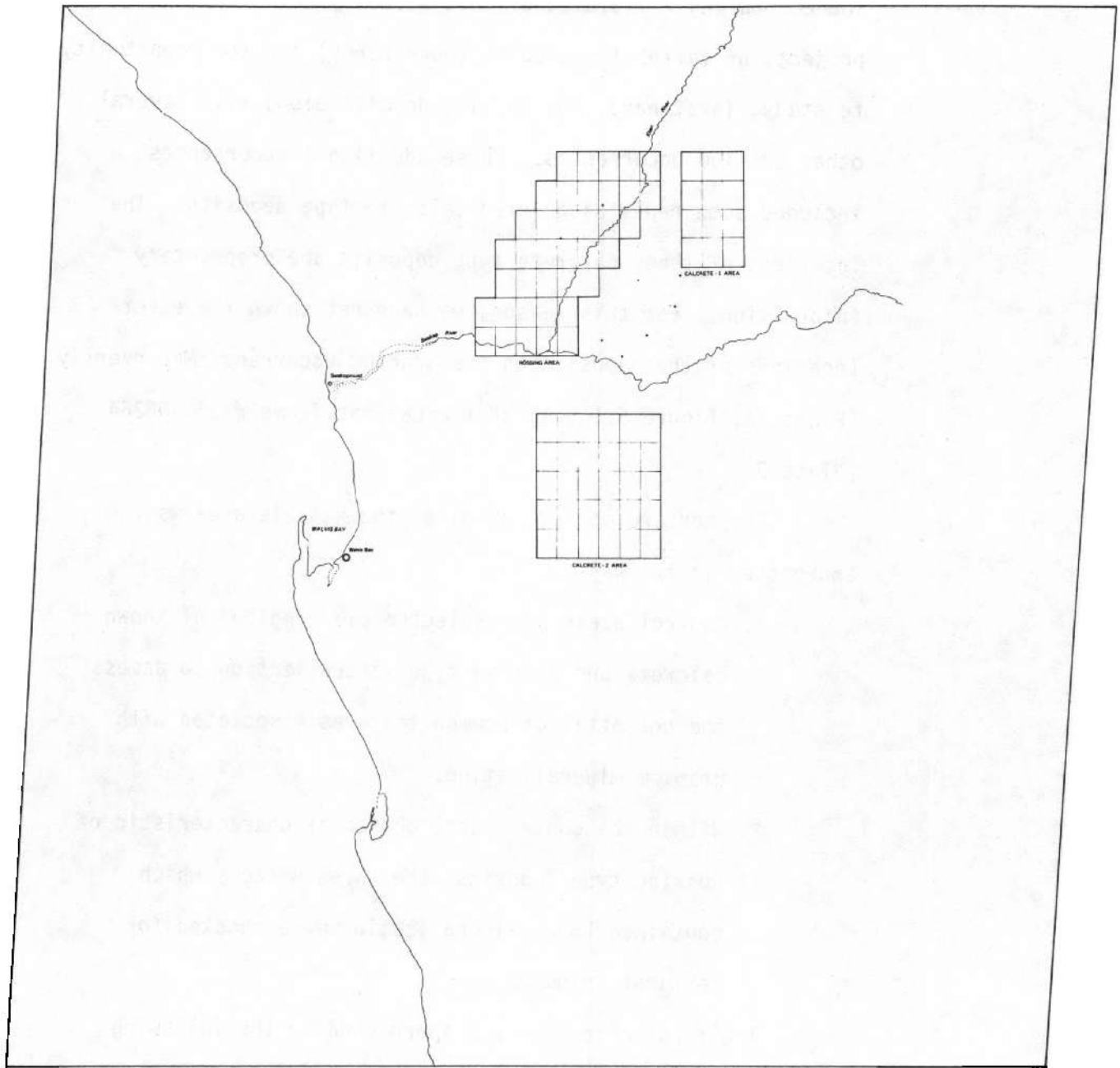
Table 5.1.8 Correlation of Texture Measure Output with Known Uranium Distribution for the Grants Training Area
Line 2

(A) Raw Data Values

Classification by Texture Measure Method	Number of Windows with Uranium Deposits	Number of Windows with no Uranium Deposits	Number of Windows in Each Uranium Potential Category
High uranium potential	16	195	211
Medium uranium potential	0	0	0
Low uranium potential	26	215	241
Total number of windows that have or lack uranium deposits	42	410	452

(B) Percentage values

Classification by Texture Measure Method	Percent of Windows with Uranium Deposits	Percent of Windows with no Uranium Deposits	Percent of Windows in each Uranium Potential Category
High uranium potential	7%	92%	47%
Medium uranium potential	0	0	0
Low uranium potential	11%	89%	53%
Total percent of windows that have or lack uranium deposits	9%	91%	



PERFORMED BY
EARTH SATELLITE CORPORATION
WASHINGTON, D. C.

**URANIUM OCCURRENCE MAP
FOR A PORTION OF
NAMIBIA**

JUNE 1979
C-1182

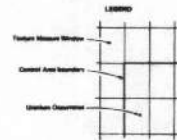


Figure 5.1.5.1. 4X-reduction of image overlay. See original for details.

the literature that could be accurately located on the Namibia scene. During a field study, not directly related to this project, an EarthSat geologist (John Berry) had the opportunity to study, first-hand, the Rossing deposit along with several other uranium occurrences. These additional occurrences included some newly discovered calcrete type deposits. The locations of these calcrete type deposits are proprietary information. For this reason, we have not shown the exact locations of the deposits on the Uranium Occurrence Map overlay (Plate 16, Figure 5.1.5.1) of the Landsat frame #1383-08264 (Plate 3).

The texture measure study of the Namibia area was approached in two ways:

1. Control areas were selected over regions of known calcrete and Rossing type mineralization to assess the potential of common textures associated with uranium mineralization.
2. Within the control area chosen as characteristic of Rossing type deposits, the three windows which contained known mineralization were checked for textural uniqueness.

The first objective was approached in the following way. Two blocks of windows were selected from areas to the south and east of the Rossing district. These areas are comprised of 30 and 12 windows for the south and east areas respectively (Figure 5.1.5.1). These areas overlie numerous newly discovered calcrete deposits and were thus combined to

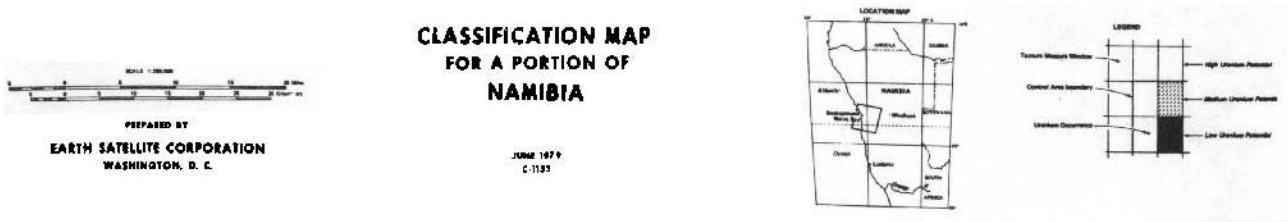
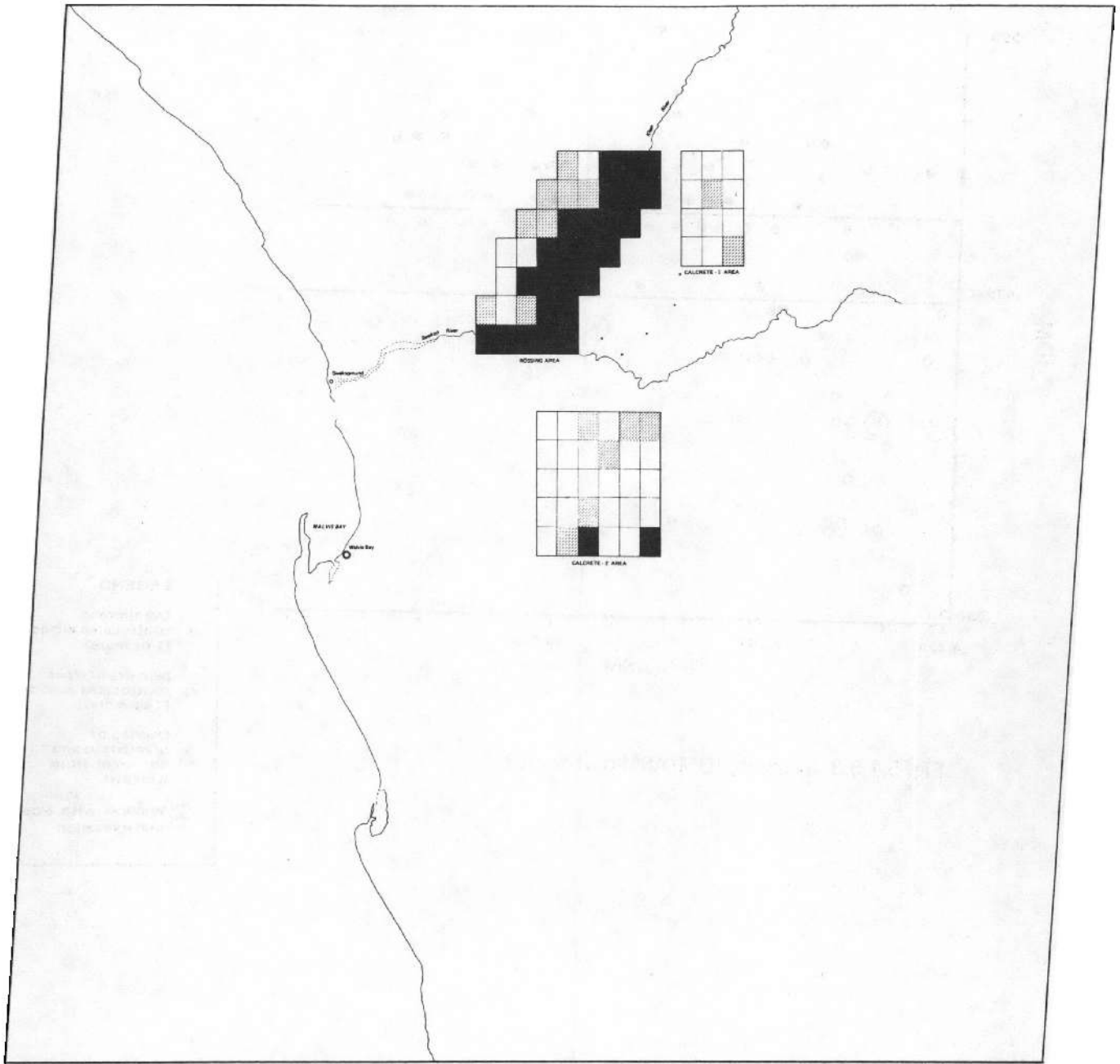


Figure 5.1.5.2. 4X-reduction of image overlay. See original for details.

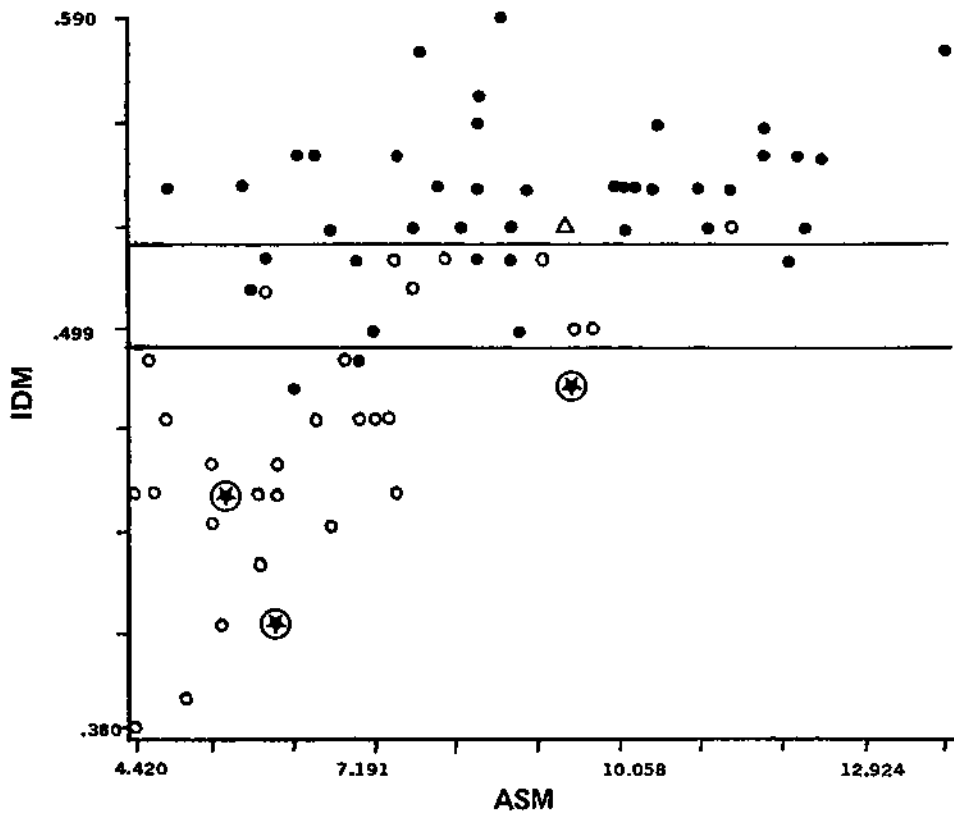
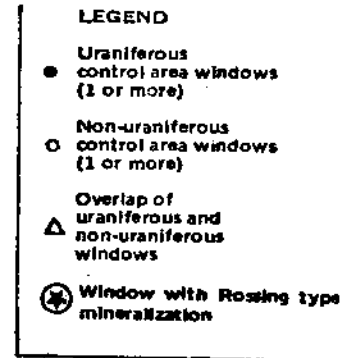


Fig. 5.1.5.3 Nambia, IDM/ASM plot for E3



create a single uranium control area. The non-uranium control area, comprised of 35 windows, was selected from a region along the Khan River (Figure 5.1.5.1). This area includes the wide northeast striking gorge of the Khan River and a parallel stretch of pediplain along the northwest side of the gorge. Two areas of Rossing type mineralization, including the Rossing deposit itself, are located within the section of Khan River gorge covered by the "non-uranium" control area. The full set of control area windows was processed using the third Eigen projection (E3) of the satellite data as the data base, and the results of the IDM/ASM operator results were plotted (Figure 5.1.5.2).

The plotted windows are reasonably separable by two parallel lines into areas of high, medium, and low uranium potential. Referring to Figure 5.1.5.3, those windows which fall above the upper line are considered to have high uranium potential, those between the lines are of medium potential, and those below the lower line are classified as having low uranium potential.

The results of the classification are shown on the Classification Map Overlay (Plate 17) to the Namibia image. The windows of the two areas comprising the uranium control areas were consistently classified as having a high potential for uranium mineralization. The non-uranium control area showed a marked division along the northern edge of the gorge. The area within the gorge was consistently classified as low potential windows, whereas, the windows located on the pediplain

to the northeast were classified as a mixture of high and medium potential. Those windows which contained Rossing type mineralization within the non-uranium control area were all classified as having low uranium potential. This indicates the predictable result that any detectable texture associated with calcrete mineralization is significantly different from that associated with Rossing type mineralization.

Further interpretation of the Landsat imagery suggests that the texture associated with the pediplain regions comprising the windows of the uranium control areas and the northwest side of the non-uranium control area are markedly different from the texture associated with the gorge of the Khan River. It is likely that, in this case, the operator has detected gross textural contrast in landforms rather than the subtle textures associated with uranium mineralization.

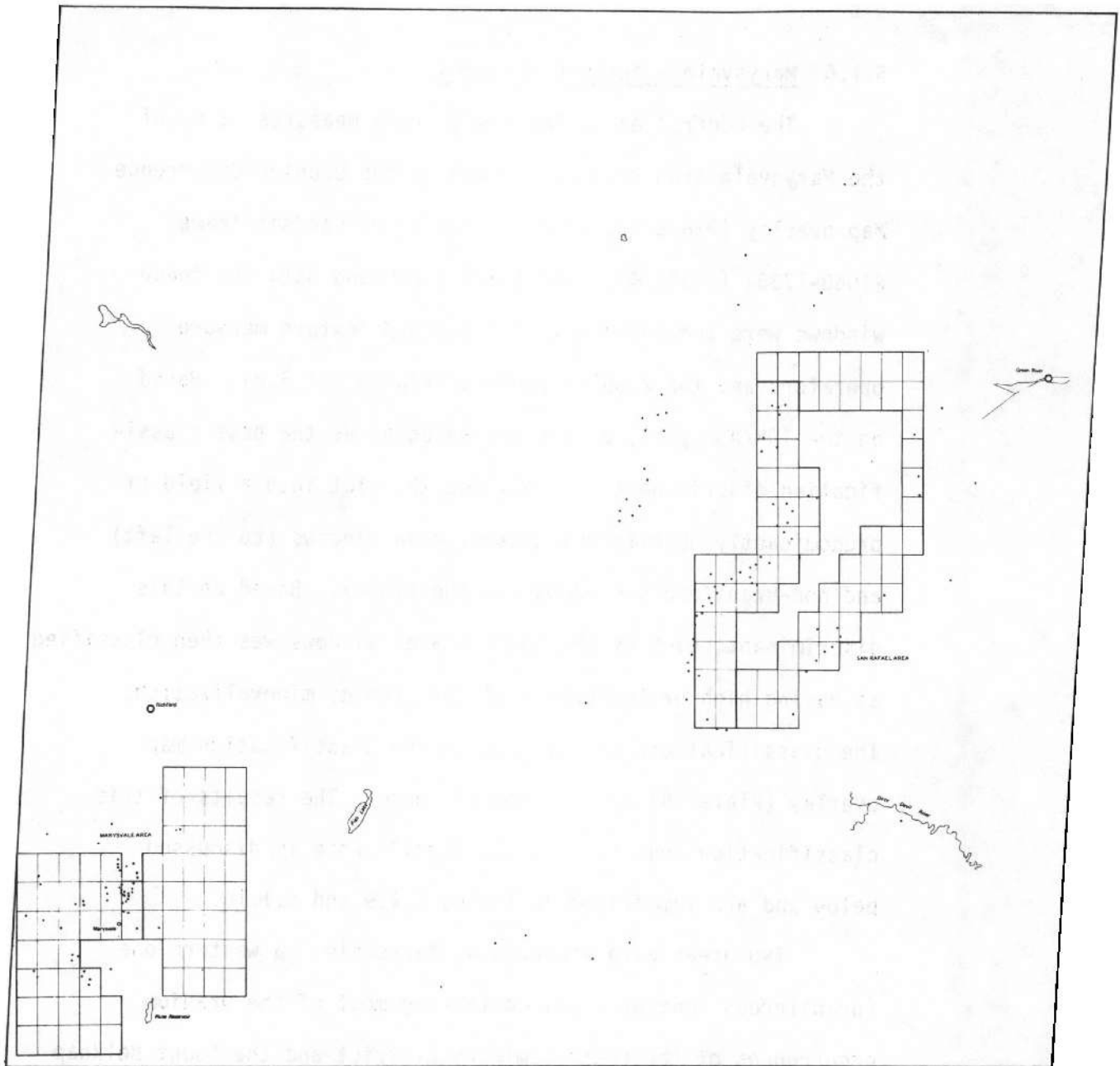
The second phase of the texture measure study on the Namibia data was aimed at distinguishing the windows overlying Rossing type mineralization from the remainder of the windows comprising the "non-uranium" control area. The three windows overlying known mineralization have been flagged on the IDM/ASM plot (Figure 5.1.5.3). These three windows are observed to be scattered throughout the plotted data. If they had shown any tendency to cluster, it may have been possible to distinguish a characteristic texture associated with the Rossing type mineralization. However, based on their broad spacing on the IDM/ASM plot, we conclude that the operator was not able to distinguish any texture that would permit the distinction of

the windows containing Rossing type mineralization from the surrounding non-mineralized areas.

5.1.6 Marysvale - Texture Measures

The control areas for the texture measures study of the Marysvale area have been drawn on the Uranium Occurrence Map overlay (Plate 18, Figure 5.1.6.1) of Landsat frame #1068-17364 (Plate 4). The third Eigenband data for these windows were processed with the IDM/ASM texture measure operators and the results plotted (Figure 5.1.6.2). Based on the IDM/ASM plot, a line was selected as the best classification discriminant. It divided the plot into a field of predominantly uraniferous control area windows (to the left) and non-uraniferous windows (to the right). Based on this discriminant, each of the control area windows was then classified as having high or low potential for uranium mineralization. The classifications are plotted on the classification map overlay (Plate 19) to the Landsat image. The results of this classification and its geologic significance is discussed below and are summarized in Tables 5.1.9 and 5.1.10.

Two areas were windowed at Marysvale: a western one (uraniferous control area) containing most of the uranium occurrences of the central mining district and the Mount Belknap Caldera, and an eastern area with similar geology and topography but with almost no uranium reported within it ("non-uraniferous" control area).



PREPARED BY
EARTH SATELLITE CORPORATION
 WASHINGTON, D. C.

**URANIUM OCCURRENCE MAP
 FOR A PORTION OF
 UTAH**

APRIL 1977
 C-1122

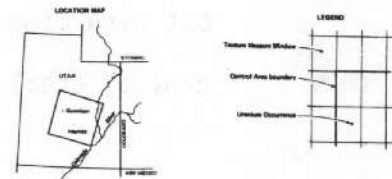


Figure 5.1.6.1. 4X-reduction of image overlay. See original for details.

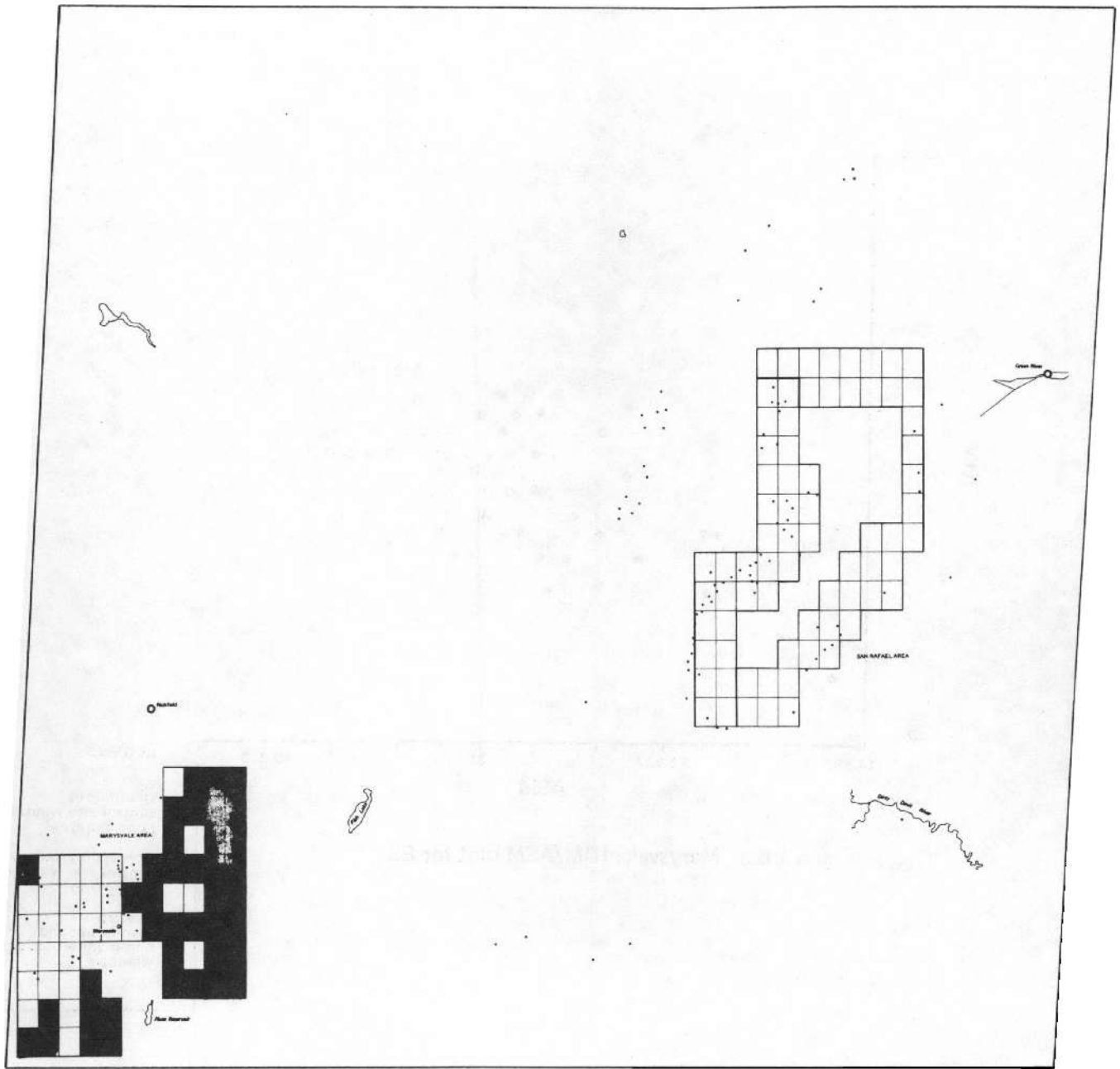


Figure 5.1.6.2. 4X-reduction of image overlay. See original for details.

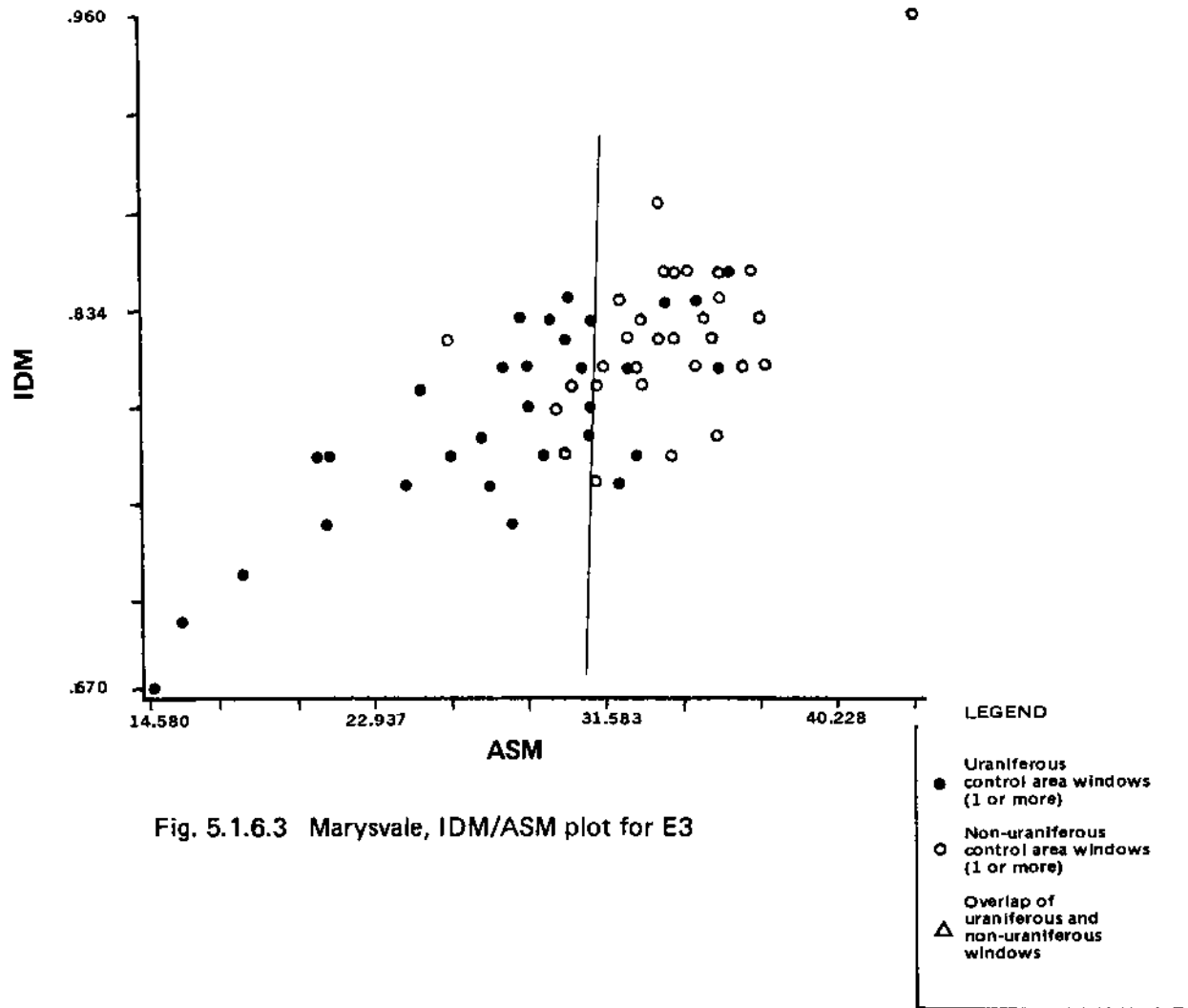


Fig. 5.1.6.3 Marysvale, IDM/ASM plot for E3

The scatter plot of IDM/ASM values for both sets of windows was made. A line could be drawn on the scatter plot (Figure 5.1.6.3) which separates fairly well the windows of the "uraniferous control area" from those of the "non-uraniferous control area." Therefore, the technique apparently works fairly well on the first order level.

However, when labeled overlays were made on each area and compared in detail with the distribution of known uranium (Plate 19, Figure 5.1.6.2), all real correlation with uranium occurrence disappears (see Tables 5.1.9 and 5.1.10). The two isolated uranium occurrences in the "non-uraniferous control area" are located in "non-uraniferous windows," although five windows in this block, including an adjacent one, are classified uraniferous. Of the 12 windows in the "uraniferous control area" classified "non-uraniferous," four contain uranium occurrences, one of them being the bulk of the central mining district. Of the 22 windows classified "uraniferous" in this block, only 9 actually contain uranium occurrences. Therefore, at the second level of comparison, the method definitely fails.

What is, in effect, being identified as "uraniferous" is light-toned fine-texture alluvium and lower slopes of mountains, and snow covered peaks. The dark, heavily vegetated intermediate slopes are classified as "non-uraniferous" along with some finer textured areas within the mountains.

The correlation with geology is very poor, except insofar as rock units which have fine textured drainage developed on them are classified as "non-uraniferous."

Table 5.1.9 Marysvale Area: Degree of Correct Classification of Known Uranium Occurrences

	<u>Number</u>	<u>% of Total</u>
Uranium occurrences falling within windows classified as having high potential for uranium mineralization.	23	55
Uranium occurrences falling within windows classified as having low potential for uranium mineralization.	19	45
Totals	42	

5.1.7 San Rafael - Texture Measures Results

In the original selection of study areas, the San Rafael Swell was selected as the official test area for the Grants training area. Based on processing volume considerations, we decided to run a preliminary test on the San Rafael area before processing an entire quarter frame. The preliminary test entailed selecting uraniferous and non-uraniferous control areas within the proposed test area and generating an IDM/ASM plot of the windows using the third Eigenband as the data source. The location of the selected control areas is shown on the Uranium Occurrence Map overlay (Plate 18, Figure 5.1.6.1) Landsat frame #1068-17364 (Plate 4). The IDM/ASM plot (Figure 5.1.7.1) was disappointing on two counts:

1. Significantly higher ASM and IDM values for the San Rafael windows placed over 95% of the windows on one

Table 5.1.10 Correlation of Texture Measure Output with Known Uranium Distribution for the Marysville Area

(A) Raw Data Values

Classification by Texture Measure Method	Number of Windows with Uranium Deposits	Number of Windows with no Uranium Deposits	Number of Windows in Each Uranium Potential Category
High uranium potential	12	17	29
Medium uranium potential	0	0	0
Low uranium potential	4	36	40
Total number of windows that have or lack uranium deposits	16	53	69

(B) Percentage values

Classification by Texture Measure Method	Percent of Windows with Uranium Deposits	Percent of Windows with no Uranium Deposits	Percent of Windows in each Uranium Potential Category
High uranium potential	41%	59%	42%
Medium uranium potential	0	0	0
Low uranium potential	10%	90%	58%
Total percent of windows that have or lack uranium deposits	23%	77%	

side (to the right) of the classification discriminant chosen for the Grants training area.

2. The uraniferous and non-uraniferous windows were strongly overlapping to the extent that we could not choose a reasonable classification discriminant.

The following is a brief discussion of each of these observations.

The main incentive for running a preliminary test on the San Rafael area was the concern over jumping Landsat frame boundaries in moving from training to test areas. When a frame boundary is jumped, that is to say when a training area is on one frame and the test area on another, several factors combine to complicate the detection of subtle textural information. With the exception of consecutive frames along the same overpass, jumping a frame boundary creates an often extreme change in atmospheric conditions. It can also present additional complications, such as changing sun angle with a change in season, and changing type and extent of vegetation cover with a change in climate.

One or several of these factors can combine to produce greatly differing ASM and IDM values over similar geology. In the case of the Landsat data for the San Rafael areas, the range of ASM values is three times larger than that for the Grants area. Likewise, the IDM values show a substantial shift towards higher values. As a result, both of the lines, drawn as the two different selections of classification discriminants at Grants, plot in the extreme lower region of the San Rafael IDM/ASM plot (Figure 5.1.7.1). By virtue of the

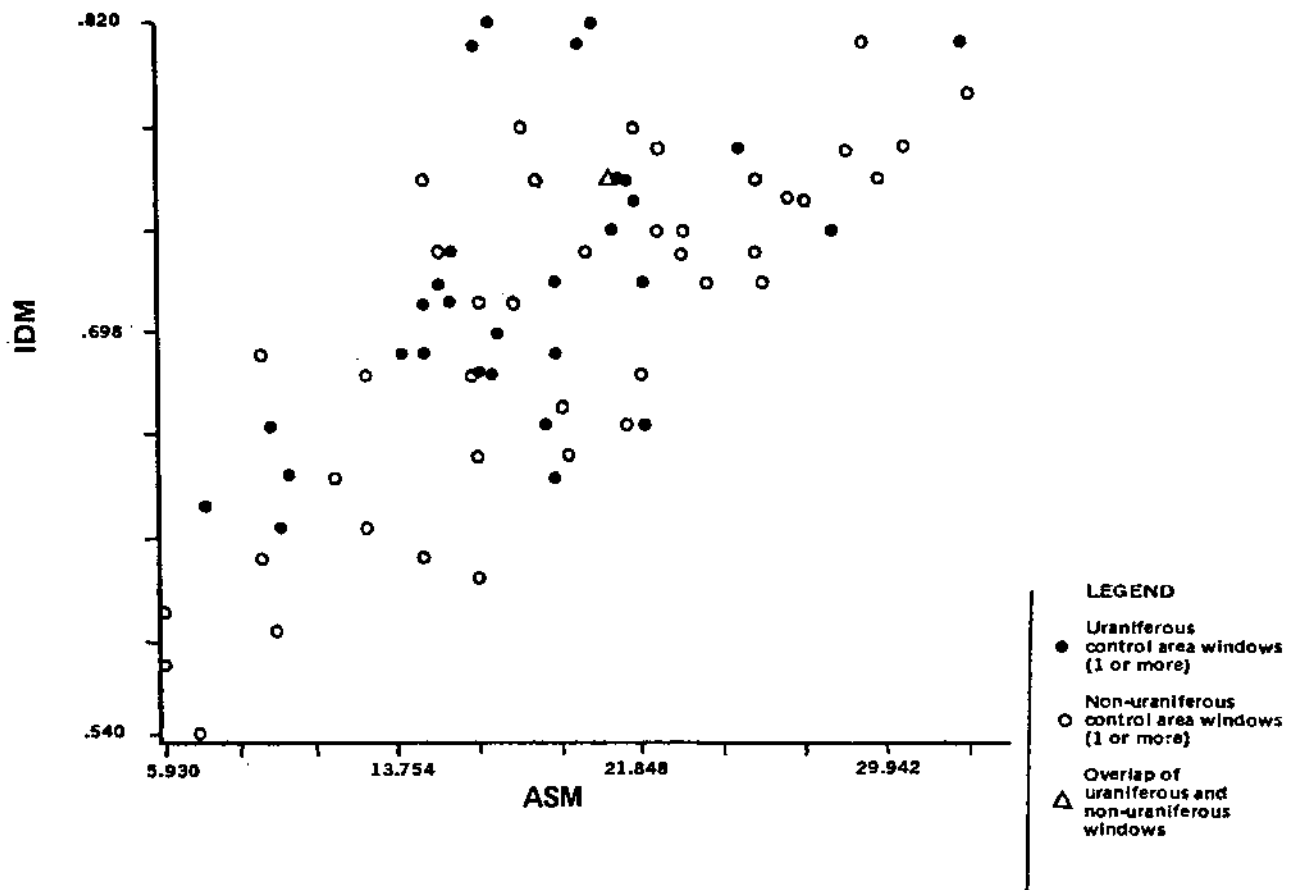


Fig. 5.1.7.1 San Rafael, IDM/ASM plot for E3

Rafael IDM/ASM plot (Figure 5.1.7.1). By virtue of the fact that over 95% of the windows lie to the right of both lines, neither could possibly serve as a valid classification discriminant. The conclusion has been drawn from this that a test area must be within the same Landsat frame as the training area, in order to avoid the inherent complications involved with moving across frame boundaries.

In addition to the higher IDM and ASM values with respect to Grants, the results of the IDM/ASM operators at San Rafael were disappointing on another count. The windows of two control areas display a nearly 100% overlap on the IDM/ASM plot. It is not possible to select a line which will adequately divide the window into predominantly uraniferous and non-uraniferous groups. This indicates that the windows selected for the two control areas are of similar texture as detected by the IDM/ASM operators. Therefore, any texture associated with uranium mineralization within the windows at the uraniferous control area is not sufficient to allow discrimination using the IDM/ASM texture measures.

5.2 Display Operators

5.2.1 Copper Mountain

Each display operator was systematically tested on Landsat band 5 of the Copper Mountain area (see Table 5.2.1.1), with generally negative results except for the edge detector when thresholded. Photointerpretative techniques were applied

to the geometric pattern display operator outputs to verify that the results were indeed negative.

Since uranium deposits at Copper Mountain are associated with fracturing, and especially with the intense fracturing in the toe of Owl Creek thrust, it is felt that the reason that the geometric pattern recognition programs in general fail at Copper Mountain is the poor inherent resolution of Landsat. However, enough encouragement was received from the results in Figure 5.2.1.4 that it is felt that the method may indeed succeed when higher resolution space-acquired data are available.

Results for each operator are summarized below.

5.2.1.1 Texture Pictures

A very tenuous relationship between uranium areas and east-west "lineaments" (Figure 5.2.1.1) visible on the texture transform and local histogram stretch of band 5 was seen. This comment also applies to the local and global histogram stretches, on which the same lineaments are seen. However, the relationship is so tenuous that it could not be of use in the exploration.

The shaded areas drawn on Figures 5.2.1.1 and 5.2.1.2 are derived from the Copper Mountain area of Figure 5.1.2.1. Some care must be exercised in comparing these figures, however, since (a) clusters of uranium occurrences have been grouped into "uraniferous areas" on Figures 5.2.1.1 etc., in order to provide a target size more nearly commensurate with the size of the 64 x 64 pixel texture measure "window";

Table 5.2.1.1 - DISPLAY OPERATORS CARRIED-OUT ON
COPPER MOUNTAIN AREA

<u>Operator</u>	<u>Band</u>	<u>Threshold</u>
Edge (E)	5	0, 1, 2, 3
Line detector (Z)	5	1, 2, 3
Thinned line detector (ZZ)	5	1, 2, 3
Global stretch (H)	5	
Local stretch (S)	5	
Texture transform (N)	5	

Copper Mountain Area

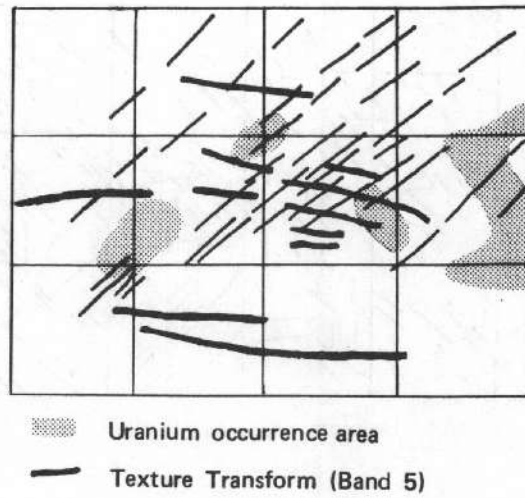


Fig. 5.2.1.1-- Lineaments drawn on Local Histogram stretch(Band 5) compared with those on Texture Transform(Band 5)

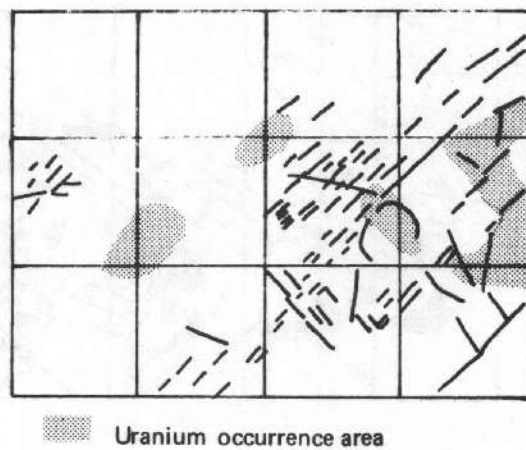


Fig. 5.2.1.2-- Lineaments drawn on Edge Detector (Band 5) at Threshold 1

Copper Mountain Area

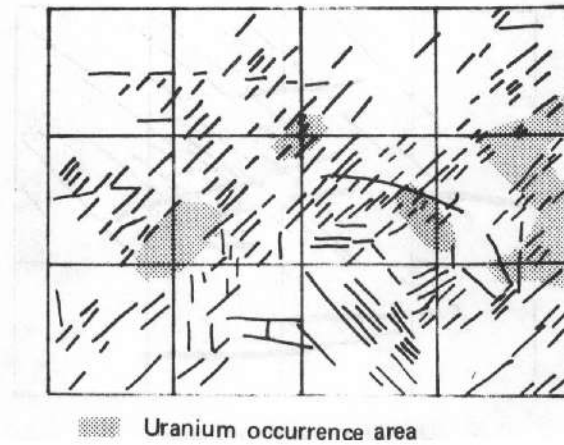


Fig. 5.2.1.3-- Lineaments drawn on Edge Detector (Band 5) at Threshold 2

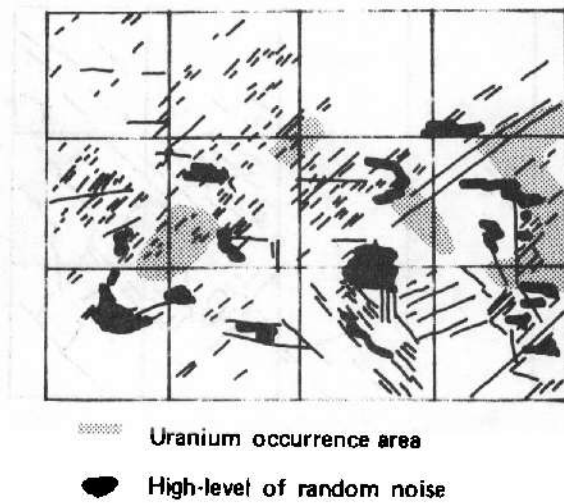


Fig. 5.2.1.4-- Lineaments drawn on Edge Detector (Band 5) at Threshold 3

and (b) Figure 5.2.11, etc. are drawn from overlays created for unsquared tape outputs. It is important to note that for texture analysis we worked throughout with unsquared tapes (see Section 2.4), since squaring creates the possibility of introducing artifacts into the data.

Thinned edges on band 5 thresholded at 1 and 2 had no relationship to uranium distribution (Figures 5.2.1.2 and 5.2.1.3). Nor did difference maps between thinned lineaments on band 5 thresholded at 3 & 2 and at 2 & 1 show any relationship to uranium (Figure 5.2.1.5).

However, a very weak inverse relationship between areas of uranium mineralization and edges thresholded at 3 on band 5 was apparent. On these displays several uranium areas appeared almost devoid of edges, but were ringed by areas of denser than normal edges (Figure 5.2.1.4). The significance of this relationship was weakened by the facts that:

1. It did not hold for all uranium areas.
2. Some known barren areas also had very low edge densities.

No correlation existed between particular lineament directions and uranium or between lineament lengths and uranium.

No significant relationship existed between any of the measures tested on Eigenband 3 and uranium.

5.2.2 Pumpkin Buttes

Display operators were run on the Pumpkin Buttes training area as shown in Table 5.2.2.1. It was decided in

Copper Mountain Area

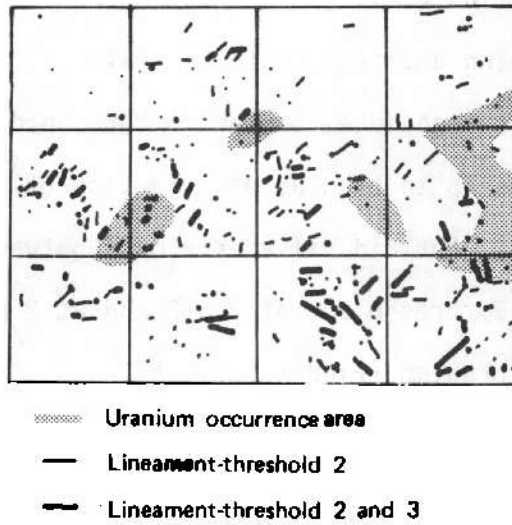


Fig. 5.2.1.5— Comparison between lineaments on Band 5 Line Detector at Threshold 3 versus Threshold 2

Table 5.2.2.1 - DISPLAY OPERATORS PROCESSES CARRIED-OUT ON
PUMPKIN BUTTES AREA

<u>Display Operator</u>	<u>Spectral Band</u>				<u>Eigen</u>			
	4	5	6	7	1	2	3	4
Texture transform (N)		X		X	X	X	X	
Local histogram stretch (S)		X		X	X	X	X	
Sub-image ("global") histogram stretch (H)		X		X	X	X	X	
Line detector (Z)		X		X	X	X	X	
Thinned line detection (ZZ)		X		X	X	X	X	

advance that Landsat bands 4 and 6 would probably add little information to that obtained from bands 5 and 7. This is so because the reflectance in bands 4 and 5 are strongly correlated and those in bands 6 and 7 are even more so. Display operators were not run on Eigenband 4 because of:

1. The very low information content of this band revealed by inspection.
2. Theoretical considerations (see Reference 4) which suggest that Eigenband 3 contains the texture information.
3. The fact that texture measures run on Eigenband 4 did not appear meaningful in the Pumpkin Buttes area.

5.2.2.1 Discussion

When overlays showing both individual deposits and uraniferous areas were placed over the displays, no obvious correlation between any feature in any of the displays and either the uranium occurrences or uranium areas was noted.

The displays were therefore manually interpreted for:

1. All lineaments (Figure 5.2.2.1).
2. Lineaments in given directions only (Figure 5.2.2.2 and Figure 5.2.2.3).
3. Major lineaments (Figure 5.2.2.3).
4. Circular features (Figure 5.2.2.8).
5. Lineament intersections (Figure 5.2.2.4).
6. Length of continuous edges, straight or bent.

No strong correlations with known uranium occurrences were found in any of these exercises. In addition, there is such a strong tendency for lineament segments to trend either 0° , 45° , 90° , or 135° with respect to image north that it is suspected that artifacts arising from the scanned nature of the Landsat data may be present.

When the natural directions of the terrain are close to coinciding with certain preferred directions associated with the scanning nature of the MSS sensor, interference effects can occur. These look like a spurious, high-frequency "shading" on the imagery, and can often be recognized because they persist across very large regions of an image. We have therefore learned to treat with caution any pronounced sets of lineaments that appear at the angles mentioned above, unless we have other reasons to believe them to be real.

In Figure 5.2.2.1, there are vague hints of an association between uraniumiferous areas and swarms of short northeast-southwest lineaments. In Figure 5.2.2.2, only northeast-southwest and northwest-southeast lineaments are plotted, and no real association between northeast-southwest lineaments and uranium is seen. However, several groups of uranium deposits occur along alignments of northwest-southeast lineaments that may represent major throughgoing lineaments. Figure 5.2.2.3 shows major throughgoing lineaments in the northwest and northeast directions; again, little real association with uranium is found.

Figure 5.2.2.4 again shows major lineaments, but emphasizes directions other than 45° - 135° with only the very

Pumpkin Buttes Area



Uranium occurrence area

Fig. 5.2.2.1--All lineaments drawn on Band 5 Line Detector (Z)

Pumpkin Buttes Area



Fig. 5.2.2.2— All lineaments trending at 45° or 135° drawn on Band 5 Thinned Line Detector(ZZ)

Pumpkin Buttes Area



Fig. 5.2.2.3— Major lineaments trending at 45° or 135°
drawn on Band 5 Line Detector(Z)

Pumpkin Buttes Area

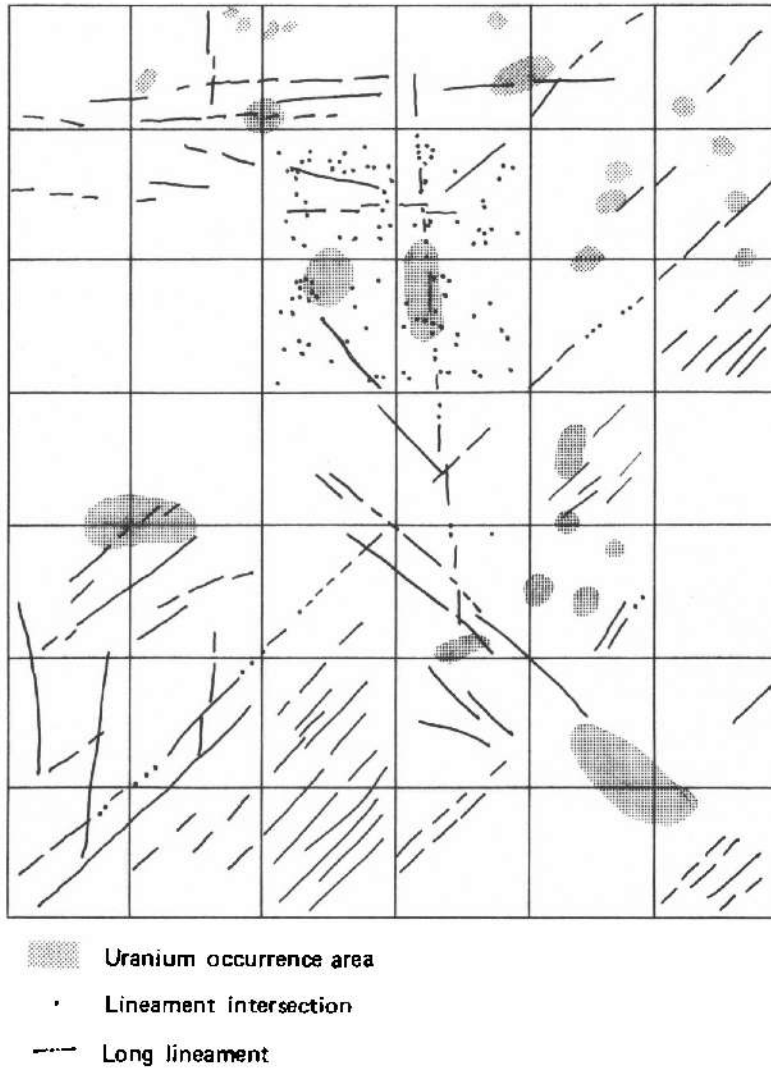
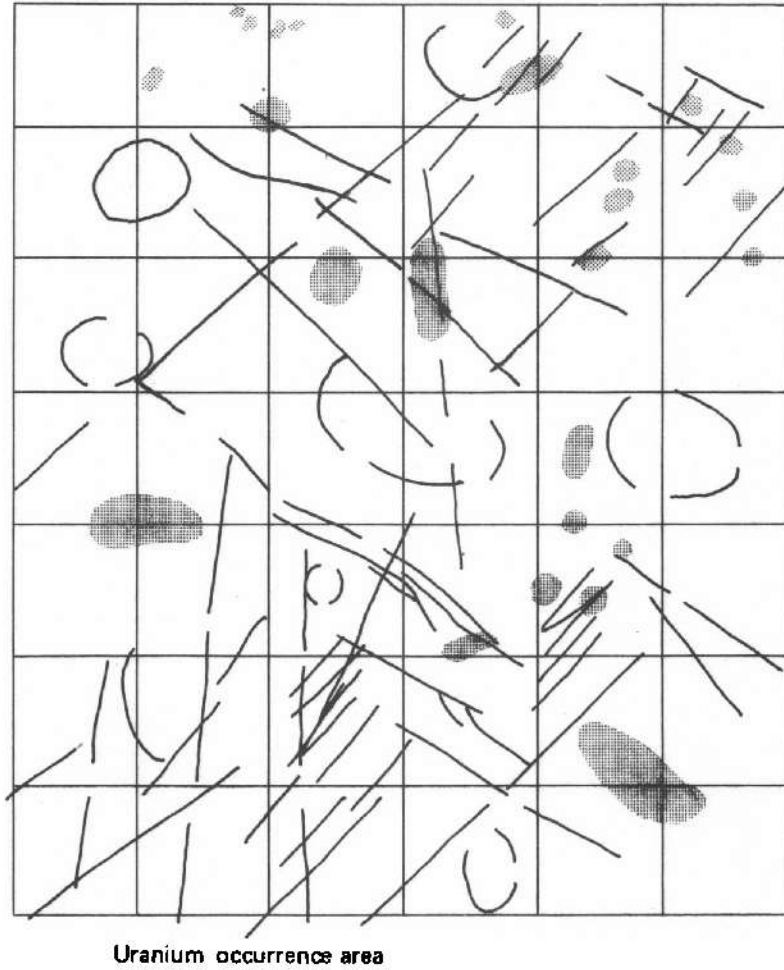


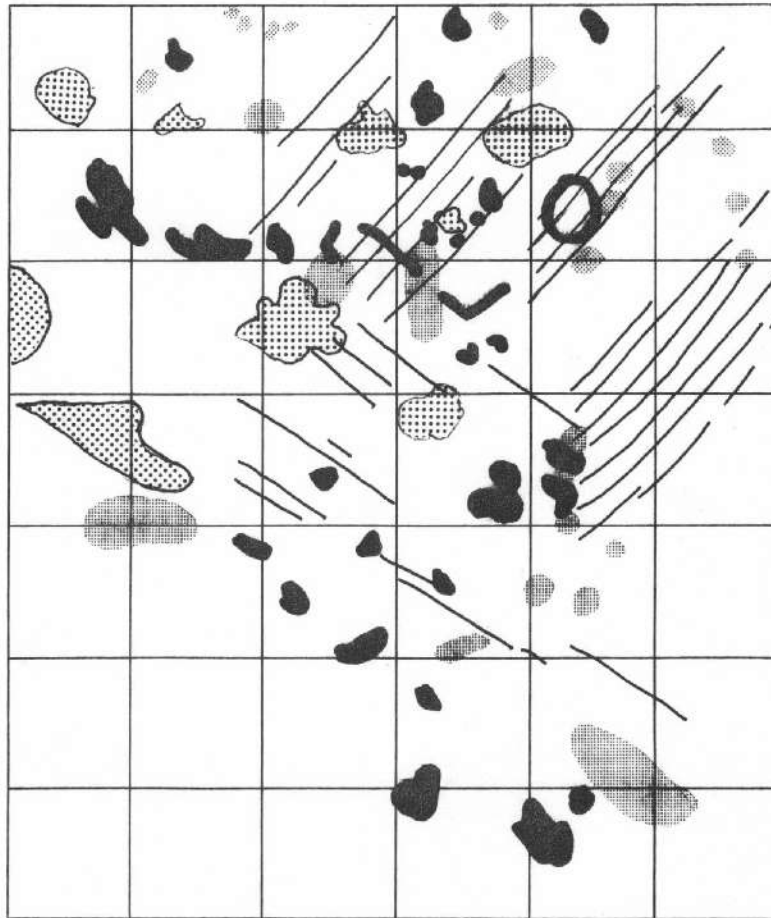
Fig. 5.2.2.4— Lineament intersections and long lineaments (excluding those trending 45° and 135°) on Band 5 Thinned Line Detector(ZZ)

Pumpkin Buttes Area



**Fig. 5.2.2.5. Lineaments and circulars on Eigenband 1
Global Histogram Stretch (H)**

Pumpkin Buttes Area



Uranium occurrence area



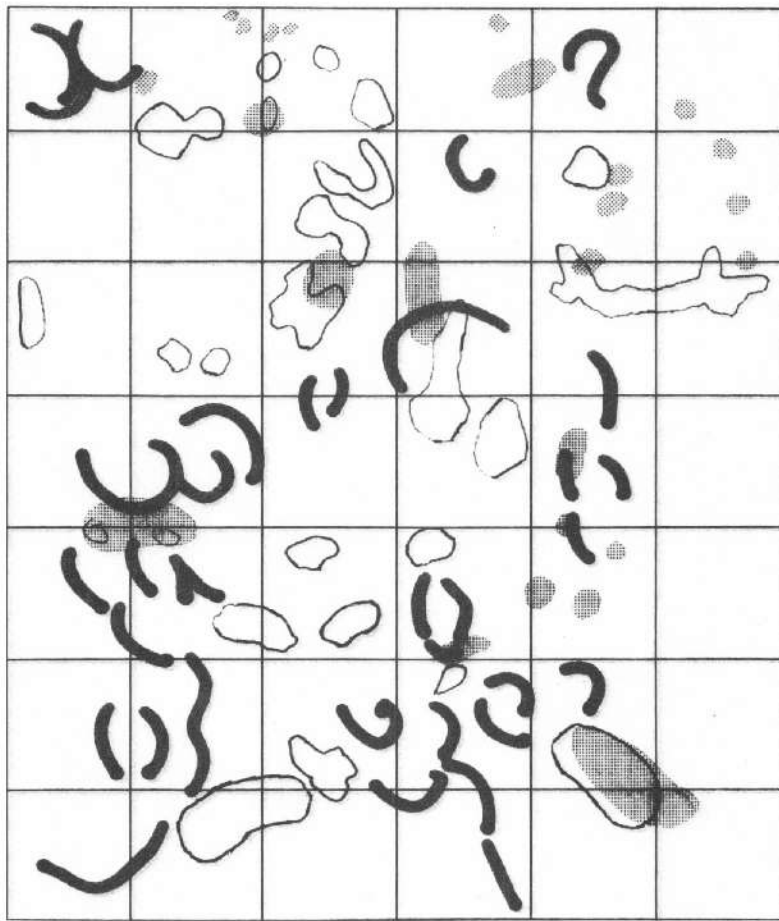


-  Dark-toned area
-  Light-toned area

Fig. 5.2.2.6— Lineaments, and extreme dark and light-toned areas on Eigenband 1 Texture Transform(N)

Pumpkin Buttes Area

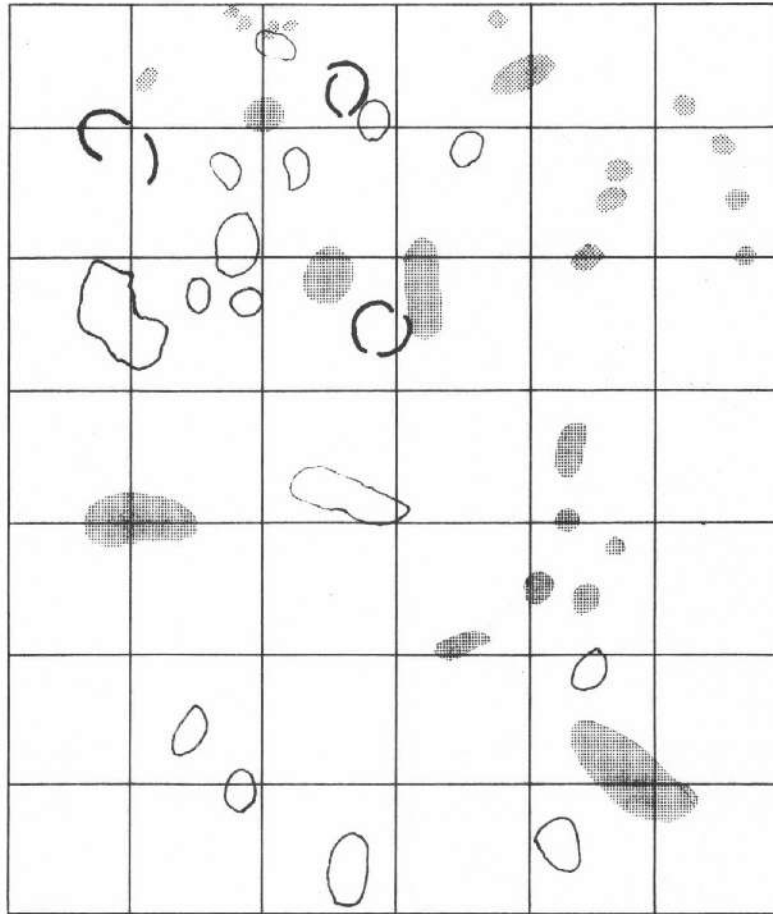


Uranium occurrence area

-  Dark-toned feature
-  Light-toned area

**Fig. 5.2.2.7-- Dark and light-toned areas on Eigenband 3
Texture Transform(N)**

Pumpkin Buttes Area



Uranium occurrence area



Circular



Low contrast feature

Fig. 5.2.2.8. Circulars and low contrast features on Eigen band 3 Local Histogram Stretch(S)

strongest of the latter shown. No correlation is apparent. Dots in Figure 5.2.2.4 represent lineament intersections, and represent an attempt to correlate density of lineament intersections with uranium. On this brief trial, no correlation is seen.

Figure 5.2.2.5 shows lineaments and circular features mapped on the global histogram stretch display. No correlation is apparent. Figure 5.2.2.6 shows lineaments, dark and light areas on the texture transform of Eigenband 1. Again, no correlation is apparent. Figure 5.2.2.7 shows dark areas and light contrast areas on the Eigenband 3 Texture Transform, and Figure 5.2.2.8 shows circular features and low contrast areas on the Eigenband 3 local histogram stretch. On neither of these are any correlations apparent.

The above comments apply to the most promising features interpreted on the most promising looking displays. Several other interpretations were done on other displays, but the results are all equally negative.

It is concluded from these exercises that:

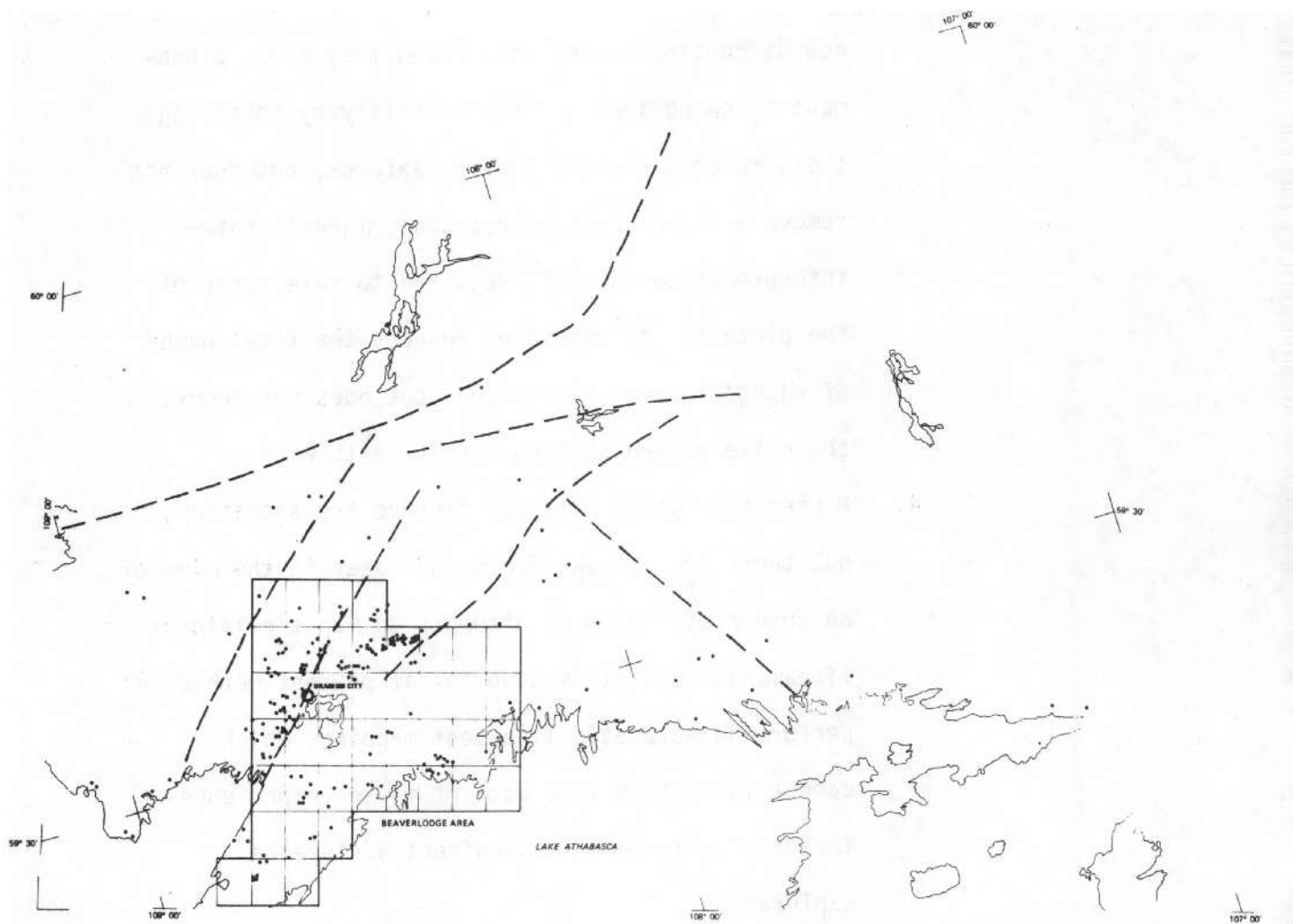
1. Landsat resolution is probably too coarse to allow automatic classification of textures or of lineaments to pick out features which are geologically significant at the scale of a uranium mining district.
2. Present automatic edge detection and lineament mapping programs are affected by artifacts inherent in the mode of Landsat data acquisition.
3. Present edge detection and lineament mapping programs are not well adapted to geologic exploration,

in that they detect all edges/lineaments, no matter how discontinuous and convoluted they are. Lineament thinning improves their utility by enhancing the straight, aligned linear features, but does not remove all the wiggly ones; thus, manual photo-interpretation is still required to make sense of the picture. Thresholding reduces the total number of edges/lineaments detected, but does not remove the noise caused by "non-linear features."

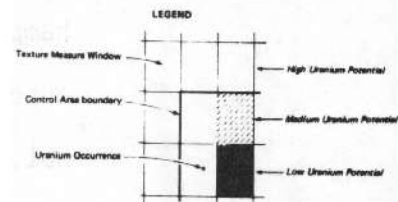
4. Higher resolution data may improve the situation, but there are so many facts and ideas in the mind of an interpreter when he attempts to map significant lineaments that it is doubtful if present methods of performing automatic lineament mapping, which cannot fully take into account these "experience factors," will be of much direct assistance to exploration.

5.2.3 Beaverlodge

Use of the display operators in the Beaverlodge area is hampered by the large number of lakes all of whose shorelines appear as sharp edges, whether geologically significant or not, but fail to appear at all as lines (see Appendix 4 for this distinction), although they may be geologically significant. Because the latter disadvantage was regarded as the greater, only the edge-detector program was run on the Beaverlodge



PREPARED BY
EARTH SATELLITE CORPORATION
 WASHINGTON, D. C.



URANIUM OCCURRENCE MAP FOR THE BEAVERLOGE AREA OF SASKATCHEWAN

JUNE 1978
 REVISED AUGUST 1979
 C-1153

Figure 5.2.3.1

Beaverlodge Area

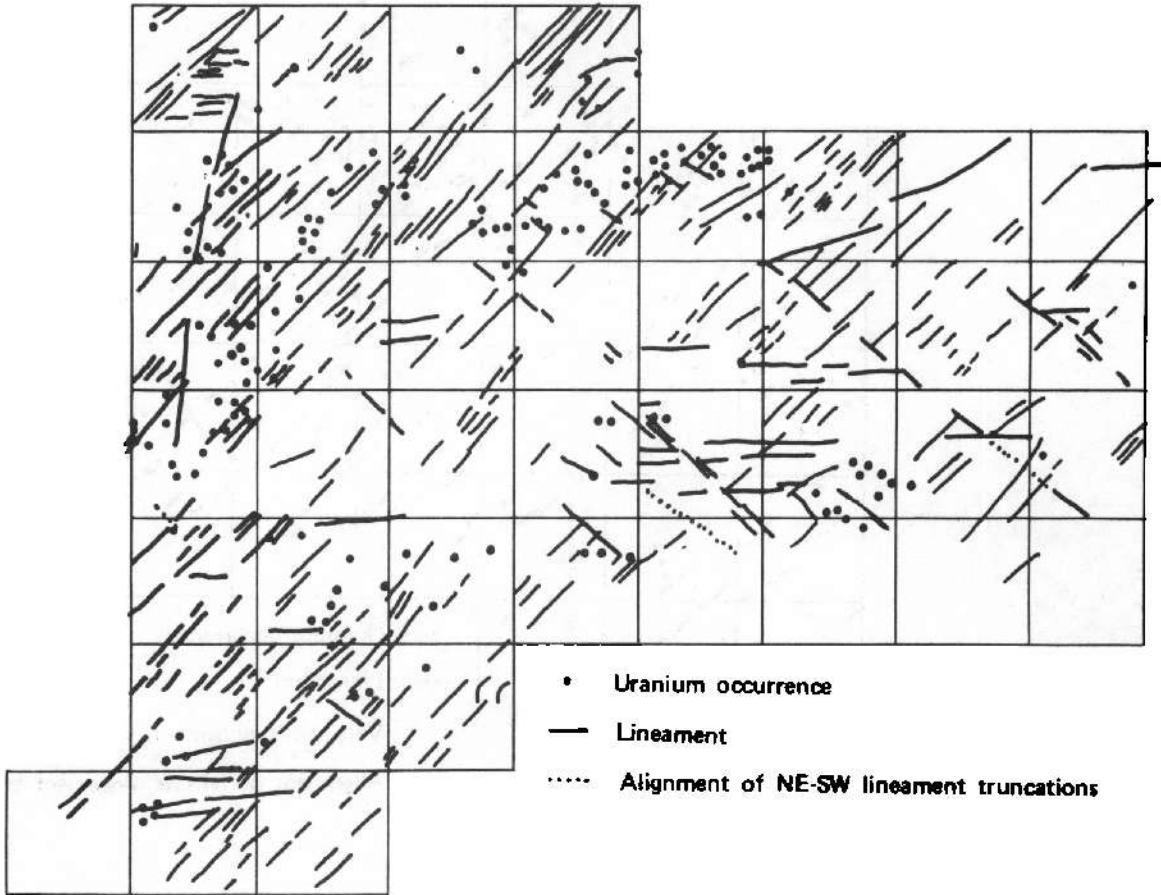


Fig. 5.2.3.2 All lineaments drawn on Band 7 Edge Detector at Threshold=1

Beaverlodge Area

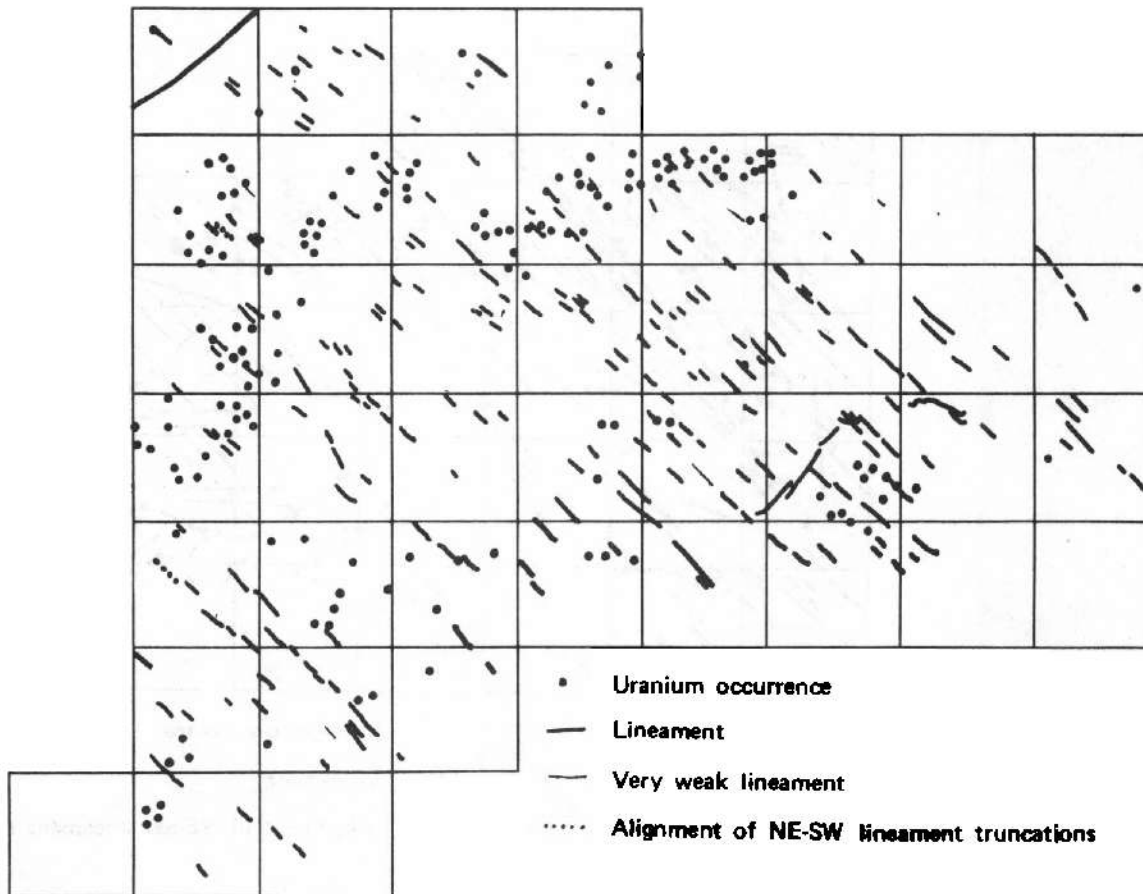


Fig. 5.2.3.3. Lineaments trending 45° and 135° drawn on E1, Edge Detector at Threshold=2.

Beaverlodge Area

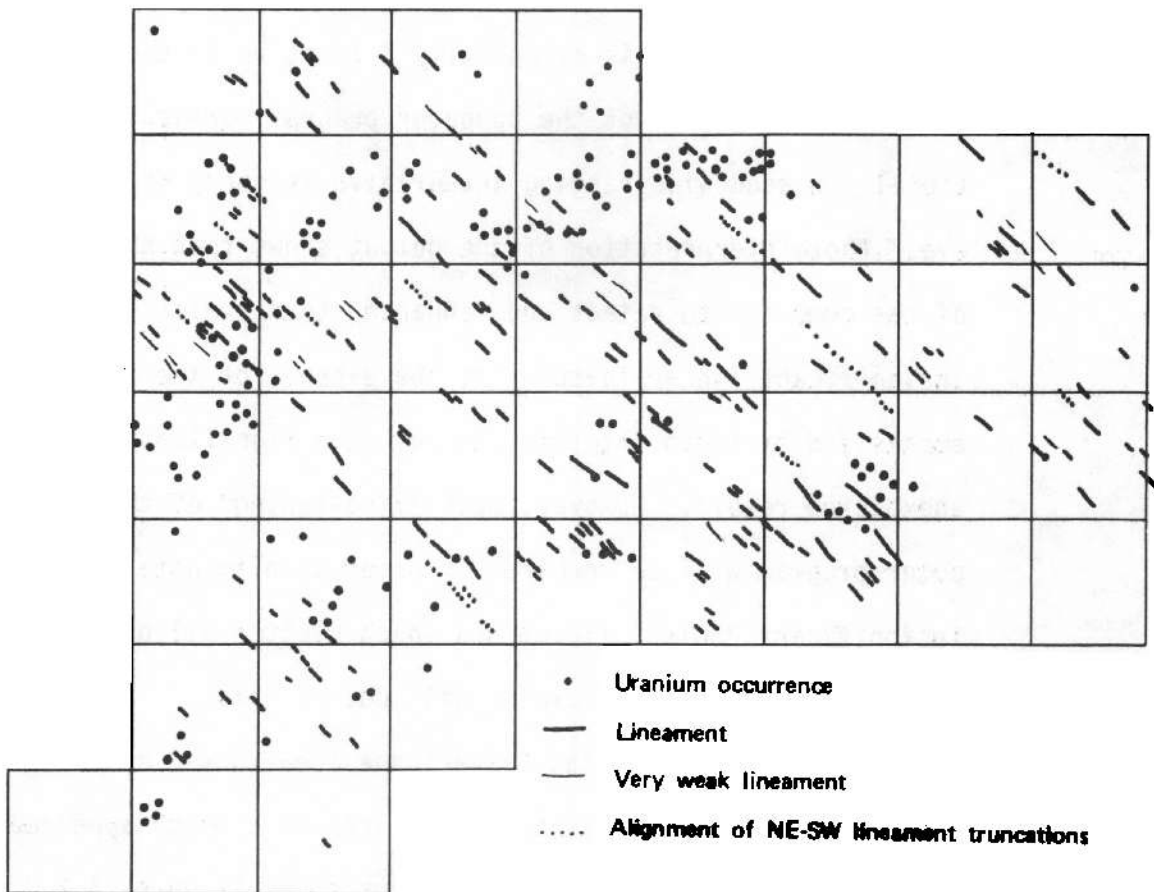


Fig. 5.2.3.4 Lineaments trending 135° drawn on Band 7 with Edge Detector at Threshold=2

area. It was run on band 7 and Eigenband 1, which show the greatest amount of geology-related information, and was run with various thresholds.

The edge detector program tends to de-emphasize the major fault-related NE-SW lineaments visible on the enhanced imagery and to emphasize the minor lineaments in the scene at their expense. This is essentially a function of the random, short-range approach of the computer program versus the directionally biased wide-ranging integrative tendency of the human eye. Photointerpretation of the output shows that the ability of the computer to detect and "enhance" these relatively insignificant linear features at the expense of the major ones emphasized by human interpreters may be a significant and unexpected result. However, much "fine-tuning" of the computer program will be required in order to eliminate the truly insignificant "noise" lineaments which clutter all of the displays. Simple thresholding will not do this.

All outputs for the Beaverlodge area showed a series of short straight northwest-southeast lineaments which appeared to correlate poorly with uranium occurrences (Figures 5.2.3.1, 5.2.3.2, 5.2.3.3, and 5.2.3.4). The color composite and band 7 images were photointerpreted for the same set of lineaments. Results were less satisfactory for band 7 than for the displays, but about the same for the color composite and the displays; however, it took much longer to interpret the color composite than the displays.

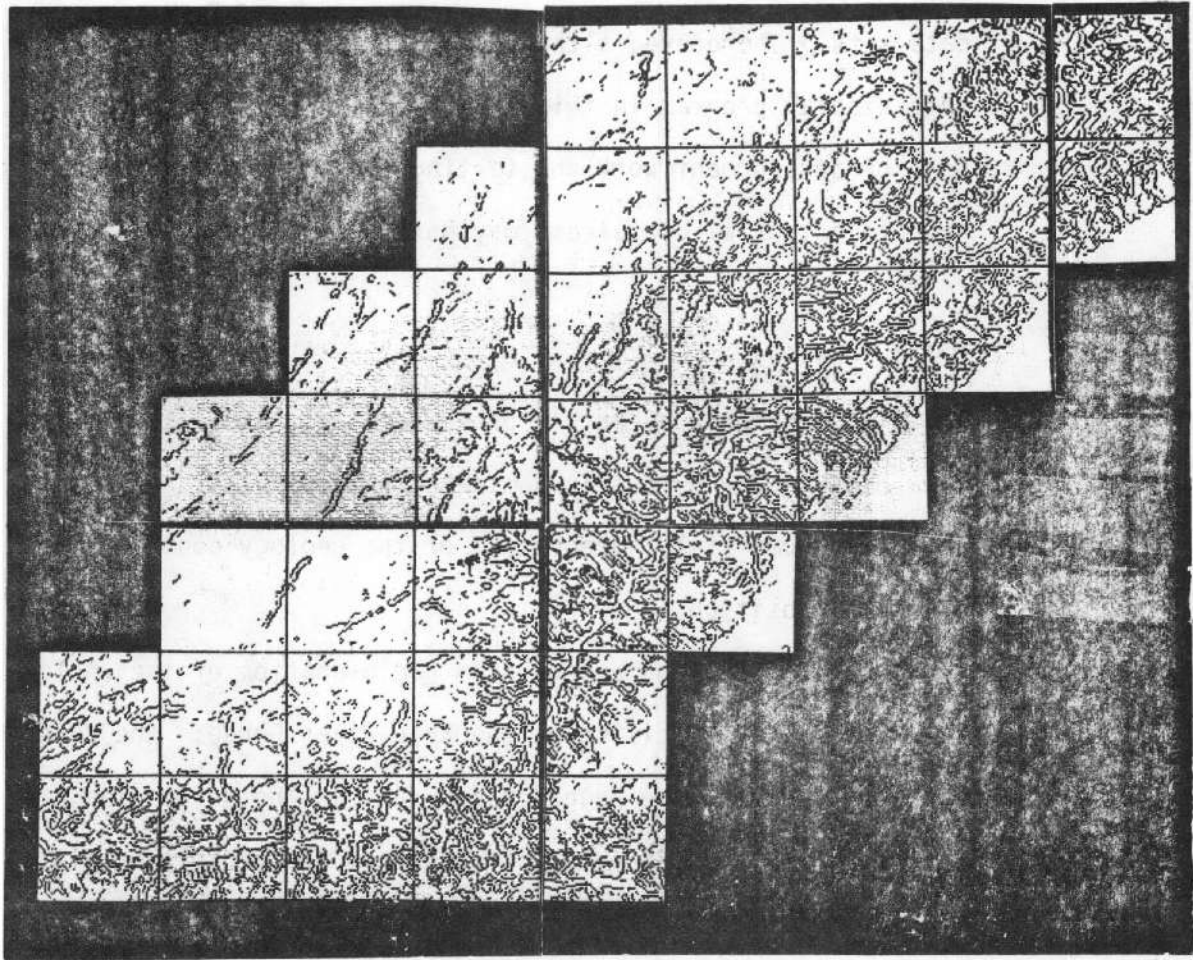


Fig. 5.2.4.1 Band 7 Edge Detector at Threshold=2 for Rossing Area of Namibia

However, in all cases, the correlation of the lineaments and ore occurrences is only tenuous, and too many lineaments are found for the method to be of practical use in exploration in an unknown area without extensive correlation with other data sets. Therefore, although some promise was shown by the edge display program in this area, it is clear that a great deal of development work and testing of the program is required and its potential usefulness may not justify the cost.

5.2.4 Rossing

The display operators proved entirely useless in this area because the output is dominated by topographic effects which are completely independent of the geology controlling uranium deposition.

This situation arises from pediplanation of the whole area followed by incision of the Khan River Gorge: the Rossing deposit occurs in the rugged topography in the gorge area, whereas the Trekkopje prospect occurs on the pediplain, although the geologies of the two are very similar. The human interpreter can see the similarity of geology on the Landsat image (on which it is obvious that both deposits occur at equivalent stratigraphic horizons at the noses of domes), because the human eye automatically takes into account the great differences of contrast and quantity of detail between the two areas. The computer program cannot do this, and so the edge detector applied to band 7 (Figure 5.2.4.1) prints out a meaningless

jumble of detail at Rossing, even when thresholded at level 2, and shows the Trekkopje area as a featureless blank. This effect was so obvious that no further display operators were run at the Namibia site.

6.0 CONCLUSIONS AND RECOMMENDATIONS

The conclusions that we present here are directed to two principal questions, which we may phrase as follows:

1. Are there unique textures associated with the presence of uranium deposits?
2. Assuming that the answer to Question 1 is affirmative, can such textures be detected using information at the resolution collected by the Landsat series of spacecraft?

Since we approached Question 2 using a particular set of texture analysis procedures on a particular set of test areas, we may add two more questions, thus:

3. Were the texture analyses performed on this project exhaustive enough to answer Question 2?
4. Was the data base of available information about test areas sufficient to answer Question 2?

We will present our conclusions by addressing these questions in the inverse order to that given above, thus our most general conclusions are those given in Section 6.4.

6.1 Conclusions Regarding the Available Data Base

1. Attempts to derive any form of texture measures that can be carried across Landsat frame boundaries were unsuccessful. Therefore, we were obliged to use training and test areas that lay on the same frame. In some test areas (notably Namibia), this meant that we had very few known uraniumiferous areas on which to train texture discrimination procedures.
2. The effectiveness of every texture measure as a method for distinguishing uraniumiferous from non-uraniferous

terrain using Landsat imagery depended on the geological type of the uranium-bearing structure. Thus we not only are limited to single frame analyses, but we can search within that frame only for uranium deposits of a type already known to be present somewhere in that frame.

3. All comparisons performed on the project are weakened by the fact that the only possible tests compare uraniferous areas with unknown areas, rather than with areas known to be non-uraniferous. The comparison of uraniferous versus non-uraniferous is possible where extensive exploration of the whole area has been performed, but such areas have had their texture modified considerably by the exploration process itself.

6.2 Conclusions Regarding the Completeness of Texture Analysis Tools Used on the Project

1. For the texture display operators, some kind of combined line and edge detector would be desirable, since neither of the two outputs can be used effectively alone.
2. In addition to the displays that show edges and lines, an improved capability to link together interrupted lineaments is needed. The present methods provide too many short and unconnected lineaments, which makes their analysis by human interpreters a major task.
3. An improved program for automatic lineament thinning would be desirable.
4. Again for the displays, some type of "intersection density" map for linears would be desirable. We do not know in

- detail how much effort would be needed to develop such a program, although the principles are clear enough.
5. On the texture measures, we were obliged to use a fairly large window (64 x 64 pixels, which is about 3.6 kms square) in order that the statistical measures developed within each window should have reasonable validity. However, there is a trade-off between the size of the window, and the ability to discern very local features of a scene. Clearly, this problem would be diminished if we had available a higher resolution satellite. For example, a similar analysis using Landsat-D would allow us to look at windows that were 1.9 kms square (which is still larger than we would wish, by an order of magnitude).
 6. Texture measures in some areas (notably Grants, Gas Hills, and Marysvale) are strongly controlled by gross geologic and geomorphological features. Thus textures potentially associated with uranium occurrences are too subtle to be detected by present techniques. Again, this situation would be improved by the availability of a higher resolution data source.

6.3 Conclusions Regarding the Detection of Uranium-Related Textures from Landsat Data

1. Of all the data sources available for analysis (which included the original Landsat bands, band linear combinations, and band ratios) the most promising for performing uranium/non-uranium discrimination based on texture is clearly Eigenband 3.

2. Of all the measures and displays used to discriminate uranium deposit areas from areas not known to contain uranium, the most successful was the texture measure pair IDM/ASM, applied to the third Eigenband of the Landsat data.
3. Although the IDM/ASM measure on Eigenband 3 fails completely for some types of terrain and geologies, we achieved some success using it for the Pumpkin Buttes/Kaycee and Gas Hills types of terrain.
4. The success of the IDM/ASM measure pair could not be explained by an analysis simply related to visible tonal values on the image. In other words, we seem to have a non-intuitive classification tool that deals with a category of image texture not readily discernible to the human eye.
5. Although the use of texture displays was limited by some of the factors mentioned in 6.2 above, there were hints that we could use them in areas where the scene relief is not too great. It is difficult to be more specific or more quantitative than this from the data available on the project.

6.4 Conclusions Regarding the Association of Texture with Uranium Deposits

1. Although visual inspection of Landsat images reveals no type of texture specifically associated with uranium occurrences, nonetheless the computed texture measures in

some types of geology did provide a capability to discriminate uranium from non-uranium areas.

2. The capability to discriminate is a weak one, since the discrimination function that we used must be separately computed for each type of geology and for each Landsat frame. Different Landsat frames possess different image properties because of variations in sun angle, atmosphere, and season. These differences are present even when we are looking at successive passes of the satellite over the same ground areas, and are more pronounced the further away that we go in space and time.
3. The discrimination capability is limited by the resolution of the system, which implies the use of large scene windows for texture measurement. There is a good chance that the relation of texture to uranium could be made much more explicit if we had available higher resolution spacecraft data.

6.5 Recommendations

1. Additional analyses of the type performed here should be performed when the higher resolution (and increased spectral coverage) data of Landsat-D becomes available. We anticipate that substantially stronger conclusions will be possible with such data.
2. Some of the results we obtained are inconclusive because of the limited data available (particularly in terms of known uranium deposits, for some training and test sites).

Therefore, we recommend that any future work should be performed on one or two areas, where there are many known occurrences, and where more exhaustive analysis can be performed.

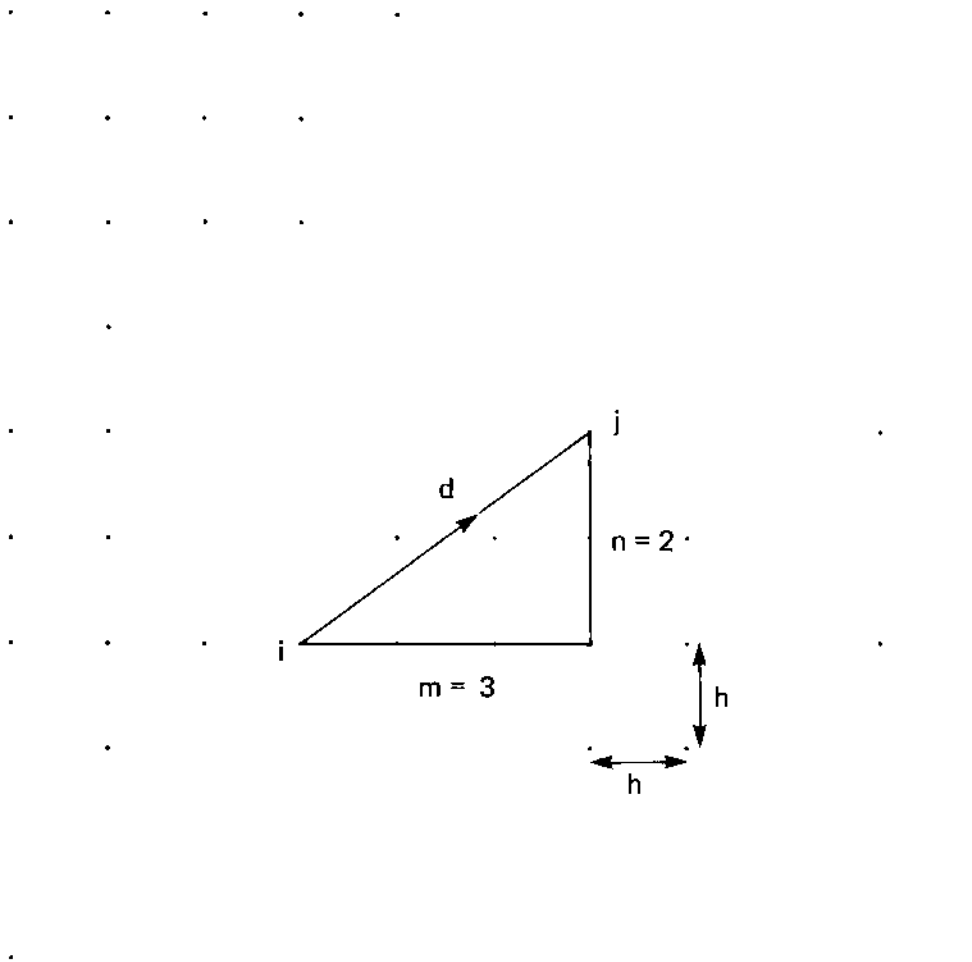
3. If additional analysis is to be performed of this type, we recommend that the additional tools described in Section 6.2 should be developed, namely, computer programs that permit improved lineament thinning and the connection of interrupted lineaments. If possible, a program that combines the main features of edge detection and of line detection should also be developed.
4. In any future work, provision should be made for more field trips to the areas that are to be analyzed.
5. Since the methods we used were limited by an inability to jump Landsat frame boundaries, methods for removing the effects of atmosphere and sun angle changes on Landsat imagery should be explored. If successful, such removal would permit a discrimination function developed for one area to be applied to another frame, and would greatly increase the potential scope of the texture classifications.

APPENDIX 1
THE USE OF TEXTURE MEASURES

In this Appendix, we develop the set of texture measures used on the project. It should be mentioned that there are other sets, based on different concepts and used by other researchers (see References 1 and 5). However, all texture measures are based on a single underlying set of ideas, though they differ in computational details.

Texture is rather an elusive property, and although we can recognize readily enough what the human eye admits as texture, defining it in quantitative terms is not easy. We regard texture as a property of the spatial distribution of the grey shades and tonal features of a black-and-white image. When a small area of the image has little tonal variation it appears as a uniform grey. When there is wide variation of tone, the eye sees texture. From this definition, it is clear that texture is resolution dependent, since a textured area may appear grey at lower spatial resolution. We will give the mathematical definition we use for texture later in this section. The main point to note is that our mathematical definition associates texture with an area, rather than a point; that the texture measures depend on the relative sizes of the discrete tonal features; and it depends on the number of distinguishable tonal features at the resolution of the sensor.

We begin with an array of points, assumed to be regular and rectangular, and with a constant separation distance (h) in both directions (see Figure A-1.1). With each point is associated a grey level value. This is an integer, and for subsequent discussion we will



Constant array spacing, h in both x- and y-directions.

$$d = h(m^2 + n^2)^{1/2}$$

Figure A-1.1 Picture element array and notation.

assume that these integers all lie between 0 and 63. As we will see later, the starting point from which the integers are counted is irrelevant - we could equally well say that the range is from 65 to 128. The range 0 to 63 is less than the range used on Landsat tapes (0 to 255). However, in practice the texture analysis was done using grey levels from Landsat that had all been divided by four and rounded so as to avoid anomalies produced by pixel re-allocation caused by the scene destriping procedure.

Consider a pair of points with x and y separations m and n , so that their distance apart is $d = h(m^2 + n^2)^{1/2}$. Let the grey levels of the two points be i and j . Now let us ask what is the probability that this should happen, i.e., what is the probability that a pair of points with relative spacing m, n , should have grey levels i and j ? We call this probability p_{ij}^{mn} .

Clearly for any general array which represents an image, the probabilities p_{ij}^{mn} are unknown. However, we can estimate them by counting how often they occur in a particular image, or a particular sub-image area. Since i and j each run over the range 0 to 63, the probabilities themselves will be an array, of dimension 64×64 , for any particular and fixed choice of m and n . Note that if we do not distinguish the choice (m,n) from the choice $(-m,-n)$, the array of p_{ij}^{mn} is symmetric in i and j .

To estimate the p 's, let us take some $R \times R$ sub-image area, where R is large compared with m and n . Now let N_{ij}^{mn} be the number of pairs of points in the $R \times R$ array with relative distance (m,n) and grey levels i and j . If N^{mn} is the total number of points in the $R \times R$ array with relative spacing (m,n) , then we can approximate p_{mn}^{ij} by using

$$p_{ij}^{mn} = m_{ij}^{mn} = N_{ij}^{mn} / N_{mn}$$

The values of m_{ij}^{mn} can be established by simple frequency counting. This gives us a 64 x 64 array, which is usually termed the co-occurrence matrix, $M(m,n)$, for a particular relative spacing (m,n) . If directions are considered irrelevant, so that all relative spacings (m,n) are considered equivalent when their distance apart is the same, then we can write $M(m,n) = M(d)$, where $d = \sqrt{(m^2 + n^2)}$. This is often done, but is not desirable when it is felt that directionality of texture may be important.

Typically, the pair (m,n) are chosen to be small integers (i.e., 1, 2 or 3). This means that we are looking at the probabilities that nearby pixels have particular grey level values i and j . Now we wish to relate the properties of the co-occurrence matrix $M(m,n)$ with our intuitive ideas of what image "texture" represents. To do so, let us assume that m and n are small and fixed. Then in a "coarse" textured region, we do not expect that neighboring pixels will have widely different grey level values, so neighbors in this case will usually have grey levels that differ by just a few from each other. Thus, we expect that in a region of coarse texture, the values of the elements m_{ij} of $M(m,n)$ will be large when i is almost equal to j , and small when i is very different from j . In other words, the matrix will have large values on and close to the diagonal, and small values well off the diagonal.

In areas of fine texture, on the other hand, large differences of grey level value may be anticipated even for near neighbors. In such a case, we will find a matrix which has large values well off the main diagonal.

In summary, evaluation of texture (fine or coarse) may be accomplished by determining suitable properties of the co-occurrence matrix $M(m,n)$, for small m and n . These properties will relate to the "spread" of the matrix away from its main diagonal, and thus measure the extent to which large differences of grey level are found at nearby image points.

Although in principle any measure derived from the matrix $M(m,n)$ could be used, we can constrain the possibilities by noting the earlier requirement, that the measures should not depend on the absolute values of the grey levels i and j , but only on their relative values. Thus, we will require that measures depend on the values $(i - j)$ rather than on the individual i and j . This means that we will be permitted to weigh any matrix element m_{ij} by functions of $(i - j)$.

To make these ideas more concrete, Figure A-1.2 shows a simple sub-image array for the case where we have two different textures, coarse and fine, and also shows the resulting matrices $M(1,1)$ that result from these arrays. As expected, we find that there is much more spread from the main diagonal where we have fine texture than where the texture is coarse.

It is possible to construct a very large number of possible texture measures. We will confine this discussion to just those measures that were actually used on this project.

1. The Angular Second Moment (ASM)

This is the simple sum $\sum_{i,j} (m_{ij})^2$. It does not depend on i and j (or even on the difference $(i - j)$), and it is smallest when all the entries are equal, i.e., when all values of i and j are equally probable. It is largest when one entry of $M(m,n)$ is non-zero and all the rest are zero. An image of "white noise," with all grey level values equally

probable, would give the smallest value for the ASM. Fine texture will produce smaller values than coarse texture.

For our simple example of Figure A-2, we find:

$$\text{ASM (coarse texture)} = .0523$$

$$\text{ASM (fine texture)} = .0352$$

2. The Entropy (ENT)

This is a concept drawn from Information Theory, and defined as $\sum_{i,j} (m_{ij}) \ln(m_{ij})$. Like the Angular Second Moment, it measures the degree of dispersion of the m , being largest when the m 's are all equal, and small when they are very unequal.

For the simple example of Figure A-1.2, we find:

$$\text{ENT (coarse texture)} = -3.0472$$

$$\text{ENT (fine texture)} = -3.5055$$

Note that neither the Angular Second Moment nor the Entropy is sensitive to whether high values are close to the diagonal or well off the diagonal; they are affected only by the spread of values evenly among all the entries of the matrix. This means that they are weak measures for any particular texture (they cannot, for example, distinguish a coarse texture from certain special fine textures with very large values for particular (and non-zero) values of $(i - j)$).

3. Contrast (CON)

This weights the matrix element with its squared distance from the main diagonal, thus: $\text{Contrast} = \sum_{i,j} (i-j)^2 m_{ij}$

The value of this function is large when there are large entries far from the diagonal, and small when all non-zero matrix elements are close

to the main diagonal. In the limiting case where all grey level values in the original array are equal, the Contrast becomes zero. This corresponds well to the usual definition of contrast, which would be zero in a region that has no variation in grey levels.

For the example of Figure A-1.2, we find:

$$\text{CON (coarse texture)} = 0 \times 54 + 1 \times 37 + 4 \times 38 + 9 \times 3 = \underline{216}$$

$$\begin{aligned} \text{CON (fine texture)} = & 0 \times 21 + 1 \times 28 + 4 \times 9 + 9 \times 19 + 16 \times 23 + 25 \times 14 \\ & + 36 \times 6 + 49 \times 7 + 64 \times 5 = \underline{1832} \end{aligned}$$

4. Inverse Difference Moment (IDM)

This is similar to the Contrast measure, except that the matrix elements are weighted proportional to the inverse square of the value of $(i - j)$, with an added factor of unity to assure that no zero divisors are encountered. Thus Inverse Difference Moment = $\sum_{i,j} (1 + (i-j)^2)^{-1} m_{ij}$.

For example of Figure A-1.2, we have:

$$\text{IDM (coarse texture)} = 1 \times 54 + 1/2 \times 37 + 1/5 \times 38 + 1/10 \times 3 = \underline{80.4}$$

$$\begin{aligned} \text{IDM (fine texture)} = & 1 \times 21 + 1/2 \times 28 + 1/5 \times 9 + 1/10 \times 19 + 1/17 \times 23 \\ & + 1/26 \times 14 + 1/37 \times 6 + 1/50 \times 7 + 1/65 \times 5 = \underline{40.97} \end{aligned}$$

As the example demonstrates, the Inverse Difference Moment is small for an area with fine texture, and large for an area with coarse texture.

5. Correlation (COR)

The correlation referred to here is not among the rows and columns of the co-occurrence matrix, although it is expressed in terms of it. The correlation is of the elements of the original picture array. It is defined by:

$$\text{Correlation} = \frac{\sum_{i,j} (ij)m_{ij} - m^2}{\sigma^2}$$

where m is the mean of the row sums and σ is the standard deviation of the row sums.

We note that the expression is independent on the actual base with respect to which i and j are measured, since addition of any constant to i and j changes the means by the same amount, leaving the correlation unchanged.

For the example of Figure A-1.2, we find:

$$\text{COR (coarse texture)} = 0.53$$

$$\text{COR (fine texture)} = 0.71$$

From these five texture measures, ten pairs can be made (taking the measures two at a time). In this project, these ten pairs were exhibited as two dimensional plots, in which the texture values for each window (chosen as 64×64 arrays of pixels) for two measures were plotted as a single point in an (x,y) coordinate system. Texture pairs were judged successful in separating uranium from non-uranium areas, according to the way in which the two-dimensional region could be separated into two parts by a line, on one side of which lay all the uranium area points, and on the other side of which lay the non-uranium points.

This was done using several different values of the relative displacement (m,n) . In early experiments on the project, it was found that the best results were obtained using the averages of the $(1,1)$, $(1,-1)$, $(-1,1)$ and $(-1,-1)$ displacement set, or the averages of the $(1,0)$, $(0,1)$, $(-1,0)$ and $(0,-1)$ displacement set. We term these the "distance-1" set.

The complete set of (m,n) values used in the experiments are as follows:

$(1,0)$, $(1,1)$, $(0,1)$, $(-1,1)$, $(-1,0)$, $(-1,-1)$, $(0,-1)$, $(1,-1)$

$(2,0)$, $(2,2)$, $(0,2)$, $(-2,2)$, $(-2,0)$, $(-2,-2)$, $(0,-2)$ $(2,-2)$

$(4,0)$, $(4,4)$, $(0,4)$, $(-4,4)$, $(-4,0)$, $(-4,-4)$, $(0,-4)$, $(4,-4)$

Figure A-1.2(a) Example, coarse texture array

1	2	3	4	5	6	7	7	7	6	5	4
2	3	4	5	6	7	8	7	6	5	4	3
2	2	3	4	5	6	7	8	8	7	6	5
2	3	4	5	6	7	8	9	9	8	7	6
3	4	4	5	6	7	8	9	8	7	6	5
4	4	5	6	7	8	9	9	9	8	7	6
4	5	5	6	7	8	9	9	8	7	6	5

(b) The co-occurrence matrix for example (a), average of $M(1,1)$ and $M(1,-1)$.

0	0	1	0	0	0	0	0	0
	3	2	4	0	0	0	0	0
		4	2	4	1	0	0	0
			8	6	5	1	0	0
				6	5	9	1	0
					9	6	9	0
						11	6	6
							7	10
								6

The matrix is unnormalized.
Probabilities are found by
dividing each element by the
sum of all the elements.

The matrix is symmetric about its principal diagonal - only the upper half is shown here.

Figure A-1.2, continued(c) Example, fine texture array

5	1	4	8	5	9	4	1	6	8	6	2
1	5	8	4	9	5	2	1	5	1	6	9
9	5	1	5	9	5	1	5	9	5	2	6
6	8	4	1	1	4	8	6	9	5	2	6
2	4	7	9	5	1	7	4	1	4	7	9
7	2	3	8	5	7	4	6	3	7	2	7
3	7	9	4	7	3	6	9	5	1	3	8

(d) The co-occurrence matrix for example (c), average of $M(1,1)$ and $M(1,-1)$.

4	3	1	5	10	7	2	3	5
	1	1	2	3	1	1	2	4
		0	5	1	0	3	0	2
			3	7	1	3	1	6
				4	3	3	6	8
					2	3	1	2
						5	3	0
							1	3
								1

The matrix is unnormalized.
Probabilities are found by
dividing each element by the
sum of all elements.

The matrix is symmetric about its principal diagonal - only
the upper half is shown here.

However, in testing the effectiveness of the measures, averages were taken of all the distance-1 sets, also over the distance-2 and distance-3 sets. Thus the comparison was done only between these averaged measures. It would have been prohibitively expensive to try and compare all sets for all texture measures.

After the first experiments, attention was concentrated on the distance-1 measures for the IDM/ASM pair. This showed the best separation of the ten pairs. When used on the third Eigenband on the image, it permitted easily the best separation lines to be drawn on the two-dimensional plots.

6. Difference Histogram Statistics

Although it was decided early in the project to use co-occurrence matrix statistics rather than difference histogram statistics as the primary tool in exploring image textures, since the latter were included in the early stages of the project, we are including for completeness a brief summary of them here.

Difference histogram statistics are basically probabilities that various local grey level differences will occur in the neighborhood of a point of an image (see References 2 and 5).

Suppose that P is any local picture property, i.e., it is a property whose value for the picture at a point (x,y) depends only on the grey levels in a small neighborhood of (x,y) . If the property can take on only a discrete set of values, $(1,2,\dots,N)$, the property will have a probability density that we can represent by the set $(h(1), h(2), \dots, h(N))$. To determine the values $h(n)$, we must determine the number of times that P has the value n in the image. Usually, we deal not with

the whole image, but with a sub-image area, such as the windows (64 x 64 pixels) that we used on this project.

The picture properties that were used for texture analysis in this work were the directional differences of grey levels. Clearly, we can look at pixels that are 1,2,3... pixels apart, and we can look at horizontal, vertical, and diagonal pixel pairs. In addition, before considering differences, we can, if we choose, average grey levels over small regions centered on each pixel.

Finally, we can use any statistic of the histogram as the choice of texture measure, for example, we can use means, variances, higher moments and so on.

The sequence of processes, and the ideas behind them, are probably best illustrated by an example. Figures A-1.1 and A-1.2 show two small windows, the first for a region of "coarse" texture, the second a region of "fine" texture. Let us consider the histogram that results from horizontal differences of grey levels, with a spacing of one pixel (i.e., we take the difference of successive horizontal 3 x 3 pixel averages, and display the histogram for the whole window).

Now let us calculate the mean of each histogram. We can see that the mean is substantially higher for coarse texture than for fine texture. Thus the histogram mean will allow us to distinguish these two types of texture.

This process also allows us to distinguish directional texture, where the texture in one direction is significantly different from the texture in a direction perpendicular to it.

Coarse texture (from Figure A-1.1) with right horizontal absolute value distance-1 difference histogram, $(n+1,m) - (n,m)$.

<u>Count</u>	11	66	0	0	0	0	0	0
<u>Grey level difference</u>	0	1	2	3	4	5	6	7
<u>Histogram mean = 0.857</u>								

Fine texture (from Figure A-1.2) with right horizontal absolute value distance-1 difference histogram, $(n+1,m) - (n,m)$.

<u>Count</u>	1	2	11	22	30	10	1	0
<u>Grey level difference</u>	0	1	2	3	4	5	6	7
<u>Histogram mean = 3.455</u>								

In more subtle cases, the means of the difference histograms may be the same, but the different textures are distinguished from some higher moment of the histogram (such as the variance).

Appendix 2 - The Creation of Eigenpictures

1. The logic for making eigenpictures. Suppose that we have N well-registered images of a scene (such as the 4 bands from Landsat, or the 13 bands from the Skylab S-192 scanner). IF $N > 3$, it is not possible to convey all the information in N bands on a 3-color composite image. However, in many cases, the information carried by each band is correlated with that in other bands. Thus the possibility exists that, by working with selected combinations of bands, a 3-color composite of 3 band combinations will contain more information about the scene than any 3 of the original bands.

This is the motivation for eigenpictures. Linear combinations of the original bands are sought such that they are:

- (1) independent of each other;
- (2) able to account for a decreasing fraction of the total variance (i.e., difference of grey levels from the mean grey level of the image), so the first band combination accounts for most of the variance, the second a lesser fraction, and so on;
- (3) any 3 band combinations (usually those that account for the largest fractions of the variance) can be used to form a 3-band color composite.

2. A geometric description of the calculation process. Although the geometric description does not help with the computational process, it gives a feel for what is going on during those calculations.

Each picture element in each band has a grey level value, say g_{mn} , where m denotes the number of the pixel (m runs from 1 to M , and for Landsat, M is about 7.6×10^6 for a full frame) and n denotes the number of the band (so n runs from 1 to N).

Imagining the bands as coordinate axes, we can think of each pixel as represented by a point in an N -dimensional space. The case $N = 2$ is easiest to visualize and is shown in Figure 1.

When all the pixels are plotted in this way, we have a cluster of M points in N -space. Usually, their distribution forms a rough ellipsoid about their centroid. On each one of the coordinate axes (i.e., in each band), one can compute the mean of the grey levels, and one can also compute the variance of the grey level distribution, and the covariance between pairs of bands. See Figure 2 for the case $N = 2$.

Note that the origin of coordinates and the orientation of the axes in this representation are both variables that we can choose for our own convenience. First, let us move the origin of coordinates to the centroid of the distribution. This means that, in each band, we use pixel grey level values $(g_{mn} - \bar{g}_n)$ in place of g_{mn} , where $\bar{g}_n =$ (mean of g_{mn}) $= \frac{1}{M} \sum_{m=1}^M g_{mn}$.

Now consider a rotation of the coordinate axes. We seek a rotation such that, in the new axes, the cross-correlation between grey level distributions referred to these new axes should vanish. In geometrical

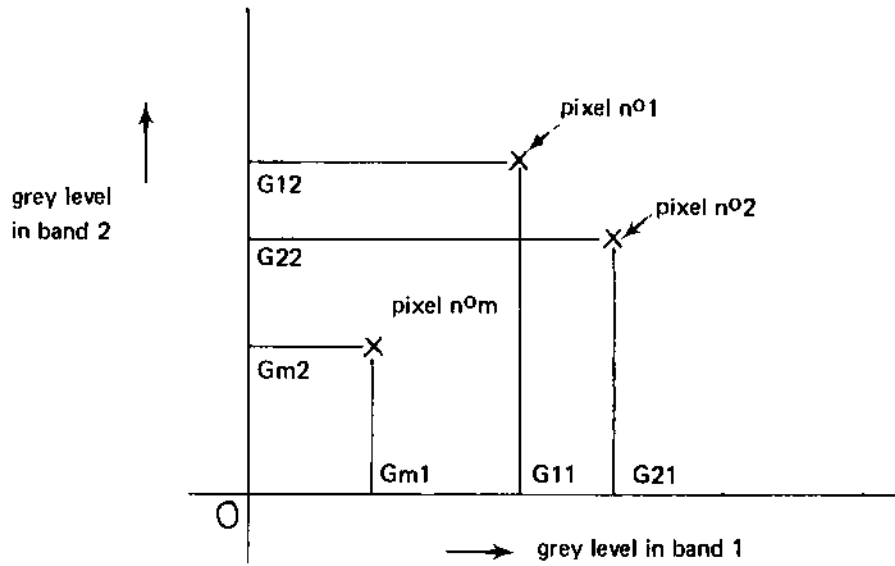


Figure A-2-1. Pixels as points in N-space.

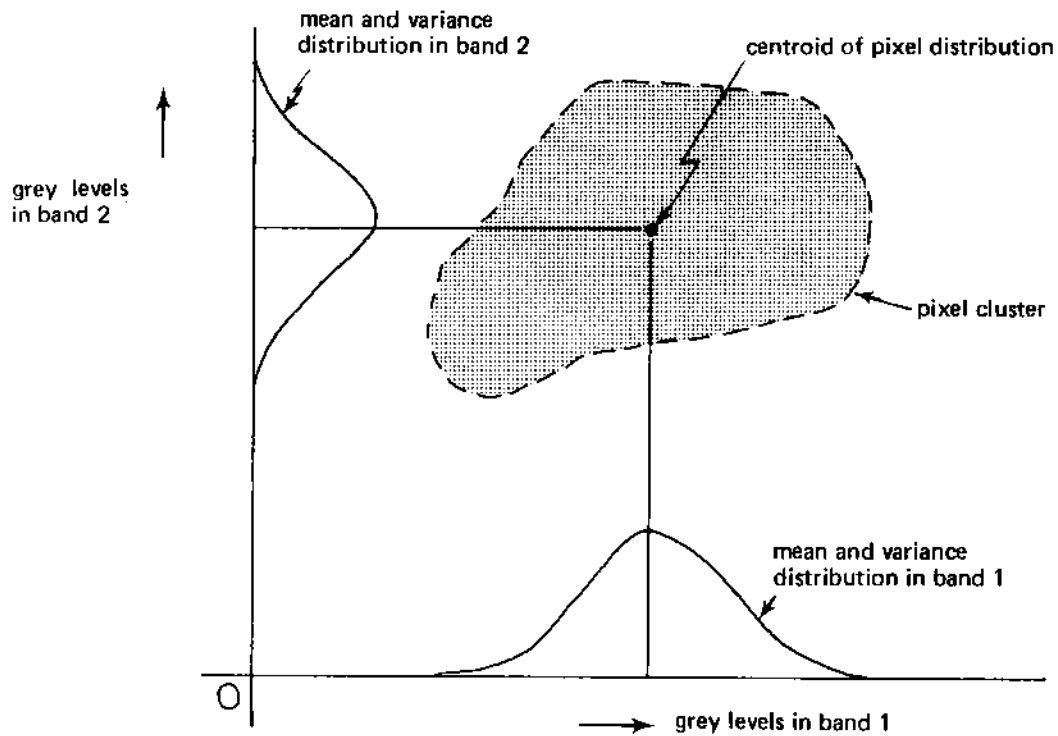


Figure A-2-2. Pixel clusters in N-space.

terms, this is achieved when our new axes coincide with the principal axes of the ellipsoid that best fits the pixel distribution. See Figure 3 for the case $N = 2$. To compute the grey levels of each pixel, we need the projections of the pixel on the new, rotated coordinate axes. These projections are simply linear combinations of the original grey levels, referred to an origin at the center of the ellipsoid.

The principal axes of the ellipsoid will in general all be of different lengths and there will be N of them. Ranking them in order of decreasing size, let their directions be vectors $\vec{R}_1, \vec{R}_2, \vec{R}_3 \dots \vec{R}_N$. These constitute the eigen-directions or principal directions for the system. They are orthogonal to each other. Note that the direction \vec{R}_1 , which points along the longest axis of the ellipsoid, is that direction along which the cluster of pixels has the most "spread." Similarly, \vec{R}_N is the shortest axis of the ellipsoid and is the direction along which the cluster of pixels is least spread. In other words, variance of data is most along \vec{R}_1 , least along \vec{R}_N .

3. The computation of eignbands. The geometric description can be translated, step by step, into a mathematical procedure, as follows:
 - a. Computation of means, variances and covariances.

$$\text{Form, for each } n, \text{ the mean } \bar{g}_n = \sum_{m=1}^M g_{mn} \quad \textcircled{1}$$

$$\text{Let } g_{mn}^1 = g_{mn} - \bar{g}_n = (\text{grey levels referred to means as origin}) \quad \textcircled{2}$$

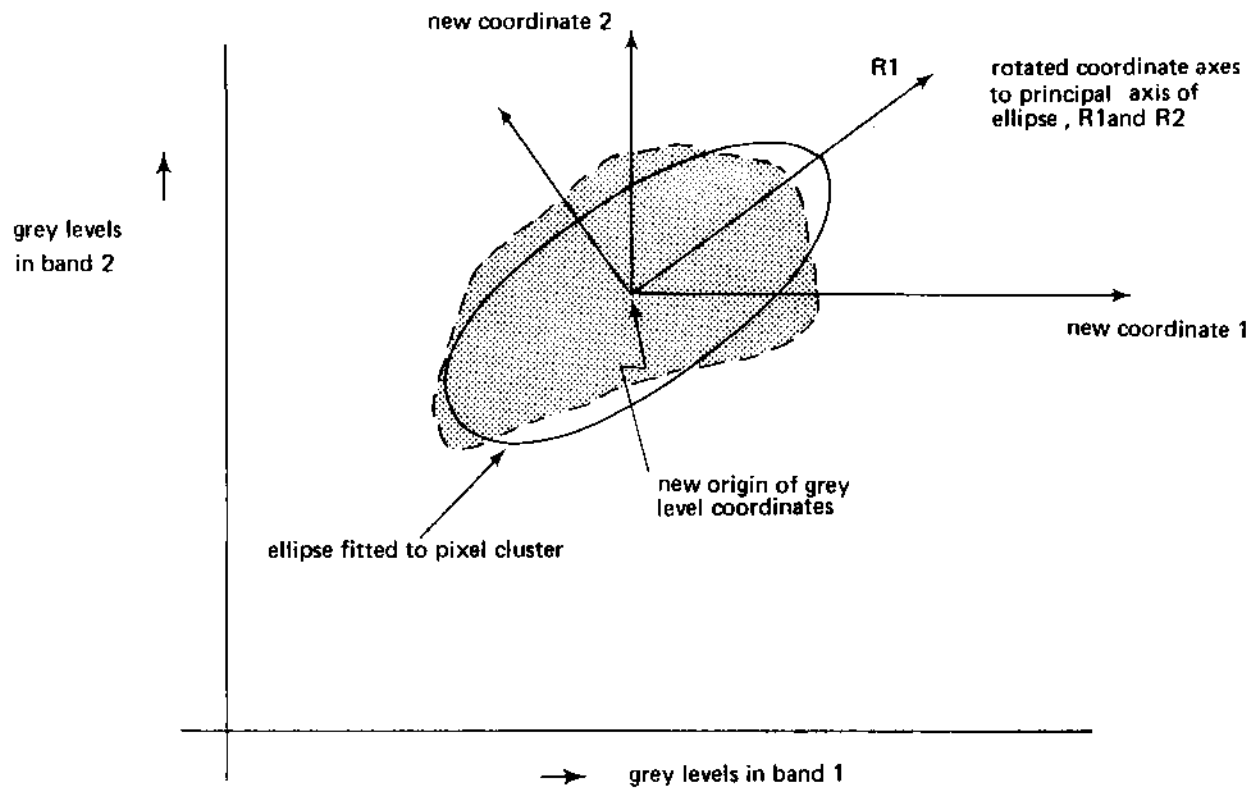


Figure A-2-3 Pixel clusters fitted to an ellipsoid.

$$\text{Variance of band } n = \sum_{m=1}^M (g_{mn}^1)^2 \equiv C_{nn} \quad (3)$$

$$\text{Covariance of bands } n \text{ and } p = \sum_{m=1}^M g_{mn}^1 g_{mp}^1 = C_{np} \quad (4)$$

The variance-covariance matrix, C , is $N \times N$ and has elements C_{nn} on the diagonal, $C_{np} = C_{pn}$ off the diagonal.

We require a rotation of coordinate axes such that the variance-covariance matrix referred to the rotated axes will be diagonal.

Consider the rotation of axes Q , where the elements of Q are Q_{ns} and the grey levels referred to the rotated axes are G_{ms} .

$$\text{Then } G_{ms} = \sum_{n=1}^N g_{mn}^1 Q_{ns} \quad (5)$$

and the variance-covariance matrix for the rotated set of axes

$$\text{is } C_{sp}^R = \sum_{m=1}^M G_{ms} G_{mp} \quad (6)$$

$$= \sum_{m=1}^M \sum_{n=1}^N \sum_{r=1}^N g_{mn}^1 Q_{ns} g_{mr}^1 Q_{rp}$$

$$= \sum_{n=1}^N \sum_{r=1}^N Q_{ns} C_{nr} Q_{rp} = Q^T C Q$$

$$\text{Thus } C^R = Q^T C Q \quad (7)$$

We require C^R to be a diagonal matrix, reflecting the fact that the covariances between bands, given by

$$\sum_{m=1}^M G_{ms} G_{mp} = 0 \quad (s \neq p) \quad (8)$$

A rotation matrix Q that will accomplish this is readily available. Let $\{\vec{q}_1, \vec{q}_2, \dots, \vec{q}_N\}$ be the N eigenvectors of C , so that $C\vec{q}_n = \lambda_n\vec{q}_n$ where λ_n is the eigenvalue of C corresponding to eigenvector \vec{q}_n . (9)

Form a matrix Q whose columns are the eigenvectors of C , ranked so that $\lambda_1 \geq \lambda_2 \geq \lambda_3 \dots \geq \lambda_N$

$$\begin{aligned} \text{Then } CQ &\equiv C(\vec{q}_1, \vec{q}_2, \dots, \vec{q}_N) \\ &= (\lambda_1\vec{q}_1, \lambda_2\vec{q}_2, \dots, \lambda_N\vec{q}_N) \end{aligned} \quad (10)$$

Now the eigenvectors of a symmetric matrix form an orthonormal set, i.e., $\vec{q}_i^T \vec{q}_j = 0$ if $i \neq j$
 $= 1$ if $i = j$

$$\text{Thus } Q^T C Q = \begin{pmatrix} \lambda_1 & 0 & 0 & \dots & 0 \\ 0 & \lambda_2 & 0 & \dots & 0 \\ 0 & & & & 0 \\ 0 & & & & 0 \\ 0 & & & & 0 \\ 0 & \dots & 0 & & \lambda_n \end{pmatrix} \quad (11)$$

Thus with this choice of Q , the variance-covariance matrix for the pixel set G_{ms} referred to rotated axes is diagonal, and the variance on the set G_{ms} for any fixed s is λ_s .

It therefore only remains to compute the related pixel sets G_{ms} .

Knowing $Q \equiv (\vec{q}_1, \vec{q}_2 \dots \vec{q}_N)$, and knowing the set g_{mn}^1 , we have at once from (5)

$$G_{ms} = \sum_{n=1}^N g_{mn}^1 Q_{ns} = \sum_{n=1}^N g_{mn}^1 q_{ns}$$

where q_{ns} is the n th element of \vec{q}_s .

The pixel set G_{ms} form an image that accounts for an amount λ_s of the total variance of the original N bands. Because the rotation of coordinates leaves the total variance unchanged, we note that

$$\sum_{n=1}^N C_{nn} = \sum_{n=1}^N \lambda_n.$$

By choosing just three rotated pixel sets, G_{m1} , G_{m2} and G_{m3} , and displaying these three band combinations as a 3-color composite, we create a single picture that accounts for the maximum possible amount of total variance of the original N bands, in a 3-band representation.

Note that eigenpictures can be made for any subimage area, and that we are not obliged to use all pixels in an area in forming the variance-covariance matrices. For example, if a scene contains significant amounts of water, snow or cloud, pixels in such areas should not be used in the variance-covariance calculation since they will give a substantial contribution to the variance (and hence affect the rotation of axes) but they contain negligible information content for the scene.

APPENDIX 3
EARTHSAT PROCESSING OF COMPUTER COMPATIBLE
TAPES AND PRODUCTION OF PHOTO PRODUCTS

Computer Compatible Tapes of Landsat data are re-formatted, then radiometrically and geometrically corrected using EarthSat's image processing software. After this, enhancement operations are performed, including edge enhancement, image ratioing, eigenbands, and contrast adjustment. Each of these operations may be applied to any image, and in each case the result is a computer tape containing image format data.

In the photo-processing of these data, the first step is to write a black-and-white positive transparency from the magnetic tape, using an Optronics film recorder. This instrument permits an array of grey level values to be written at 25, 50, and 100 micron spacing with as many as 100 discrete density levels being displayed on the final color print. For EarthSat's standard products, the black-and-white images are written at a scale of 1:1,140,000. If black-and-white products are required, the film positives are used to create prints at any scale from contact to a full frame at 1:185,000. When scales larger than this are required, they are prepared in sections appropriate to the demand. The maximum sheet size which can be handled measures 40" x 72". A typical 1:250,000 full frame print in either black-and-white or color is delivered on a sheet 34" x 34". If identification information is required at the top and bottom of the image, the largest single sheet scale is approximately 1:192,000.

For color imagery, any three black-and-white transparencies of a single scene are accurately pin-registered, and a color negative is

composited using the three additive primary colors as shown in Figure A.3.1. In EarthSat's standard edge-enhanced color product, these film records of bands 4, 5, and 7 of the original Landsat scene regulate the transmission of blue, green, and red light respectively to a single sheet of color negative film. Figure A.3.3. illustrates the formation of a color negative image. Chemical processing produces yellow dye in the blue-sensitive layer of this material, magenta-dye in the green-sensitive layer, and cyan dye in the layer sensitive to red. As indicated in Table (A-3.1.), combinations of dyes in the color negative reveal the additive primary colors blue, green, and red as well as their subtractive complements yellow, magenta, and cyan as shown in Figure A.3.2. When viewed against a white light (composed of blue, green, and red), the yellow dye layer subtracts the blue and passes green and red which are the components of yellow. The magenta dye layer subtracts the green, passes blue and red which is seen as magenta. The cyan layer subtracts red, passes blue and green and is viewed as cyan. The presence of both magenta and cyan subtract green and red and pass the blue. Yellow and cyan dyes subtract blue and red and pass green. Yellow and magenta dyes subtract blue and green and pass red.

If yellow, magenta, and cyan dyes are present in full strength in the color negative, all three additive primaries will be subtracted and the result will be no light transmission or black. When no dye has been formed in the color negative, the transmission of blue, green and red is viewed as the original white light source. As densities in the film positives vary, they will alter the exposure during the compositing of the color negative. As exposure decreases, so will the concentrations of dye which reduces the subtractive filtration of white light.

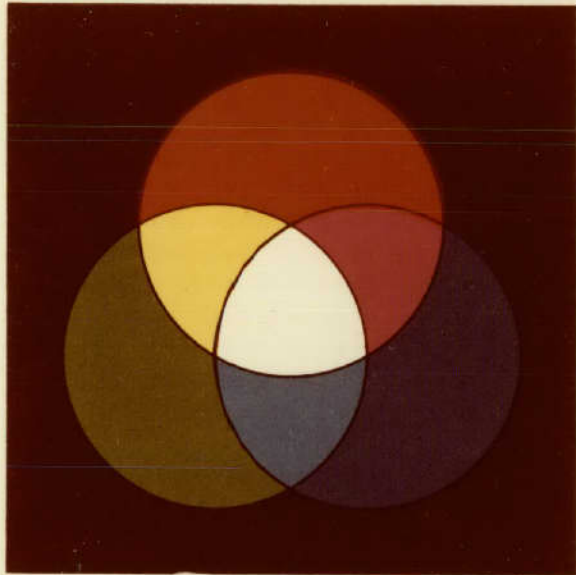


Figure A.3.1. Result of the additive mixing of colors (three spotlights).

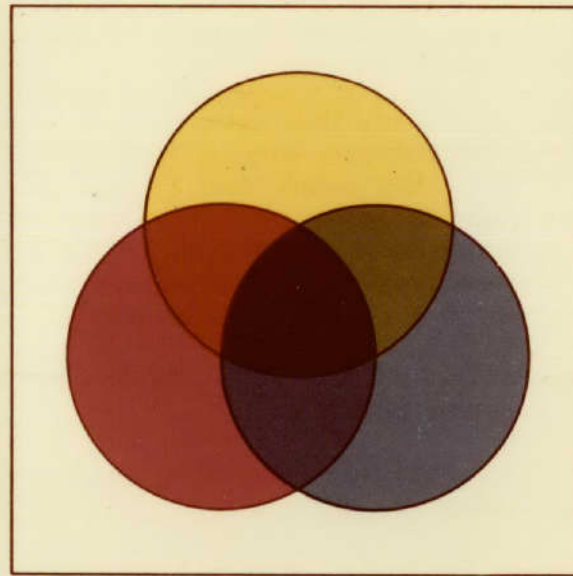


Figure A.3.2. Diagram of the subtractive combination of colors (such as in printing and painting).

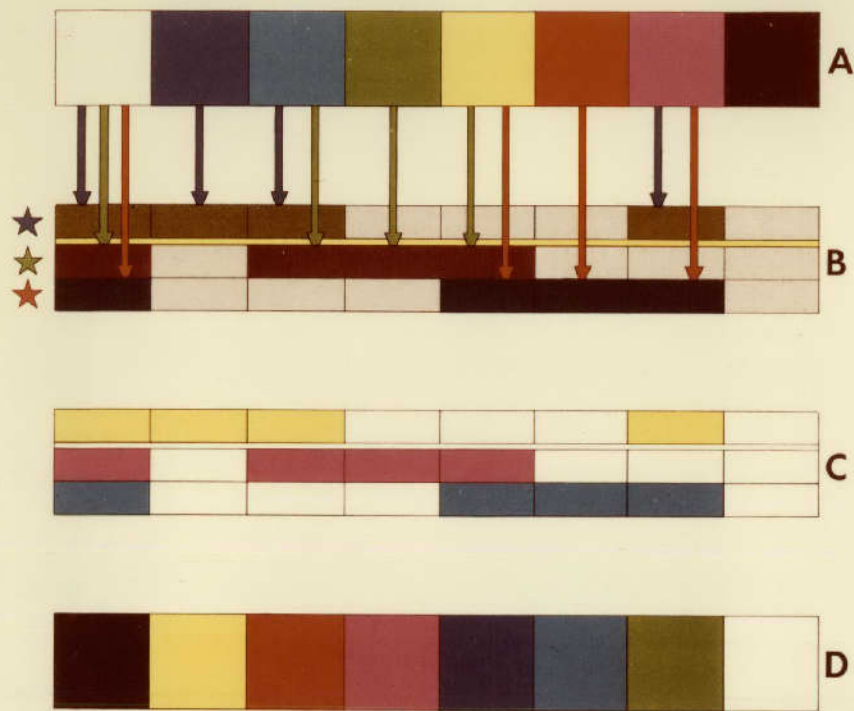


Figure A.3.3. Formation of negative images.

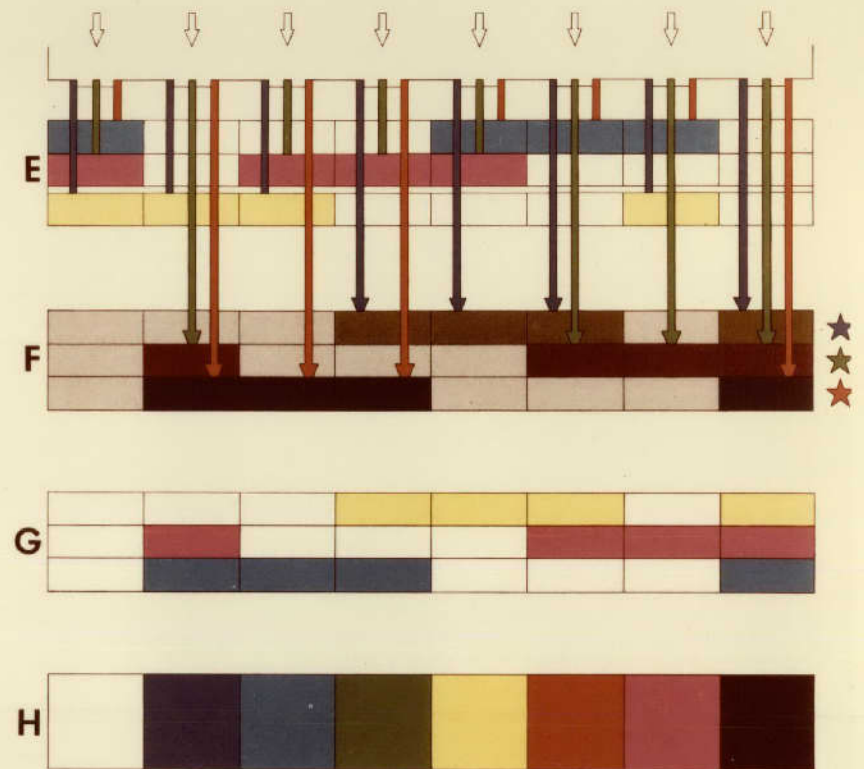
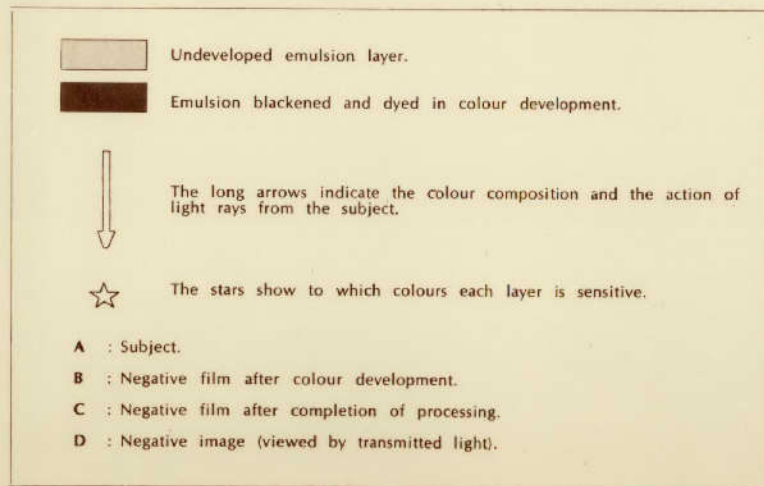
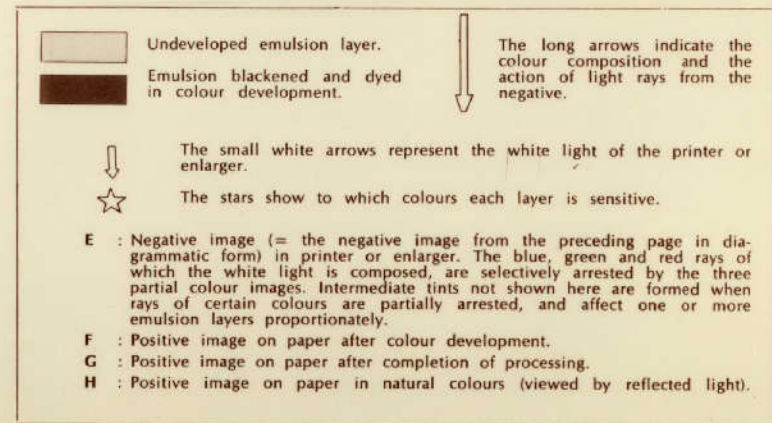


Figure A.3.4. Formation of positive images.



The final product is a color positive print viewed by reflected light. The formation of positive images as diagrammed in Figure A.3.4 is essentially a repetition of the process which produced the color negative. The light transmitted through the color negative to the print is further regulated by a system of yellow, magenta, and cyan filters in the photographic enlarger. Like the transparent base of the color negative, the reflective white paper base of the print material is coated with three gelatin layers light-sensitive to the additive primaries. Their dye response is similar to that of the color negative and the colors viewed in the print further demonstrate the principles of the subtractive process. The combinations of dyes which transmitted color in the negative have their direct counterpart in reflecting a full range of colors in the print.

While the longevity of these dyes is being extended by research within the photographic industry, only the silver image of the black-and-white positive transparencies is regarded as a reliable source for future information retrieval. These separate records of the several wavelengths of light recorded and transmitted by the satellite are processed for archival permanence and may, at any time, be used to remake a color negative which may have suffered from storage time and conditions.

TABLE A.3.1

RESULTS OF VARIOUS DYE COMBINATIONS IN A COLOR NEGATIVE

<u>Band 4 (Blue)</u>	<u>Band 5 (Green)</u>	<u>Band 7 (Red)</u>	<u>Activated Dye Layer</u>	<u>Color Viewed In Negative</u>
Dark	Light	Light	Magenta + Cyan	Blue
Light	Dark	Light	Yellow + Cyan	Green
Light	Light	Dark	Yellow + Magenta	Red
Light	Dark	Dark	Yellow	Yellow
Dark	Light	Dark	Magenta	Magenta
Dark	Dark	Light	Cyan	Cyan
Light	Light	Light	Yellow + Magenta + Cyan	Black
Dark	Dark	Dark	No Dye	White

APPENDIX 4

TEXTURE AND LINEAMENT DISPLAY OPERATORS

In addition to the texture measures and the standard enhancement of images used in the GEOPIC processing, a number of special enhancements were used, designed to emphasize local textures and local patterns.

These were applied to sub-image areas (GEOPIC processing is for the whole image) and their results are shown in the main report. This Appendix summarizes the mathematics of the operators that were applied and discusses their effects.

1. Edge detection

An edge is defined as a single rapid change in grey level value, as distinguished from a line, which is a double change of grey level; for example, a rapid change of grey level occurs at the edge of a narrow river, but usually returns to the original value at the other side. At the boundary of a large lake, on the other hand, the grey levels change and remain at the changed value for the whole interior of the lake.

The edge extraction operator computes differences of average grey level in the neighborhood of a pixel, and suppresses small values of these differences, leaving large values to be displayed. Specifically, we proceed as follows:

We form the average grey level over a square array of pixels surrounding a particular point, thus:

$$A(m,n) = \sum_{-N/2=i}^{N/2} \sum_{-N/2=j}^{N/2} g(i,j)$$

where $g(i,j)$ is the grey level at pixel at lattice point $((i+m)h,(j+n)h)$.

Now we form the absolute value of the differences between values of $A(m,n)$ at horizontal and vertical neighbors, thus:

$$D_H(m,n) = |A(m+1,n) - A(m,n)|$$

$$D_V(m,n) = |A(m,n+1) - A(m,n)|$$

Finally, the differences are shapened, by selecting the largest differences within a region. To do this, we set the value of $D_H(m,n)$ to zero, if we find a larger value of $D_H(m,n)$ somewhere within a horizontal distance $(-Nh/2, +Nh/2)$ of the pixel (m,n) , and we set the value of $D_V(m,n)$ to zero if we find a larger value of $D_V(m,n)$ within a vertical distance $(-Nh/2, +Nh/2)$ of the pixel (m,n) .

Finally, the edge at (m,n) is defined to be the maximum value of the pair $D_H(m,n), D_V(m,n)$, thus: $E(m,n) = \max(D_H(m,n), D_V(m,n))$.

Clearly, there will be places where both $D_H(m,n)$ and $D_V(m,n)$ are set to zero, which will mean that edges are reinforced by the spaces this generates between them.

For the work on this project, the displays were created using $N = 2$, i.e., averages were taken over 2×2 neighborhoods.

2. Line detection

The line detection operator is also based upon examining differences of average grey levels computed over $N \times N$ pixel blocks, but in this case we are looking for a double change of grey level. This is done as follows:

First, we compute the average, $A(m,n)$, over an $N \times N$ block, as before. We now consider the following 14 neighborhoods of (m,n) where the pixel location (m,n) is underlined, and where each symbol shown represents the value of $A(m,n)$ for that site:

abc abc abc	abc abc abc	abc abc abc	abc abc abc	abc abc abc	abc abc abc	abc abc abc
c bc abc ab a	cc bbc aab a	c bcc abb aa	ccc bbb aaa	c ccb bba aa	cc cbb baa a	c cb cba ba a

Now let A , B and C denote the average grey level of the three values of $A(m,n)$ denoted as the a's, b's and c's, respectively, in each of the above 14 groups. For each group, if each b is greater than its horizontally or vertically adjacent a and c, we compute $V = B - (A + C)/2$.

Otherwise, we set $V = 0$.

Let V_{\max} be the greatest value of V for any of the 14 groups. Then the required value for the output display at location (m,n) is V_{\max} .

This process produces output values only where thin lines are present; the computed value is zero for step changes and for isolated high values.

For this project, we again used $N = 2$ in computing $A(m,n)$, i.e., we averaged over 2×2 neighborhoods.

3. Grey scale stretching

Global grey level stretching, i.e., an adjustment of the histogram for the whole image, is routinely applied during creation of the GEOPIC products. In addition, the effects of two types more local operators was investigated. These were a fixed window local grey level stretch, and a moving window local grey level stretch.

In both cases, the procedure consisted of setting the lowest 7.5% of grey levels to 0, and the highest 7.5% to 63. The remaining grey levels were linearly stretched to fill the range (0,63).

In the fixed window local stretch, 64x64 pixel windows were each processed in this way.

In the moving window local stretch, 11x11 neighborhoods of each pixel were processed in this way, and the grey level transformation that resulted was applied to the center pixel only. Thus each pixel had a different grey level stretch calculation and grey level stretch operator.

In both cases, radiometric comparisons between different parts of the image are lost, and local contrast is gained. The technique is designed to maximize the detail visible in each part of the image.

4. The texture transform

This operator produces an output display image in which each pixel's grey level is an estimate of the local image texture.

The procedure to accomplish this is as follows:

- (a) Compute the unnormalized co-occurrence matrices $M(m,n)$ for the set $S: (m,n) = (1,0), (0,1), (1,-1), (-1,1), (-1,0), (0,-1), (1,1)$ and $(-1,-1)$, i.e., for all the distance-1 cases (see Appendix 1).
- (b) At each pixel, we determine the eight grey level pairs (i,j) for the pixel and each of its 8 neighbors. For each pair, we select the appropriate (i,j) entry from the appropriate co-occurrence matrix $M(m,n)$. Call this entry N_{mn}^{ij} .
- (c) At each pixel, we now compute the sum $s(x,y) = \sum_{m,n \text{ in } S} \log(N_{mn}^{ij})$. If all the N_{mn}^{ij} in the sum s are small, this means that the pixel is an "unusual" one, since the number of pixels in the whole image with a similar set of neighboring grey levels is

small. If the sum is large, many pixels in the image have a similar pattern of neighbors as the one under consideration. Thus the sum measures the likeliness of each pixel, compared with the likeliness of all other pixels in the image.

- (d) To produce a display output of the likeliness, the array of values of $s(x,y)$ for all (x,y) in the image are scaled to the range $(0,63)$ using a linear grey level stretch, and the polarity reversed (i.e., $(63 - i)$ replaces i). The resulting display shows bright grey levels for points that have improbable grey level combinations in their immediate neighborhood.

APPENDIX 5: Return Beam Vidicon Data from Landsat-3, Thematic Mapper Data from Landsat-D and Synthetic Aperture Radar Data from SEASAT-1

Two new visible and near-IR wavelength instruments, on Landsat-3 and on the as-yet-unflown Landsat-D, may have a significant effect on the use of texture information in uranium exploration. Both instruments offer substantially better spatial resolution than the Multi-Spectral Scanners of Landsat's -1, -2, and -3. In addition, data from any successor to the now-inactive SEASAT-1 spacecraft could be of great utility.

The Return Beam Vidicon (RBV) of Landsat-3 began to return data in March of 1978. At this time (April 1979) little data is available, but that situation should change in the next year or two. In addition, digital RBV data, which is still completely unavailable, should be obtainable from the EROS Data Center.

Landsat-3 carries two RBV cameras, each covering an area about 99 kilometers square. The cameras are mounted side by side, with a center overlap of about 15 kilometers. Together they image a swath of total width 185 kilometers, and thus cover the same ground track as the MSS on the spacecraft. The two cameras are otherwise essentially identical. Each one produces a single band of data covering the spectral range from 0.505 to 0.75 micrometers, and each offers a ground resolution of about 35 meters. Although the early images available for inspection from the RBV's have been of poor contrast, the amount of ground detail that can be seen on them is strikingly better than even the best enhanced MSS images (which probably approach 50 meters ground resolution in the best circumstances). It would certainly be informative to subject

such RBV data, when it becomes available in digital form, to the same type of texture analyses that were performed in this project for MSS data.

Landsat-D is scheduled for launch in late 1981. In addition to the MSS (identical with that of Landsat's -1, -2, and -3), Landsat-D will carry a Thematic Mapper. The spacecraft will be placed in a rather lower orbit than the present Landsat's, with a mean height of 705 kilometers rather than 915 kilometers. This, plus the increased angular resolution of the Thematic Mapper, should offer ground resolution of about 30 meters in the visible and near-IR channels. Equally significant, Landsat-D will have additional spectral channels in wavelengths that are of importance to geology. The channels and their expected ground resolutions are as follows:

0.45 to 0.54 micrometers:		30 meter resolution.			
0.52 to 0.60	"	"	30	"	"
0.63 to 0.69	"	"	30	"	"
0.76 to 0.90	"	"	30	"	"
1.55 to 1.75	"	"	32	"	"
2.08 to 2.35	"	"	32	"	"
10.4 to 12.5	"	"	120	"	"

The satellite also has a 16-day repeat cycle for ground coverage, compared with the 18-day cycle of the first three Landsat's.

The improved spatial and spectral properties of the the Thematic Mapper could make a crucial difference to the value of Landsat data for uranium exploration. It has been noted in other remote sensing applications (Reference 6), particularly ones with a need for spatial detail, that there is a "thresholding" effect for system resolution. The usefulness of the data remains approximately constant until some critical value of the resolution is reached, then with a relatively small improvement a whole new

class of applications become feasible. This suggests that the use of texture discriminators for uranium exploration should be re-evaluated when Landsat-D becomes available.

Finally, there is the possible use of synthetic aperture radar data from spacecraft. SEASAT-1 was launched in June of 1978, and carried a radar with approximately 25 meters ground resolution. Unfortunately, a power failure in October 1978 meant that no more data could be received from any of the on-board instruments. Little data has been made available over land areas, but a first inspection of a single flight strip by EarthSat staff shows that a number of geological features are readily visible on the radar imagery, more so than on any other remotely sensed data source. For the long term, radar data may prove to be a most useful type of space-sensed data for applications to geological exploration.

APPENDIX 6A.6.0 Computer Output Exhibits

The computer printouts of the texture measure results are bound under separate cover. The tables of this appendix are designed as an index to these bound collections.

In order to keep the computer costs within reasonable limits and to facilitate interpretation, smaller subsets of the training areas (control areas) were processed before processing a one quarter frame training area. Where possible, the control areas were selected so as to contain approximately 40 windows over uraniumiferous ground and 35 windows over non-uraniferous ground. Uraniferous windows are plotted with the letter "A," non-uraniferous windows are plotted with the letter "B." The first three letters of the axes labels follow the standard texture measure abbreviations established in Appendix 1.

A.6.1 Copper Mountain, Wyoming

The printouts of the Copper Mountain control areas are largely concerned with the development of the approach by which the various measures were calculated and displayed. These early runs were performed entirely on MSS bands 5 and 7. Later in the project, after learning that the third Eigenband (E3) contained the most texture information at the Pumpkin Buttes training area, the texture measures for the Copper Mountain control areas were rerun using E3.

COPPER MOUNTAIN, WYOMING

<u>Label</u>	<u>Date</u>	<u>Band</u>	<u>Description</u>
CM-1	10/22	MSS 5	Difference histogram values, Distance = 1, uranium control area.
CM-2	10/22	MSS 5	Difference histogram values, Distance = 1, non-uranium control area.
CM-3	10/22	MSS 5	Co-occurrence matrices, Distance = 1, uranium control area.
CM-4	10/22	MSS 5	Co-occurrence matrices, Distance = 1, non-uranium control area.
CM-5	9/6	MSS 5	Difference histogram values, Distance = 2, uranium control area.
CM-6	9/18	MSS 5	Difference histogram values, Distance = 2, non-uranium control area.
CM-7	10/22	MSS 5	Co-occurrence matrices, Distance = 2, uranium control area.
CM-8	10/22	MSS 5	Co-occurrence matrices, Distance = 2, non-uranium control area.
CM-9	11/12	MSS 7	Difference histogram values, Distance = 1, uranium control area.
CM-10	11/12	MSS 7	Difference histogram values, Distance = 1, non-uranium control area.
CM-11	11/12	MSS 7	Co-occurrence matrices, Distance = 1, uranium control area.
CM-12	11/12	MSS 7	Co-occurrence matrices, Distance = 1, non-uranium control area.

CM-13	11/12	MSS 7	Difference histogram values, Distance = 2, uranium control area.
CM-14	11/12	MSS 7	Difference histogram values, Distance = 2, non-uranium control areas.
CM-15	11/12	MSS 7	Co-occurrence matrices, Distance = 2, uranium control area.
CM-16	11/13	MSS 7	Co-occurrence matrices, Distance = 2, non-uranium control areas.
CM-17	12/24	E3	Co-occurrence matrices, Distance = 1, uranium control area.
CM-18	12/24	E3	Co-occurrence matrices, Distance = 1, non-uranium control area.
CM-19	10/23	MSS 5	PLOTS (bar), Distance = 1, calculated from co-occurrence matrix.
CM-20	10/23	MSS 5	PLOTS (pair), Distance = 1, calculated from co-occurrence matrix.
CM-21	10/23	MSS 5	PLOTS (bar), Distance = 2, calculated from co-occurrence matrix.
CM-22	10/23	MSS 5	PLOTS (pair), Distance = 2, calculated from co-occurrence matrix.
CM-23	11/29	MSS 5	PLOTS (pair), Distance = 1, calculated from difference histogram.
CM-24	11/29	MSS 5	PLOTS (pair), Distance = 1, calculated from co-occurrence matrix with improved 'IDM' feature.
CM-25	10/24	MSS 7	PLOTS (bar), Distance = 1, calculated from co-occurrence matrix.
CM-26	10/24	MSS 7	PLOTS (pair), Distance = 1, calculated from co-occurrence matrix.
CM-27	10/24	MSS 7	PLOTS (bar), Distance = 2, calculated from co-occurrence matrix.
CM-28	10/24	MSS 7	PLOTS (pair), Distance = 2, calculated from co-occurrence matrix.
CM-29	10/24	MSS 7	PLOTS (bar), Distance = 1, calculated from the difference histogram.
CM-30	10/24	MSS 7	PLOTS (pair), Distance = 1, calculated from the difference histogram.
CM-31	10/24	MSS 7	PLOTS (bar), Distance = 1, calculated from the difference histogram, uranium area only.

CM-32	10/24	MSS 7	PLOTS (pair), Distance = 2, calculated from the difference histogram, uranium area only.
CM-33	12/24	E3	PLOTS (pair), Distance = 1, calculated from co-occurrence matrix (unstretched).
CM-34	12/27	E3	PLOTS (pair), Distance = 1, calculated from co-occurrence matrix (stretched).

A.6.2 Pumpkin Buttes, Wyoming

The Pumpkin Buttes, Wyoming training area, both MSS 5 and MSS 7 as well as all four eigen bands (E1, E2, E3, and E4), were used as data bases for the texture measure processing of the control areas. It was through this broad based approach that E3 was determined as the most useful data base and the IDM/ASM texture measure pair as the most useful texture discriminant. A quarter frame training area, which included the two control areas, and a quarter frame test area were processed using the E3 data base.

To aid the interpretation of the classifications, a new type of plot was developed (NPLOT) which individually identified each window on the pair plots (PLOT). NPLOTS were generated for the Pumpkin Buttes, Grants, Marysvale, and Southwest Africa control areas.

PUMPKIN BUTTES, WYOMING

<u>Label</u>	<u>Date</u>	<u>Band</u>	<u>Description</u>
PB-1	12/13	MSS 5	PLOTS.
PB-2	12/13	B7	PLOTS.
PB-3	12/13	E1	PLOTS.
PB-4	12/13	E2	PLOTS.
PB-5	12/13	E3	PLOTS (unstretched).
PB-6	12/20	E3	PLOTS (stretched).

PB-7	1/19	E3	NPLOTS (stretched).
PB-8	1/16	E3	PLOTS (stretched), test new IDM.
PB-9	1/5	E4	PLOTS (unstretched).
PB-10	1/7	E4	PLOTS (stretched).
PB-11	1/16	E4	NPLOTS (stretched).
PB-12	3/19	E3	Window labels for uranium and non-uranium control areas - final choice of line discriminant.
PB-13	3/19	E3	Window labels for one-fourth frame training area - using "best line discriminant."
PB-14	3/19	E3	Window labels for one-fourth frame test area, using "best line discriminant."
PB-15	3/14	E3	Window labels for uranium and non-uranium control areas - several rejected line discriminants.
PB-16	3/19	E3	Window labels for one-fourth frame training area, rejected line discriminant.
PB-17	3/19	E3	Window labels for one-fourth frame test area, rejected line discriminant.

A.6.3 Grants, New Mexico

At Grants, New Mexico, texture measures were calculated for only the third eigen band. A quarter frame sized training area was run in addition to the control areas. The larger training area included both the uraniferous and non-uraniferous control areas.

GRANTS, NEW MEXICO

<u>Label</u>	<u>Date</u>	<u>Band</u>	<u>Description</u>
GT-1	1/15	E3	PLOTS (stretched).
GT-2	1/16	E3	NPLOTS (stretched).
GT-3	1/31	E3	Window labels for control areas using line #1.
GT-4	2/6	E3	Window labels for control areas using line #2.

GT-5	1/31	E3	Window labels for one-fourth frame training area using line #1.
GT-6	1/31	E3	Window labels for one-fourth frame training area using line #2.

A.6.4 Southwest Africa

The texture measures are applied to E3 data for three control areas on the Southwest Africa image. In reference to Plate 16, the two calcrete areas were combined into a single uranium control area.

SOUTHWEST AFRICA

<u>Label</u>	<u>Date</u>	<u>Band</u>	<u>Description</u>
SA-1	1/11	E3	PLOTS (stretched).
SA-2	1/13	E3	NPLOTS (stretched).
SA-3	1/20	E3	Window labels, control areas.

A.6.5 Marysvale, Utah

In the Marysvale region, the texture measures calculated for the E3 data base for the two control areas.

MARYSVALE, UTAH

<u>Label</u>	<u>Date</u>	<u>Band</u>	<u>Description</u>
MV-1	2/6	E3	PLOTS (stretched), ASM/IDM only.
MV-2	2/6	E3	NPLOTS (stretched), ASM/IDM only.
MV-3	2/6	E3	Window labels, control areas.

A.6.6 San Rafael, Utah

The San Rafael area in Utah was processed by applying the texture measures to the E3 data base for selected control areas and uraniumiferous and non-uraniferous areas.

SAN RAFAEL, UTAH

<u>Label</u>	<u>Date</u>	<u>Band</u>	<u>Description</u>
SR-1	3/7	E3	PLOTS (stretched).

APPENDIX 7A.7.0 DELIVERABLE IMAGE PRODUCTS

Original image product deliverables for this project are provided as a separate package. The list of them is given here for the sake of completeness.

A) Color composite computer-enhanced images - 1:250:000 scale

1 - Poison Spider (I.D. 1786-17135)	Plate 1
2 - Grants, New Mexico (I.D. 1515-17180)	Plate 2
3 - Namibia (Swakopmund, Windhoek) (I.D. 1383-08264)	Plate 3
4 - San Rafael Swell (Overthrust) (I.D. 1068-17364)	Plate 4
5 - Uranium City, Saskatchewan (I.D. 1396-17531)	Plate 5
6 - South Park, Colorado (I.D. 1802-17030)	Plate 6
7 - Durango (Lake City) (I.D. 5433-16342)	Plate 7
8 - Iron Mountain, N. Michigan (I.D. 1774-16044)	Plate 8

B) Color composite Eigenimage, Eigenbands 1, 2, and 3

1 - Poison Spider (I.D. 1786-17135)	Plate 9
-------------------------------------	---------

C) Color composite ratio, bands 4/5, 5/6, and 6/7

1 - Poison Spider (I.D. 1786-17135)	Plate 10
-------------------------------------	----------

D) Uranium occurrence maps and classification maps (as overlays)

1 - Poison Spider (occurrence map)	Plate 11
2 - Poison Spider (classification map)	Plate 12
3 - Grants, New Mexico (occurrence map)	Plate 13
4 - Grants, New Mexico (classification map #1)	Plate 14

5 - Grants, New Mexico (classification map #2)	Plate 15
6 - Namibia (occurrence map)	Plate 16
7 - Namibia (classification map)	Plate 17
8 - San Rafael Swell (occurrence map)	Plate 18
9 - San Rafael Swell (classification map)	Plate 19
10 - Uranium City (Beaverlodge area), Saskatchewan	Plate 20

APPENDIX 8

ANNOTATED GEOLOGICAL BIBLIOGRAPHY.

GENERAL LITERATURE

Conel, J.E., Abrams, M.J., and Goetz, A.F.H., 1978, A Study of Alteration Associated with Uranium Occurrences in Sandstone and its Detection by Remote Sensing Methods, Jet Propulsion Lab Pub. 78-60, Volumes I and II.

Discussion of spectral detection of uranium alteration (San Rafael Swell is one of the test area).

Engineering and Mining Journal, 1978, November, Uranium Expansion: The Rush is On.

Discussion and general geology of exploration development of various uranium districts throughout the world.

Everhart, D.L. and Wright, R.J., 1952, The Geologic Character of Typical Pitchblend Veins, U.S. Atomic Energy Commission, RMO-1035.

Summary of uranium mineral associations, paragenesis, structural relationships and host rock information for the deposits at Marysvale, Utah and Beaverlodge, Saskatchewan.

Lampley, C.M. and Wells, M.B., Studies of Airborne Optical Detection of Uranium Ore, Bendix 77-037-S.

Ruzicka, V., Conceptual Models for Uranium Deposits and Areas Favorable for Uranium Mineralization in Canada, Geol. Surv. Can., Paper 77-1A (1977).

Presentation of models for the genesis of various types of uranium deposits.

Spirakis, C.S. and Condit, C.D., 1975, Preliminary Report on the Use of Landsat-1 Reflectance Data in Locating Alteration Zones Associated with Uranium Mineralization Near Cameron, Arizona, USGS Open File 75-416.

Discussion of various image enhancement techniques used to detect uranium mineralization near Cameron, Arizona.

USGS Prof. Paper 455, Geology of Uranium Bearing Veins in the Conterminous U.S.

Discussion of the distribution, mineralogy, petrography, paragenesis, and alteration of vein type uranium deposits in the U.S.

United Nations 1956, Proceedings of the International Conference on the Peaceful Uses of Atomic Energy, Volume 6 Geology of Uranium and Thorium.

A collection of papers discussing various aspects of uranium ore deposits in the world.

GRANTS

Brookins, D.G., 1976, Uranium deposits of the Grants New Mexico Mineral Belt, GJB-16(76), USERDA Open File.

Chapman, Wood and Griswold, 1973, New Mexico State Bureau Mines and Mineral Resources, Map 31, Geologic Map and Grants Uranium Region.

Dodd, P.H., 1956, Some examples of uranium deposits in the upper Jurassic Morrison Formation on the Colorado Plateau, In: Proc. of the Intern' Conf. on the Peaceful Use of Atomic Energy, United Nations, pp. 615-623.

Discussion of local stratigraphy and structure as well as ore mineralogy and controls.

Fitch, D.C., 1971, New Mexico State Bureau of Mine and Mineral Resources Circular 118, Exploration Geology Methods in the Grants Mineral Belt.

Discussion of uranium ore types, occurrences, ore controls, and exploration guides.

Gabelman, J.W., 1956, Uranium Deposits in Limestone, In: Proc. of the Intern'l Conf. on the Peaceful Use of Atomic Energy, United Nations, pp. 338-345.

Discussion of ore control and occurrence in the Todilto Limestone of the Grants area.

Gilkey, A.K., 1953, U.S. Atomic Energy Commission RME-3050, Fracture Patterns of the Zuni Uplift.

Discussion of faults and joints as possible uranium ore control.

Granger, H.C., 1968, USGS Prof. Paper 600-B, pp. 60-70, Localization and Control of Uranium Deposits in Southern San Juan Mineral Belt, New Mexico.

Hackman, R.J. and Olson, A.B., USGS Map I-981 Geology, Structure and Uranium Deposits of the Gallup 1° x 2° Quad New Mexico and Arizona. Scale 1:250,000.

Hilpert, L.S. and Freeman, V.L., 1956, Guides to Uranium Deposits in the Gallup-Laguna Area, New Mexico, In: Proc. of the Intern'l Conf. on the Peaceful Use of Atomic Energy, United Nations, pp. 346-349.

Discussion of local stratigraphy and structure and of ore guides.

Hilpert, L.S. and Moench, R.H., 1960, Economic Geology Volume 55, #3, p. 429-463, Uranium Deposits of the Southern Part of the San Juan Basin, New Mexico.

Detailed survey of local uranium deposits, discussing stratigraphy, structure, mineralogy, ore controls, and ore guides.

Kelley, V.C. (Chairman), 1963, New Mexico Bureau of Mines and Mineral Resources Memoir 15, Geology and Tectonics of the Grants Mineral Belt.

A collection of papers discussing various aspects of the stratigraphy, structure, distribution, and genesis of the local uranium deposits.

Konigsmark, T.A., 1955, U.S. Atomic Energy Commission RME-76, Color Changes and Uranium Deposits of the Upper Morrison Formation, NE Flank of the Zuni Uplift, New Mexico.

Discussion of local uranium ore distribution and possible ore guides.

Mathewson, D.E., 1953, Reconnaissance for Uranium in the Morrison Formation North of Bluewater, McKinley County, New Mexico, U.S. Atomic Energy Commission RME-57.

Discussion of uranium ore mineralogy and distribution with a presentation of possible ore guides.

Pierson, C.T., 1977, Factors Controlling Localization of Uranium Deposits in the Dakota Sandstone, Gallup and Ambrosia Lake Mining Districts, McKinley Co., New Mexico, USGS Open File Report 77-766.

Rapaport, I., 1952, Interim Report on the Ore Deposits of the Grants District New Mexico, U.S. Atomic Energy Commission, RMO-1031.

Discussion of ore mineralogy and genesis and possible ore guides.

Reinhardt, E.V., 1952, Practical Guides to Uranium Ores on the Colorado Plateau, U.S. Atomic Energy Commission, RMO-1027.

Discussion of ore distribution and ore guides.

Roeber, M.M., 1972, New Mexico State Bureau of Mines and Mineral Resources, Circular 118. Possible Mechanics of Lateral Enrichment and Physical Positioning of Uranium Deposits, Ambrosia Lake Area, New Mexico.

Discussion of the relationship of fracturing and faulting to the occurrence of secondary ore.

Santos, E.S., 1963, Relation of ore deposits to the stratigraphy of host rocks in the Ambrosia Lake Area, in: Geology and Technology of the Grants Uranium Region, N.M., Bureau of Mines and Min. Res. Mem. 15, pp. 53-59.

Vizcaino, H.P. and O'Neill, A.J., 1977, Preliminary Study of the Uranium Potential of Tertiary Rocks in the Central San Juan Basin, New Mexico, GJBX-78(77).

LAKE CITY, COLORADO

Burbank, W.S. and Pierson, C.T., 1953, USGS Circular 236, Preliminary Results of Radiometric Reconnaissance of Parts of the NW San Juan Mountains, Colorado.

Discussion of uranium mineralization in Ouray and San Juan counties, and Thorium mineralized in Gunnison County, with a generalized geologic map at a scale of 1' = 10 miles.

Derzay, R.C., 1956, The Los Ochos Uranium Deposit, In: Proc. of the Intern'l Conf. on the Peaceful Use of Atomic Energy, United Nations, pp. 468-472.

Discussion of local stratigraphy and structure and ore controls and mineralogy.

Eckel, E.F., 1949, USGS Prof. Paper 219, Geology and Ore Deposits of the LaPlata District, Colorado.

Detailed discussion of local ore deposits with the history, development, and location of individual mines. A geologic map of the area is included at a scale of 1:31,680.

Gallagher, G.L., Edmond, C.L., D'Andrea, R.F., 1977, Preliminary Evaluation of the Uranium Favorability in the Area NW of Gunnison, Colorado, GJBX-61(77).

King, R.V., Leonard, B.F., Moore, F.B., Pierson, C.T., 1953, Uranium in the metal mining districts of Colorado, USGS Circular 215.

Discussion of the occurrence, mineralogy, and exploration guides.

Lipman, P.W., 1976, USGS Map I-962, Geologic Map of the Lake City Caldera Area, Western San Juan Mountains, Colorado.

Lipman, P.W., Doe, Bruce R., Hedge, Carl E., and Steven, Thomas A., 1978. Petrologic evolution of the San Juan volcanic field, southwestern Colorado: Pb and Sr isotope evidence. G.S.A. Bull., v. 89, p. 59-82.

Attributes Oligocene andesitic volcanism to plate subduction, but Miocene-Pliocene bimodal calderan volcanism to magma generated from mantle sources. Since the ore deposits in the region are associated entirely with the latter, this is a conclusion of fundamental importance.

Lipman, P.W., Steven, A. Thomas, Luedke, Robert A., and Burbank, Wilbur S., 1973. Revised volcanic history of the San Juan, Uncompahgre, Silverton, and Lake City calderas in the western San Juan Mountains, Colorado. Jour. Research, U.S.G.S., v. 1, no. 6, p. 627-642.

A clear exposition of the volcanic history of the area, based on very detailed stratigraphic work and a substantial amount of age-dating.

Maxwell, J.C., 1977, Uranium Hydrogeochemical and Stream Sediment Reconnaissance in the San Juan Mountains, GJBX-27(77).

Malan, R.C. and Ransport H.W., 1959, Econ. Geol. 54, p. 1-19, Geology of the Uranium Deposits in the Cochetopa Mining District, Colorado.

Olson, J.C., 1976, Uranium Deposits in the Cochetopa District, Colorado, In Relation to the Oligocene Erosion Surface, USGS Open File 76-222.

General description of the Los Ochos Uranium Deposit and possible mechanism of ore genesis is presented.

Pierson, C.T., Weeks, W.F., and Kleinhampl, F.J., 1958, USGS Bull. 1046-O, Reconnaissance for Radioactivity in the Metal Mining Districts of the San Juan Mountains, Colorado.

Generalized description of each ore district and discussion of several radioactive anomalies.

Schmitt, L.J. and Raymond, W.H., 1977, USGS Bull. 1434, Geology and Mineral Deposits of the Needle Mountains District, Southwest Colorado.

Detailed study of the local mineral potential, structural geology, and geochemistry. A geologic map is included at a scale of 1:31,250.

Tweto, O. et al., 1976, Preliminary Geologic Map of Montrose, 1° x 2° quad, Colorado USGS Map MF-761, Scale 1:250,000.

Steven, T.A. et al., 1974, Geologic Map of Durango 1° x 2° quad, SW Colorado, USGS Map I-764, Scale 1:250,000.

MARYSVALE

Callaghan, E., 1973, Mineral Resources Potential of Puite Co., Utah and Adjoining Area. Utah Geological and Mineralogical Survey Bull. 102.

Discussion of mineralogy and occurrence of various mineral deposits as well as regional structure and stratigraphy.

Cunningham, C.C. and Steven, T.A., 1977, USGS Open File Report 77-568, Mount Belknap and Red Hills Calderas and Associated Rocks, Marysvale Volcanic Field, West Central Utah.

Discussion of the local structure, stratigraphy, and petrology.

Cunningham, C.C. and Steven, T.A., 1978, Geology of the Delano Peak, NW Quad Utah, USGS Map MF-967, Scale 1:24,000.

Files, G.F., 1978, Uranium in Volcanic Environments in the Great Basin, U.S. D.O.E. GJBX-98(78).

Gruner, J.W., Fetzer, W.G. and Rapaport, I., 1951, Econ. Geol., Volume 46, #3, pp. 243-251, The Uranium Deposits Near Marysvale, Utah.

Generalized discussion of structure and stratigraphy of uranium deposits.

Kerr, P.F., 1952, A Geologic Guide to the Marysvale Area, U.S. Atomic Energy Commission, RMO-924.

Discussion of the local stratigraphy and structure of uranium ore occurrences and their origin.

Kerr, P.F., 1956, Rock Alteration Criteria in the Search for Uranium, In: Proc. of the Intern'l Conf. on Peaceful Use of Atomic Energy, United Nations, pp. 679-683.

Discussion of ore guides at Marysvale.

Kerr, P.F. et al., 1957, Marysvale, Utah, Uranium Area Geol. Soc. Am., Special Paper 64.

Detailed discussion of the local stratigraphy and structure of uranium ore occurrences, mineralogy, and origin.

Kerr, P.F., 1968, The Marysvale, Utah Uranium Deposits, In: Ore Deposits of the United States 1933-1967, The Graton Sales Volume (J.D. Ridge, editor), AIMMPE.

Discussion of local stratigraphy and structure of uranium ore occurrences, mineralogy, and origin.

Steven, T.A., Cunningham, C.G., Naeser, C.W., Mehnert, H.H., 1977, USGS Open File Report 77-569, Revised Stratigraphy and Radiometric Ages of Volcanic Rocks and Mineral Deposits in the Marysvale Area, Utah.

Discussion of the local stratigraphy and structure of uranium mineralization.

Steven, T.A., Rowley, P.D., Cunningham, C.G., 1978, Geology of the Marysvale Volcanic Field, West Central Utah, Bigham Young Univ. Geol. Studies, vol. 25, pt. 1, pp. 67-70.

General discussion of the local geology.

Steven, T.A., 1978, USGS Map MF-962, Geologic Map of Sevier SW Quad, Utah, scale 1:24,000.

Walker, G.W. and Osterwald, F.W., 1956, Relation of secondary uranium minerals to pitchblend-bearing veins at Marysvale, Puite Co., Utah, In: Proceedings of the Intern'l Conf. on Peaceful use of Atomic Energy, p. 283-287, United Nations.

Discussion of ore control, guides and origin of the primary and secondary uranium deposits.

THIS PAGE BLANK

NORTHERN MICHIGAN

Kalliokoski, J., 1976, Uranium, Thorium, and Potassium Content of PreCambrian Rocks of the Upper Peninsula Michigan and Northern Wisconsin; GJBX-43(77), Supplement to GJBX-48(76).

Summary of the geology of Northern Michigan and Wisconsin with a discussion of known uranium occurrences and potentially uraniumiferous rock types. Comparisons with producing districts of similar lithology in other continents is presented. A model for a "Lake Superior Type" uranium occurrence is proposed.

ROSSING

Anon, 1970, Working Group 4, Uranium Deposits of Unusual Occurrence In: Uranium Exploration Geology, Internat. Atomic Energy Agency, Vienna 1970, p. 369-370.

Brief discussion of the Rossing deposit.

Armstrong, F.C., 1974, Uranium Resources of the Future Porphyry Uranium Deposits, p. 625-635, In: Formation of Uranium Ore Deposits International Atomic Energy Agency, May 1974, Athens.

Discussion of a geologic model for "porphyry" uranium deposits, with examples cited.

Von Backstrom, J.W., 1970, The Rossing Uranium Deposits Near Swakopmund, Southwest Africa: In: Uranium Exploration Geology, Internat. Atomic Energy Agency, Vienna 1970, p. 143-150.

Brief description of the geology and mineralization of the Rossing deposit.

Berning, J., Cook, R., Hiemstra, S.A., and Hoffman, U., 1976, The Rossing Uranium Deposit Southwest Africa, Economic Geology, Volume 71, pp. 351-368.

Description of local geology, ore mineralogy, and ore distribution of the Rossing deposit. Exploration techniques used at Rossing are also described.

Frommurze, H.F., Gevers, T.W., and Rossouw P.J., 1942, The Geology and Mineral Deposits of the Karibib Area, Southwest Africa, Dept. of Mines, Geological Survey.

Discussion of the local stratigraphy and structure of various mineral occurrences.

Haughton, S.H., Frommurze, H.F., Gevers, T.W., Schwellnus, C.M., and Rossouw, P.J., 1939, The Geology and Mineral Deposits of the Omaruru Area Southwest Africa, Dept. of Mines Geological Survey.

Merifield, P., Orme, A., Kohl, M., Kolker, O., 1978, The distribution of calcretes and gypcretes in SW USA and their uranium favorability based on a study of deposits in western Australia and Southwest Africa (Namibia), GJB-29(78).

Rogers, J.J.W., 1977, Preliminary report on a visit to Southwest Africa In: Nishimori et. al., Uranium Deposits in Granitic Rock, USERDA GJBX-13(77).

Smith, D.A.M., 1965, The Geology of the Area Around the Khan and Swakop Rivers in Southwest Africa, Southwest Africa Geological Survey, Memoir 3.

Discussion of the local stratigraphy and structure and of various mineral occurrences and mines.

SAN RAFAEL

Bain, G.W., 1960, Patterns to Ores in Layered Rocks, Economic Geology, Volume 55, p. 695-720.

Johnson, H.S., 1957, Uranium Resources of the San Rafael District, Emery Co., Utah - A Regional Synthesis, USGS Bull. 1046-D.

Hawley, C.C., Robeck, R.C., Dyer, H.G., 1968, Geology, Altered Rocks and Ore Deposits of the San Rafael Swell, Emery Co., Utah, USGS Bull. 1239.

Discussion of stratigraphy, structure, mineralogy and occurrence of various mineral deposits and selected mines.

Isachsen, Y.W., 1956, Geology of Uranium Deposits of the Shinarump and Chinle formations in the Colorado Plateau, In: Proc. of the Intern'l Conf. on the Peaceful Use of Atomic Energy, United Nations, pp. 350-367.

Discussion of ore distribution, mineralogy, exploration guides, and possible genesis.

Mickle, D.G., Jones, C.A., Gallagher, G.L., Young, P. and Dubyk, W.S., Uranium Favorability of the San Rafael Swell Area, east central Utah, GJBX-72(77).

Williams, P.L. and Hackman, R.J., 1971, Geology, Structure and Uranium Deposits of the Salina Quad, Utah, USGS Map I-591. Scale 1:250,000.

SASKATCHEWAN

Agarwal, R.G., 1962, Regional Correlation of Geological and Geophysical Data in the Lake Athabasca Area, Dept. of Mineral Resources, Rept. #75, Sask. Geol. Survey.

Geologic and aeromagnetic maps at 1:253,440, of the region bounded by 112° to 102° longitude and 60° to 59° latitude.

AMOK (Canada) Ltd., 1974, The Carswell Circular Structure and Cluff Lake Uranium Ore Bodies: In Sask. Geol. Soc. Special, Pub. #2, pp. 47-61, G.R. Parslow (editor).

Description of the local stratigraphy and structure. Also a discussion of the distribution and genesis of uranium ores.

Beck, L.S., 1969, Dept. Mineral Resources, Report #126, Sask. Geol. Survey, Uranium Deposits of the Athabasca Region.

Detailed discussion of local and regional structure and stratigraphy and a summary of uranium ore mineralogy, genesis, distribution, and controls. Geologic, uranium occurrence and various other maps are included.

Beck, L.S., 1970, Canadian Institute of Mining and Metallurgy Transaction, Volume 73, pp. 59-69, Genesis of Uranium in the Athabasca Region and its Significance in Exploration.

Discussion of the local structure and stratigraphy, and of uranium ore mineralogy, distribution, genesis, and controls.

Campbell, D.D., 1957, Canadian Mining and Met. Bull., Volume 50 #545, pp. 542-549, Geology and Ore Control at the Verna Mine Beaverlodge, Sask.

Detailed discussion of local structure and stratigraphy and of uranium ore controls.

Dahlkamp, F.J., 1977, Details of Uranium Occurrence and Mode of Origin: Northern Saskatchewan Royal Soc. of London Meeting: Theoretical and Practical Aspects of Uranium Geology.

Discussion of uranium ore mineralogy, distribution and paragenesis of the Beaverlodge, Rabbit Lake, Cluff Lake, Key Lake, and Maurice Bay regions.

Dahlkamp, F.J., 1978, Geologic appraisal of the Key Lake U-Ni Deposits, Northern Saskatchewan Econ. Geol., vol. 73, pp. 1430-14449.

The structure, mineralogy and genesis of the Key Lake deposit is discussed.

Dunn, C.E. (editor), Uranium in Saskatchewan, 1976, Saskatchewan Geol. Society Special Pub. 3.

Collection of papers discussing various aspects of uranium in Saskatchewan.

Gracie, A.J. and DeZoysa, T.H., 1973, North Saskatchewan Uranium Tour: La Ronge - Rabbit Lake - Beaverlodge - Cluff Lake, in Sask. Geol. Society Special Pub. #1, F. Simpson (editor).

Discussion of local uranium ore occurrences and controls.

Hoeve, J. and Sibbald, T.I.I., 1978, On the genesis of Rabbit Lake and other unconformity-type uranium deposits in Northern Saskatchewan, Canada Econ. Geol., vol. 73, pp. 1450-1473.

The structure, mineralogy, and geochemistry of the Rabbit Lake deposit.

James, D.R., 1978, Saskatchewan Uranium Exploration Richardson Securities of Canada, Canadian Research Report.

Discussion of general geology and exploration development of the Athabasca region.

Knipping, H.D., 1974, The Concepts of Supergene versus Hypogene Emplacement of Uranium at Rabbit Lake, Sask. in Sask. Geol. Soc. Special Pub. #2, G.R. Parslow (editor).

Brief discussion of geology and geochronology of the Rabbit Lake deposit.

Koepfel, V., 1968, Age and history of uranium mineralization of the Beaverlodge areas, Saskatchewan, Geol. Survey of Canada Paper 67-31.

Discussion of the structure and origin of uranium mineralization in the Beaverlodge district.

Langford, F.F., 1974, Origin of Australian Uranium Deposits: A Universal Process that can be Applied to Deposits in Saskatchewan, Sask. Geol. Soc. Special Pub. #2, G.R. Parslow (editor).

Discussion of the genesis of the Beaverlodge uranium deposit.

Lintott, K.G., Pyke, M.W. and Netolitzky, R.K., 1976, Uranium - Recent Developments in Saskatchewan, Presented at the Prospectors and Developers Ass. Ann. Meeting, March 1976.

Discussion of structure, stratigraphy, and ore genesis of the Rabbit Lake, Carswell structure and Key Lake deposits.

Munday, R.J., Uranium mineralization in Northern Saskatchewan, Presented at the C.I.M.M. Ann. Meeting, April 1978.

Discussion of regional stratigraphy and structure and uranium ore distribution and genesis at Rabbit Lake, Beaverlodge, Key Lake, Carswell dome and other locations.

Olsson, W., 1974, The Geology and History of Eldorado's Hab Mine Beaverlodge, District in: Saskatchewan Geol. Soc. Special Pub. #2, pp. 149-173, G.R. Parslow (editor).

Discussion of logical geology of Hab Mine with examples of uranium ore controls.

Ramaekers, P.P., and Dunn, C.E., 1977, Geology and Geochemistry of the eastern margin of the Athabasca Basin, in: Saskatchewan Geological Society Special Pub. #3, C.E. Dunn (editor), pp. 297-323.

Discussion of sedimentology, structure, and geochemistry of the Athabasca formation.

Robertson, D.S., 1974, Uranium Deposits of Canada, Geoscience Canada, Volume #2, p. 8-21.

Discussion of the structure, ore types, ore controls, and sources of the Beaverlodge, Rabbit Lake, and Cluff Lake deposits.

Schiller, E.A., 1978, Saskatchewan Uranium Exploration, Mining Magazine June 1978, pp. 563-565.

Brief discussion of the local general geology and exploration development.

Sibbald, T.I.I., Munday, R.J.C., and Lewry, J.F., 1977, The Geological Setting of Uranium Mineralization in Northern Saskatchewan, in: Saskatchewan Geological Society Special Pub. #3, C.E. Dunn (editor), pp. 51-100.

Discussion of the structure, stratigraphy, origin, mineralogy, and distribution of uranium deposits in northern Saskatchewan.

Simpson, F., 1973, The mineral endowment of Saskatchewan in Saskatchewan Geol. Soc. Special Pub. #1.

Tremblay, L.P., 1970, Canadian J. Earth Sciences, Volume 7 #280, pp. 281-305, The Significance of Uranium in Quartzite in the Beaverlodge Area.

Summary of the structure, stratigraphy, and ore guides for the Beaverlodge Area with a discussion of uranium ore genesis.

Tremblay, L.P., 1972, Geol. Survey of Canada, Memoir 367, Geology of the Beaverlodge Mining Area.

Detailed discussion of the local structure and stratigraphy and of the distribution, origin, mineralogy, and controls of the uranium deposits.

SOUTH PARK, COLORADO

Gallagher, G.L., 1976, GJBX55(76), Uranium Favorability of Precambrian rocks in the Badger Flats Elkhorn Thrust area, Park and Teller Co., Colorado.

Young, P., Mickle, D., 1976, GJBX54(76), USERDA Open File, Uranium Favorability of Tertiary Rocks in Badger Flats Elkhorn Thrust area, Park and Teller Co., Colorado.

WYOMING

Armstrong, F.C., 1970, Wyoming Geological Association Guidebook 22nd Field Conference, pp. 31-44, Geologic Factors Controlling Uranium Resources in the Gas Hills District.

Discussion of ore occurrence and exploration guides.

Childers, M.O., 1974, Uranium occurrences in Upper Cretaceous and Tertiary Strata of Wyoming and northern Colorado, *The Mountain Geologist*, Vol. II, #4 (Oct. 1974), p. 131-14.

Discussion of the stratigraphy and structure of uranium occurrences in the Shirley Basin, the Powder River Basin and the Cheyenne Basin.

Davis, J.F., 1970, Wyoming Geol. Ass. Guidebook 22nd Field Conf., pp. 21-29, Uranium Deposits of Powder River Basin.

Granger, H.C. and Warren, C.G., 1978, Some speculations on the genetic geochemistry and hydrology of roll-type uranium deposits, Wyoming Geol. Ass. Guidebook, p. 349-361.

Discussion of the genesis of roll-type uranium deposits.

Grutt, E.W., 1956, Uranium Deposits in Tertiary Clastics in Wyoming and Northern Colorado, *In: Proc. of the Intern'l Conf. on Peaceful Use of Atomic Energy, United Nations*, pp. 392-402.

Discussion of local stratigraphy, structure, ore mineralogy and ore occurrences and controls of deposition.

Harshman, E.N., 1961, USGS Prof. Paper 424C, pp. C4-C6, Paleotopographic Control of a Uranium Mineral Belt, Shirley, Wyoming.

Harshman, E.N., USGS Prof. Paper 450D, pp. 8-10, Alteration as a Guide to Uranium Ore, Shirley Basin, Wyoming.

Discussion of color alteration of sandstone as an ore guide.

Harshman, E.N., 1972, Prof. Paper 745, Geology and Uranium Deposits, Shirley Basin Area, Wyoming.

Discussion of the local stratigraphy and structure and the mineralogy, paragenesis and distribution of uranium ore deposits.

King, J.W. and Austin, R., 1966, *Mining Engineering*, Volume 18, p. 73-75, Some Characteristics of Roll-Type Uranium Deposits at Gas Hills, Wyoming.

Discussion of the roll-type uranium ore deposits.

Love, J.D., 1952, USGS Circular 176, Preliminary report on the uranium deposits in the Pumpkin Buttes area, Powder River Basin, Wyoming.

Discussion of local stratigraphy and structure and description of individual deposits.

Love, J.D. and Keefer, W.R., 1963, Laramide vertical movements in central Wyoming, Contributions to Geology Univ. of Wyoming, Vol. 2, p. 47-54.

Discusses the activity of major laramide faults in central Wyoming.

Lover, 1954, USGS, Circular 352, Preliminary Report on Uranium in the Gas Hills Area.

Melin, R.E., 1964, Description and Origin of Uranium Deposits in Shirley Basin, Wyoming, Economic Geol., Vol. 59, p. 835-849.

Discussion of local geology and the mineralogy, alterations, origin and geometry of the uranium deposits.

Nkomo, I.T., Stuckless, J.S., Thaden, R.E., and Rosholt, J.N., 1978, Petrology and uranium mobility of a granite of early Precambrian age from the Owl Creek Mountains, Wyoming, in, Wyoming Geol. Ass. Guidebook, 30th Annl. Field Conf., 1978, p. 335-348.

Granite in the Copper Mountain area is 2.645 b.y. old. Most samples appear to have lost uranium through weathering processes in the Tertiary. Two samples from severely fractured granite near the North Canning Deposit have highly anomalous concentrations of uranium (40-70 ppm).

Rackley, R.J., 1972, Am. Ass. Pet. Geol. Volume 56, p. 755-790, Environments of Wyoming Uranium Deposits.

Discussion of the genesis and alteration of the uranium deposits located in the Shirley, Powder River, Wind River, and Great Divide Basins.

Raines, G.L., Offield, T.W., Santos, E.S., 1978, Remote-sensing and subsurface definition of facies and structure related to uranium deposits Powder River Basin, Wyoming, Econ. Geol., vol. 73 p. 1706-1723.

Discussion of uranium exploration in the Powder River Basin using computer processed remotely sensed data in combination with subsurface and surface geology.

Seeland, D.A., 1978, USGS Bull. 1446, Eocene Fluvial Drainage Patterns and Their Implication for Uranium and Hydrocarbon Exploration in the Wind River Basin, Wyoming.

Discussion of the regional sedimentation patterns with respect to the genesis and distribution of uranium deposits in the Wind River Basin.

Sharp, W.N., McKay, E.J., McKeown, F.A., White, A.M., 1959, Geology and uranium deposits of the Pumpkin Buttes area of the Powder River Basin, USGS Bull. 1107H.

Detailed discussion of stratigraphy, structure, mineralogy, occurrence, genesis, and exploration guides of the uranium deposits.

Sharp, W.N., McKeown, F.A., McKay, E.J., White, A.M., 1956, Geology and Uranium Deposits of the Pumpkin Buttes area, Wyoming, In: Proc. of the Intern'l Conf. on the Peaceful Use of Atomic Energy, United Nations, pp. 403-406.

Discussion of ore occurrences and controls of deposition.

Sharp, W.N., McKeown, F.A., McKay, E.J., White, A.M., 1956, USGS Prof. Paper 300, Geology and Uranium Deposits of the Pumpkin Buttes Area, Powder River Basin, Wyoming.

Discussion of local uranium ore guides and types of deposits.

Sharp, W.H., and Gibbons, A.B., 1964, Geology and Uranium Deposits of the Southern part of the Powder River Basin, Wyoming, USGS Bull. 1147-D.

Discussion of the stratigraphy, structure, exploration guides, distribution, and mineralogy of these uranium deposits. Various mines are also described.

Snow, C.D., 1978, Gas Hills uranium district, Wyoming - a review of history and production, Wyoming Geol. Ass. Guidebook p. 329-334.

Discussion of the production history of Gas Hills uranium district.

Stahl, R.L., 1974, Detection and delineation of faults by surface resistivity measurements, Bureau of Mines Report of Investigations #7824.

Discussion of fault detection by electrical resistivity profiling in the Gas Hills uranium district, Wyoming.

Troyer, M.L., McKay, E.J., Soister, P.E., Wallace, S.R., 1954, Summary of Investigations of Uranium Deposits in the Pumpkin Buttes area, Wyoming, USGS Circular 338.

Discussion of local stratigraphy and structure and of ore mineralogy and exploration guides.

Yellich, J.A., Cramer, R.T., Kendall, R.G., 1978, Copper Mountain, Wyoming, Uranium deposit - Rediscovered, in: Wyoming Geol. Ass. Guidebook, 30th Annl. Field Conf., pp. 311-327.

Discussion of the occurrence, structure, and stratigraphy.

Zeller, H.D., et al., 1956, USGS Mineral Investigation Field Studies, Map MF-83, Preliminary Geologic Map of the Gas Hills Uranium District, Wyoming.

Zeller, H.D., 1957, Wyoming Geol. Ass. Guidebook #12, p. 156-159, The Gas Hills Uranium District and Some Probable Controls for Ore Deposition.

Discussion of local mineralogy, structure, and ore deposition controls.

APPENDIX 9A.9.0 REFERENCES ON TEXTURE ANALYSIS

1. "Use of textural features in the analysis of Landsat images,"
by H.K. Ramapriyan, S.H. Chang and R.L. McKinney: Proceedings
of the 1978 AFIPS National Computer Conference (1978).

 2. "A comparative study of texture measures for terrain classification,"
by Joan S. Weszka and Azriel Rosenfeld: Report TR-361, Computer
Science Center, University of Maryland (1975).

 3. "Stability and dimensionality of Karhunen-Loeve multispectral
image expansions," by Gabriel E. Lowitz: Proceedings of the
Third International Joint Conference on Pattern Recognition,
held in Coronado, California (November, 1976).

 4. "Further experiments in terrain classification by texture
analysis," by Charles R. Dyer, Joan S. Weszka, and Azriel Rosenfeld:
Report TR-417, Computer Science Center, University of Maryland
(1975).
- "Detection of hazy anomalies in Landsat imagery by texture
analysis," by Charles S. Dyer, Joan S. Weszka, and Azriel Rosenfeld:
Report TR-429, Computer Science Center, University of Maryland
(1975).

5. "Textural features for image classification," by R.M. Haralick, K. Shanmugan, and I. Dinstein: IEEE Transactions on Systems, Man and Cybernetics, Volumen SMC-3, Number 6 (1973).

"Visual texture analysis: an overview,:" by Azriel Rosenfeld:
Report TR-406, Computer Science Center, University of Maryland
(1975).

6. "Manual of Remote Sensing," Chapter 9, The American Society of Photogrammetry (1975).

APPENDIX 10GLOSSARY

ASM - angular second moment, a measure of image texture. See Appendix 1.

CCT - Computer Compatible Tape, in particular one derived from Landsat imagery.

co-occurrence matrix - an array of pairs of grey level values, in which the individual matrix elements are a measure of the probability that a particular pair of grey levels occur in an image.

CON - contrast, a measure of image texture. See Appendix 1.

convolution filter - a one dimensional convolution filter can be represented by

$$C_R = \sum_{i=-n}^n X_i Y_{R+i}$$

where $X_{-n} \dots X_0 \dots X_n$ are the filter coefficients, $Y_{R-n} \dots Y_{R+n}$ represent a segment of the data stream to be filtered, R is the current filter position, $2n+1$ is the filter size and C_R is the R th filter output.

COR - correlation, a measure of image texture. See Appendix 1.

edge - in an image, a significant change in grey level values associated with a particular direction and a particular region of an image.

eigenband - a digital linear combination of two or more bands of Landsat MSS data, chosen to maximize information content and band separability.

ENT - entropy, a measure of image texture. See Appendix 1.

epigenetic mineral - mineral of later origin than the enclosing rock, usually implies formation by hydrothermal action.

grey level - the discrete tonal reflectance value part of an image. For the work performed here, all grey level values were normalized to lie in the range (0, 63).

grey level stretch - a mapping of grey level values, such that every pixel in an image is assigned a new grey level depending uniquely on its old grey level value.

histogram - the frequency distribution of grey level values in an image or sub-image.

- IDM - inverse difference moment, a measure of image texture. See Appendix 1.
- line - in an image, a double change in grey level value associated with a particular direction and region of an image, and taking place within the span of a few pixels (a line is a limiting case of two edges, where the edges move closer and closer together).
- lineament - a mappable, linear feature of a surface, whose parts are aligned in a rectilinear or slightly curvilinear relationship and presumably reflects a subsurface phenomenon.
- MSS - the Multi-Spectral Scanner that is carried as the primary sensor in the Landsat spacecraft.
- ore control - any geologic feature (tectonic, lithologic, geochemical, etc.) considered to have influenced the formation of ore.
- ore guide - any natural feature, e.g., alteration products, or a certain structure or plant growth, known to be indicative of an ore body.
- pixel - a picture element, the smallest individual component of a digitized image.
- primary ore - the first generation of ore or protore formed in a district or mine.
- ratio - a band combination of Landsat MSS data, in which pixel-by-pixel ratios of grey level values are computed to create a new grey level and hence a new image band.
- RBV - Return Beam Vidicon, a television-format recording instrument, panchromatic on Landsat-3 and 3-camera on Landsat-1 and -2 (Note: the instrument failed early in the lifetime of both Landsat-1 and -2, and little data is available).
- secondary ore - ore or mineralization which has migrated a (usually) short distance from a pre-existing "primary" ore. There may be several generations of secondary ore.
- supergene - a mineral deposit or enrichment formed by descending solutions. A mineral formed by weathering processes from a different pre-existing mineral; usually used with reference to ore minerals.
- syngenetic mineral - mineral formed contemporaneously with the enclosing rock.
- uranium deposit - an occurrence large enough and rich enough to be of economic interest.
- uranium occurrence - any record, specifying the location of uranium mineralization.

uranium ore body - a deposit large enough and rich enough to be mined at a profit at current market prices.

texture - the spatial distribution of grey levels in an image. When grey level values show slow change over many pixels, the image has coarse texture; when grey levels show rapid change over a few pixels, the image displays fine texture. Texture depends on image resolution, the size of discrete tonal features, and the number of such features.

APPENDIX 11

1. X-Directional Derivative Images

The x-directional derivative (XDD) is a convolution filter (see Glossary) designed to enhance edges or lines in an image. The filter is termed x-directional because it operates on a single scan line at a time, and scan lines lie in the x direction if the image is regarded with respect to a conventional Cartesian coordinate system. The XDD thus gives greatest enhancement to edges which lie perpendicular to the scan direction. Edges lying parallel to the scan direction are not enhanced at all. An advantage of this property is the suppression of radiometric striping caused by detector miscalibration. Radiometric striping appears as a series of edges parallel to the scan direction and as such receives no enhancement.

An XDD image contains no spectral information whatsoever. Instead of indicating reflected energy, the grey levels indicate the degree of texture in the image. Medium grey tones indicate a region of uniform reflectance while light and dark tones indicate the presence of positive and negative edges respectively.

Two different x-directional filters were tested on the first eigenband image of the Poison Spider, Wyoming scene. The first filter differences two adjacent pixels to obtain a derivative while the second filter calculates a derivative using a 5 pixel segment of the scan line. The first filter ("unsmoothed") gives the greatest degree of enhancement to the sharpest edges and the result can often be a harsh, noisy image. This did not appear to be the case in the Poison Spider scene, probably because of the noise free quality of the first eigenband image.

The second filter ("smoothed") gives the greatest enhancement to medium edges. It may be equated with performing a mild smoothing operation to reduce noise prior to calculating the image derivative. This filter also exhibits the tendency to "spread" out edges due to its 5 pixel length.

2. Geological Evaluation

Both the smoothed and unsmoothed versions of the XDD images were evaluated see Figures A.11.1 and A.11.2. Some geological formations were identifiable by their signature on the XDD image. However, in all cases these formations were more easily recognizable on the standard color composite image: for example, the Sundance formation.

It was difficult to accurately recognize some cultural features as being human origin when interpreting the XDD image; other cultural features (e.g., an interstate highway) were very obvious.

Although the smoothed image was less pleasing and further from reality than the unsmoothed versions, more linear features and other features of geological origin were visible upon it.

In the Copper Mountain, Kaycee and Poison Spider areas, there was no correlation between the known occurrence of uranium and any of the following features of the XDD: lineament length, direction, strength, or smoother than average or rougher than average areas. However, in the Pumpkin Buttes area, there was a weak correlation between clusters of deposits and rougher than average areas. It is therefore concluded that the XDD will be of little use in uranium exploration in this type of terrain.



- LEGEND
- Local Unsmoothed
 - Regional Unsmoothed
 - Smooth Region
 - Smooth Region



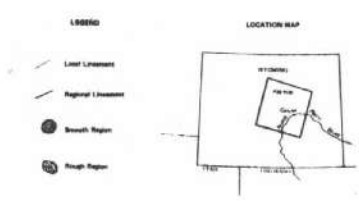
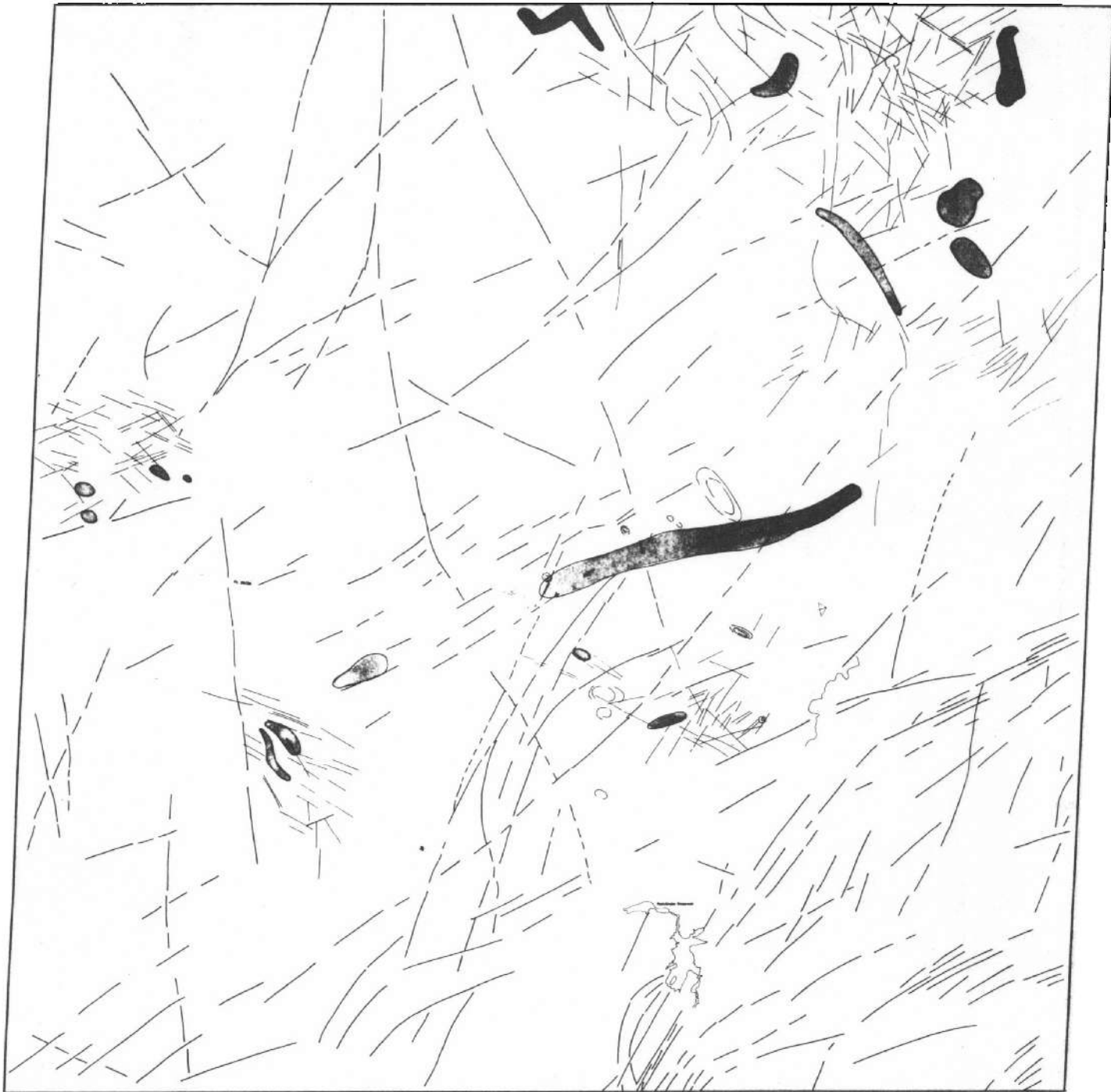
**PARTIAL INTERPRETATION OF THE
UNSMOOTHED X DIRECTIONAL DERIVATIVE
OF THE POISON SPYDER FRAME,
A PORTION OF WYOMING**

AUGUST, 1979

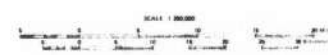
SCALE 1:100,000

PREPARED BY
EARTH SATELLITE CORPORATION
WASHINGTON, D. C.

Figure A.11.1 4X reduction of image overlay.
See original for details.



**PARTIAL INTERPRETATION OF THE
SMOOTHED X DIRECTIONAL DERIVATIVE
OF THE POISON SPYDER FRAME,
A PORTION OF WYOMING**



PREPARED BY
EARTH SATELLITE CORPORATION
WASHINGTON, D. C.

MAR 67, 1977

**Figure A.11.2 4X reduction of image overlay.
See original for details.**

